1990

Interaction Properties of Geogrids in Reinforced Soil Walls, Testing and Analysis.

Khalid A. Farrag
Louisiana State University and Agricultural & Mechanical College

Order Number 9123187

Interaction properties of geogrids in reinforced-soil walls, testing and analysis

Farrag, Khalid A., Ph.D.

The Louisiana State University and Agricultural and Mechanical Col., 1990

U·M·I
300 N. Zeeb Rd.
Ann Arbor, MI 48106

INTERACTION PROPERTIES OF GEOGRIDS IN REINFORCED-SOIL WALLS, TESTING AND ANALYSIS.

A Dissertation

Submitted to the Graduate Faculty of the
Louisiana State University and
Agricultural and Mechanical College
in partial fulfillment of the degree of
Doctor of Philosophy

in

The Department of Civil Engineering

by
Khalid A. Farrag
B.S. in C.E., Cairo University, 1977
M.S. in C.E., Louisiana State University, 1986
Dec. 1990

ACKNOWLEDGMENT

The author wishes to express his sincere thanks to his major advisor Dr. Ilan Juran for his guidance and supervision during the period in which this study was carried out, and to Dr. Y. Acar, the committee Chairman, for his advice through the last portion of this study. My appreciation also extends to the other members of the committee for their suggestions.

The author wishes to thank the Board of Regent, Louisiana Transportation Research Center (LTRC), and Conwed Plastics for their financial support. The suggestions from the staff of LTRC and Conwed Plastics during testing are also highly appreciated.

Finally, sincere appreciation is forwarded to my wife Elisabete for her help and support throughout my study.

TABLE OF CONTENTS

LIST OF TABLES

LIST OF FIGURES

ABSTRACT

The considerable development of the geosynthetics and their increasing use in soil reinforcement in the last decade made it necessary to develop methods of measuring the interaction properties and modeling load transfer in reinforced soil structures. The current testing procedures and interpretation schemes demonstrate significant limitations related to the equipment design, testing methodology and data interpretation. In order to address these limitations, a pull-out box and direct shear box were constructed and instrumented. The design of these boxes overcomes most of theses limitations and provides the capability of conducting displacement-rate controlled tests for the evaluation of short-term behavior of the soil-reinforcement system, and load-controlled tests to evaluate the confined time-dependent performance of the geosynthetics. The accuracy of the testing facility was evaluated through comparison of test results with those provided by the manufacturers. The reproducibility of test results were evaluated through repetitive tests performed on the geogrids under the same testing parameters. A parametric study on the geogrids under different testing conditions (i.e pull-out displacement-rate, confining pressures, soil compaction, soil density and boundary conditions) was conducted to evaluate the equipment sensitivity to the variations in testing conditions and to provide a reliable data base for the evaluation of the effect of these parameters on the soil-geogrid interface properties.

A data analysis procedure and interpretation methodology were established to determine the interface properties and the confined material characteristics of the geogrid reinforcement. The applicability of the load-transfer model was evaluated through comparison between the interface parameters evaluated from pull-out tests with those measured directly from the tests performed in the large direct shear box.

The interface properties and confined material characteristics of the geogrid reinforcement were utilized in a design model for the stability analysis of reinforced soil structures. This model is implemented in a computer program to calculate the forces in the reinforcements and the predicted failure planes. Design charts are presented where the maximum tension force at each reinforcement level and the inclination of failure surface can be predicted for different soil characteristics and reinforcement extensibilities. In order to evaluate the design assumptions considered in this model, the predicted tension forces and inclinations of failure surfaces were compared with those measured in laboratory model tests, full-scale model walls, and embankments of different soil data and reinforcements.

CHAPTER 1

INTRODUCTION

The considerable growth in using various materials to reinforce soil made it necessary to develop methods of measuring the interaction properties and modeling the load transfer mechanism at the soil-reinforcement interface. The selection criteria for a specific material in reinforcement of the soil is governed by the pull-out performance of the reinforcement, its tensile strength, and its time-dependent behavior when placed in the soil. Two different types of materials are used as tension resisting elements in reinforcing the slopes and embankments; namely,

i) inextensible reinforcement (such as metal strips and welded wire meshes),

ii) extensible geosynthetic reinforcement (such as woven and non-woven geotextiles and geogrids).

The use of inextensible materials in soil reinforcement have been investigated. Studies led to development of well-established testing procedures for evaluation of design parameters for soils reinforced with metal strips (Schlosser and Elias, 1978; Forsyth, 1978; Elias, 1979; and Schlosser et al., 1983). However, the effect of corrosion on the long term durability of metal inclusions limited their application and led to the use of polymer extensible materials. These extensible materials have different constitutive properties and structures that influence their behavior and consequently the testing methodology and interpretation.

Inextensible reinforcement moves as a rigid member in the soil with a constant shear stress distribution along its length. While extensible reinforcement exhibits more complex soil interaction mechanism. Non-uniform shear stress and displacement distributions are developed along the soil-inclusion plane with a large portion of the shear being mobilized at the loading application point (Juran et al., 1988; Juran and Chen, 1988; Christopher, 1976; and Tzong and Cheng-Kuang, 1987). This non-uniform shear stress distribution raises a basic difficulty in evaluating the scale effect for a reliable interpolation of laboratory pull-out test results to field conditions.

In addition, all polymer materials exhibit time-dependent behavior and stress relaxation which affect the long term stability of the reinforced structures. Therefore, the interpretation methods established for inextensible inclusions can not apply to the development of appropriate design procedure for the extensible inclusions.

A wide variety of geotextiles and geogrids are now available for civil engineering application (Bonaparte et al., 1987). In selecting a specific geotextile or geogrid for reinforcement of embankments and slopes, the following aspects of performance should be considered:

i) stress-strain relationship and creep behavior of the reinforcement when placed in the soil,

ii) pull-out performance of the reinforcement and its load transfer mechanism.

The majority of stress-strain and creep property tests of geotextiles and geogrids are currently performed on unconfined samples (Shrestha and Bell, 1982a-b; Andrawes et al., 1986; Richards and Scott, 1986; Rowe and Ho, 1986; and Myles, 1987). Consequently, the measured properties differ from those obtained under confined conditions and can not be used to determine the appropriate design parameters for the soil-reinforcement systems. Moreover, no standard testing procedure for the properties of the confined reinforcement currently exists. The large number of factors that affect the interface properties of the confined reinforcement raises major difficulties in comparing test results. Knochenmus (1987) and Juran et al. (1988) showed a wide scatter in the available confined pull-out test results. These differences in results are partially due to the use of different pull-out devices, the associated boundary effects, testing procedures, and soil placement and compaction schemes.

In order to develop a methodology for evaluation of the in-soil mechanical characteristics and interface properties of geosynthetic reinforcement, it is necessary to establish reliable testing equipment, procedure, and appropriate interpretation scheme. The specific objectives of this research are:

(1) to design, construct and calibrate a large pull-out box and a large direct shear box which will provide the capability of evaluating the performance of different types of geogrids and geotextiles,

(2) to develop a reliable testing procedure and data interpretation method for evaluation of the short term and long term pull-out performance of geosynthetic reinforcements,

(3) to utilize the measured interface properties and the in-soil material characteristics in a design model in order to evaluate the stability of reinforced soil structures.

The scope of this research focuses on testing and performance evaluation of the geogrid reinforcements in dense granular soils. It involves five tasks:

(1) Review of the Available testing Procedures: A comprehensive review of the available testing equipment, procedures, and data interpretation methods is conducted in order to evaluate the limitations of the current state of practice and to provide guidelines for the design of the testing facility.

(2) Design of a Testing Facility: A testing facility is designed, constructed, and instrumented for evaluation of both short term and long term geogrid performance. The facility is designed to provide the capability of conducting two basic testing modes: (a) displacement-rate controlled and (b) load controlled modes. In the displacement-rate controlled mode, the geogrid is subjected to a constant pull-out displacement rate during the test and pull-out load is recorded. This testing procedure (which is most commonly used) provides the interface parameters related to the short term performance of the

reinforcement such as peak and residual pull-out resistance and the level of front displacement at the peak pull-out load. In the load controlled mode, pull-out loads are applied incrementally to the inclusion and maintained constant during a specified period. The displacements along the inclusion are recorded and data interpretation yields time-dependent response parameters related to the long term performance of the inclusion.

(3) Performance Evaluation Study: A pull-out and direct shear testing programs were impiemented in order to evaluate the performance of the facility (i.e. the reproducibility of the results and accuracy of the monitoring system), to assess the effect of the rigid boundaries on test results, and to provide a data base for development of testing procedures (e.g. soil compaction, loading mode and displacement rate).

(4) Development of Data Analysis Procedure: A data interpretation scheme is developed in order to determine the interface properties and confined material characteristics of geogrid reinforcements.

(5) Soil-reinforcement Design Model: The soil-reinforcement interface properties are implemented in a computer program in order to analyze the state of stresses in the reinforcement and to evaluate the stability of the reinforced soil structures.

The detailed literature review of the existing testing equipment is presented in Chapter 2. The design and instrumentation of both the pull-out and

direct shear boxes are presented in Chapter 3. Sample preparation, testing procedure and performance evaluation of test results are presented in Chapter 4. A parametric study to assess the effect of different testing parameters on the in-soil performance of the geogrids is presented Chapter 5. Chapter 6 provides an interpretation scheme and data analysis procedure in order to determine the soil-geogrid interface parameters needed to evaluate the stability of reinforced soil structures. Chapter 7 contains a design model for the stability analysis of reinforced soil structures. Chapter 8 contains conclusions on the pull-out and direct shear testing procedures, the effect of testing parameters on soil-geogrid interaction mechanism, and a discussion of the data analysis procedure and the stability of reinforced-soil structures.

CHAPTER 2

REVIEW OF THE EXISTING GEOSYNTHETIC TESTING PROCEDURES

The in-soil mechanical characteristics and interface properties of geosynthetics have been experimentally modelled by monitoring:

i) the in-soil mechanical properties of the geosynthetic (i.e. its confined stress strain relationship and creep behavior),

ii) the soil-geosynthetic interface properties (i.e. shear stress-strain relationship and pull-out resistance).

Research on these parameters has been conducted using various equipment and testing procedures which made it difficult to consistently compare the performance of different geosynthetic specimens. An evaluation of these equipment and testing procedures is presented herein.

2.1) IN-SOIL MECHANICAL PROPERTIES OF GEOSYNTHETICS:

The unconfined stress-strain properties of geotextiles can be determined by testing the geotextile specimen in a wide width strip test according to the procedures presented in ASTM D4595-86. However, when the geosynthetic materials are embedded in the soil, their stress-strain properties are significantly affected by soil confinement (McGown et al., 1982; Knochenmus, 1989; and Juran et al., 1988).

The results of confined extension tests performed by Siel et al. (1987) and McGown et al. (1982) show that the confining pressure increases the tensile strength and deformation modulus of the geotextile material. These results are presented, respectively, in Figures (2.1-a and b). The figures demonstrate the effect of confining pressures on the deformation modulus. The effect is more predominant on geogrids which have transversal elements. In such geogrids, lateral earth resistance on the transversal elements restricts elongation and hence, increases strength and deformation modulus..

Currently, no standard testing procedure or apparatus exists for measuring the "in-soil" stress-strain material properties. Several investigators have determined these properties by testing geotextiles in modified direct shear boxes. In these boxes, the rear end of the specimen is clamped to the back of the box; while the front of the specimen is subjected to an extension force. Siel et al. (1987) used a modified shear box of 6.5 inch long, 4.75 inch wide and 2.5 inch deep (Figure 2.2) to study the stress-strain properties of non-woven geotextiles in compacted sand. While, El-Fermaoui and Nowatzki (1982) used a modified shear box of 2.5 inch long, 2.5 inch wide and 1.5 inch deep to obtain the confined extension properties of woven and non-woven geotextiles.

The disadvantage of using small shear boxes with dimensions similar to the conventional ones is the boundary effect of the box walls on the soil-geotextile interaction. Moreover, such small boxes can not be used to evaluate the elongation of the large representative samples of geogrids.

Another major shortcoming in using such devices is that confined extension test produces a combined effect of shear stress and extension along the specimen; thereby inducing a non-uniform tension force distribution along the geotextile (Knochenmus, 1989). Additional instrumentations to measure displacement distribution along the specimen and the load at its rear end are necessary to de-couple the shear-extension effect.

Leshchinsky and Field (1987) used a direct shear box modified to contain a metal platform in the lower box (Figure 2.3) to ensure that the geotextile remains exactly at the shear plan. They measured the tension forces in both ends of the geotextile specimen to estimate displacement and friction force distribution along its length.

McGown et al. (1982) developed a custom-built apparatus (Figure 2.4) to evaluate the effect of confining pressure and specimens size on the confined extension properties of geotextiles. Their apparatus consists of two air pressure diaphragms which are placed on each side of the geotextiles. A soil layer can be compacted between the diaphragm and the geotextile. Their results, shown in Figure (2.1-b), demonstrate the effect of confinement and sample dimensions on the confined properties of the geotextiles.

Knochenmus (1989) developed a confined extension testing device (Figure 2.5) in which extension loads on both sides of the specimen and the developed pore pressures in the soil sample can be monitored.

Attempts have also been made to determine the confined stress-strain properties of the geotextiles using other devices. Christopher et al. (1986) proposed a 'zero span' confined tension test in which the specimen is confined by means of pressure controlled metal clamps. Their apparatus is shown in Figure (2.6). Surface treatments were used on the clamp faces to simulate granular soil conditions. Several shortcomings of this apparatus are related to the difficulty in simulating the frictional conditions of the wide range of granular and soft soils on the clamp surfaces. Moreover, the device does not account for many parameters influencing the confined extension properties such as the development of pore pressures in saturated fine soils, soil dilatancy and soil particle interlocking on the specimen surface. Triaxial tests have also been carried out to investigate the stress-strain properties and time-dependent behavior of samples reinforced with horizontal disks of fabrics (Holtz et al., 1982; and Broms, 1977). Figure (2.7) shows the reinforced soil sample in the triaxial test. In this test, the strains in the fabric are difficult to be monitored and they are associated with different boundary conditions than those encountered in the field.

Although the "in-soil" stress-strain properties can be determined in confined extension tests, the development of an appropriate load transfer mechanism raises the need for other tests to determine the geogrid interface properties (i.e. the shear stress-strain and pull-out resistance).

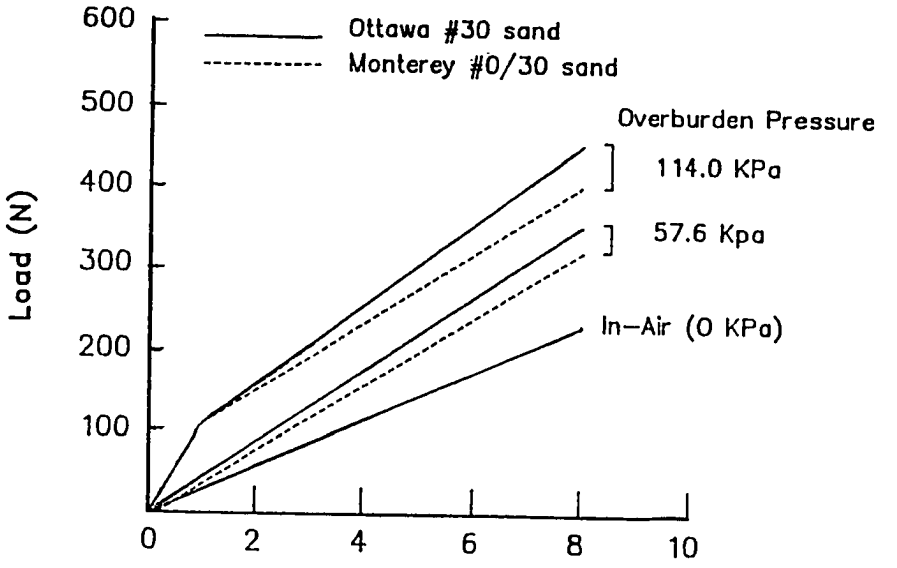

(a) After Siel et al., 1987.

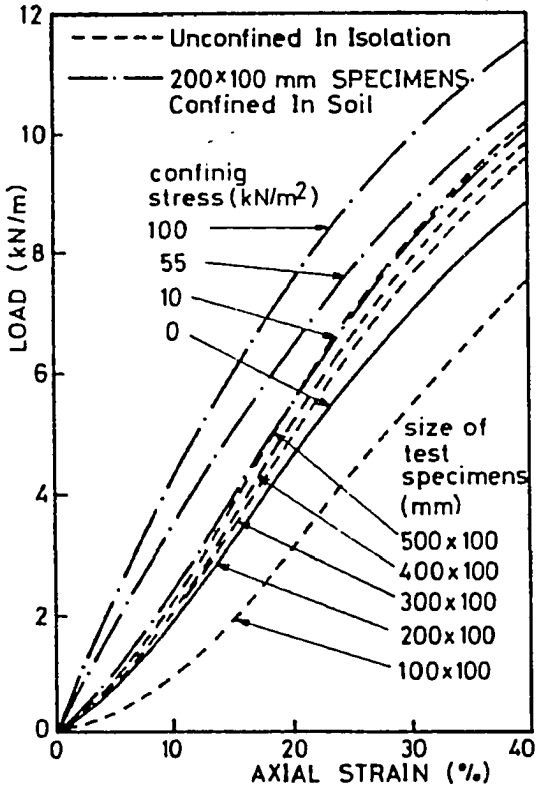

(b) After McGown et al., 1982.

Figure 2.1 Unconfined and Confined Extension Tests on Geotextiles.

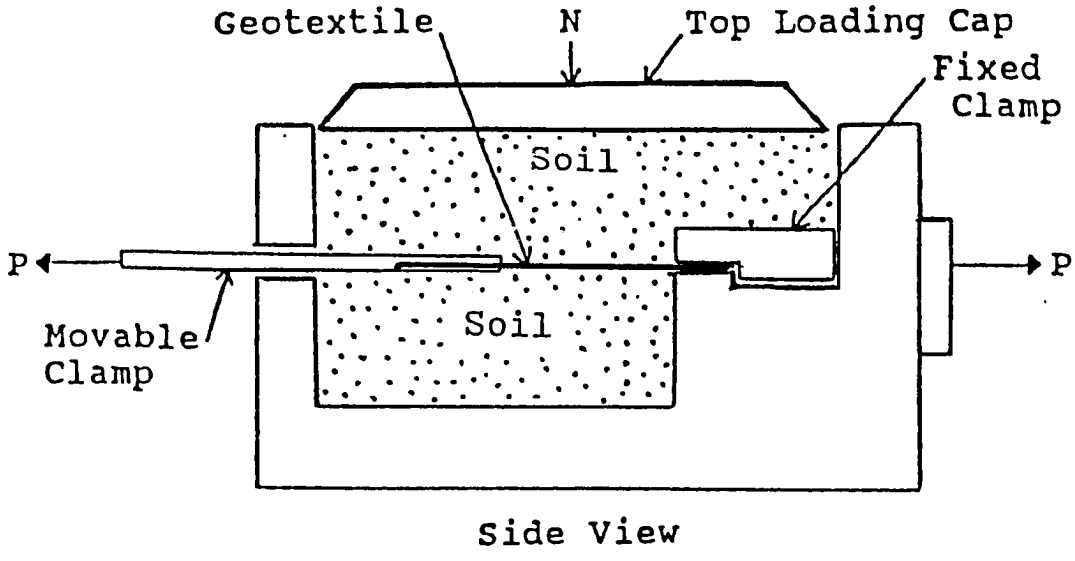

Figure 2.2 Modified Shear Box for Confined Extension Tests.
(After Siel et al., 1987)

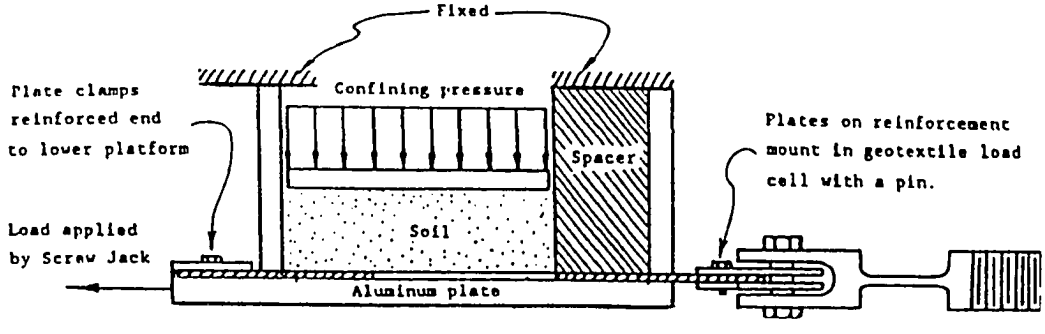

Figure 2.3 Confined Extension Testing Device on Geotextiles.
(After Leshchinsky and Field, 1987)

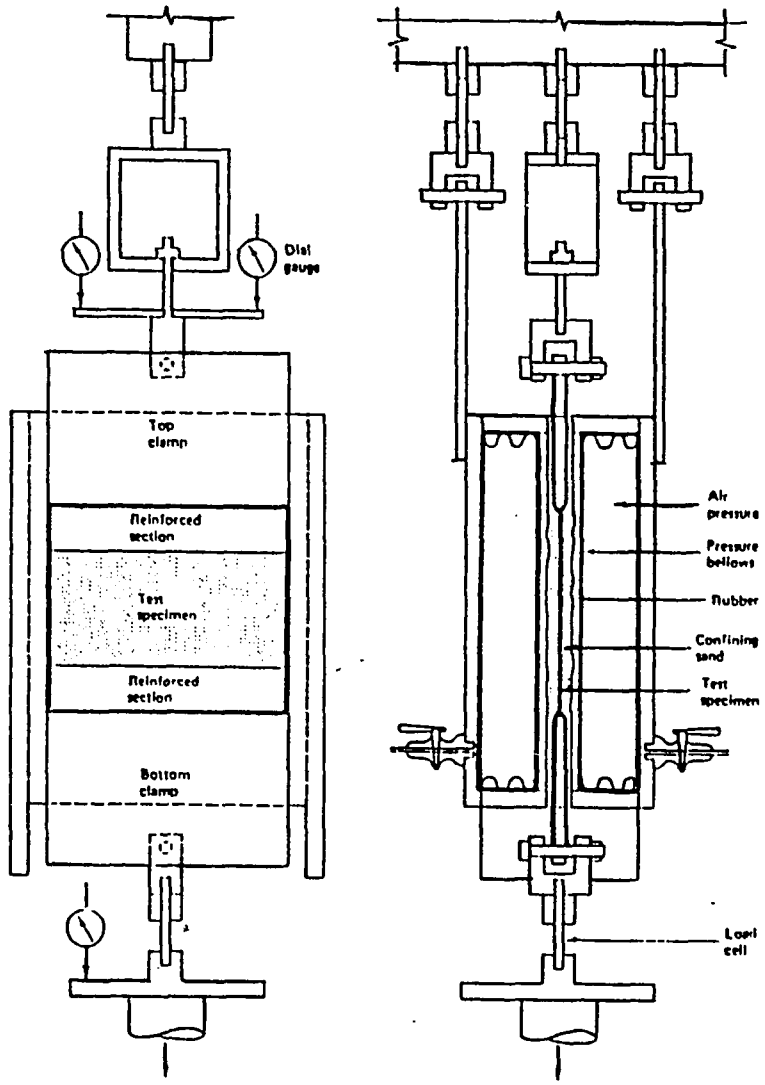

Figure 2.4 Confined Extension Testing Apparatus.
(After McGown et al., 1982)

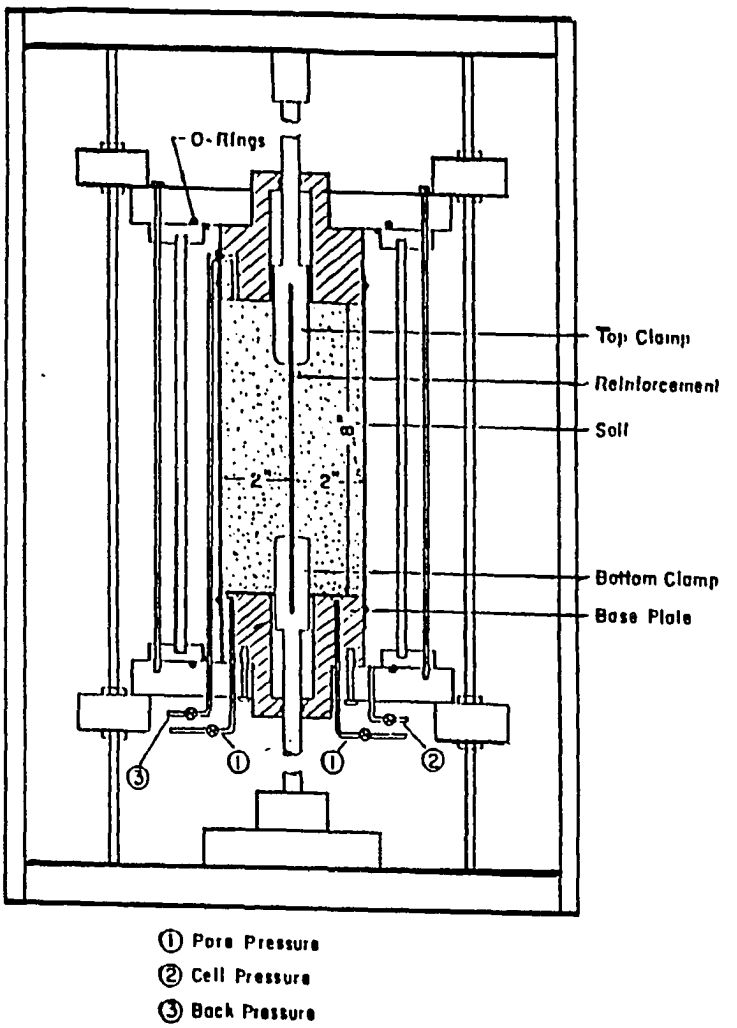

Figure 2.5 Confined Extension Testing Apparatus.
(After Knochenmus, 1989)

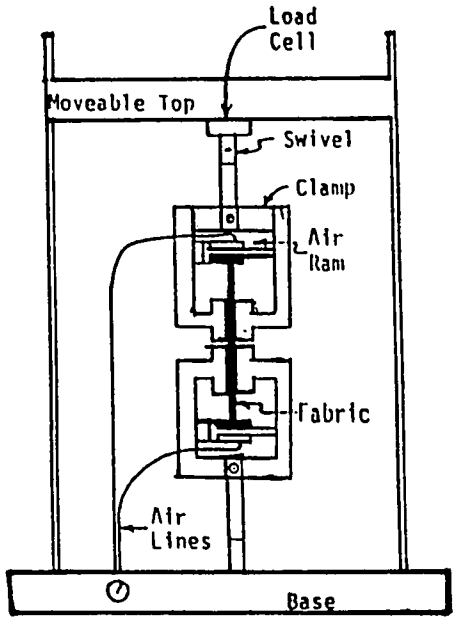

Figure 2.6 'Zero Span' Confined Extension Apparatus.
(After Christopher et al., 1986)

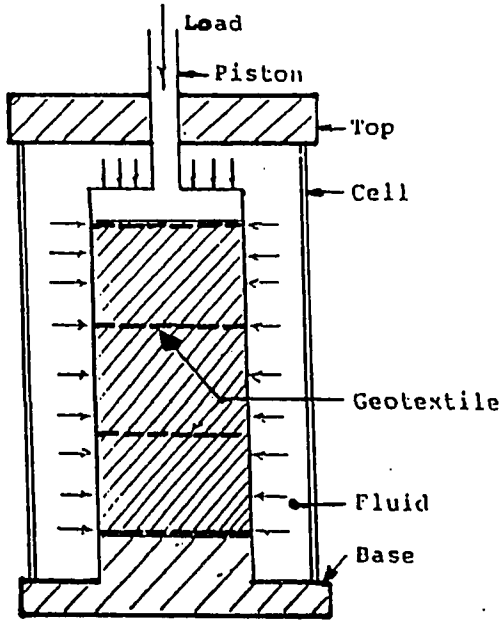

Figure 2.7 Triaxial Cell with Reinforced Soil Sample.
(after Broms, 1977)

2.2) SOIL-GEOSYNTHETIC INTERFACE PROPERTIES:

The shear stress-strain relationship developed at the soil-reinforcement interface can be tested in both direct shear and pull-out boxes. In the direct shear box, tests are usually conducted in accordance with the conventional procedure of tests on un-reinforced soil samples. The horizontal displacement required to mobilize the shearing stresses are measured along with the vertical displacements of loading plates. Typical shear boxes used to determine the soil-geosynthetic frictional properties are shown in Figures (2.8a-b). Test results are usually expressed as the efficiency factor which is the ratio between the soil-reinforcement interface friction angle and the soil friction angle (tan δ/ tan ϕ).

Different shear boxes have been utilized to evaluate the shear strength at the soil-reinforcement interface. The sizes of shear boxes ranged from the conventional ones (Richards and Scott, 1985) and small boxes of 4 in. long by 4 in. wide (Martin et al., 1984) to relatively larger shear boxes of 10 in. by 10 in. (Saxena and Budiman, 1985) and 12 in. by 12 in. (Degoutte and Mathieu, 1986; and Williams and Houlihan, 1987). The shortcoming of using small shear boxes is due to their inability in measuring the large deformations required to mobilize the interface friction between soil and geosynthetics. Moreover, the large dimensions of most of the geogrid patterns do not allow using representative samples in such small boxes. Myles (1982) and Miyamori et al. (1986) used direct shear devices with the lower boxes of bigger dimensions than the upper ones. The advantage of using a lower box of bigger dimensions

is to subject the reinforcement to a higher shear strain level without loss of shear area. A comparison of dimensions of the shear boxes, reinforcements and soil types used, and testing procedures is shown in Table (2.1).

Direct shear test results provide the local shear stress-strain relationship at the soil-inclusion interface. However; in order to determine the pull-out resistance of the reinforcement, pull-out tests have to be performed. Since pull-out resistance integrates the non-uniform variation of the shear stress-strain along the reinforcement, pull-out tests incorporate the reinforcement extensibility effect on the interface parameters. Consequently, the interface frictional parameters obtained from shear and pull-out tests can vary. Both tests are associated with different testing procedures, loading paths and boundary conditions. In selecting the most appropriate type of test it is essential to adequately simulate field conditions. For soil reinforcement applications, pull-out tests should be used since it is more representative of field conditions and failure mechanism of embankments and slopes (Juran et al., 1988).

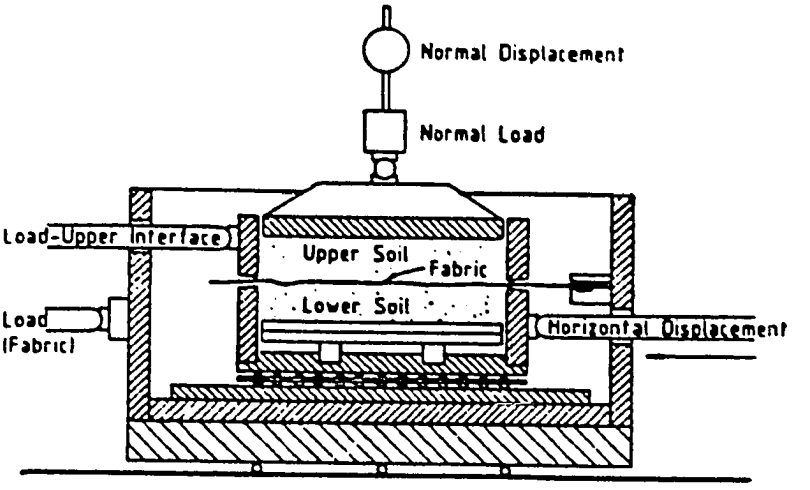

(a). After Rowe et al. (1985).

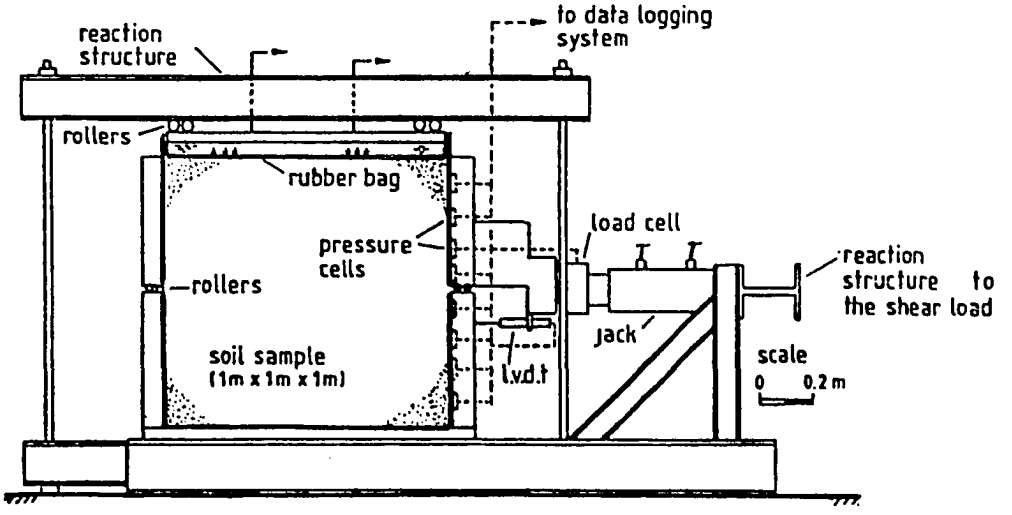

(b). After Palmeira and Milligan (1989).

Figure 2.8 Soil-Geosynthetic Direct Shear Test Devices.

References	Device Description	Reinforcement Type (*)	Soil Type	Notes
[1] Williams and Houlihan, (1987)	Shear box 12x 12 in^2.	- Trevira 1155 [2] - Typer 3401 [2] - Nicolon 900 [1] - PVC membrane - Polyethelen [4]	- Ottawa 20/30 - Concrete sand - Glacial till - Saprolite - Gulf coast clay.	- [δ] = 10-45 deg. - Rate = 0.01 in/min.
[2] Miyamori et al. (1986)	Lower box 47.8 x 40.8 cm^2, upper box 31.6 x 31.6 cm^2.	- Poyster needle-punched [1]	Poorly graded dry and wet sand.	- [δ/φ] = .72-.78 dry sand, = .64- .86 wet sand. - Rate = .5 mm/min - [σ] = 50-500 Kpa - Fabric glued to wooden block in lower box.
[3] Degoutte and Mathieu, (1986)	Shear box 30 x 30 x 30 cm^3.	- Geotextile [1,2] - PVC [4]	- Sand [φ] = 33° - Sandy clay [φ] = 33.5°	- [δ] = 35-39 deg. - Soil in one side of box - [σ] = 200-1200 Kpa
[4] Saxena and Budiman, (1985)	Shear box 10 x 10 in^2.	- Celanese 600 [1] - Monsanto [2]	- Sandy clay, 45% Ottawa - Saturated Lime stone balast.	- [δ] = 23.8- 27 deg. for C-34 = 17.2- 22 deg. for 600X - Rate 0.03 in/min - [σ] = 10-30 psi
[5] Formazin and Batereau, (1985)	Shear box	- Non-woven - Woven	- Saturated sand	- [δ] = 22-35 deg.
[6] Richards and Scott, (1985)	Shear box 2x2 in^2.	-Bidium U-14 [2] -Terrafix [1] -Mirafi T700 [1]	- Quartz angular sand [φ] = 38°.	- [δ] = 31-41 deg.

(1) Reinforcement type:
[1] wooven geotextile,
[2] non-wooven geotextile,
[3] geogrid,
[4] other materials.

(2) φ = soil friction angle
δ = interface friction angle.

Table 2.1 Comparison of Geosynthetic Direct Shear Tests.
[from avaliable experimental data]

- Table 2.1 [Continued] -

References	Device Description	Reinforcement Type	Soil Type	Notes
[7] Martin et al. (1984)	Shear box 10 x 10x 2.54 cm^3	- EPOM FML [4] - PVC FML [4] - Typar 3401 [2] - Polyfilter X [1] - Mirafi 500 X [1]	Concrete sand (φ) = 24 deg.	-[δ] = 20-30 deg. -Soil in one side. -Rate = .127 mm/min. -[σ] = 14-100 Kpa
[8] Myles, (1982)	Upper box .1 m^2, lower box .35 x .4 m^2	- Needle-punched Polypropelene [2] - Woven Polyster	Leighton Buzzard sand .4-.85 mm	-[δ] = 36-44 deg. -Fabric glued to wooden plate in lower box. -Rate = 10-75 mm/min. -[σ] = 30, 60 and 300 Kpa.
[9] Jacobsen, (1985)	Shear box 17.5 x 10 cm^2, circular end plate to acheive shear at different angles.	- Fibertes needle-punched [2]	Quartz angular sand	-[σ] = 3-5 m of sand

(1) Reinforcement type:
[1] wooven geotextile,
[2] non-wooven geotextile,
[3] geogrid,
[4] other materials.

(2) φ = soil friction angle
δ = interface friction angle.

Table 2.1 [Continued].

In the pull-out tests, the rear end of the specimen is free while the front end is clamped to the pull-out loading machine. Pull-out tests were used to provide the load-displacement relationship at the facing of the geosynthetic specimen and its pull-out resistance. Since no standard design for pull-out testing devices exist, box dimensions and testing procedures differ for every box. The dimensions of the box are usually chosen to reduce the boundary effects. Figures (2.9 to 2.12) show typical pull-out testing equipment. A summarized review of most of the available equipment and testing parameters is presented in Table (2.2).

The review of the existing pull-out tests shows a large variety of testing equipment and procedures which makes it difficult to compare test results. It also indicates some significant limitations which the investigators tried to overcome with different degrees of success. Most of these limitations are related to:

(1) Most of pull-out tests were performed with controlled displacement rates. Various pull-out rates were recorded in the literature (varying from 0.1 mm/min till 20 mm/min). Although Myles (1982) has studied the frictional resistance of the geotextile interface in direct shear tests under different strain rates (10-75 mm/min) and showed little sensitivity of test results, the effect of displacement rate on pull-out results has to be evaluated. Moreover, very few pull-out tests under load controlled mode are available in the literature.

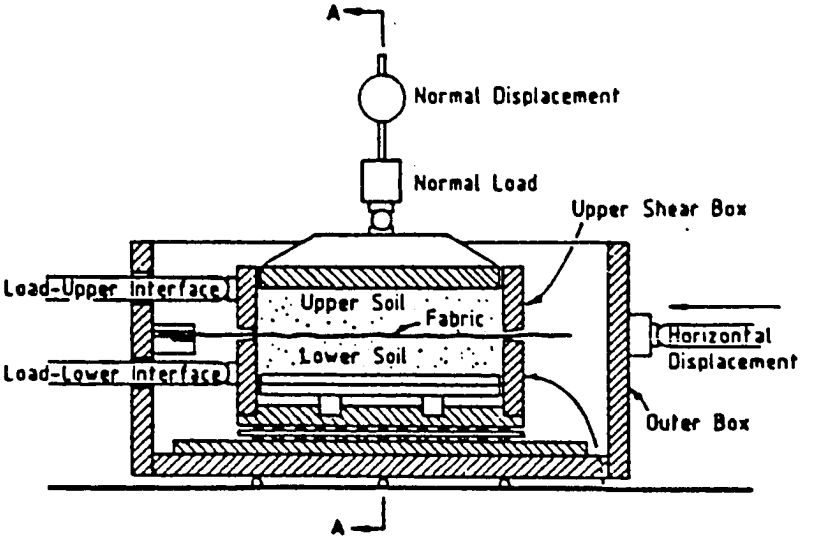

Figure 2.9 Pull-out Testing Device.
(After Rowe et al., 1985)

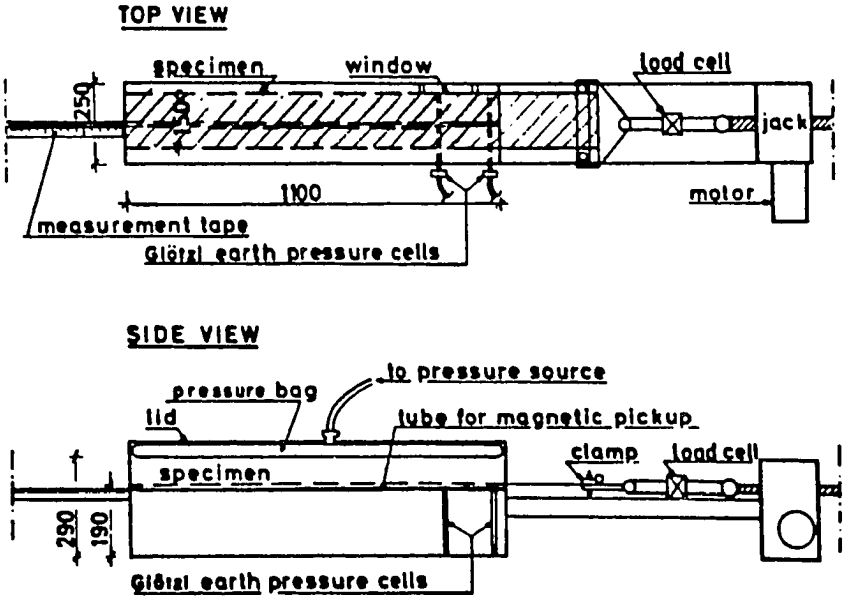

Figure 2.10 Pull-out Testing Device.
(After Holtz, 1977).

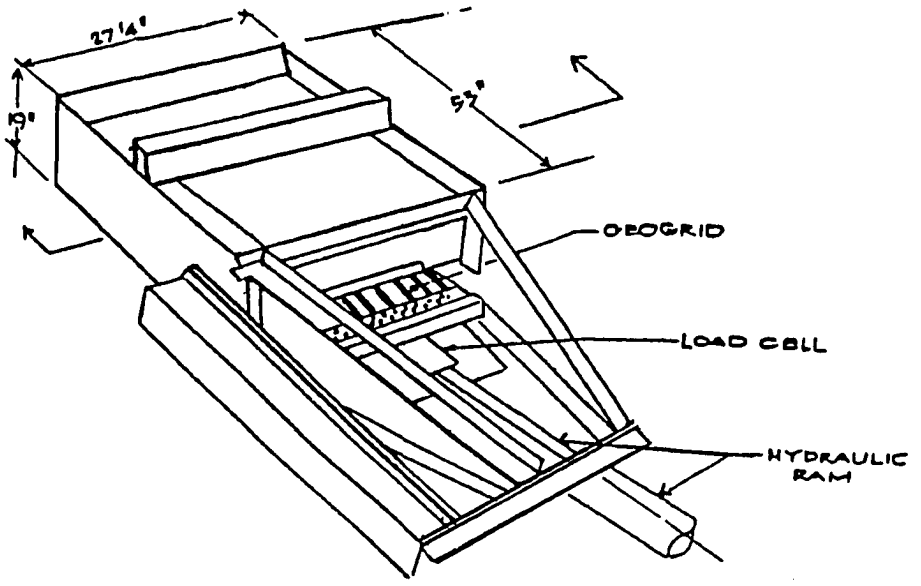

Figure 2.11 Geosynthetic Pull-out Box.
(After Christopher, 1976)

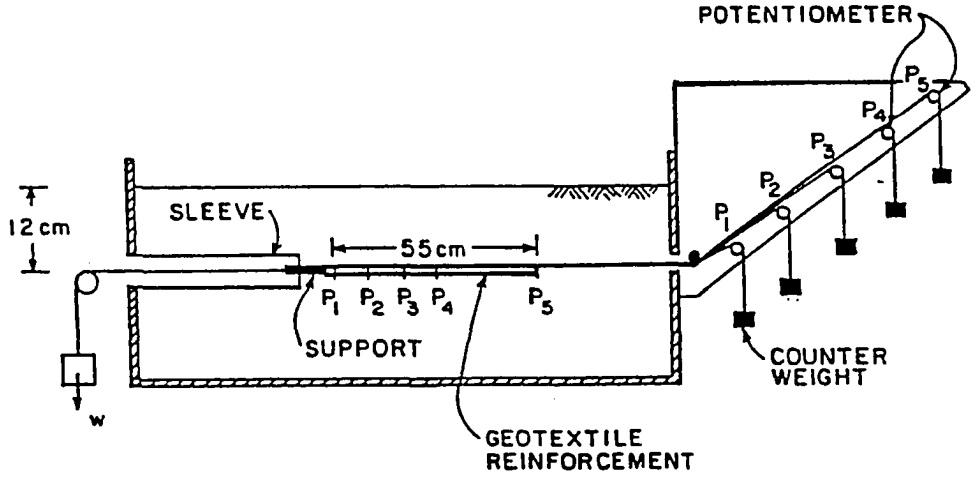

Figure 2.12 Displacement Monitoring Along the Reinforcement in Pull-out Test.
(after Juran and Chen, 1989)

References	Pull-out Box [length x width x height] in^3.	Reinforcement type (1)	Soil type	Notes
[1] Elias, (1979)	36 x 36 x 18	Smooth and ribbed metal strips [4]	- Residual silt - Kaoline clay - Wyoming sand	- Strain rate 0.3 in/min. - rigid front face.
[2] Tzong and Cheng-Kuang, (1987)	48 x 48 [sample width = 18 in.]	- Trivera 1127 [2]	- Ottawa sand, density=107 pcf	- Load controlled test. - [σ]= 4.34 psi.
[3] Brand & Duffy (1987)	12 x 12 [sample size 10 x 10 in^2.]	- Tensar SS2 [3] - Tensar SR2 [3] - Tensar SR3 [3] - Tensar TT2 [3]	- Bentonite clay	- Strain rate 0.01 cm/min. - [σ] =12-48 Kpa
[4] Christopher, (1976)	48 x 30 x 18	- Tensar SS2 [3] - Signode TNX [3]	- Fontainbleau dense sand	- Strain rate 0.1 mm/min. - Rigid front face with sleeves. - [σ] = 440, 660, 800 psf.
[5] Koerner, (1986)	18 x 18 x 8	- Geomembranes [4] - C2-600 [2] - Tensar SR2	- Well graded concrete sand	- Rigid front face.
[6] Ingold, (1983)	19.7x 11.2x 11.8	- Nelton 1168 [3] - Tensar SR2 [3] - Welded wire mesh [4] - mild steel sheets	- Borham wood pit sand	- water filled air bag. - rigid front face.
[7] Holtz, (1977)	42 x 10 x 11	- Woven polyster [1]	- Tullinge sand - G-12 rounded sand.	

(1) Reinforcement type:
[1] woven geotextile
[2] non-woven geotextile
[3] geogrid
[4] other material.

Table 2.2 Comparison of Geosynthetic Pull-out Tests.
[from available experimental data].

Table 2.2 [Continued].

References	Pull-out Box [length x width x height] in^3.	Reinforcement type (1)	Soil type	Notes
[8] Rowe et al. (1985)	Pull-out and shear box on samples 6 x 6.	- Permealiner [1] - Mirafi [1] - Geolon 1250 [1] - Terrafix [2] - Tendar SR2 [3]	- Loose silty sand.	- Strain rate 1.0 mm/min. - Rigid front face.
[9] Johnston, (1985)	54 x 54 x 36	- Tensar SR2 [3]	- Medium to coarse sand.	- Strain rate 4.4 mm/min.
[10] Anderson, (1984)	72 x 60 x 48	- Welded wire mesh [4]	- Silty sand - Washed sand - Pea gravel	- Strain rate 0.8 mm/min
[11] Jewell, (1980)	Modified shear and pull-out box 10 x 6 x 6	- welded wire steel [4]	- Leighton Buzzard sand	- Strain rate 0.1 mm/min. - Rigid front wall.

(1) Reinforcement type:
[1] woven geotextile
[2] non-woven geotextile
[3] geogrid
[4] other material.

Table 2.2 [Continued].

Tzong and Cheng-Kuang (1987) examined the pull-out interaction mechanism under imposed loading-controlled conditions. Load-controlled pull-out tests are necessary if the in-soil time-dependent interface parameters need to be evaluated.

(2) The interaction between the soil and the box side walls can affect the pull-out test results. The applied confining stresses can be partially carried out by the side wall friction causing a reduction in the normal pressure applied at the reinforcement level (Johnston, 1985). Anderson and Nielsen (1984) minimized the interaction with the side walls by keeping the edge of the specimen at 1.5 ft from the side walls. Jewell (1980) lubricated the walls with silicon and covered them with a thin rubber membrane to provide frictionless boundary. Several investigators confined the soil within a flexible membrane to insure uniform distribution of normal stress by means of air pressure (Christopher, 1976) or de-aired pressurized water (Ingold, 1983).

(3) The interaction between the reinforcement-soil system and the rigid front wall can also influence test results. As the reinforcement is pulled out from the box, the lateral earth pressure developed at the front face can result in an increase in pull-out resistance. Christopher (1976) incorporated sleeves around the pull-out slot to transfer the pull-out application point far behind the rigid front wall. Other investigators ((Williams and Houlihan, 1987) used flexible front face to minimize its effect. Johnston (1985) used pull-out box with the front face removed to prevent interaction with the soil-reinforcement system.

(4) The thickness of soil differs in each box according to its clear height (Table 2.2). If soil thickness is small, the interaction between the soil-reinforcement system and the rigid plates at the top and bottom of the box may restrain soil dilatancy and the mobilized shear resistance at the interface and, consequently, affecting pull-out resistance. Brand and Duffy (1987) determined pull-out resistance of geogrid in different thickness of clay. Their results show that as the soil thickness increased, pull-out resistance decreased until a minimum force state is reached.

(5) An apparent increase in the pull-out resistance of the inclusion was recorded with the increase in soil relative density and normal pressure (Ingold, 1983; and Koerner, 1986). Johnston (1985) attributed recorded variations in the normal pressure on the reinforcement level to the uneven sample compaction. Different sample preparation and compaction procedures were utilized to insure uniform soil density. Soil compaction was achieved by means of electric jack hammer (Johnston, 1985), standard proctor hammer (Saxena and Budiman, 1985), hand tamping devices (Elias, 1979) and by mechanical tamping (Anderson, and Nielsen, 1984). A hopper with flexible tube was also used to insure uniform soil placement in the box (Jewell, 1980).

(6) Several investigators (Christopher, 1976; Koerner, 1986; and Brand and Duffy, 1987) clamped the reinforcement outside the box. The disadvantage of this technique is that the unconfined front portion of the reinforcement results in a variation of the effective interface area during the test.

(7) The existing pull-out testing equipment are usually instrumented to monitor displacement, pull-out rate, and mobilized pull-out resistance at the facing. Most of these equipment lack the proper instrumentation to monitor the internal deformations along the interface. For extensible reinforcement, monitoring the displacements at different locations along the inclusion is a key element in a proper development of a load transfer mechanism. Jewell (1980) used an x-ray device and placed short lead markers in the soil to detect the internal deformations in the sand. However, the maximum penetration depth (15 cm) of the x-ray limited the sample width used in this experiment. Christopher (1976) used extensometers to measure the displacements at various locations along the inclusion. Juran and Chen (1989) described a mechanism where they hooked inextensible ,tell-tail, wires to the reinforcement through slots at the rear wall (Figure 2.12) in order to monitor the displacements at different locations along the inclusion.

2.3) CONCLUSIONS:

The soil-reinforcement interface properties can be measured in both direct shear and pull-out tests. The interface friction coefficient is usually presented as the efficiency factor which is the normalized value with the soil to soil friction coefficient (tan δ/ tan ϕ). Efficiency factors ranging from 0.6 to 1.0 for geotextiles and values larger than one for geogrids were commonly reported. The review of the available test results demonstrated that there exists significant variations in the results obtained from both direct shear and pull-out tests. Jewell et al. (1984) and Johnston (1985) found out that the frictional resistances for various inclusions in dense sand were greater in pull-out tests than those obtained from direct shear tests. Similar results were recorded by Schlosser and Guilloux (1979). They attributed the higher values in pull-out tests to the higher sample dilation which increases the local vertical pressure on the reinforcement. Ingold and Templeman (1979) found equal values from both tests for geogrids tested under low confining pressures. However, under higher normal stresses, higher shear strength values were produced in pull-out tests. Koerner (1986) reported higher shear resistance of geogrids in pull-out tests. However, unlike the results of Ingold, he found out that under higher confining pressures direct shear tests give higher shear resistance. Rowe et al. (1985) found out that both tests give approximately equal values of shear resistance for geotextiles tested in loose fine grained soil. Since loose sand has low tendency for dilation, restrained expansion has no effect on normal

stresses. Figure (2.13) shows a comparison between the efficiency factors obtained by various investigators from both pull-out and direct shear tests.

The different testing methods in both direct shear and pull-out boxes, the associated boundary conditions and the corresponding soil dilatancy behavior lead to different design parameters. Moreover, a fundamental difference between both tests is that direct shear tests provide uniform shear stress-displacement parameters; while these values are distributed non-uniformly along the extensible reinforcement in pull-out tests.

The review of the available testing equipment has also showed that many factors influence the measured interaction properties. These factors are related to testing equipment and procedure, boundary condition, soil and reinforcement type, soil placement and compaction, soil dilatancy behavior, and overburden pressure. Several techniques are used in determining the effect of these factors on test results; however, only with limited success.

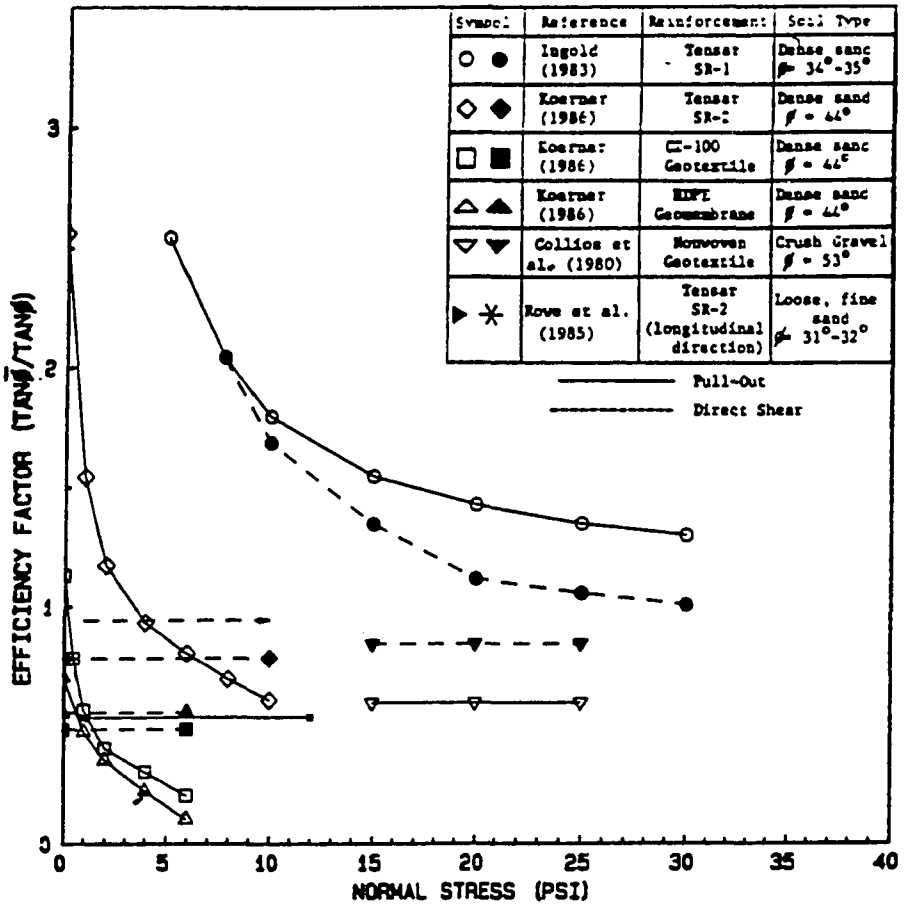

Figure 2.13 Comparison of the Efficiency Factor Obtained from Direct Shear and Pull-out Tests.
(After Juran et al. 1988)

CHAPTER 3

EQUIPMENT DESIGN AND INSTRUMENTATION

3.1) DESIGN CONSIDERATIONS:

Several pull-out facilities have been designed and used to determine the soil-reinforcement interface properties of geosynthetics. A detailed review of the available testing equipment is presented in the previous chapter to provide guide lines for the design of the pull-out and direct shear testing equipment. The review showed a large variety in the typed of available equipment and testing procedures. It also showed some significant limitations which should be considered in the design of the proposed equipment. These limitations are mainly related to:

(i) Loading Scheme:

In most of the equipment reviewed, tests have been done under constant displacement rates. Tests under various displacement rates should be performed in order to evaluate their effect on the results. Moreover, the equipment should provide the capability of conducting tests under load controlled mode in order to assess the confined creep parameters of the soil-reinforcement system. This testing scheme is of importance specifically for geosynthetic materials which exhibit time-dependant deformations.

(ii) Rigid Wall Boundary Effects:

The rigid walls of the boxes influence test results by imposing boundary conditions on the interface. The proposed equipment should provide, through modular design, the flexibility in sample and box dimensions for the evaluation of the boundary condition effects.

The side wall friction can partially carry out the applied normal pressure and, thereby, affecting the confinement at the interface. Side wall friction can be minimized by applying the normal pressure within a flexible membrane. Box dimensions have also to be of adequate size to keep the confined specimen far from box walls. In order to investigate the effect of the passive earth resistance at the front wall, sleeves have to be incorporated into the design to insure that the soil-reinforcement interaction is carried out far from the front face. Soil pressure at the facing must be measured and a parametric study has to be performed to determine the sleeve length at which this effect is minimal. In order to evaluate the effect of top and bottom plates on the interaction mechanism, tests with different soil thickness above and under the reinforcement have to be performed.

(iii) Soil Placement and Compaction:

The frictional resistance of the inclusion is influenced by the relative density of the soil. When interface shear stresses are mobilized during testing, dense soil tends to dilate. As this dilation is restrained in the box, normal stress

increases at the vicinity of the inclusion. Furthermore, in geogrid reinforcement, soil compaction increases the lateral resistance on the transversal elements and, consequently, their shear resistance. A soil placement and compaction procedure should be developed in order to facilitate sample preparation and insure that the soil density is compacted uniformly to the desired density throughout the box.

(iv) The Specimen Clamping Mechanism:

In pull-out tests, the clamping of the reinforcement to the loading device outside the box leads to an unconfinement of the front portion of the reinforcement. The unconfined elongation of the front part implies variation of the interface area of the reinforcement during the test. The clamping mechanism has to insure in-soil clamping of the specimen to maintain uniform confinement and a constant interface area of the specimen during pull-out.

(v) Instrumentation:

The results of pull-out tests are influenced by the extensibility of the inclusion. In order to evaluate the frictional resistance along extensible materials, an interpretation method that incorporates the inclusion extensibility has to be adopted. Accordingly, the instrumentation must be capable of measuring the relative displacements at different locations along the confined reinforcement.

3.2) EQUIPMENT DESCRIPTION:

The testing facility consists mainly of the following:

i) A pull-out box of dimensions 60 in. long, 36 in. wide and 36 in. high.

ii) A large direct shear box with the lower part of dimensions 60 in. long, 36 in. wide and 24 in. high, while the upper box is of dimensions 27 in. by 27 in. and 15 in. deep.

iii) A hydraulic loading system for each box, which is capable of performing under both constant pull-out displacement-rate and constant pull-out load.

iv) A sand handling system; which consists of an elevated sand hopper and a sand vacuum machine, that facilitates sand placement, removal and compaction control for both boxes.

v) Instrumentation and data acquisition system to control and monitor the input testing and response parameters (e.g. displacement rate, pull-out load and displacements at different locations along the reinforcement).

Figure (3.1) shows a side view of the pull-out box, the loading frame and the sand handling equipment. Figure (3.2) shows a front view of the box, the loading frame and the clamping plates. Figures (3.3) and (3.4) give the longitudinal and cross sectional details of the pull-out box. The direct shear box is shown in Figure (3.5), and its cross sectional details are shown in Figure (3.6). Both boxes were constructed with ASTM A36 mild steel. The details of

the cross sections of the testing equipment are shown in Appendix A.

i) The Pull-out and Shear box Details:

The main elements of the pull-out and direct shear boxes are:

1) ¼ in. bottom and side wall steel plates which can be assembled to modify the length of the box. The boxes were assembled in bolted modular units to adjust the length to 30 in., 45 in. and 60 in. and to adopt any increase in the box dimensions in the future. For the tests performed in this study, box length was kept at 60 in. For the pull-out box, the width of the box was chosen to keep the standard sample, of 1 ft wide, at a distance 1 ft from each side of the box wall to reduce the effect of side wall friction on the soil-specimen interaction. The level of the hydraulic ram can be adjusted to allow pulling out the inclusion at different heights in soil in order to evaluate the effect of soil thickness on test results.

2) A modular front wall is designed of 4 in. by 4 in. rectangular beams. The front wall contains a slot of 2 in. height to permit pulling the clamping plates out of the box. In the pull-out box, the modular units permit an evaluation of the effect of the rigid front boundary by using slots with variable opening sizes and different facing types.

3) A modular rear wall of 2 in. by 4 in. rectangular beams. In the pull-out box, five slots are located in the rear wall to permit the instrumentation for displacement measurements along the reinforcement.

4) A loading frame , shown in Figure (3.1), which is bolted to the front face of the box to support the hydraulic loading device.

5) An air bag of 2 in. thickness. It is used to apply the vertical overburden pressure when inflated through the air pressure source. The pressure system is able to apply a normal pressure up to 30 psi. A cover plate of ½ in. thickness is used to confine the air bag above the soil. The cover plate is placed under rectangular beams which are bolted to the box wall to enclose the air bag.

6) Sleeve plates, shown in Figure (3.3), of 4 inch width x ½ inch thick. The plates are placed on the top and bottom of the slot in the front wall of the pull-out box. The sleeves are placed at the facing to transfer the pull-out load far behind the box rigid front face. The sleeves minimize the lateral stress transfer to the rigid facing during pull-out which would result in an apparent increase of the pull-out resistance of the inclusion. The sleeves are designed in modular units to evaluate the minimum sleeve length required to eliminate the effect of the rigid front face.

7) Two clamping plates, shown in Figure (3.2), of 1/8 in. thick. In the shear box, the clamping plates are bolted to the upper box; while, in the pull-out box, they are bolted to the reinforcement inside the box.

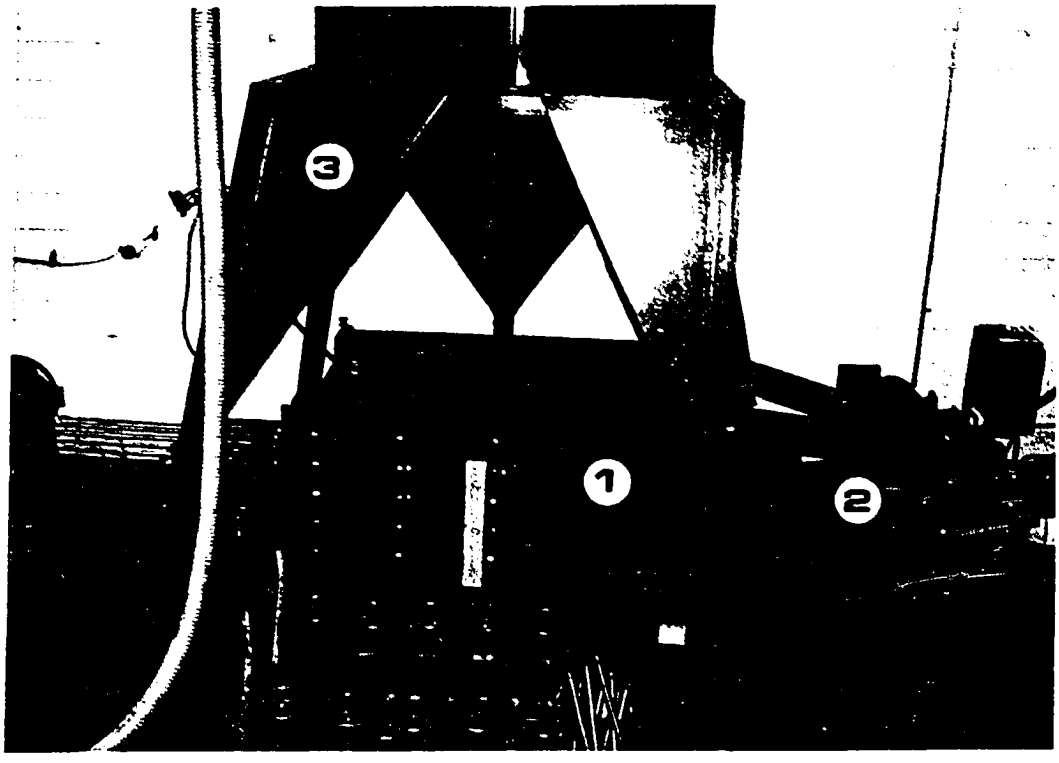

1) Pull-out Box
2) Loading Frame
3) Elevated Sand Container.

Figure 3.1 Side View of the Pull-out Box.

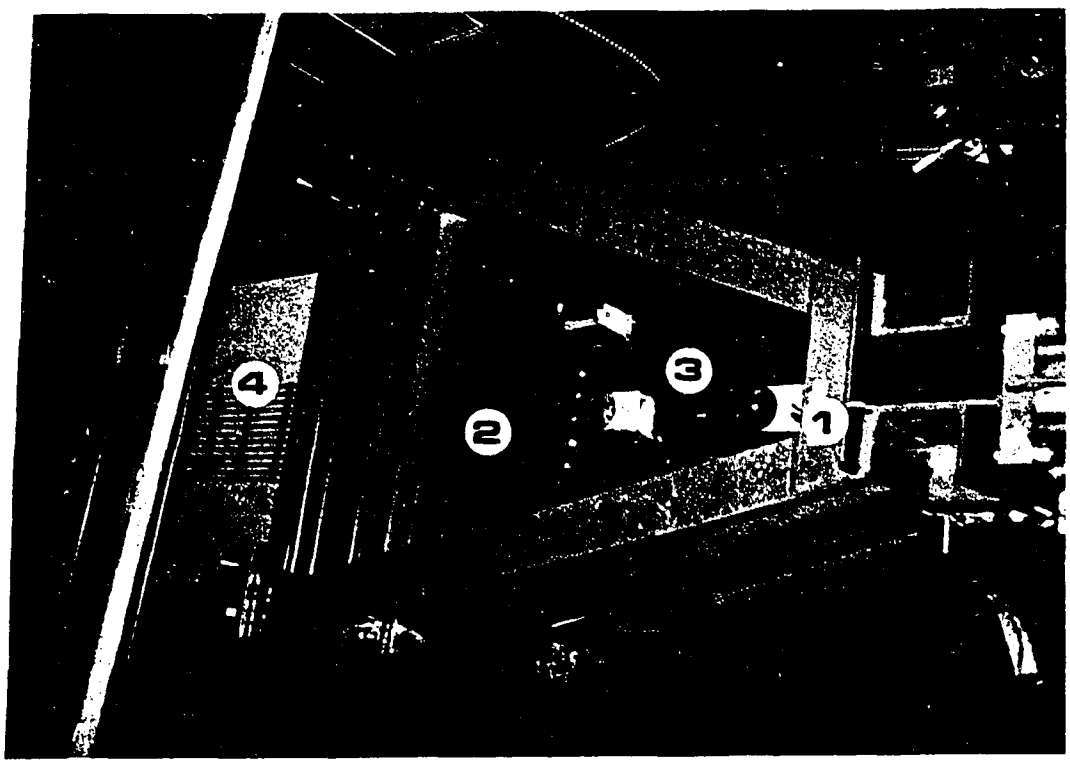

1) Loading Frame
2) Clamping Plates
3) Load Cell
4) Geogrid Reinforcement.

Figure 3.2 Front View of the Pull-out Box and Loading Frame.

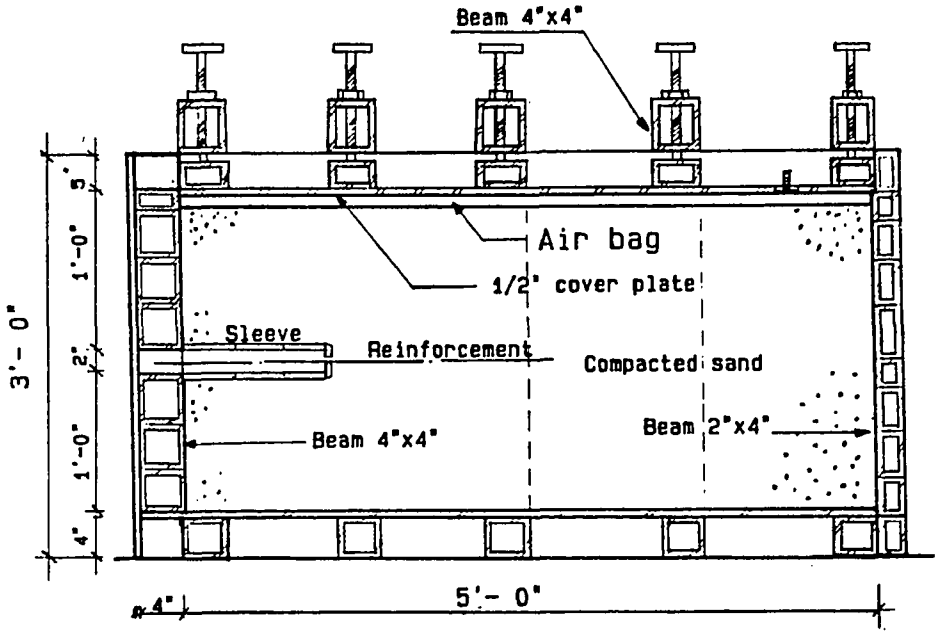

Figure 3.3 Longitudinal Cross-Section of the Pull-out Box.

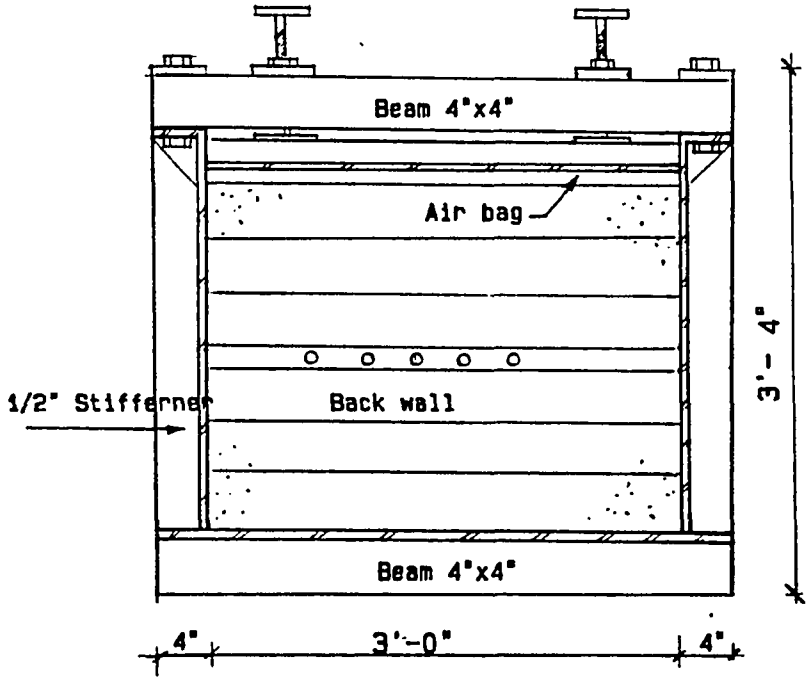

Figure 3.4 Cross-Section of the Pull-out Box.

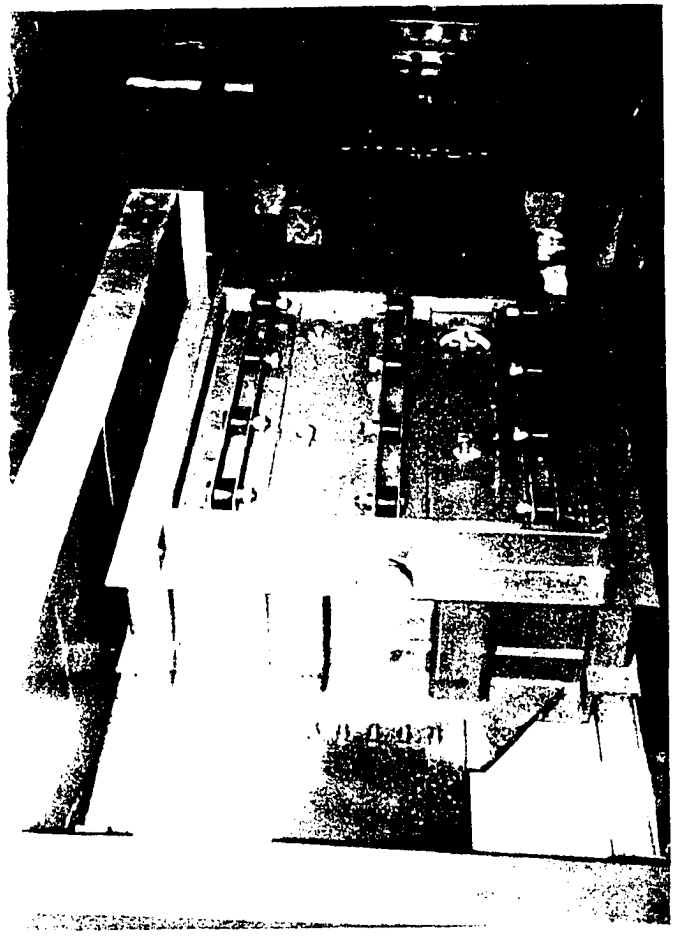

Figure 3.5 View of the Large Direct Shear Box.

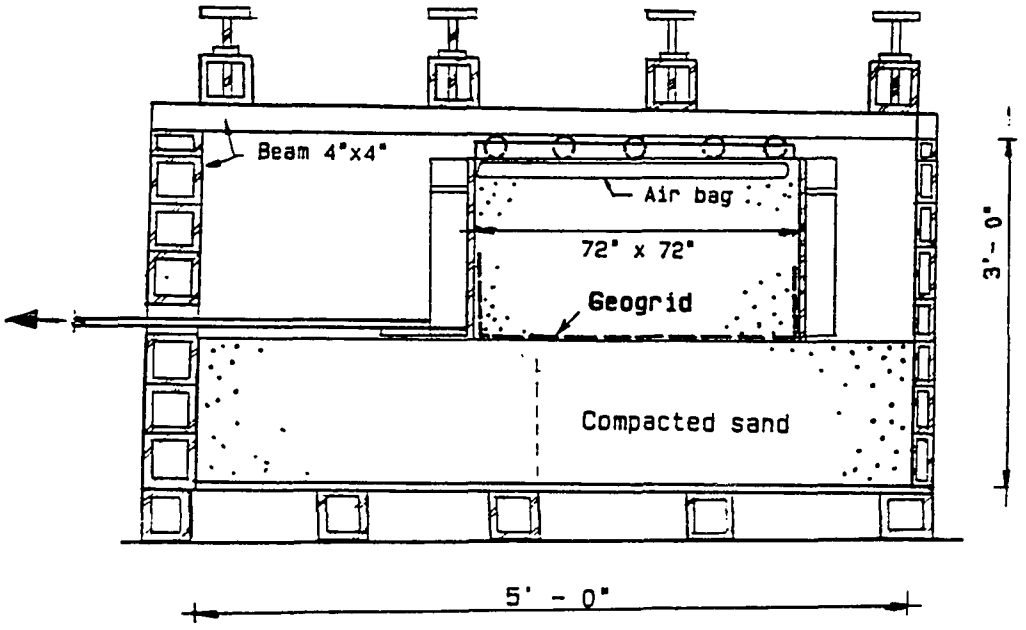

Figure 3.6 Cross-Section of the Direct Shear Box.

ii) The hydraulic Loading System:

The pull-out load is applied by a hydraulic system. The system includes three basic units:

i) hydraulic ram model Miller H67B (Figure 3.7). The ram is mounted on the loading frame and applies the pull-out load on the clamping plates. The hydraulic piston of the ram is 5 in. diameter and is able to apply 18 inch maximum pull-out displacement. A servo valve is mounted on the ram which controls the piston pull-out displacement rate.

ii) hydraulic power supply unit which consists of a hydraulic pump model Miller of 5 HP and 20 gallon fluid reservoir capacity and a cooling system. The details of the power unit are shown in Figure (3.8). The pump is able to operate under two loading schemes, namely: (a) Pressure-control scheme; where the pump fluid is controlled by a low pressure proportional control valve. The pressure is measured directly in the hydraulic ram by a test gauge; and (b) Velocity-control scheme; Where the pump operates under a constant pull-out velocity with variable pressures up to 3000 psi. The constant fluid rate is controlled mainly by the servo valve mounted on the hydraulic ram. The pump is controlled to operate under either of theses schemes from the control box unit.

iii) control box unit (Figure 3.8); where the commands to the hydraulic pump can be sent manually by the control keys in the board or through the computer when the control board is connected to the data acquisition system.

iii) Sand Handling Facility:

In order to minimize operator's effort and control the sand placement procedure, a sand handling facility has been specially designed and constructed. This facility is shown in Figure (3.9) and it consists of:

1) A heavy duty movable sand vacuum model 'Invincible': The sand is vacuumed out from the box through a flexible hose and the dust is filtered out to a dust container of 3 ft^3 capacity. The vacuum machine stores the sand in the elevated hopper.

2) Elevated sand hopper of capacity 54 ft^3 of sand: The hopper is used to store the sand when vacuumed from the box. The hopper supporting system is designed to permit its movement above the two boxes. To place the soil back into the box, the hopper is moved above the box and the sand is loaded back by gravity through the flexible hopper outlet. The outlet is elevated to 55 in. above ground in order to permit positioning the outlet above the box.

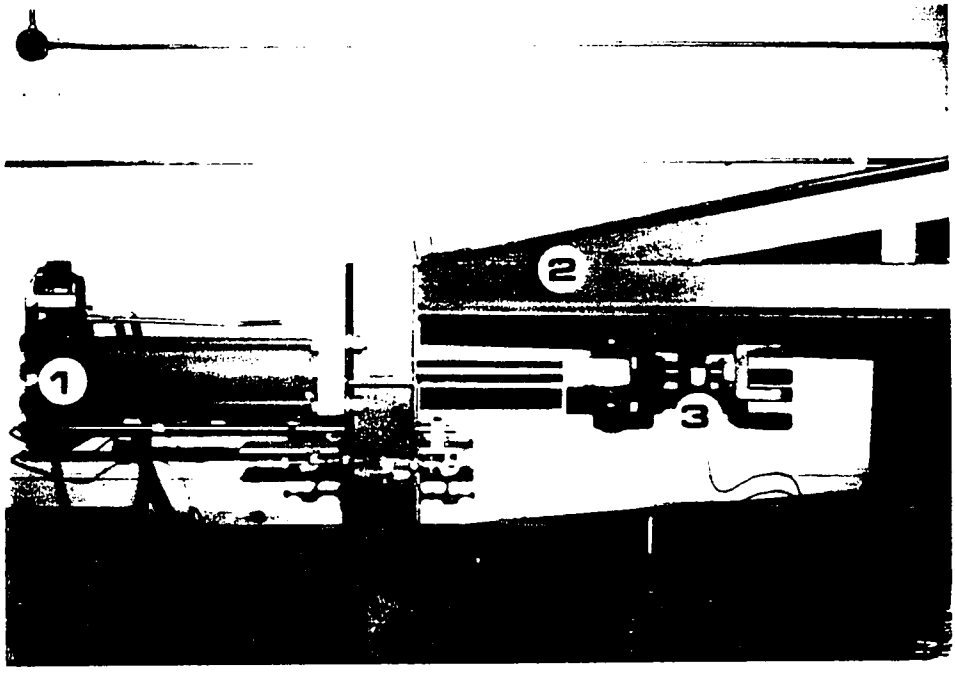

1) Hydraulic Ram
2) Loading Frame
3) Load Cell.

Figure 3.7 View of the Loading Frame.

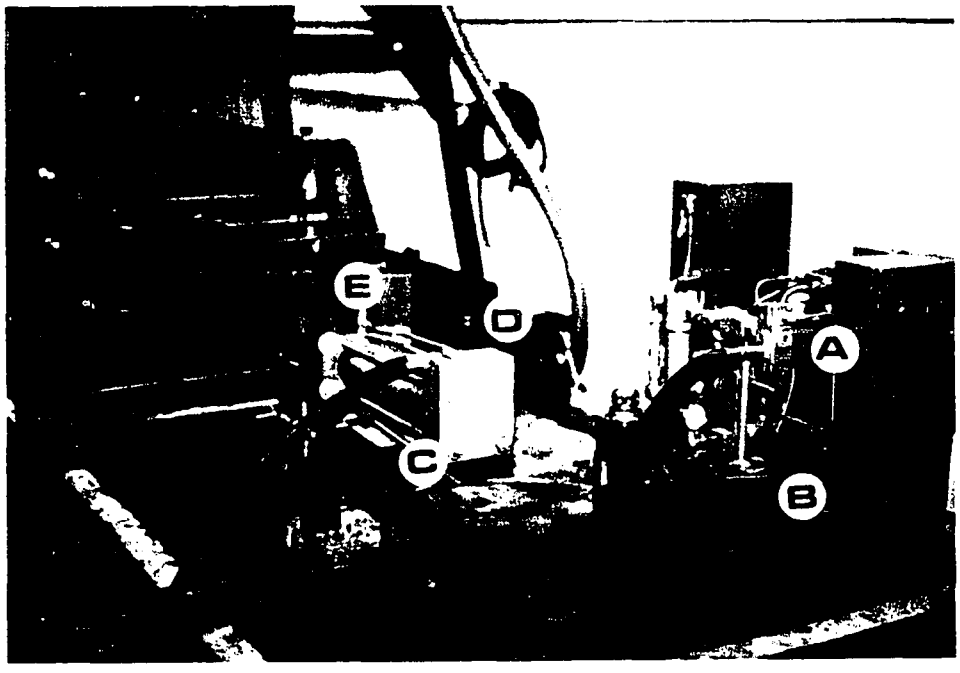

A) Control Box
B) Fluid Reservoir
C) Hydraulic Ram
D) Servo Valve
E) Low Pressure Gauge.

Figure 3.8 Details of the Hydraulic loading System.

A) Elevated Hopper
B) Vacuum System
C) Hopper Outlet.

Figure 3.9 View of the Sand Handling Facility.

3.3) INSTRUMENTATION AND DATA ACQUISITION:

The instruments used to measure the interaction response and the input testing parameters, for both of the pull-out and direct shear boxes, consist mainly of:

1- load cell used to measure the pulling force applied from the hydraulic loading system,

2- linear variable differential transformers (LVDT's) to measure the displacement at the pull-out application point,

3- velocity transducers for measuring the front displacement rate of the reinforcement,

4- pressure cells used to measure the internal earth pressure inside the box,

5- manometer gauge to measure the normal pressure applied from the air bag.

Moreover, in the pull-out box, LVDT's are placed at the back of the box to measure the displacements at different points along the reinforcement. The specifications of these instruments and the results of their calibration tests are presented in Appendix A. The measured response is monitored by a data acquisition system. The data acquisition system is used to:

i) translate the output response from the measuring instruments into digital values in the computer,

ii) display and store the output data into the computer system,

iii) translate the operator's digital commands from the keyboard to analogous values in the control box.

(i) Load and Pressure Measurements:

The pull-out force is measured by a load cell attached to the hydraulic piston and the clamping plates as shown in Figure (3.7). The load cell of 20 Kips capacity operates when an excitation voltage is sent to the load cell from the load cell conditioner. The conditioner, shown in Figure (3.10), also reads and stabilizes the output signal and converts it to the data board in the computer. The load cell response is a voltage output in millie-volts (mV) and it corresponds to the magnitude of the applied load in pounds. Calibration tests were performed on the load cell by applying different predetermined loads on the load cell and monitoring its response. The results of these tests, which show the relationship between the applied load in Lbs and the output response in mV are shown in Appendix A.

When load-controlled pull-out tests are performed, the load can be either manually controlled by the pressure valves in the hydraulic pump or computer controlled through D/A channel of the data control board.

The earth pressure on the facing wall is measured using two earth pressure cells model 'GeoKon 3650' with maximum pressure of 100 psi. The pressure cells are 2 in. diameter and consist of two circular stainless steel plates welded together and spread apart by a narrow cavity.

External pressure acting on the cell is balanced by an equal pressure induced in the internal fluid by an excitation voltage. The excitation voltage of 10 volts DC is supplied from a stabilized power supply (Figure 3.10). The pressure is converted by the pressure transducer into an electrical signal which is transmitted to the data control board in the computer. Calibration tables to convert this output response (in mV) to the magnitude of the applied pressure (in psi) are provided by the manufacturer. These values were checked by testing the cells in a triaxial pressure chamber. Predetermined incremental air pressure was applied and the voltage output was monitored. The calibration values of the earth pressure cells are shown in Appendix A. The earth pressure cells are fixed on the facing wall in the locations shown in Figure (3.11).

(ii) Displacement Measurements:

The geogrid front displacement in the pull-out box and the upper box displacement in the direct shear box are monitored by means of Linear Variable Differential Transformers (LVDT's). These LVDT's are mounted on the loading frame and are shown in Figure (3.7). The LVDT's used are of 18 in. length and stroke length of ±10 in. An excitation DC voltage of 15 volts is sent by means of stabilized power supply. Displacement is monitored as the core rod moves inside the LVDT causing an output voltage response equivalent to the displacement. The relationship between the core rod displacement and the output voltage is provided by the manufacturer.

These calibration tables are presented in Appendix A and they are utilized in the A/D channels of the data control board to convert the voltage values to digital output.

For the geogrid extensible reinforcement, non-uniform shear stresses and displacements are developed along the reinforcement with the large shear being mobilized at the front portion of the inclusion (Christopher, 1976; and Juran and Chen, 1988). Therefore, It is necessary to monitor the displacements at different locations along the reinforcement in order to determine the reinforcement length which is effectively mobilized under a specific level of pull-out load. In order to measure the displacements at different locations in the confined inclusion, five LVDT's are mounted at the level of the inclusion on a rear table in the pull-out box. The displacement rods of the LVDT's are connected to the geogrid by 'tell-tale' inextensible wires through slots in the box rear wall. The wires are connected to the transversal ribs of the geogrid and kept stretched by means of counter weights through the rear table. A detail of the setup at the rear table is shown in Figure (3.12) and a view of the displacement instrumentation of the geogrid at the rear table is shown in Figure (3.13).

(iii) Displacement-rate Measurements:

A velocity transducer is mounted on the loading frame of both boxes to measure the front displacement-rate. The velocity transducer measures the rate

of the core rod displacement when it is moved inside the transducer shaft. An excitation voltage of 5 volts is sent by the DC power supply. The output voltage is calibrated by applying several predetermined velocities and the equivalent output voltages are monitored. The displacement-rate is measured for the following purposes:

(i) to compare the displacement-rate at the front during pull-out with the command value sent by the computer when the test is conducted under a displacement-rate controlled mode.

(ii) to measure the variation of front displacement-rate when the test is conducted under constant loading scheme.

When displacement-rate controlled tests are performed, a command is sent to operate the hydraulic ram under a constant velocity. The command is sent to the hydraulic pump through the D/A channel of the data control board in the computer. The velocity control is calibrated by operating the pump with different command values (in volts) and measuring the output voltage response of the transducer. The velocity transducer output is then equivalent to the displacement-rate calculated from the time-displacement measurement. In displacement-rate controlled tests, the pressure of the hydraulic pump is kept constant at a high value (1000 psi) in order not to affect the velocity control procedure.

(iv) Data Acquisition:

The output response parameters (i.e. displacement, velocity, load and pressure) measured, respectively, by the LVDT's, velocity transducers, load cells and pressure cells; are transmitted to display and storage in the computer through a data acquisition system. A schematic diagram of the instrumentation and the data acquisition system is shown in Figure (3.14) and a view of the data acquisition control system is shown in Figure (3.15).

A data translation board (model DT-2801 AD/DA) is plugged into one of the computer system extension slots. The data translation board includes 8 differential (16 single-ended) A/D channels and two D/A channels. The dual function of the board is to:

(i) translate the digital commands, sent by the operator, to analogous ones through the D/A channels,

(ii) translate the analogous output data of the tests to digital data to display and storage through the A/D channels.

The data input and output are simultaneously monitored and stored in the computer. The data translation board is connected to the measuring instruments through a screw terminal board model DT707. The screw terminal board is shown in Figure (3.10). The connection scheme of the screw terminal board is:

(i) each of the measuring instruments is connected to one of the A/D channels of the screw terminal,

(ii) the screw terminal A/D channels are connected to the control box in the hydraulic system. These channels translate the commands to the hydraulic loading system for either hydraulic ram velocity control or pressure control.

A schematic diagram of the screw board showing the assigned channels to each instrument is shown in Figure (3.16). The data acquisition board is programmed and controlled from the computer keyboard through the software "Labtech Notebook'. The software supports the data control management and organizes data display and storage.

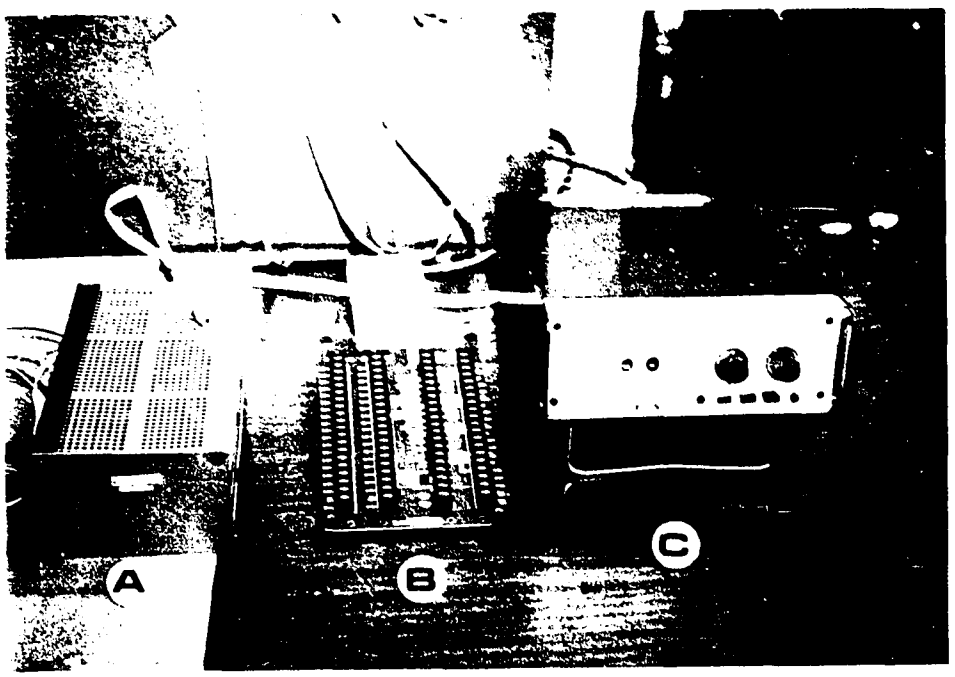

A) Stabilized Power Supply
B) Screw Terminal Board
C) Load Cell Conditioner.

Figure 3.10 Data Acquisition Supporting Instruments.

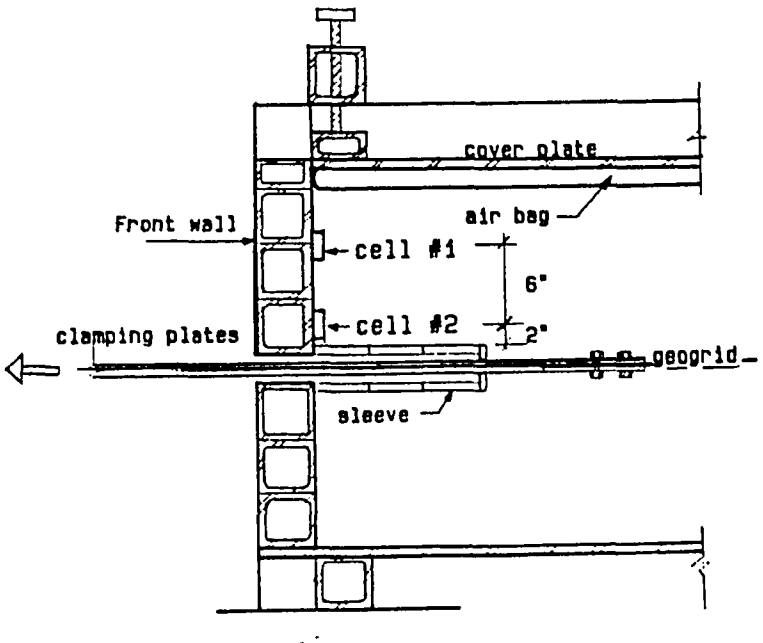

Figure 3.11 Locations of the Earth Pressure Cells.

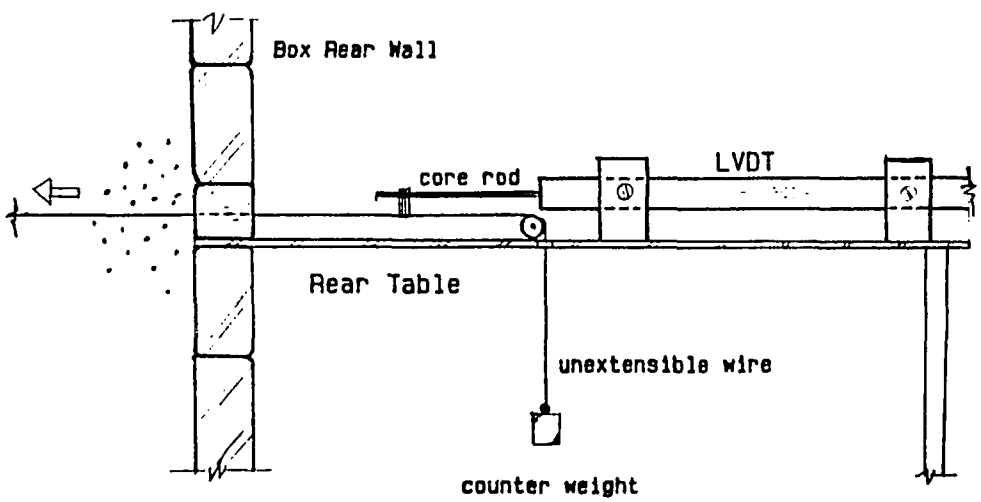

Figure 3.12 Detail of the 'Tell-tale' and the Rear Table.

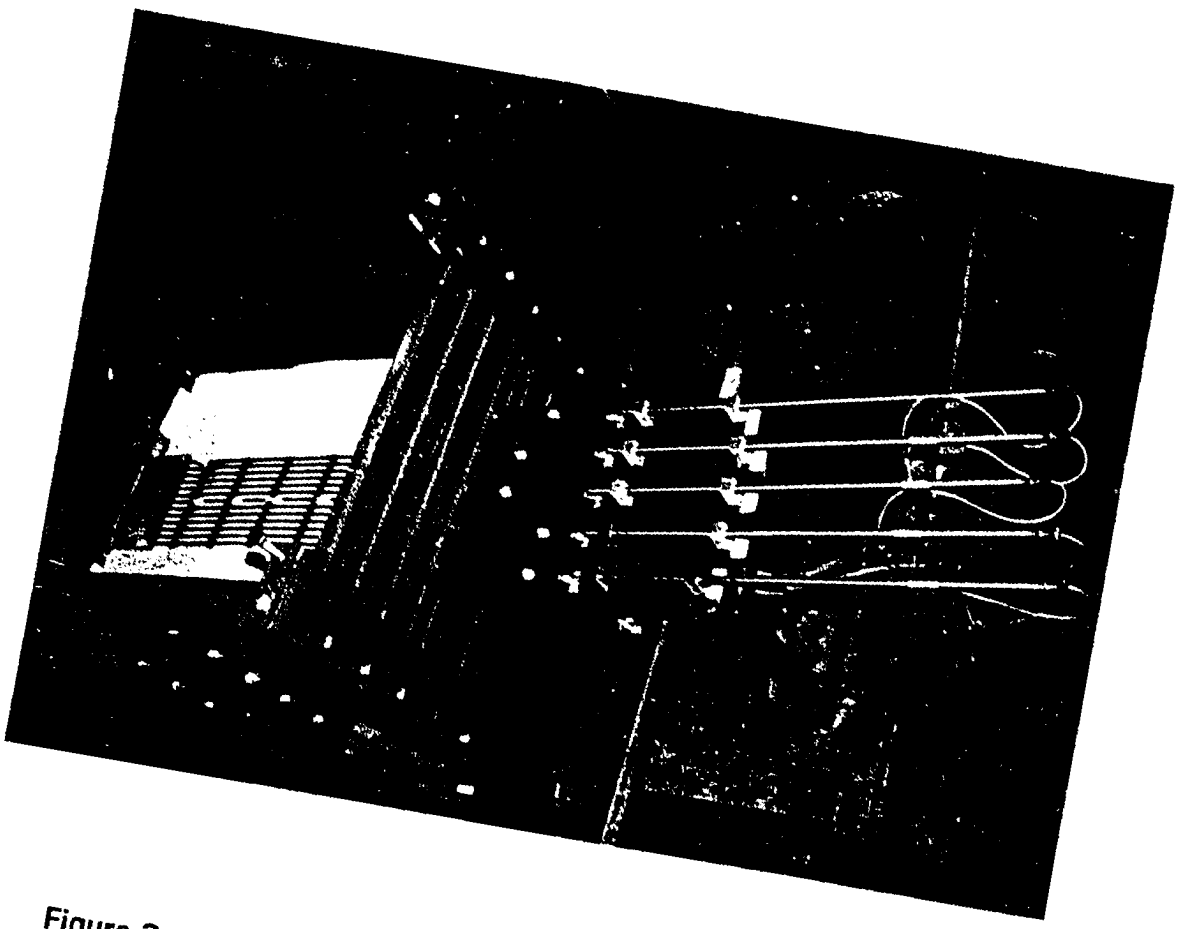

Figure 3.13 Displacement Instrumentation of the Geogrid.

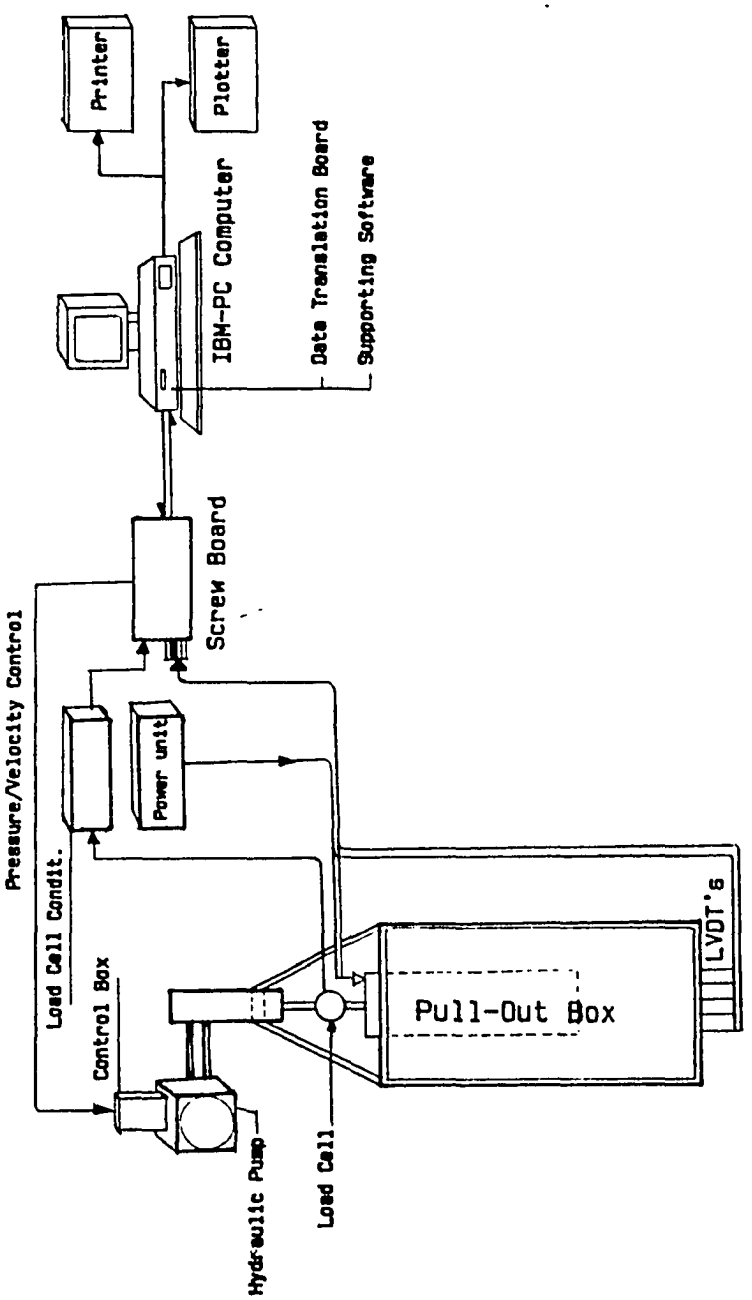

Figure 3.14 Schematic View of the Data Acquisition System.

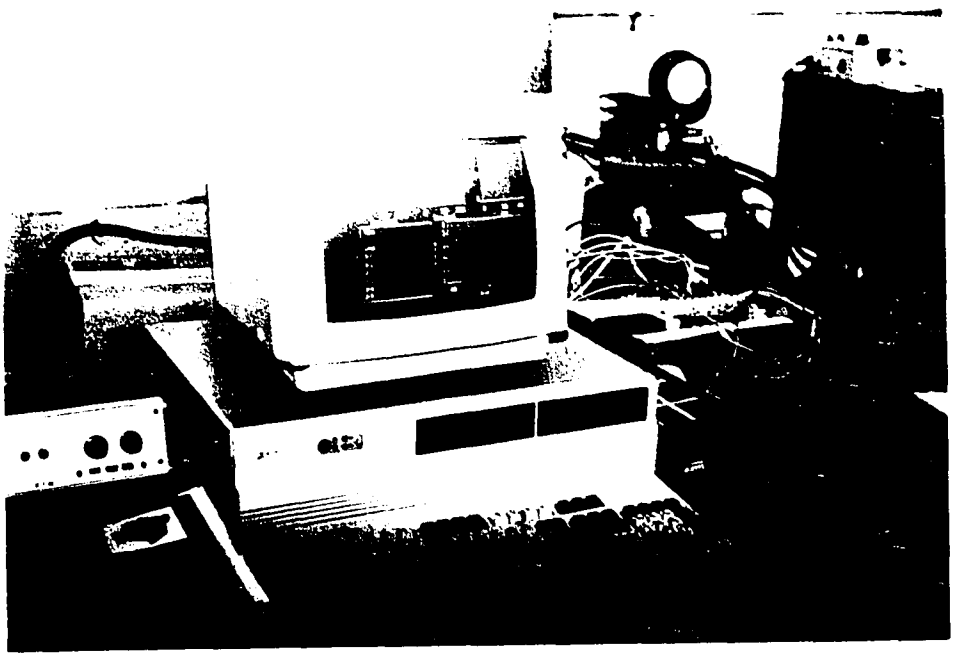

Figure 3.15 View of the data Control System.

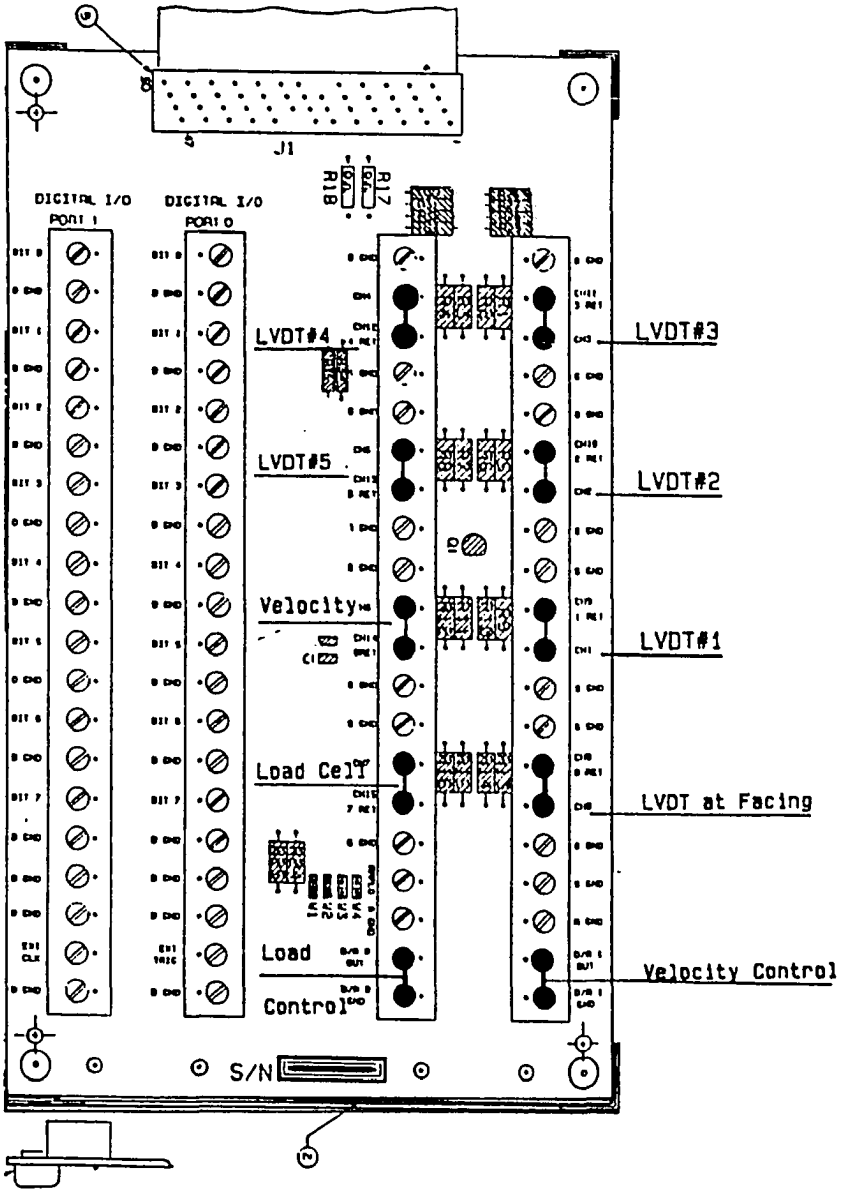

Figure 3.16 Connection Scheme of the Screw Terminal Board.

CHAPTER 4

TESTING PROCEDURE AND DATA INTERPRETATION

4.1) INTRODUCTION:

Several pull-out and direct shear tests were conducted in order to evaluate the performance of the testing facility, the effect of testing parameters and to provide the data base for the development of an analytical data interpretation procedure. These tests are:

(1) Unconfined extension tests: These tests were conducted on the geogrid specimens under constant extension-rates. Results were compared with the index test results provided by the manufacturers. These tests are aimed to evaluate the equipment performance, the accuracy of the control and monitoring system, and the material behavior in the unconfined state.

(2) Pull-out tests: Constant displacement-rate pull-out tests were conducted under the same testing conditions (e.g. confining pressure, soil density, boundary conditions, and pull-out rate) to evaluate the equipment reproducibility and the pull-out performance of the geogrid. Tests were also conducted under variable testing conditions to evaluate the effect of testing parameters on the pull-out resistance.

(3) Direct shear tests: These tests were conducted to evaluate the shear stress-strain characteristics at the soil-geogrid interface. Results of these tests were also used to evaluate the interface parameters calculated from the pull-out

tests using the proposed data analysis procedure.

(4) Load-controlled pull-out tests: Stepped load-controlled pull-out tests were performed to determine the unconfined and confined time-dependant parameters of the geogrid. In these tests, loads were applied incrementally and maintained constant during specific times. A data analysis procedure was adopted to predict the critical creep load and strain. Long term (500 hour) creep tests were performed to evaluate the confined creep strain of the geogrid under the critical creep load.

The testing methodology and interpretation of test results are discussed in this chapter. The procedures used in specimen preparation, soil compaction, and calibration of soil density are presented.

4.2) SOIL COMPACTION AND SPECIMEN PREPARATION:

Soil compaction and relative density significantly affect pull-out test results (Knochenmus, 1987; and Juran et al., 1988). In dense sand, as soil particles are displaced in the vicinity of the reinforcement, the soil tends to dilate. This dilation is restrained by the surrounding soil. This results in a normal stress concentration at the soil-reinforcement interface which increases the pull-out resistance of the soil.

For a given relative density, soil placement and compaction can have a significant effect on the results obtained from the pull-out box. Uneven soil

placement and compaction would result in a sample with higher tendency for arching or non-uniform soil dilation. Previous studies (Rowe et al., 1985; and Johnston, 1985) showed that non-uniform sample dilation leads to uneven normal pressures along the inclusion. Inadequate soil placement and poor compaction of soil layers would result in differential settlement of the inclusion, which may lead to an incorrect measurement of the interface pull-out resistance. The compaction process should be adequately adopted for each type of soil in order to simulate, as closely as possible, the compaction process used in the field. The compaction techniques and the calibration procedure used to determine the amount of compaction effort needed to produce the required relative soil density are discussed herein.

i) Soil Placement:

The sand used in this study is a uniform blasting sand. Its grain size distribution is shown in Figure (4.1). The shear stress characteristics under different confining pressures, determined from the conventional direct shear test, are shown in Figure (4.2). The maximum and minimum soil density tests were conducted according to ASTM D4253-83 and D4254-83, respectively. The values of 99 pcf (1.58 t/m^3) and 110.9 pcf (1.77 t/m^3) were obtained, respectively, for minimum and maximum soil density.

The sand is placed into the pull-out box by pouring it from the elevated hopper through a flexible outlet. The elevated hopper is moved during pouring

to permit uniform filling of sand along the box. The sand is placed in four layers of 6 inch each, leveled and compacted to the desired relative density. Figure (4.3) shows the sand placement scheme in the box. Compaction was applied manually using a vibrating electric hammer. A predetermined number of blows was applied on each layer in a regular pattern.

After compaction, the density was measured with a nuclear density gauge model 'TROXLER 3440'. Figure (4.4) shows the soil density measurement in the pull-out box. The gauge rod was embedded 8 in. to 12 in. into the soil and the density is measured at 9 different locations to insure uniform density distribution at each layer.

ii) Compaction Control:

In order to simulate the compaction process commonly used in the field, a compaction process which consists of coupling vibration and hammering effect has been adopted. A vibrating electric hammer was modified to hold a compacting plate of 5 inch diameter allowing manual compaction of the soil layers.

Calibration tests were performed in order to establish the compaction effort and sequence required to achieve the required relative density. For the purpose of performance evaluation study, calibration tests were performed with two different sand placement procedures, namely:

(a) Variable falling height: In this procedure, the level of the outlet pipe in

the hopper was fixed. This leads to different sand falling height from the hopper outlet to each of the sand layers in the box.

(b) Constant falling height: In this procedure, the hopper outlet is connected to a long flexible hose to keep sand falling height constant from the outlet to each layer.

Under each of these two soil placement methods, different compaction efforts were applied to the sand layers; namely,

1- No compaction: the hopper outlet was moved above the box to permit uniform fill and the soil layers were leveled with minimum disturbance to achieve minimum soil density.

2- 40 blows per layer: Soil was compacted by applying 40 blows uniformly at each layer.

3- 110 blows per layer.

4- 200 blows per layer.

At each layer, density was measured after compaction and before placing the following layer. Density was measured again when upper sand layers were removed in order to assess the effect of the weight of the upper layers on the density of the compacted sand. The details of compaction schemes and results of density measurement are shown in Appendix B. The relationship between the applied number of blows and the resulting soil density, for the two cases of variable and constant sand falling heights, are shown in Figures (4.5-a and b), respectively. These curves can be used to estimate the number of blows per

layer necessary to obtain a desired soil density. The figures show that, under the same compaction effort, the first method of sand placement (i.e. variable falling height) induces a looser state of sand at the lower layers. The constant falling height procedure (which maintains the falling distance constant above each layer) allows better control of compaction and results in soil densities independent of falling height. The effort induced in leveling each layer should also be the same in order to reduce the effect of sand placement on the density.

The results in Figure (4.5) indicate that after compacting a specific layer, the successive placement and compaction of the following layers results in an additional increase in sand density which should be taken into consideration when the number of blows is to be determined. A systematic and consistent sand placement, leveling and compaction techniques should be used in order to achieve a reproducible initial state of soil density.

iii) Reinforcement Preparation:

Two different types of geogrids, commonly used in soil reinforcement, were tested. These geogrids are: (a) geogrid 'TENSAR SR2', and (b) Geogrid 'CONWED'. For both types of geogrids, standard specimens of 1 ft width x 3 ft length were tested in the pull-out box. In the large shear box, the specimens had the same size as the upper box (i.e. 27 in. width x 27 in. length).

In the pull-out box, the standard specimen width allows keeping its edge at 1 ft from the side walls of the box to reduce boundary effects. The specimens were bolted to the clamping plates and placed over 1 ft of sand. A sleeve of 1 ft length was used around the clamping plates at the front wall. The sleeve transfers the pull-out application point far behind the front wall in order to reduce the effect of front rigid boundary on test results. Figure (4.6) shows the placement of the geogrid in the pull-out box.

The displacement distribution along the confined geogrid is measured by five LVDT's placed at the 'tell-tail' table. Figures (4.7-a) and (4.7-b) show the locations of the displacement measurements along the geogrids 'Tensar' and 'Conwed', respectively. The LVDT's are connected to the transversal ribs of the geogrid through non-extensible wires. The wires extend through 1/2 inch plastic tubes embedded in the sand to prevent the frictional resistance of the sand to the movement of the wires. A sand layer of 1 ft thick is placed above the reinforcement and the confining pressure is applied from the air bag.

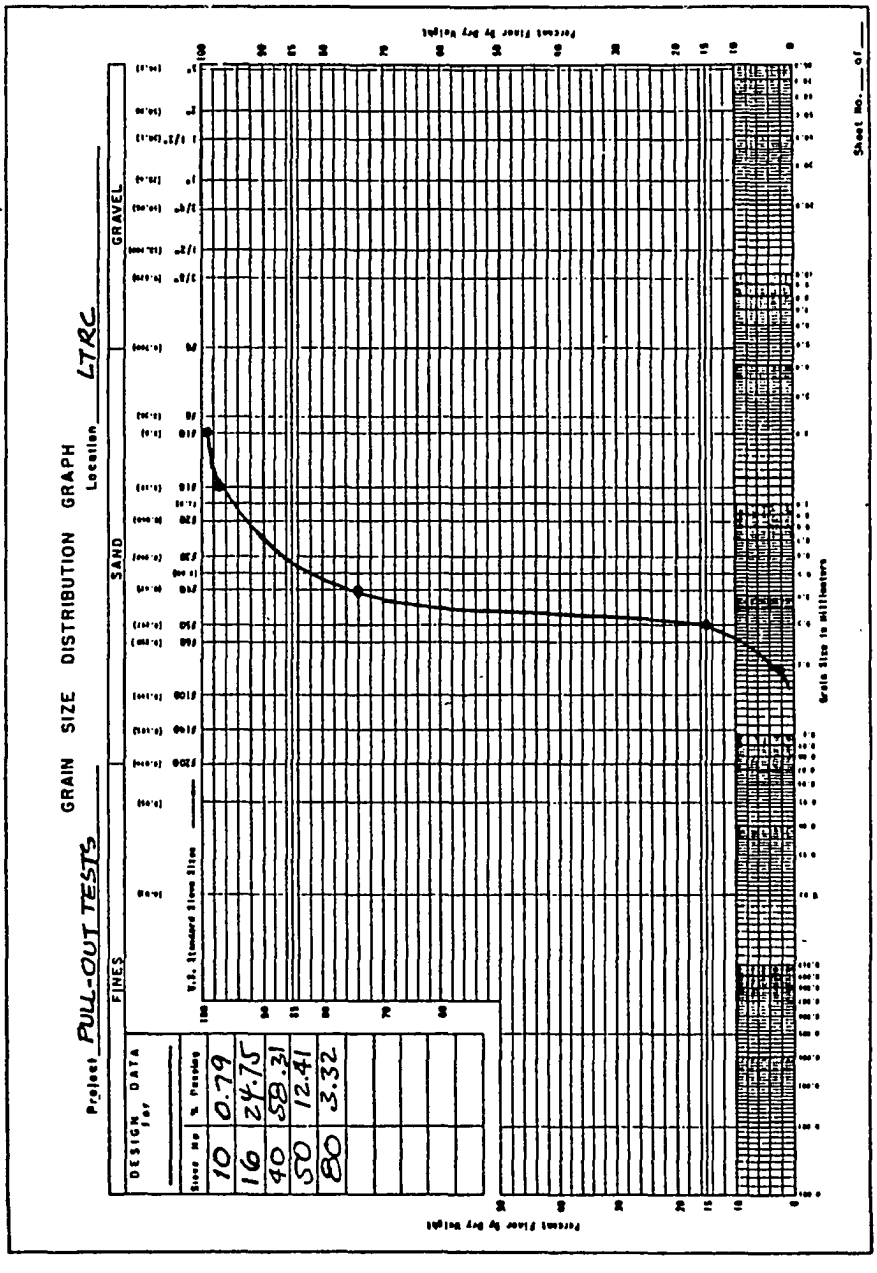

Figure 4.1 Grain Size Distribution of the Blasting Sand.

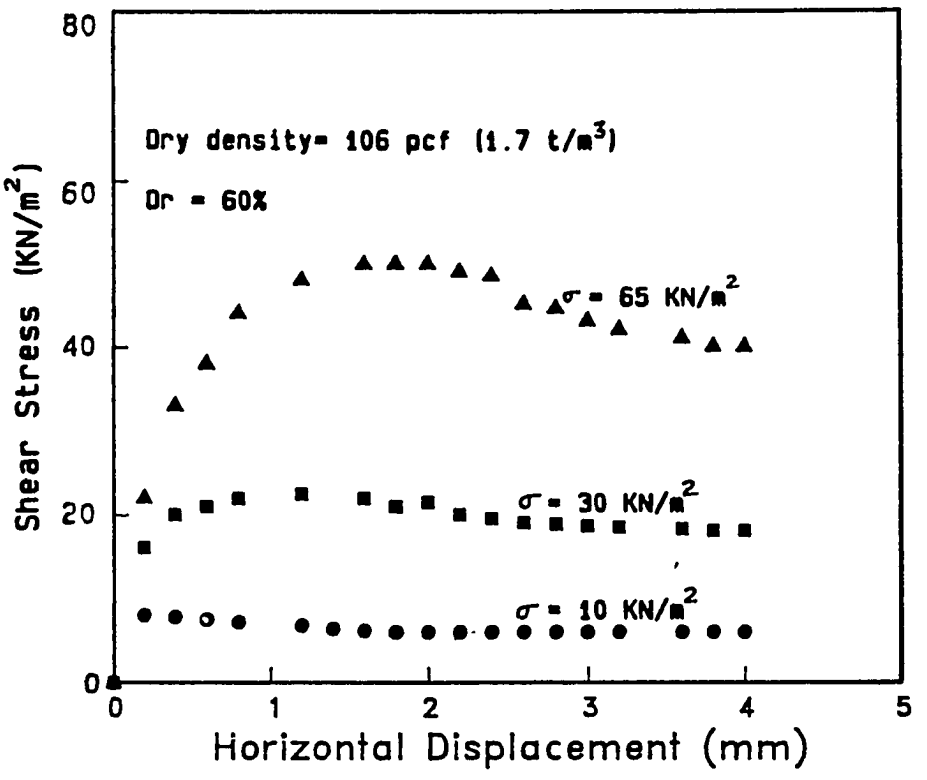

Figure 4.2 Direct Shear Test Results on the Sand.

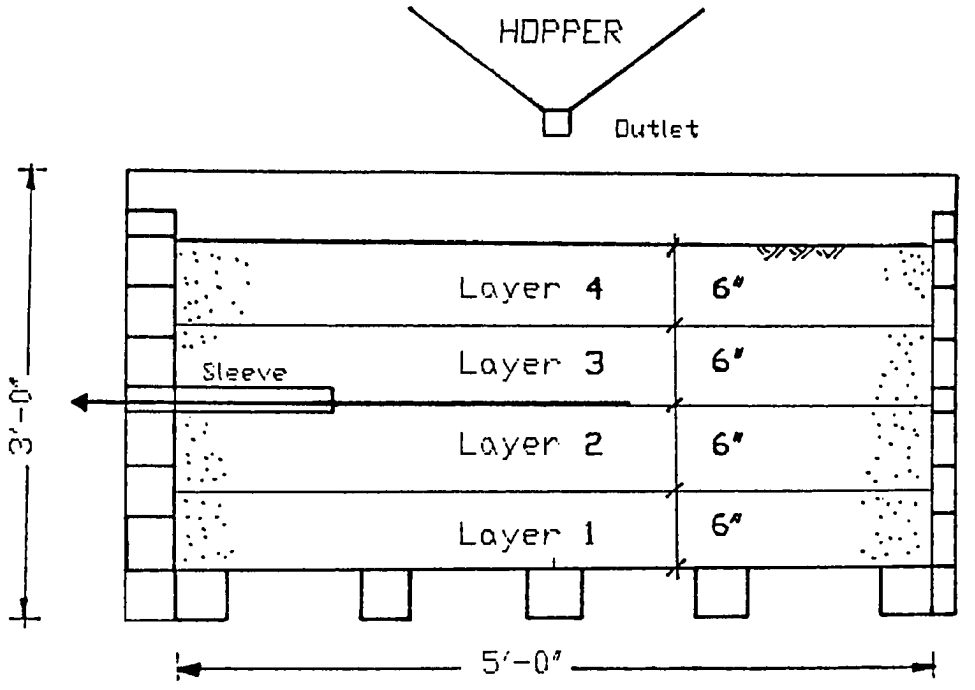

Figure 4.3 Sand Placement in the Pull-out Box.

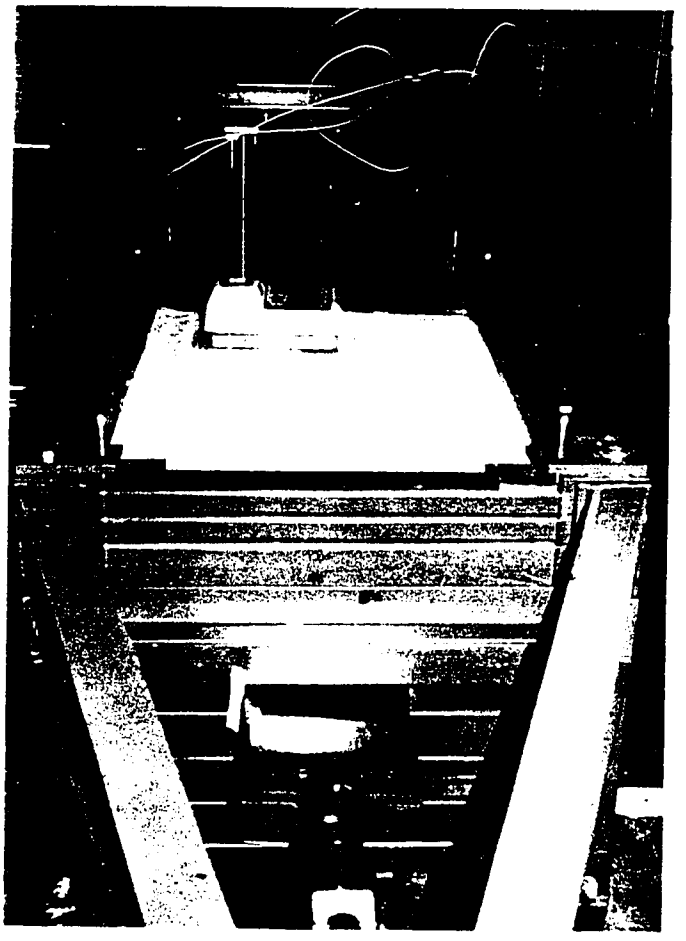

Figure 4.4 Soil Density Measurements in the Pull-out Box.

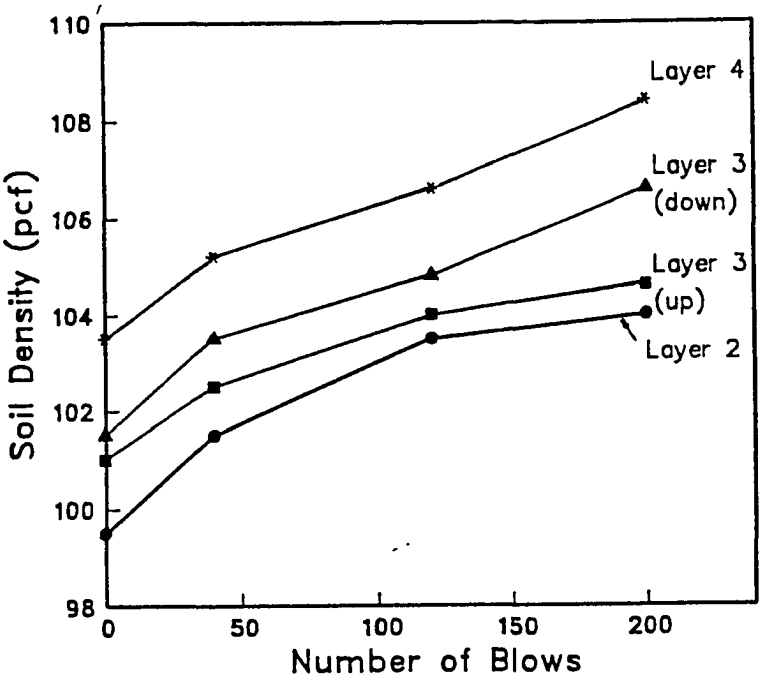

(a) Variable Falling Height Procedure,

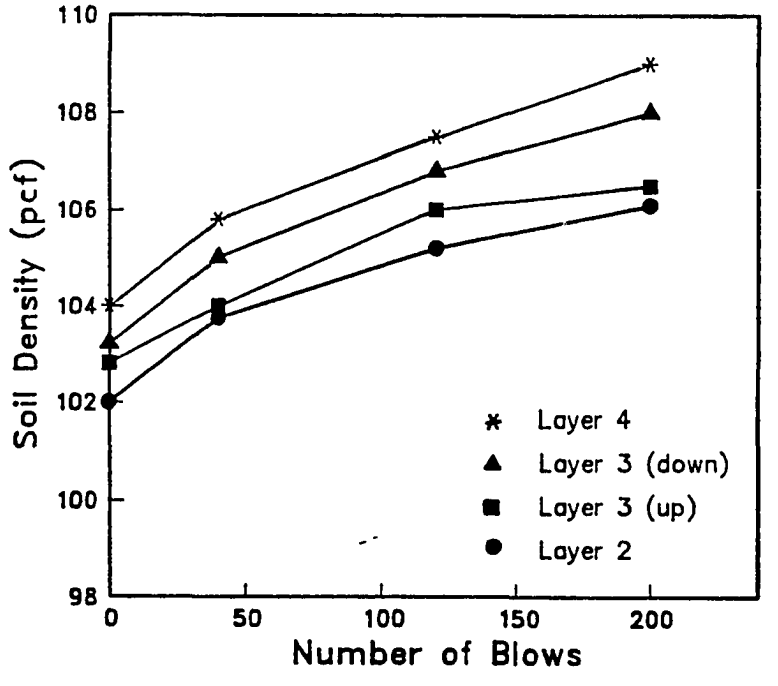

(b) Constant Falling Height Procedure,

Figure 4.5 Calibration of Sand Density with Compaction.

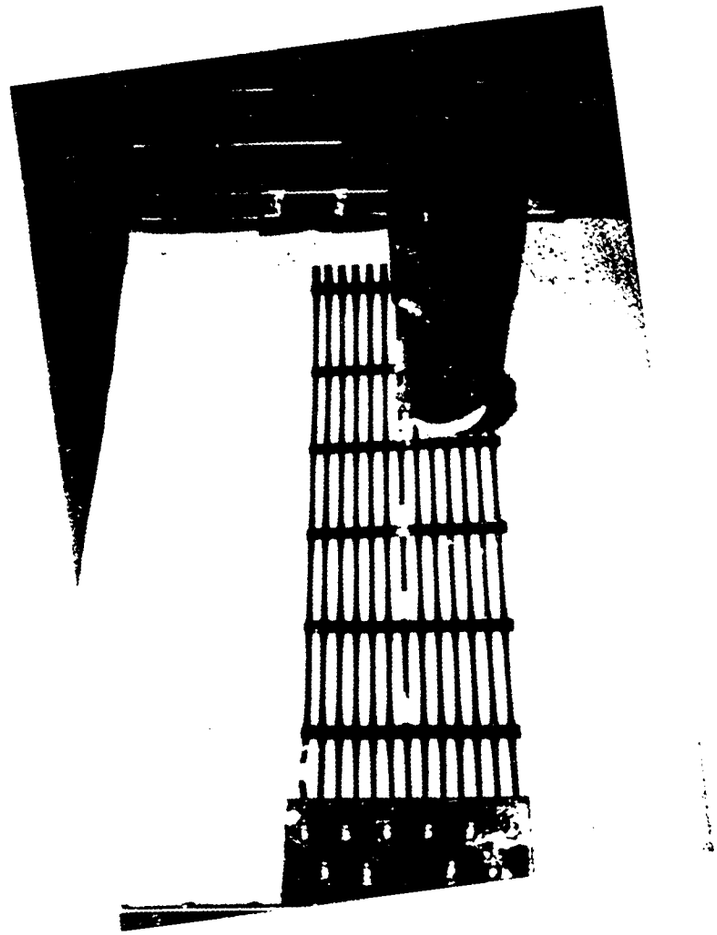

Figure 4.6 Placement of the Geogrid in the Pull-out Box.

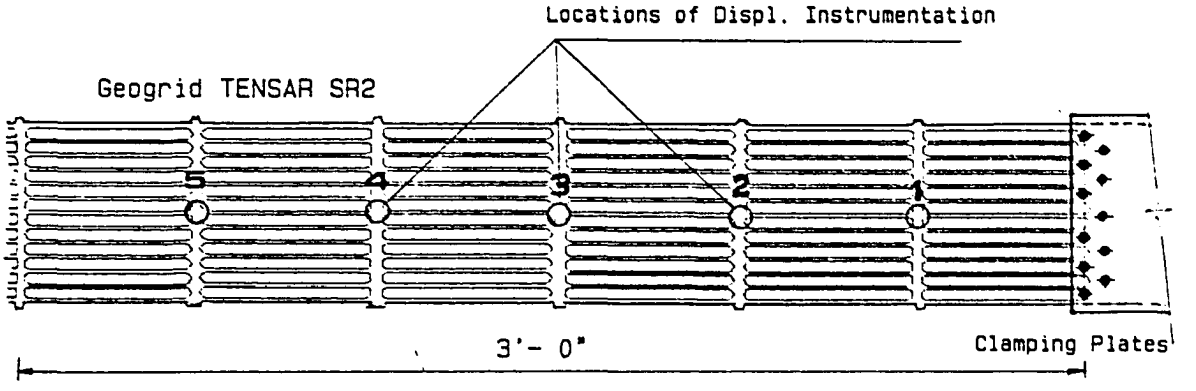

(a) Geogrid 'TENSAR SR2'.

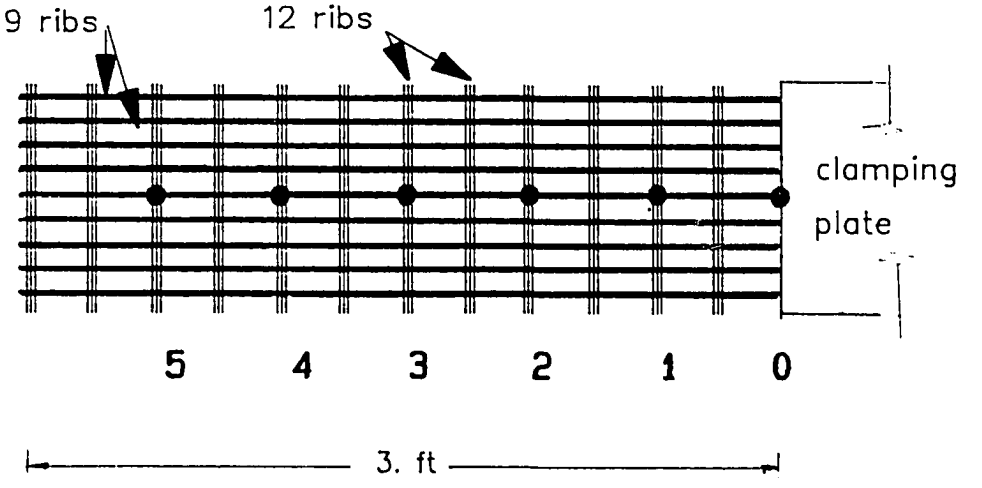

(b) Geogrid "CONWED'.

Figure 4.6 Instrumentation of Geogrid Specimens in Pull-out Box.

4.3) DISPLACEMENT-RATE CONTROLLED TESTS:

i) Unconfined Extension Tests:

Unconfined extension tests were performed on the geogrids in order to evaluate the material behavior in the unconfined state and the equipment performance and its reproducibility in the displacement-rate controlled mode. The unconfined stress-strain test results were compared with the index tests provided by the manufacturers.

Unconfined extension tests were performed on geogrids 'Tensar SR2' and 'Conwed'. In these tests, the front face of the specimens were bolted to the clamping plates while the rear ends were clamped to rear wall of the pull-out box. A computer command was sent to operate the hydraulic pump with a constant pull-out velocity of 2 mm/min. The front displacement, the velocity and the load were monitored during the test. Figures (4.8-a) and (4.8-b) show the unconfined stress-strain relationships of geogrids 'Tensar' and 'Conwed', respectively. The index test results of both geogrids, provided by the manufacturer, are plotted in their respective figures. The figures show that the measured unconfined response compares fairly well with the index results of the geogrids.

ii) Pull-out Tests:

Pull-out tests were conducted on both 'Tensar' and 'Conwed' geogrids in order to evaluate their pull-out resistance and interface parameters. In these

tests, standard testing conditions were maintained constant in order to evaluate the reproducibility of pull-out test results. A confining pressure of 7 psi (48.2 KN/m^2), an average soil density of 104 pcf (1.67 t/m^3), a soil thickness of 2 ft, a displacement-rate of 6 mm/min, and a sleeve length of 12 in. were kept constant in the pull-out standard tests. In these tests, geogrid specimens of 1 ft width and 3 ft length were tested. Figures (4.6-a and b) show the dimensions and the points of displacement measurements along the geogrids tested in the pull-out box.

Figure (4.9) shows the load-displacement relationships from a series of pull-out tests on 'Tensar' geogrid samples tested under the standard testing conditions. The figure shows that the results yield similar pull-out resistance, interface stiffness modulus, and front displacement at peak. Figure (4.10) shows the results of a series of tests conducted on 'Tensar' geogrid under a confining pressure of 7 psi, average soil density of 105.5 pcf (1.69 t/m^3), and a displacement rate of 10 mm/min. The figure shows that an increase in the soil density and displacement-rate results in an increase in the peak pull-out resistance of the geogrid. The effect of variation of testing parameters (e.g. soil density, confining pressure, displacement-rate, and boundary conditions) on the pull-out response of the geogrids will be discussed in detail in chapter 5.

Figure (4.11) shows the pull-out response from a series of tests on geogrid 'Conwed' of standard specimen sizes and under confining pressures of 7 psi, and average soil densities of 106 pcf (1.7 t/m^3).

The measured front displacements at different nodes along 'Tensar' geogrids are shown in Figure (4.12). The figure shows that the slopes of the displacement curves at the front correspond to the controlled input velocity. The displacements at different nodes along the geogrid are monitored by means of the LVDT's at the rear table. Figures (4.13) and (4.14) show, respectively, typical time-nodal displacement relationships for 'Tensar' and 'Conwed' geogrids. The results show the progressive load transfer mechanism along the geogrid. The interpretation of the results in these figures shows that:

(i) At the front node (i.e. at node 0), the slope of the front displacement verses time is constant and is equal to the controlled pull-out displacement rate.

(ii) At early stages of pull-out response, the difference in the slopes of nodal-displacement curves indicates progressive movement of the geogrid nodes during testing. This progressive load transfer leads to higher extension at the front part of the geogrid with practically no strain at the rear nodes.

(iii) The slopes of time-nodal displacement curves become practically equal at the later stages of testing, indicating that the geogrid extension is fully mobilized along its length. At this stage, the geogrid moves as a rigid body without any further extension at this stage. The specific point on the displacement curve where the slopes become practically equal indicates the occurrence of the slippage failure of the reinforcement which is attained at the peak pull-out resistance.

To illustrate the progressive load transfer mechanism along the geogrid

in pull-out tests, the nodal displacements are normalized with respect to the front displacement (i.e. node 0). The normalized displacements at different loading levels are plotted along the geogrid length in Figures (4.15) and (4.16) for geogrids 'Tensar' and 'Conwed', respectively. The figures show that at an early stage of testing (at loading level 40% of peak pull-out load), the front nodes of the geogrid (nodes 1 and 2) develop their displacement response while no displacements are practically monitored at the rear nodes (nodes 4 and 5). At this early stage of pull-out loading, the grid experiences an extension response at the front part without slippage and the strained length of the geogrid is its effective adherence length. At a later stage of pull-out testing, the geogrid reaches its peak strength, the rear node undergoes displacement, and the geogrid experiences a combined extension-displacement response. This combined response is mobilized along the reinforcement till, at a later stage of post peak response, the normalized displacement curve becomes practically linear. The linear displacement along the geogrid specimen demonstrates that the geogrid experiences a rigid body movement without further extension.

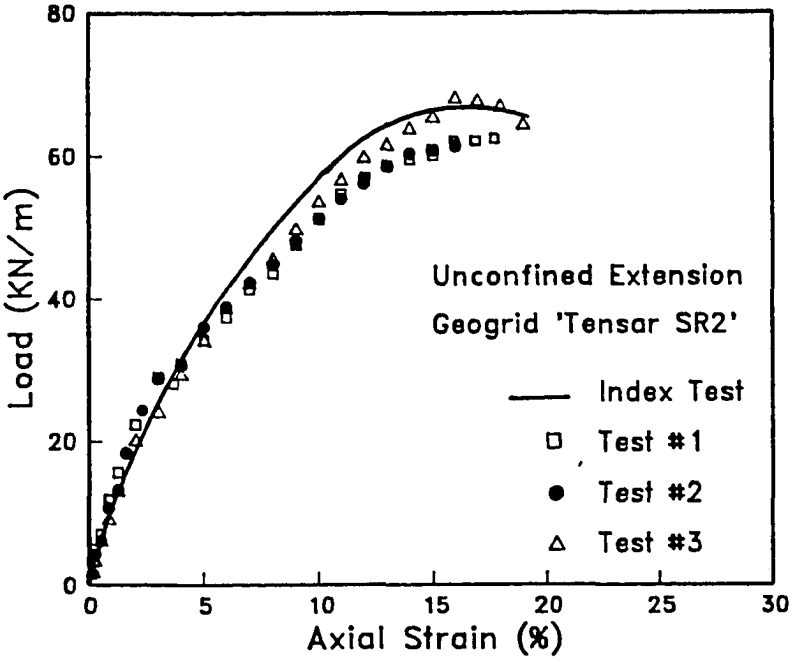

(a) Geogrid 'Tensar'

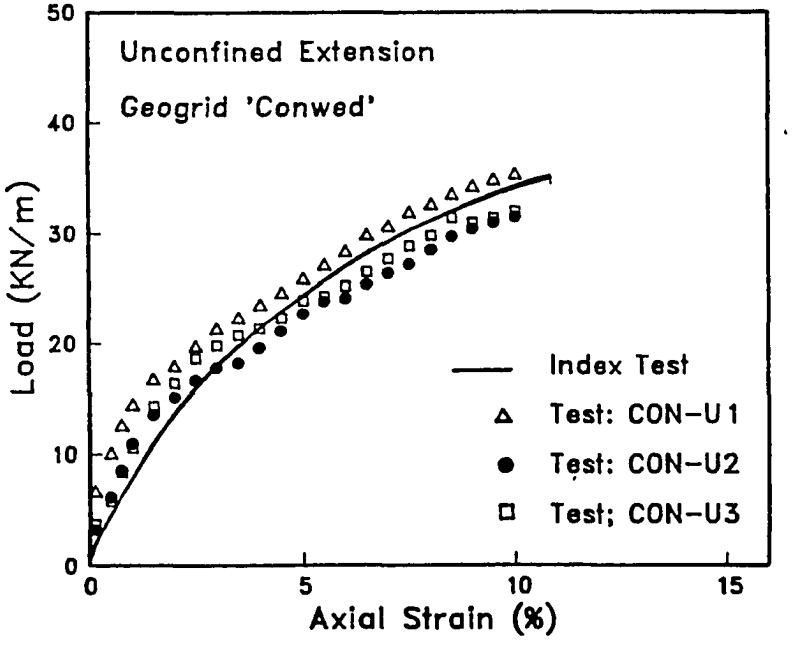

(b) Geogrid 'Conwed'.

Figure 4.8 Unconfined Extension Test Results on Geogrid.

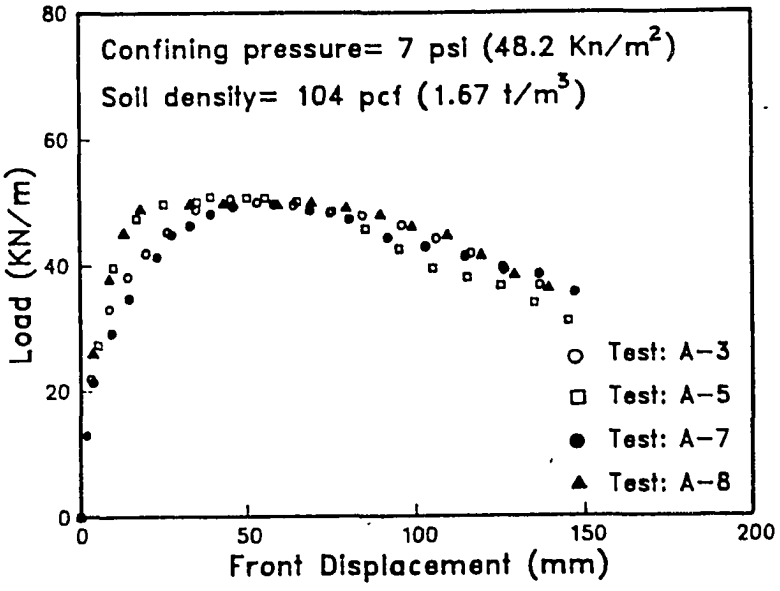

Figure 4.9 Pull-out Test Results on Geogrid 'Tensar SR2'.

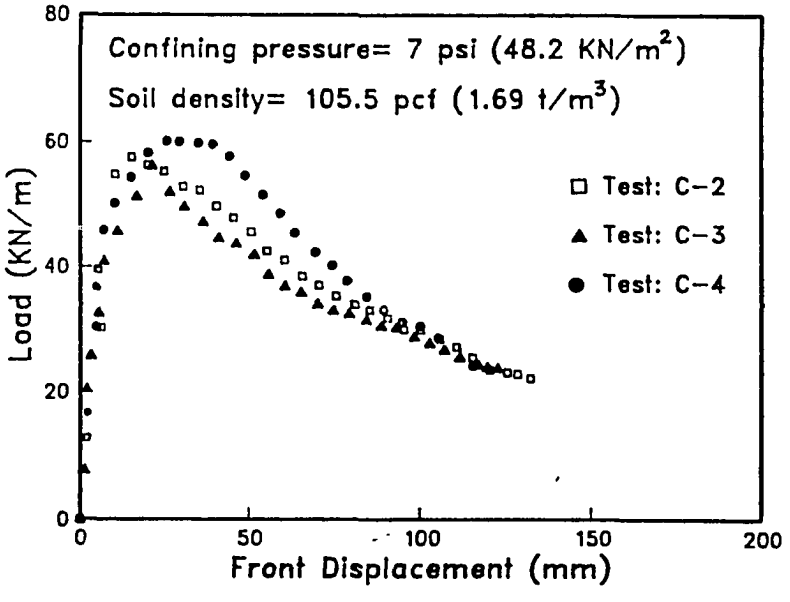

Figure 4.10 Pull-out Test Results on Geogrid 'Tensar SR2'.

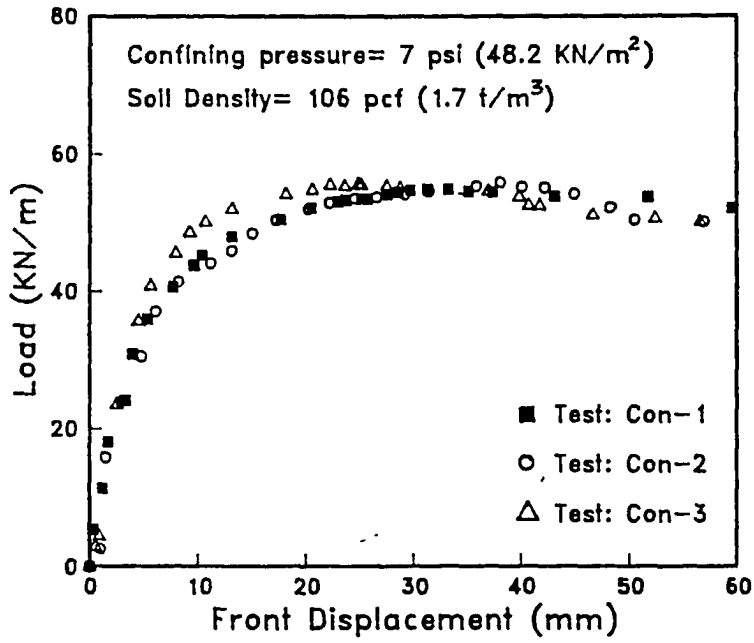

Figure 4.11 Pull-out Test Results on 'Conwed' Geogrid.

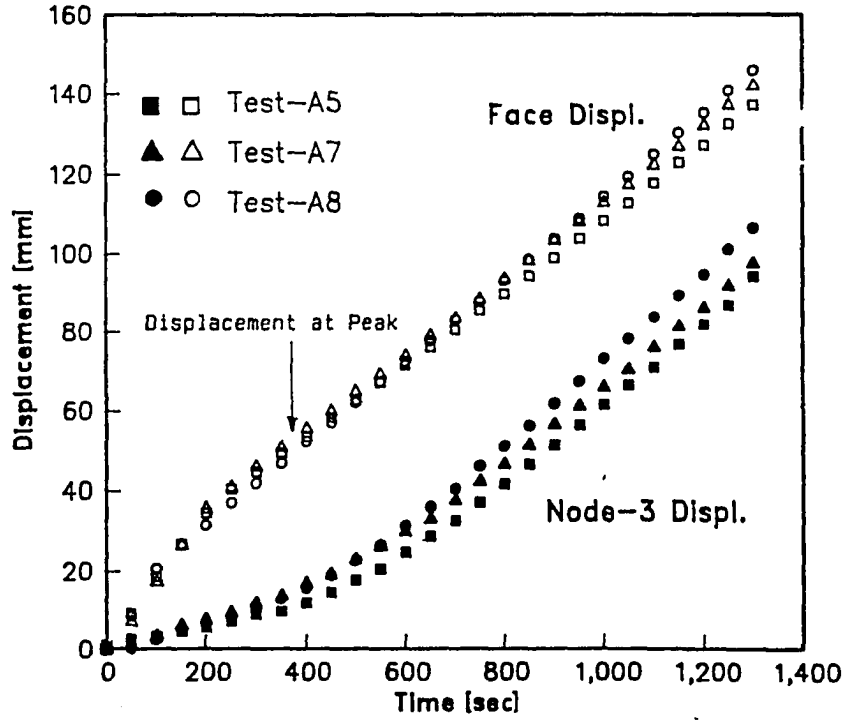

Figure 4.12 Measurement of Front Displacement in Pull-out Tests.

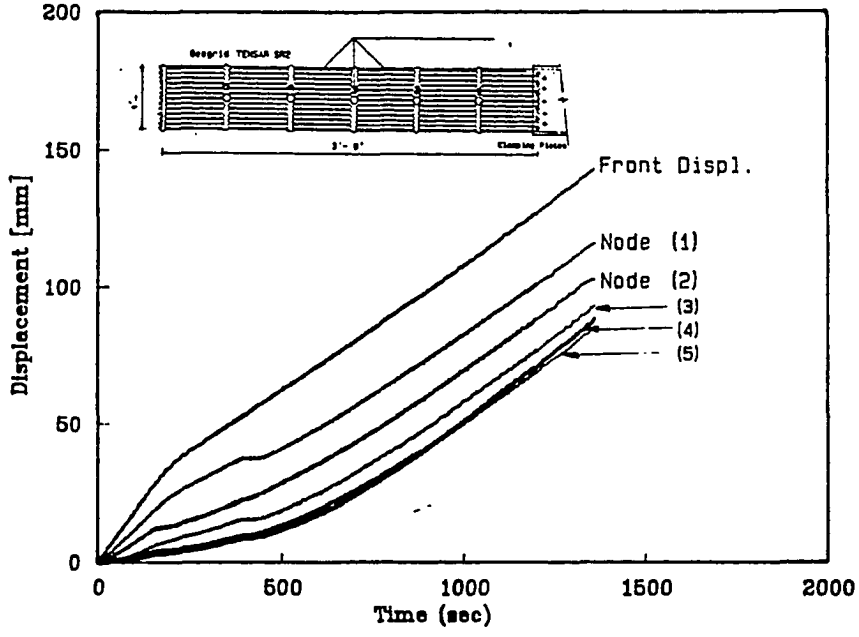

Figure 4.13 Time-Nodal Displacement Relationship for Geogrid 'Tensar SR2' in Pull-out tests.

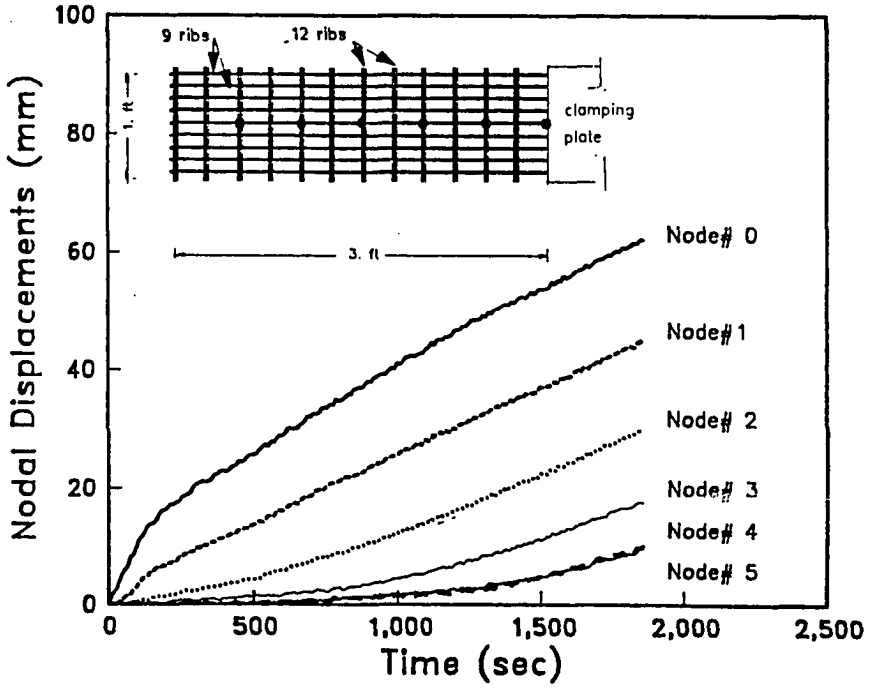

Figure 4.14 Time-Nodal Displacement Relationship for 'Conwed' Geogrid in Pull-out Tests.

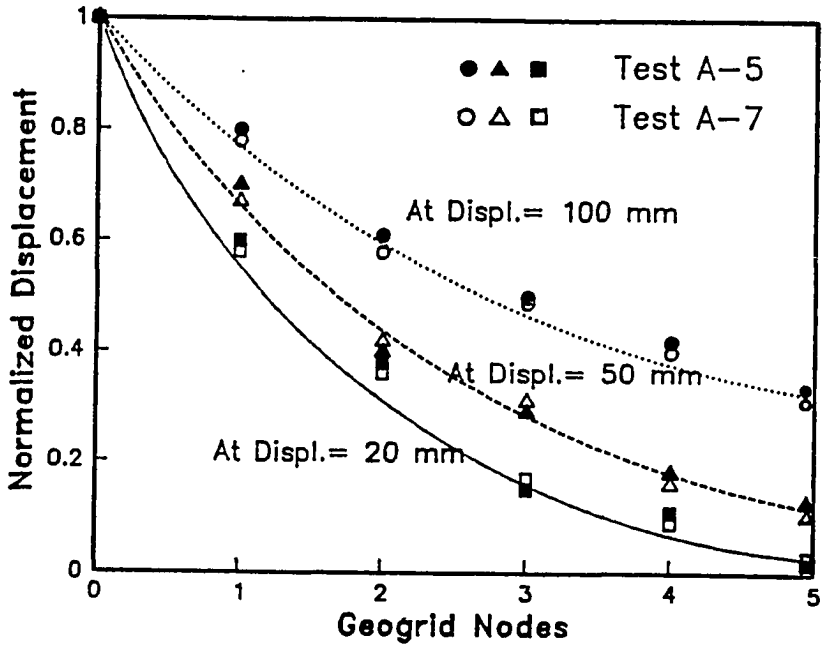

Figure 4.15 Normalized Displacements Along the 'Tensar' Geogrid Specimen.

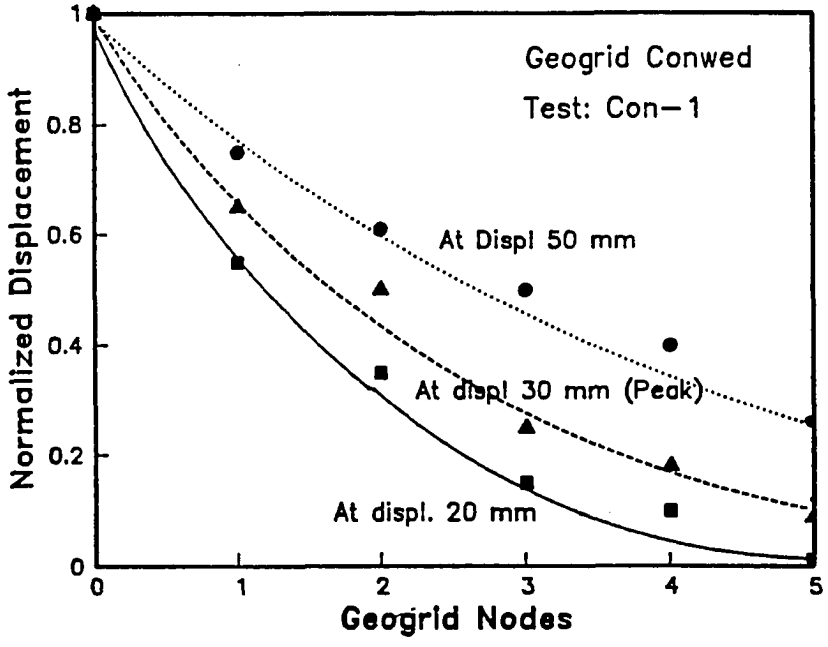

Figure 4.16 Normalized Displacements Along the 'Conwed' Geogrid Specimen.

4.4) DIRECT SHEAR TESTS:

In the direct shear test, the clamping plates are bolted to the upper shear box which is permitted to move between the lower box and the confining beams on its top (see Figure 3.5). Calibration tests were conducted without the sand in the box and the resistance induced by the friction between the box walls and the upper beams was measured.

Direct shear tests were performed on sand to sand interface, without the geogrid, in order to determine the shear stress-strain characteristics of the sand. the soil internal friction angle (ϕ) was equal to 29.8 degrees under confining pressure of 7 psi and average soil density of 106 pcf. Direct shear tests were then performed with the geogrid sample at the interface. Geogrid samples of 72 in. by 72 in. were placed on the bottom of the upper shear box. An interface friction angle (δ) equals 32 degrees was obtained under the same testing conditions. Figure (4.17) shows the effect of geogrid reinforcement on the frictional interaction at the interface. An efficiency factor (tan ϕ/ tan δ) of 1.1 is obtained under the specified confining pressure and soil density. This value is similar to results obtained by other different investigators (Koerner, 1986; and Ingold, 1983) where efficiency factors more than one were recorded at the interface of 'Tensar SR2' geogrid.

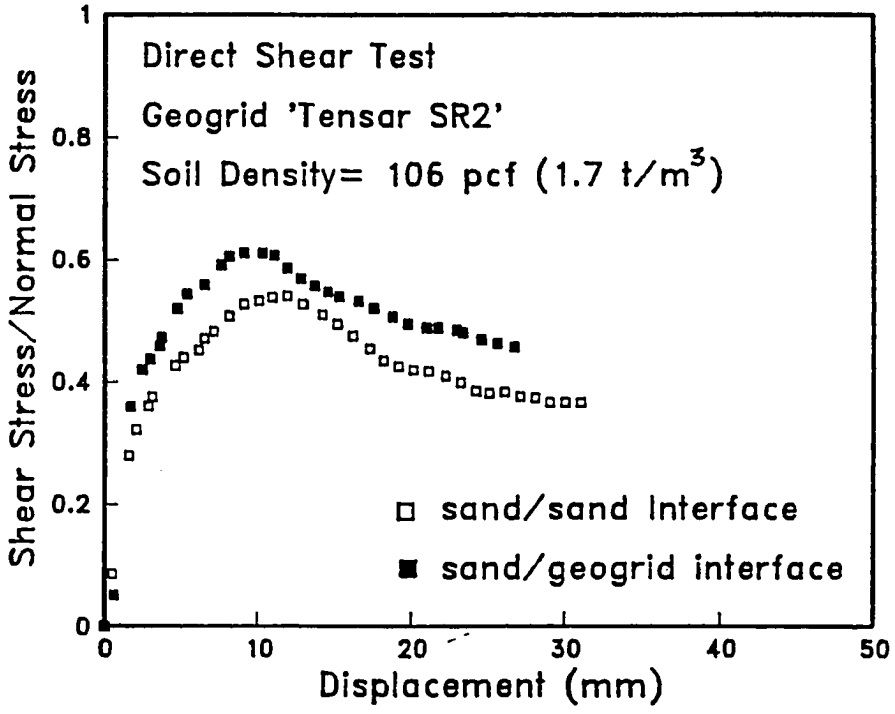

Figure 4.17 Effect of Reinforcement on the Frictional Resistance in Direct Shear Test.

4.5) LOAD-CONTROLLED TESTS:

When geosynthetic reinforced samples are subjected to sustained loading conditions, the strain response consists of an elastic strain followed by a time-dependant creep strain (Figure 4.18). The main design concerns for the long term stability of the reinforced earth structures are:

(i) to predict the long term creep displacement under a constant pull-out load,

ii) to evaluate the critical creep load (or creep strain) below which creep rupture is unlikely to occur.

In order to determine the long term creep displacement under a constant load, load controlled pull-out tests are performed and displacement is monitored with time.

The critical creep pull-out load can be determined by subjecting the specimen to a stepwise increasing load over a time interval. This interval can be determined at each load level when the deformation is stabilized. The critical creep load can be established following a procedure similar to that used for ground anchors (Christopher et al., 1989) which is illustrated in Figure (4.19). In this procedure, the measured front displacement, for each load, is plotted versus Log time (T). An upward concavity of the creep curve indicates an accelerated creep failure. The slope of the displacement versus Log (T) is plotted against the applied pull-out load to determine the critical creep load Tc.

The creep strain induced by a specific loading can be determined as the sum of the strains produced by the previous load increments (Vyalov, 1986). This concept of strain superposition is illustrated in Figure (4.20). Stepped load tests has the advantage that one specimen is tested under the different loading levels which reduces the effect of testing parameters on the results.

In the load-controlled pull-out tests, the loads are incrementally applied to the inclusion and maintained constant during a specified period. The induced load, displacement and velocity at the front are recorded during the test. Three types of load-controlled tests were performed; namely:

(i) load-controlled extension tests on the unconfined geogrid,

(ii) Stepped load-controlled pull-out tests on the confined geogrid to determine the critical creep load,

(iii) long term pull-out tests under a constant load to evaluate the creep pull-out displacement of the confined geogrid.

i) Unconfined Load-Controlled Extension Tests:

Unconfined extension tests were performed on geogrid 'Tensar' of 1 ft width and 3 ft length. The purpose of these tests was to evaluate the time-dependent unconfined behavior of the geogrid under stepped loading conditions and to evaluate the performance of the testing facility under this testing mode. A stepwise increasing load was applied to the samples starting from 10% of the maximum strength of the unconfined geogrid. The load was increased to

40% and 70% of the maximum load. Figure (4.21) shows the unconfined time-dependent strains in these tests.

ii) Stepped Load-Controlled Pull-out Tests:

Stepped load-controlled pull-out tests were conducted on the "Conwed' geogrid. In these tests, the specimens were subjected to different loading levels defined as percentages of the maximum pull-out resistance (Tmax) obtained from displacement-rate controlled tests. Figures (4.22) and (4.23) show the front displacement verses time relationship of the geogrid under confining pressures of 7 psi and soil density of 107 pcf. In these tests, the specimens were subjected to stepwise loads increasing from 20% Tmax to 85% Tmax at time intervals of about 1800 min. for each step.

In order to interpret the critical creep pull-out loads, the measured front displacements, for each loading level, were plotted versus log (time) as shown in Figure (4.24). In these curves, the displacement-rate curves indicate stabilized creep with time till a loading level of about 70% Tmax where creep pull-out rate starts to accelerate. The maximum displacement rates at each load level were plotted against the normalized pull-out load (T/Tmax) in Figure (4.25) in order to estimate the critical creep load (Tc). The long term creep displacement under the critical creep load (Tc) was evaluated in a long term (500 hr) pull-out test under the critical creep load.

iii) Long Term Pull-out Tests:

Long term pull-out tests were conducted on 'Tensar' geogrid specimens subjected to pull-out load equals (Tc) in a soil dry density of 107 pcf. The value of Tc was estimated from Figure (4.27) and was taken as 65% of the maximum pull-out resistance of the geogrid. Figure (4.26) show the creep displacement of the geogrid specimen under confining pressures of 7 psi. The Log (displacement-rate) versus log (time) relationship of the geogrid is plotted in Figure (4.27). The Figure shows an upward of the creep curve indicating an accelerated creep.

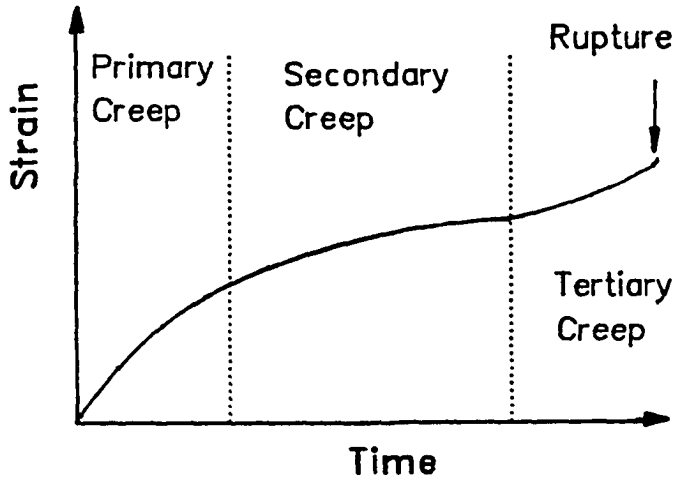

Figure 4.18 Illustration of Creep Concept.

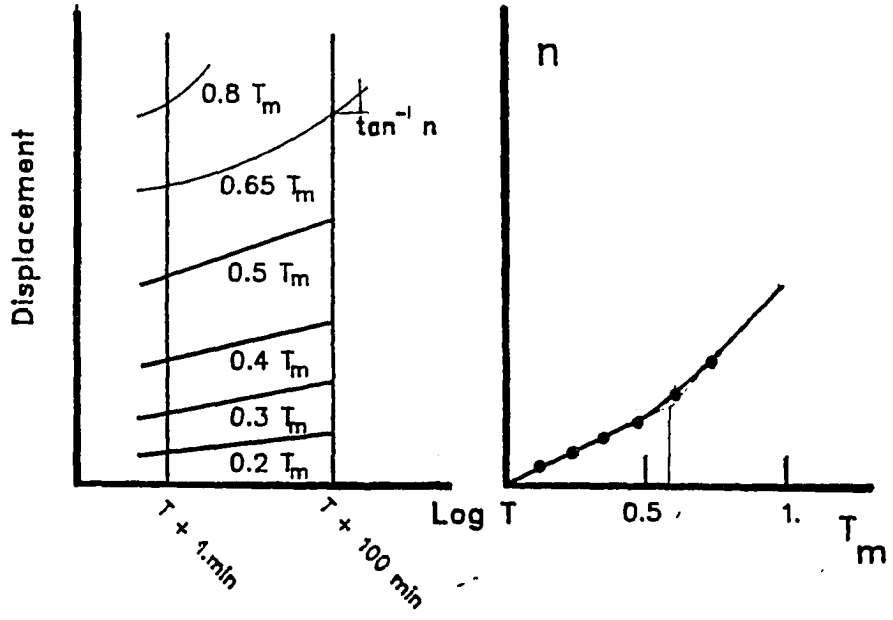

Figure 4.19 Determination of the Critical Creep Load. (After Christopher et al. 1989).

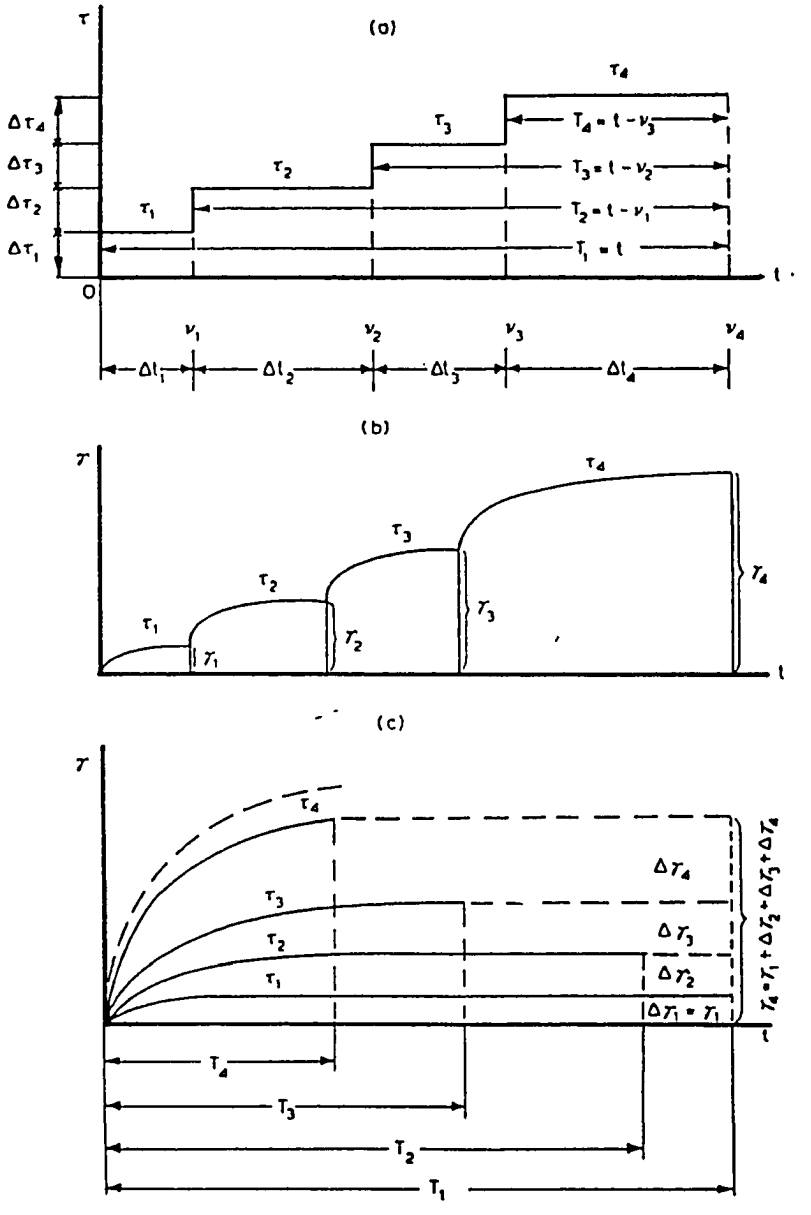

Figure 4.20 Concept of Strain Superposition in Stepped Loading Tests. (After Vyalov, 1986).

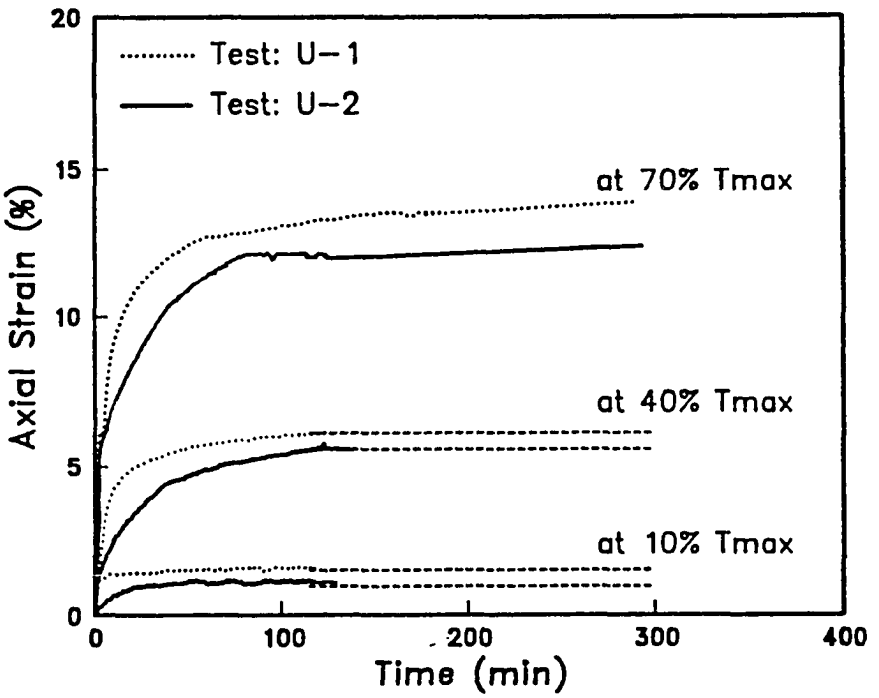

Figure 4.21 Unconfined Load-Controlled Tests on Geogrid 'Tensar'.

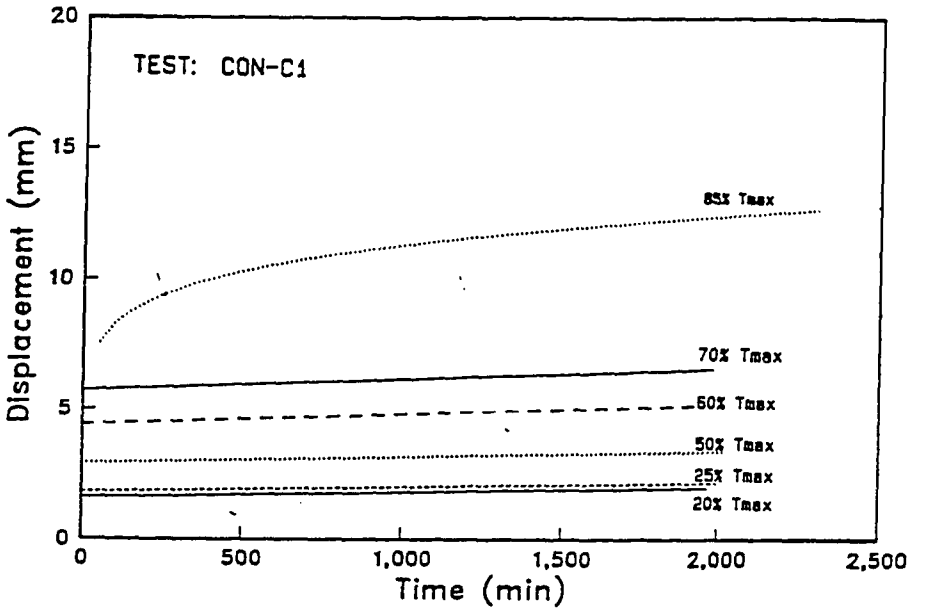

Figure 4.22 Stepped Load-Control Test on Geogrid 'Conwed'.

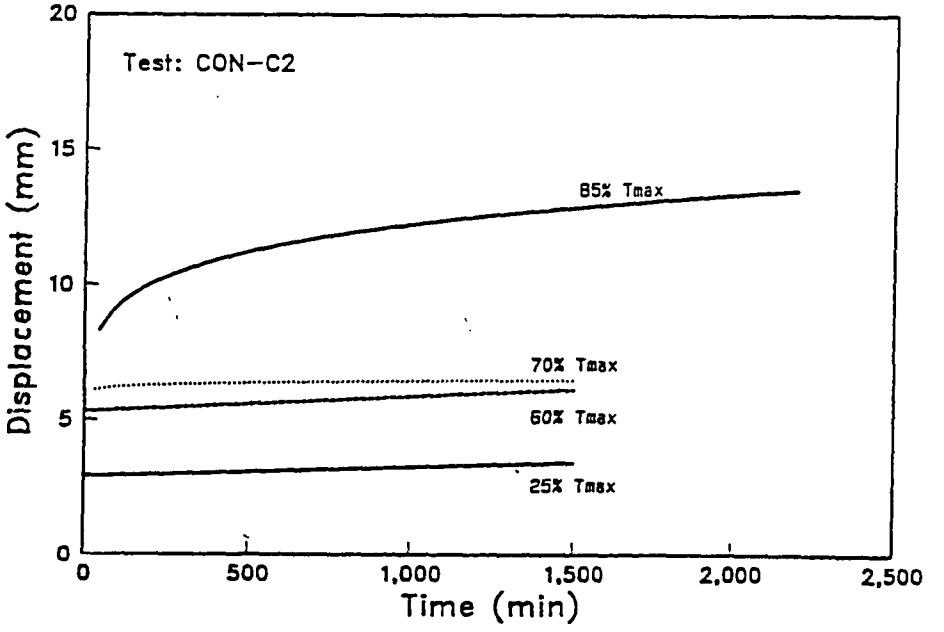

Figure 4.23 Stepped Load-Control Test on Geogrid 'Conwed'.

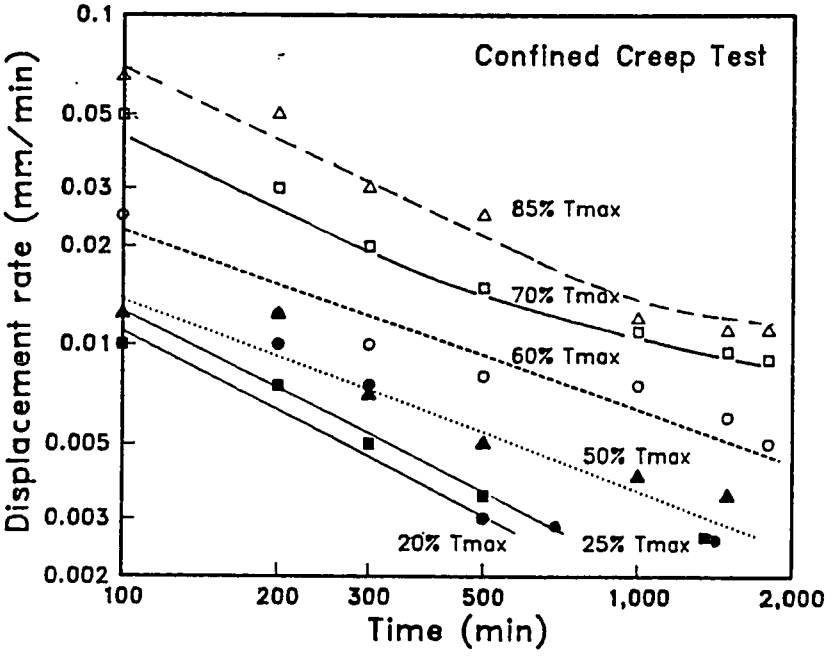

Figure 4.24 Log(Dipl. rate) versus Log (Time) in Creep Tests on 'Conwed'.

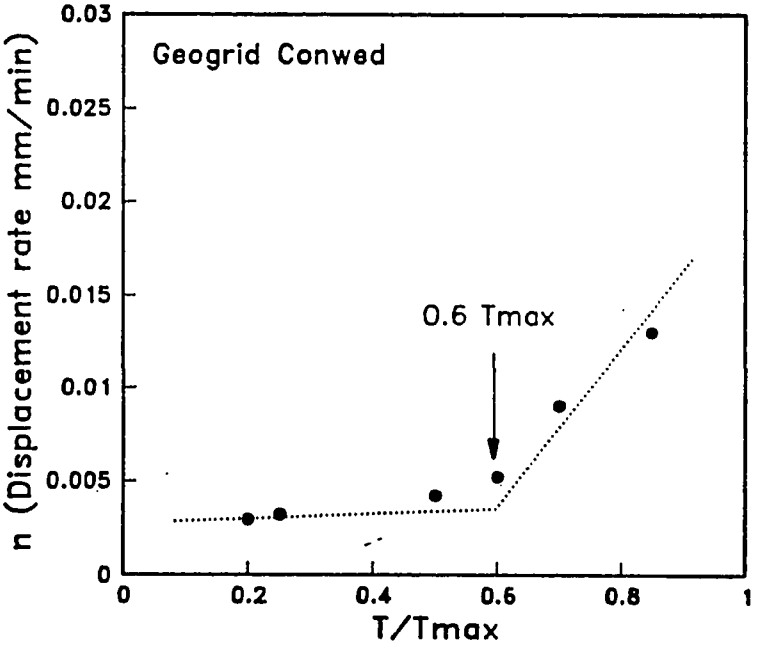

Figure 4.25 Determination of the Critical Creep Load.

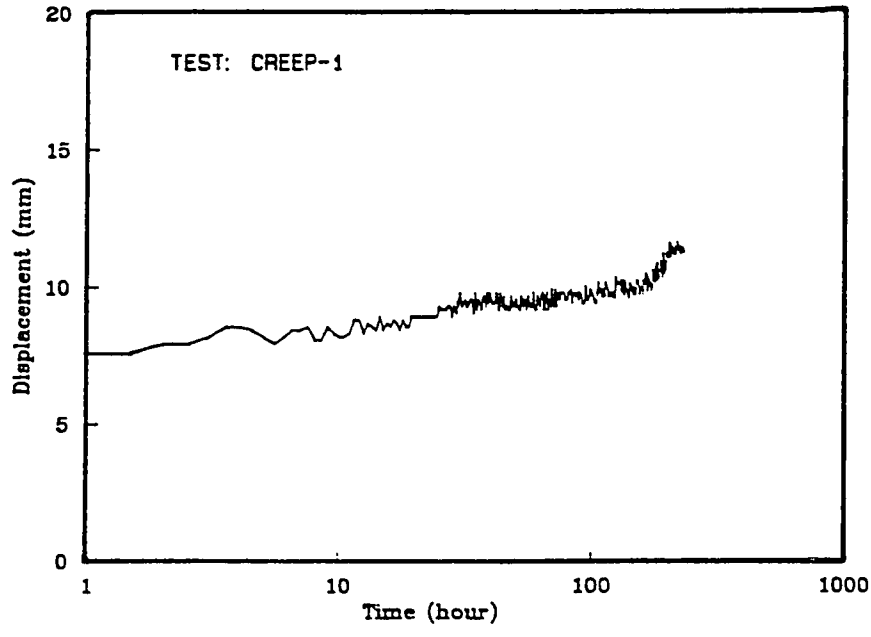

Figure 4.26 Results of Creep Test on Geogrid 'Conwed'.

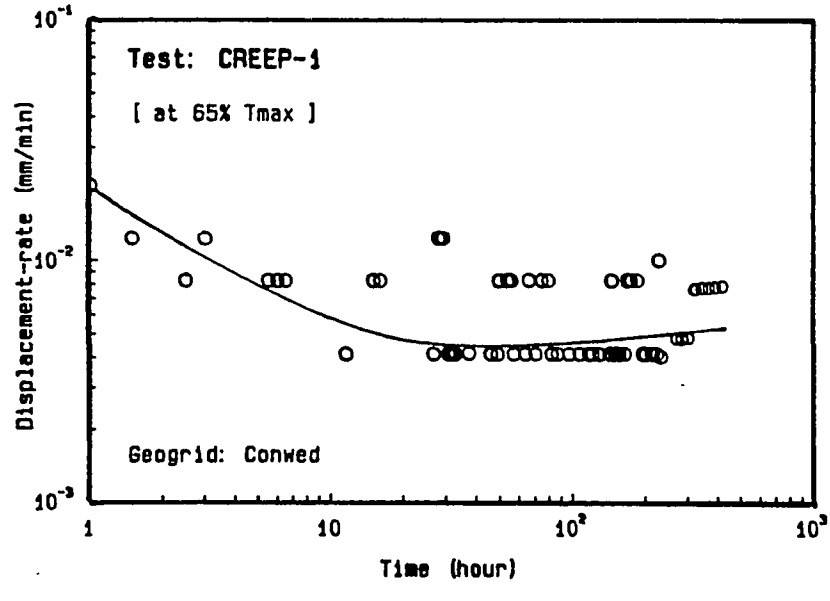

Figure 4.27 Results of Creep Test on Geogrid 'Conwed'.

CHAPTER 5

EFFECT OF TESTING PARAMETERS ON THE INTERACTION MECHANISM

5.1) INTRODUCTION:

The soil-reinforcement interaction involves mainly three basic load-transfer mechanisms:

(i) lateral friction on the soil-reinforcement interface (as in geotextiles, strips and bars),

(ii) passive earth pressure on the transversal elements of geogrids, welded wire meshes and bar mats,

(iii) particle interlocking as in the geotextiles and geogrids.

Load transfer in most of the geosynthetic materials is a combination of these mechanisms. Mobilization of these mechanisms requires different magnitudes of displacements that would substantially affect the interaction performance. The relative contribution of each mechanism to the total pull-out resistance depend on many factors, namely:

(i) material properties (e.g. its type, geometry, extensibility and creep properties),

(ii) soil characteristics (e.g. its relative density, shear strength and grain size distribution),

(iii) loading conditions (e.g. overburden pressure, displacement-rate and testing boundary conditions).

The major objective of the performance evaluation study is to assess the sensitivity of test results to the changes in the testing parameters and establish a data base for the development of a reliable interpretation procedure. For this purpose, a parametric study was conducted and the effects of the main testing parameters (i.e. geogrid type, displacement rate, confining pressure, rigid box boundaries, soil compaction and relative density) on the soil-geogrid interaction response were investigated. The tests performed for this parametric study are shown in Table (5.1). The table shows the main testing parameters for each test. The detailed results of these tests are presented in Appendix C.

Test	Material	Sample width [cm]	Confining pressure [KN/m^2]	Displ. rate [mm/min]	Soil density [t/m^3]	Soil thick [cm]	Sleeve length [cm]	Notes
(a) Displacement-rate Extension Tests:								
#1	Tensar-SR2	30	Unconfined	3	--	--	--	sample
#2	,,	30	extension	3	--	--	--	clamped
#3	,,	30	tests.	3	--	--	--	at end.
Con-U1	Conwed X3022	30	Unconfined	2	--	--	--	,,
Con-U2	,,	30	extension	2	--	--	--	
Con-U3	,,	30	tests.	2	--	--	--	
Con-U4	,,	30		2	--	--	--	
Con-U5	,,	30		2	--	--	--	
Con-U6	,,	30		2	--	--	--	
(b) Displacement-rate Pull-out Tests:								
C1	Tensar-SR2	30	48	10	N/M(*)	60	30	standard
C2	,,	30	48	10	1.69	60	30	tests.
C3	,,	30	48	10	1.69	60	30	
C4	,,	30	48	10	N/M	60	30	
C5	,,	30	48	10	N/M	60	30	
A3	,,	30	48	6	1.66	60	30	
A4	,,	30	48	6	1.67	60	30	
A5	,,	30	48	6	1.67	60	30	
A7	,,	30	48	6	1.67	60	30	
A8	,,	30	48	6	1.67	60	30	

(*) Not measured

Table 5.1 List of Pull-out Tests.

Test	Material	Sample width [cm]	Confining pressure [KN/m^2]	Displ. rate [mm/min]	Soil density [t/m^3]	Soil thick [cm]	Sleeve length [cm]	Notes
A1-a	Tensar-SR2	30	70	6	1.73	60	30	
A1-b	,,	30	70	6	1.74	60	30	
A2	,,	30	48	6	1.73	60	30	
A6-a	,,	30	34	6	1.68	60	30	
A6-b	,,	30	34	6	N/M	60	30	
A9	,,	30	48	10	1.63	60	30	
A10	,,	30	48	10	1.65	60	30	
A11	,,	30	48	2	1.67	60	30	
P1	Tensar-SR2	30	48	20	1.67	60	no-sleeve	
P2	,,	30	48	20	1.67	60	20	
P3	,,	30	48	20	N/M	60	30	
B1	Tensar-SR2	30	48	6	1.65	40	30	
B2	,,	30	48	6	1.65	40	30	
B3	,,	30	48	6	1.66	80	30	
B4	,,	30	48	6	N/M	20	30	
Con-1	Conwed X3022	30	48	2	1.70	60	30	
Con-2	,,	30	48	2	1.71	60	30	
Con-3	,,	30	48	2	1.70	60	30	
Con-4	,,	30	96	2	1.71	60	30	
Con-5	,,	30	96	2	1.71	60	30	
Con-6	,,	30	96	2	1.71	60	30	

Table 5.1 [Continued].

Test	Material	Sample width [cm]	Confining pressure [KN/m^2]	Displ. rate [mm/min]	Soil density [t/m^3]	Soil thick [cm]	Sleeve length [cm]	Notes
Con-P1	Conwed X3022	30	140	2	1.71	60	30	
Con-P2	,,	30	140	2	1.72	60	30	
Con-P3	,,	30	140	2	1.72	60	30	
Con-P4	,,	30	185	2	1.73	60	30	
Con-P5	,,	30	185	2	N/M	60	30	
Con-P6	,,	30	185	2	N/M	60	30	
Con-L1	Conwed X3022	30	48	2	N/M	60	30	without
Con-L2	,,	30	48	2	N/M	60	30	transv.
Con-L3	,,	30	96	2	N/M	60	30	ribs.
Con-L4	,,	30	96	2	N/M	60	30	
(c) Load-Controlled Pull-out Tests:								
U1	Tensar-SR2	30	Unconfined	--	--	--	--	stepped
U2	,,	30	,,	--	--	--	--	loading.
Load-1	Tensar-SR2	30	48	--	1.69	60	30	creep
Con-C1	Conwed X3022	30	48	--	1.71	60	30	stepped
Con-C2	,,	30	48	--	1.71	60	30	loading.
Con-C3	,,	30	96	--	1.71	60	30	
Con-C4	,,	30	96	--	N/M	60	30	
Creep-1	,,	30	48	--	1.72	60	30	500 hr.
Creep-2	,,	30	96	--	N/M	60	30	500 hr.

Table 5.1 [continued]

5.2) EFFECT OF TESTING PARAMETERS ON INTERACTION RESPONSE:

(i) Reinforcement Type:

The mobilized shear resistance at the soil-reinforcement interface reinforced soil systems depends on the type of reinforcement. In case of geogrids, the interface shear strength is primarily mobilized, as illustrated in Figure (5.1), by the skin friction and passive resistance against transversal ribs. For coarse grained soils, the openings in the geogrids may allow soil particles to interlock between the ribs and, thereby, increasing its shear strength. The skin friction between the soil and the geogrid depends on the type of soil and the surface roughness of the geogrid. The contribution of soil resistance at the transversal ribs to the overall shear strength of the geogrid depends on many factors such as confining pressure, geogrid geometry and grain size distribution of soil. The effect of soil friction at the soil-geogrid interface is shown in Figure (5.2). The figure shows the results of pull-out tests on 'Conwed' geogrids performed with and without their transversal ribs. These tests were performed under confining pressures of 7 psi (48.2 KN/m^2) and 14 psi (96.4 KN/m^2). The figure shows that an average value of 75% of the overall pull-out resistance of this specific geogrid is attributed to the frictional resistance on the longitudinal ribs.

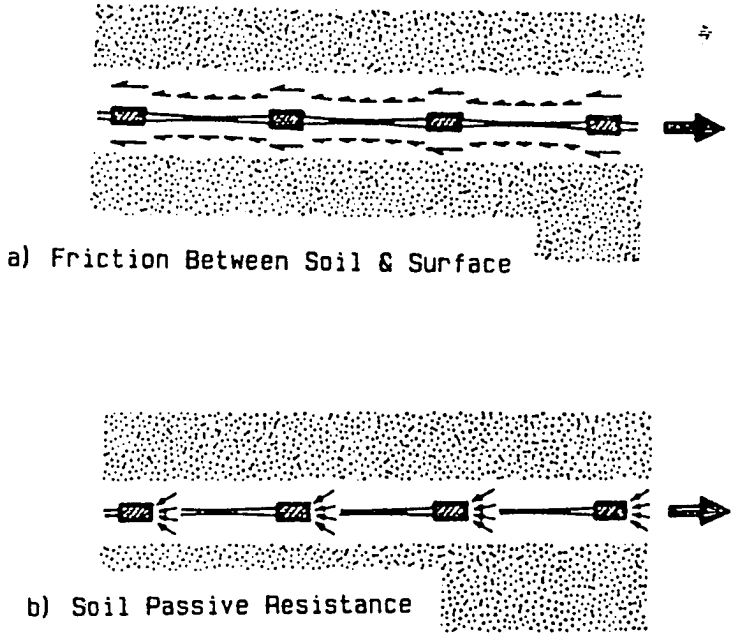

Figure 5.1 Load Transfer Mechanism for Geogrids.

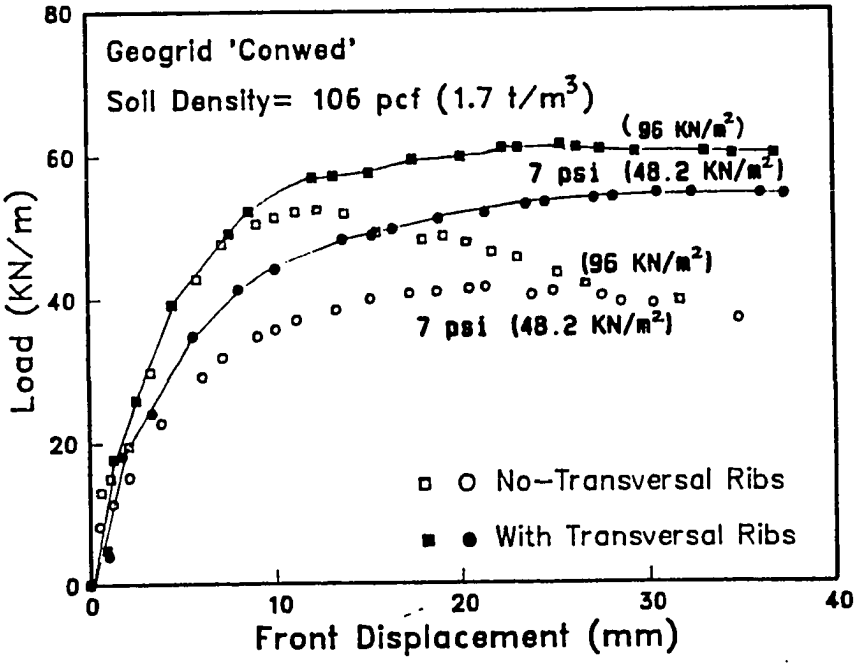

Figure 5.2 Pull-out Tests on Geogrids With and Without the Transversal Ribs.

(ii) Displacement Rate:

Currently, no standard testing procedure that specifies the displacement-rate for pull-out tests exists. For unconfined extension tests, ASTM Designation D4595-86 recommends a standard rate of strain of 10 ±3% per min for wide strip method test. Rowe and Ho (1986) performed wide strip tests on geogrids at strain rates from 0.2% to 10% per min. They showed that the geogrid tension strength varies according to the applied rate of strain. It should be noticed that the wide strip test is an index test under unconfined conditions and does not represent the reinforcement response under confinement. Under confining conditions, reinforcement experiences its peak pull-out strength at much lower strain levels and test duration should be relevant to the observed fabric behavior in field conditions.

For pull-out tests, most of the previous studies were conducted under different displacement-rates. Table (5.2) shows the values of pull-out displacement rates used by different investigators. The displacement rates varied from 0.1 to 15 mm/min. In order to investigate the effect of displacement-rate on pull-out response, tests were performed on geogrid 'Tensar' under four different pull-out displacement-rates, while maintaining the other testing parameters constant. These pull-out displacement rates are:

i) 0.033 mm/sec (2 mm/min)

ii) 0.10 mm/sec (6 mm/min),

iii) 0.18 mm/sec (10 mm/min),

iv) 0.33 mm/sec (20 mm/min).

In these tests, sample dimensions of 1 ft (.3 m) width and 3 ft (1 m) long, an applied normal stress of 7 psi (48.2 KN/m^2), and an average soil density of 104 pcf (1.67 t/m^3) were maintained. Figure (5.3) shows the pull-out response of the geogrid under these different displacement-rates. The Figure shows that the increase in the displacement-rate from 2 to 20 mm/min results in a reduction in the peak pull-out resistance and interface stiffness modulus.

Figure (5.4) shows the effect of displacement-rate on nodal displacements. The plotted displacements were measured at the front point (node 0), and at 2 ft (0.61 m) from the geogrid front end (node 4). The slopes of the curves at node (0) are constant and consistent with the input commands of displacement-rates. The slopes of the displacement curves at node (4) show that higher displacement-rates result in a faster mobilization of shear stresses at the rear nodes.

In order to evaluate the effect of the applied displacement-rate on the displacement distribution along the geogrid, displacements along the nodal points are normalized with respect to the front displacement (i.e at node 0) and are plotted along the geogrid in Figure (5.5). The Figure illustrates that, at peak pull-out level, higher displacement-rates result in a more uniform shear strain mobilization along the inclusion.

The effect of displacement-rate on the geogrid pull-out resistance and its interface stiffness modulus are shown, respectively, in Figures (5.6) and (5.7).

The figures show that the peak pull-out resistance and the interface stiffness modulus appear to be less sensitive to the changes of displacement-rates under 6 mm/min. These results suggest that in order to reduce the effect of displacement-rate on pull-out results, pull-out displacement-rate should not exceed 6 mm/min.

Box	Testing Method	Testing rate
- Caltrans Box (Johnston, 1985) [54"x36"x20"]	displacement rate controlled pull-out on Tensar SR2	2%/min. (4.4 mm/min)
- V. Elias Box (Elias, 1979) [36"x36"x18"]	displacement rate controlled on metal strips	0.1 in/min (2.5 mm/min)
- STS Box (Christopher,86) [48"x30"x18"]	displacement rate controlled pull-out on Tensar SR2.	0.1 mm/min
- Utah State U.Box (Anderson,1984)	displacement rate controlled on wire mesh.	0.8 mm/min
- Drexel U. (Koerner, 1986)	displacement rate controlled pull-out on tensar SR2.	0.25-15.2 mm/min
- U. of Grenoble (Gourc, 1980)	displacement rate controlled pull-out on Tensar SR2.	0.25 in/min (6 mm/min)

Table 5.2 Comparison Between Testing Strain Rates for Different Pull-Out Boxes, (After Knochenmus, 1987)

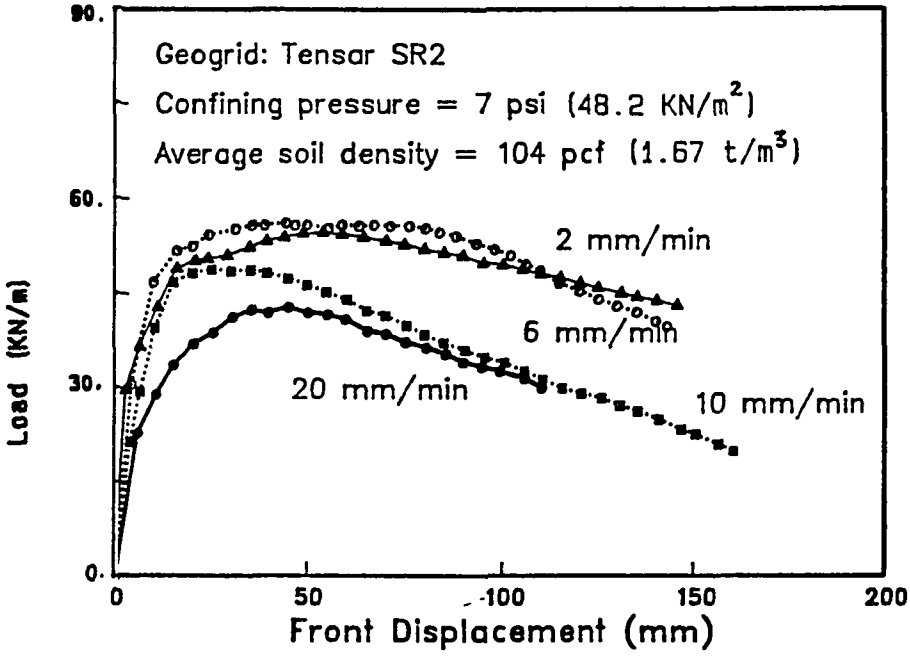

Figure 5.3 Effect of Displacement-rate on Pull-out Response.

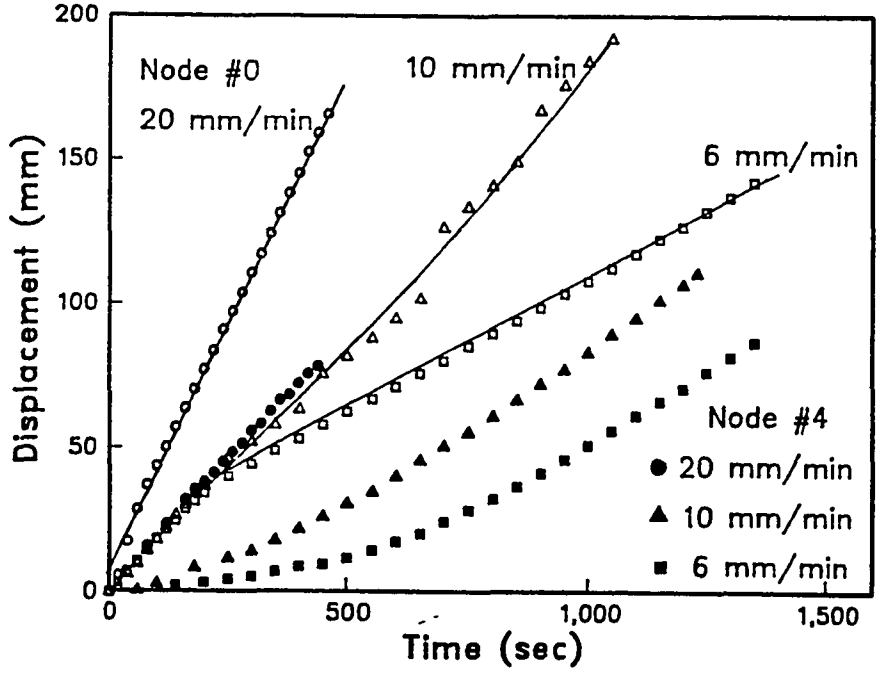

Figure 5.4 Effect of Displacement-rate on Nodal Displacements.

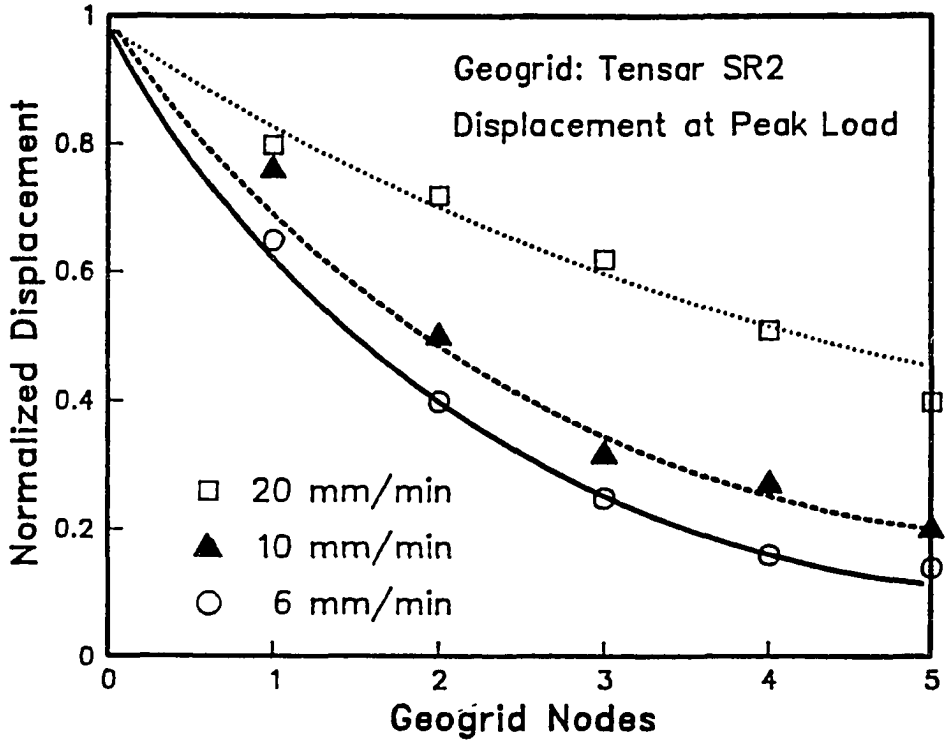

Figure 5.5 Effect of Displacement-rate on Displacement Distribution.

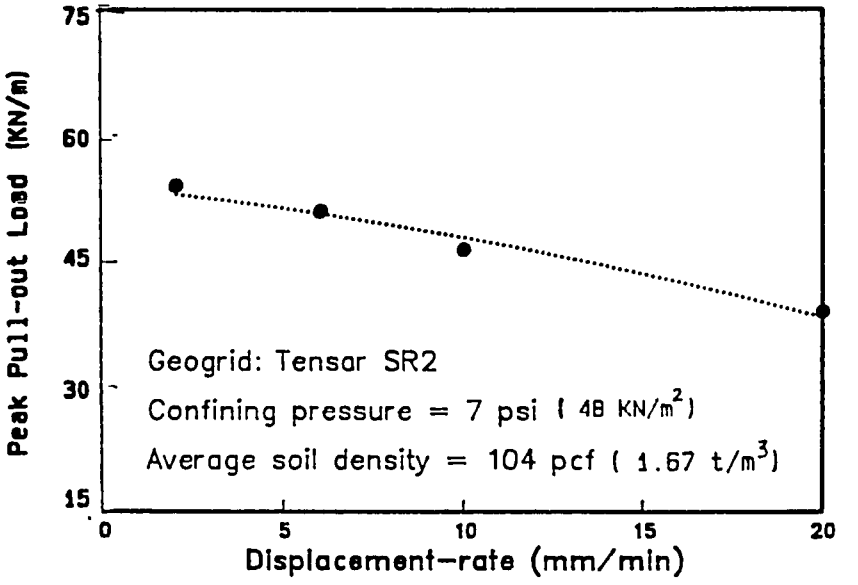

Figure 5.6 Effect of Displacement-rate on Pull-out Resistance.

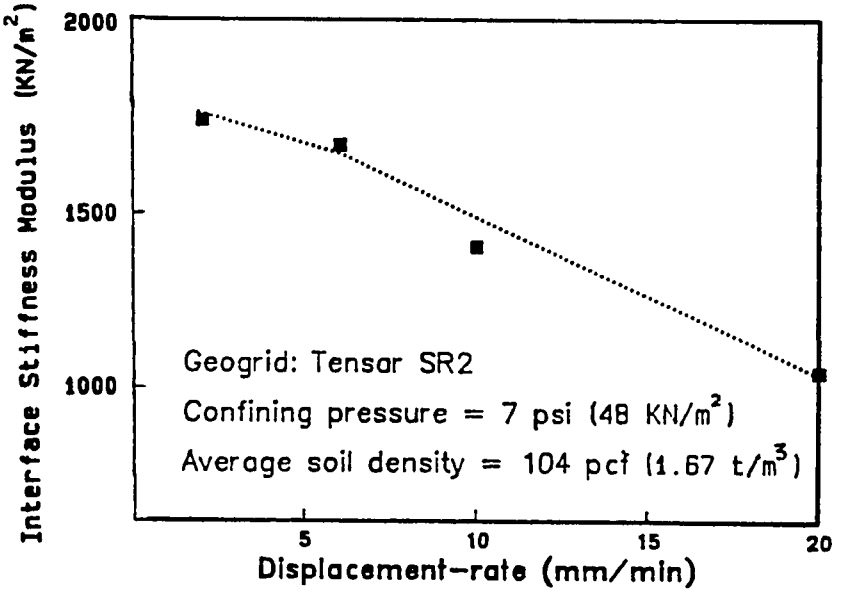

Figure 5.7 Effect of Displacement-rate on Interface Stiffness Modulus.

(iii) Soil Compaction and Relative Density:

The frictional resistance of the inclusion is highly influenced by the soil relative density (Juran et al. 1988). Dense soils tend to dilate when shear stresses are mobilized along the reinforcement interface. As the dilatancy is restricted by the surrounding soil, this results in a normal stress concentration at the interface and consequently an apparent increase of the pull-out resistance.

To evaluate the effect of the relative soil density on the pull-out response, tests were performed with the soil compacted to different relative densities under the same confining pressure; namely:

i) average soil density of 102 pcf (1.62 t/m^3),

ii) average soil density of 104 pcf (1.67 t/m^3),

iii) average soil density of 105.5 pcf (1.7 t/m^3),

iv) average soil density of 108 pcf (1.73 t/m^3).

Figures (5.8) and (5.9) show the effect of soil density on geogrid 'Tensar' tested, respectively, with pull-out displacement-rates of 6 mm/min and 10 mm/min. In these tests, the geogrid was subjected to constant confining pressure of 7 psi (48.2 KN/m_2). The figures show that an increase in the soil relative density results in an increase of the peak pull-out resistance and interface stiffness modulus of the geogrid.

Soil compaction increases the lateral earth pressure on the geogrid transversal elements and the mobilized frictional resistance at the interface.

Consequently, it restrains geogrid movement and slippage. Figure (5.9) shows that when the soil was compacted to a relative density of 85%, the restrained geogrid movement resulted in a significant increase in the interface stiffness modulus and the pull-out strength. In this test, the reinforcement failed by successive rupture of its longitudinal ribs at a very low front displacement.

The nodal-displacement distribution along the geogrid are normalized with respect to the front displacement and plotted in Figure (5.10). The figure shows the effect of soil density on the mobilized shear distribution along the geogrid. The higher soil density results in a higher shear stress concentration at the vicinity of the point of application and, ultimately, rupture failure at the front element. Low soil density leads to a more uniform mobilization of the interface shear stresses along the reinforcement.

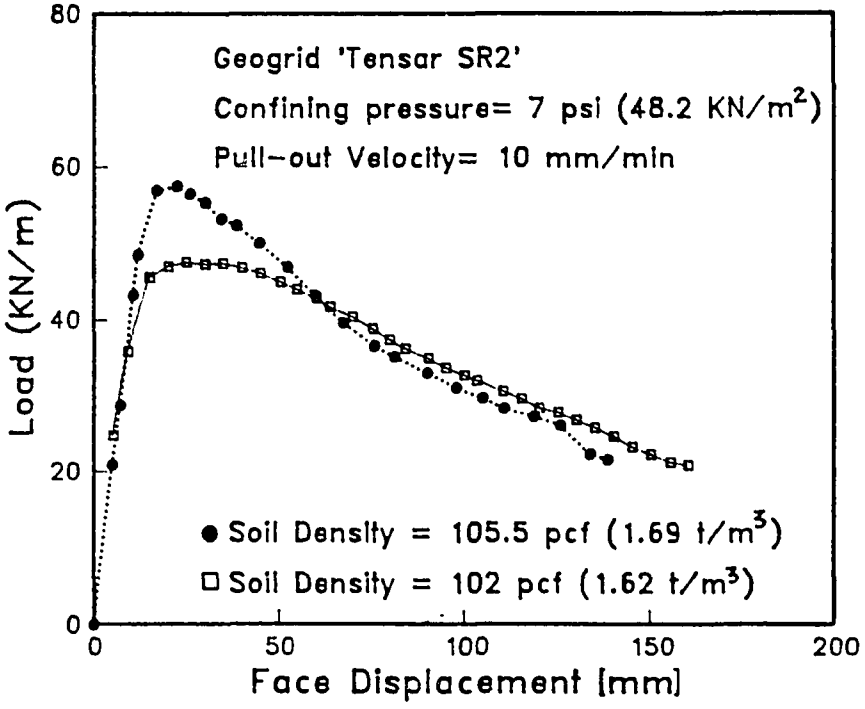

Figure 5.8 Effect of Soil Density on Pull-out Response of 'Tensar' Geogrid.

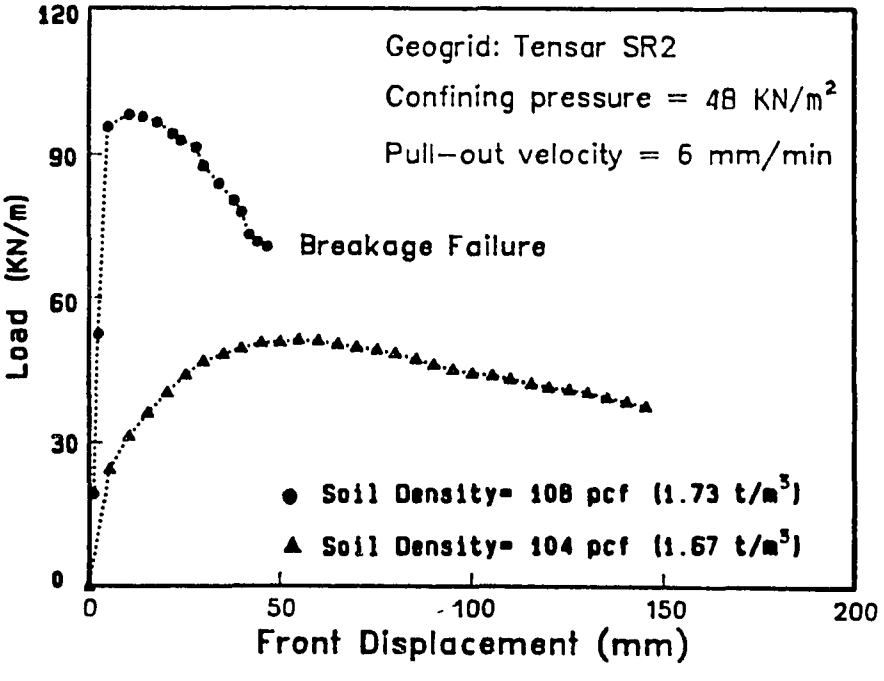

Figure 5.9 Effect of Soil Density on Pull-out Response of 'Tensar' Geogrid.

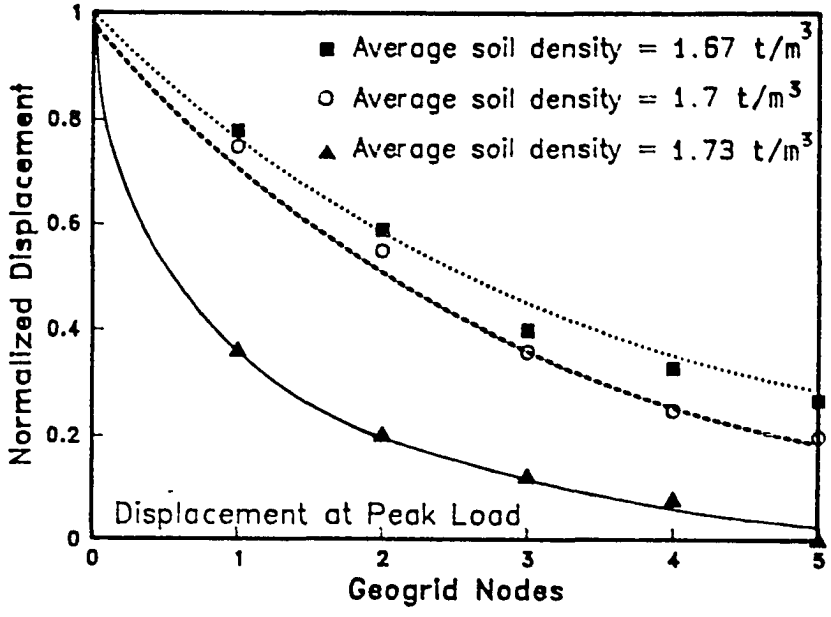

Figure 5.10 Effect of Soil Density on Displacement Distribution Along the Geogrid.

(iv) Confining Pressure:

The effect of confining pressure on the frictional resistance of the reinforcement has been demonstrated by several investigators (McGown et al., 1982; and Juran and Chen, 1989). For geogrid reinforcement, the confined elongation during pull-out testing is restrained by the passive resistance of the soil and particles interlocking within the transversal geogrid elements. The restrained elongation results in an apparent increase of the tensile strength and of the stiffness modulus.

Figure (5.11) shows the effect of the confining pressure on the pull-out response of 'Tensar' geogrids measured under confining pressures of 5 psi (34 KN/m_2) and 7 psi (48 KN/m_2). These tests were performed with displacement-rate of 6 mm/min and sand average density of 104 pcf (1.67 t/m_3). The results show that an increase in the confining pressure results in an increase the pull-out resistance of the geogrid. Although the increase in the confining pressure reduces soil tendency to dilate, it results in an increase in the passive soil resistance to the transversal ribs and, consequently, an increase in the geogrid pull-out resistance.

The effect of soil confinement on the extension behavior of geogrid 'Tensar' is illustrated in Figure (5.12). In the unconfined tests, the samples were clamped to the box rear wall; while, in the confined tests, the specimens were tested under normal stresses of 7 psi (48.2 KN/m_2) and 10 psi (70 KN/m_2), and soil density of 108 pcf (1.74 t/m_3). The figure shows that an

increase in the confining pressure results in an increase in the pull-out resistance and the geogrid ultimatly demonstrates successive ruptures of the longitudinal ribs at lower strain levels.

Figure (5.13) shows test results of geogrid 'Conwed' when tested under confining pressures of 7 psi (48.2 KN/m_2), 14 psi (96.4 KN/m_2) and 21 psi (140 KN/m^2). The Figure shows similar effect of confinement on the pull-out resistance of the geogrid. The results in Figures (5.12) and (5.13) show that 'Conwed' geogrid demonstrates rupture at a much higher confining pressure than 'Tensar' geogrid. This is mainly due to the small thickness of 'Conwed' transversal ribs (1 mm), compared to the relatively thick transversal ribs of 'Tensar' (4.5 mm), which requires higher confinement to mobilize passive soil resistance at the transversal ribs.

These results suggest that the design criteria for geogrid reinforced soil structures should take into account the in-soil confined extension properties derived from pull-out tests rather than the material properties obtained from unconfined extension tests. Although a lower (and consequently more conservative) peak strength is obtained from unconfined tests, the unconfined behavior of the geogrid is substantially more ductile and its strain level at peak is higher than that obtained under confined conditions. This may results in non-conservative design values for the admissible geogrid extension and the related structure displacements.

The normalized displacement distribution along the 'Tensar' and

"Conwed' geogrids under different confining pressure are shown, respectively, in Figures (5.14) and (5.15). The figures illustrate the effect of the confining pressure on the mobilized load transfer along the reinforcement.

The soil-geogrid interface shear stress is more uniformly mobilized along the geogrid under low confining pressures. The increase in the confining pressure restrains the geogrid displacement and results in a higher mobilization of the soil-geogrid interface shear stresses near the pull-out application point, a lower mobilization of the shear stresses at the rear, and consequently a shorter effective adherence length.

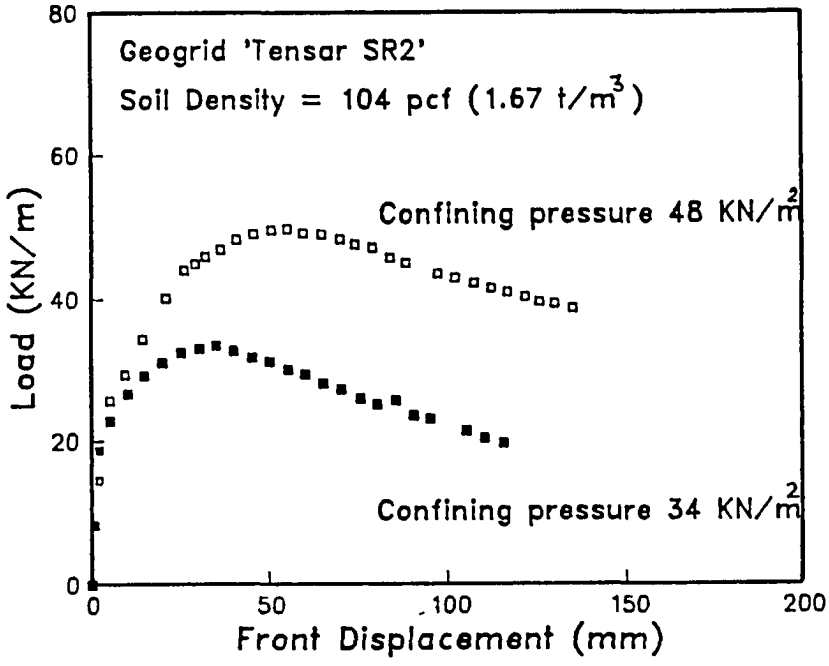

Figure 5.11 Effect of Confining Pressures on Pull-out Resistance of 'Tensar' Geogrid.

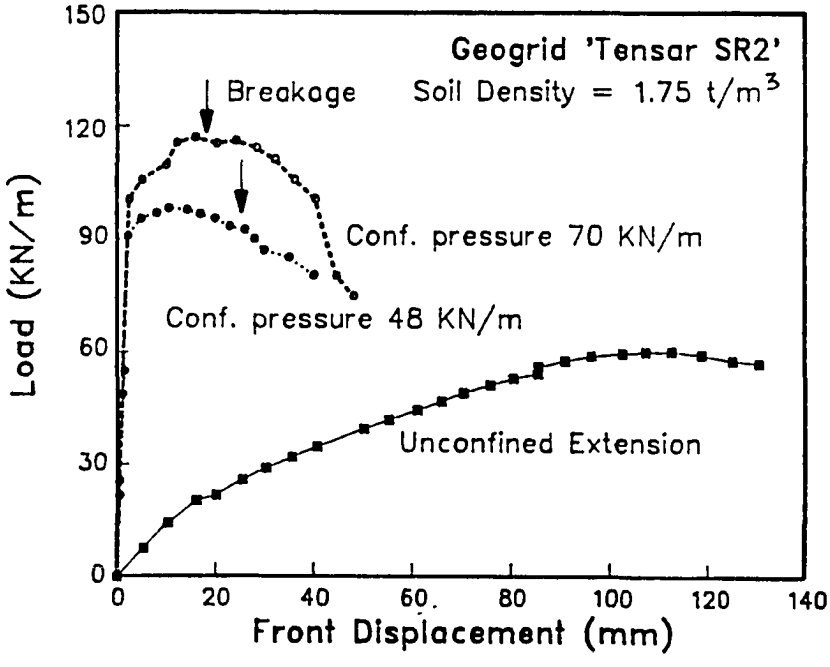

Figure 5.12 Effect of Confining Pressure on the Extension Behavior of 'Tensar' Geogrid.

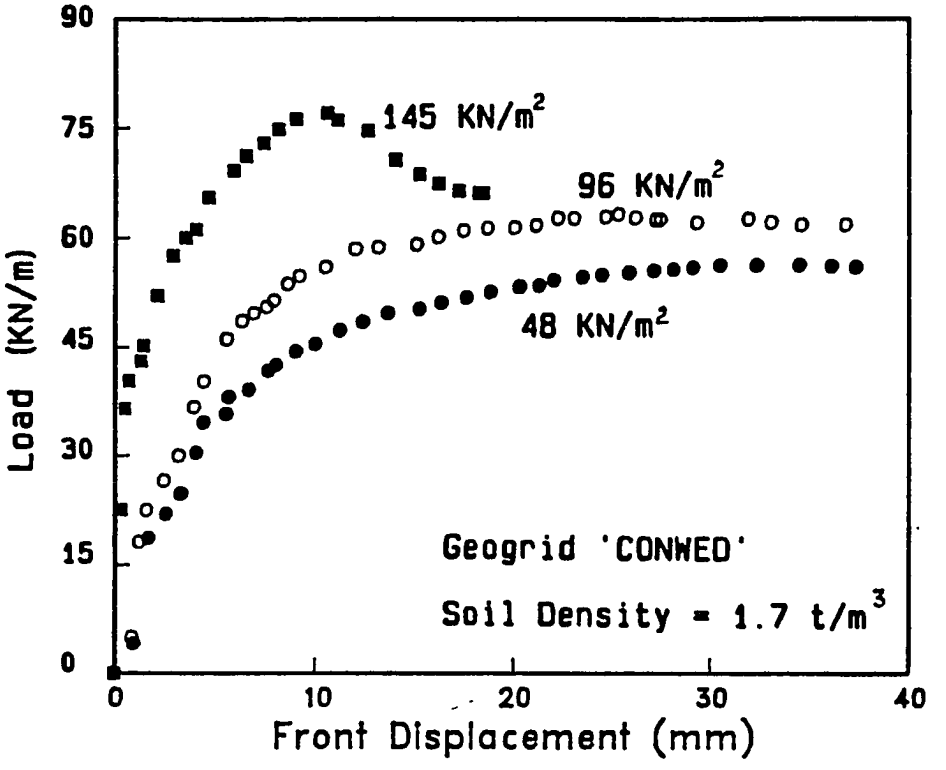

Figure 5.13 Effect of Confining Pressure on the Pull-out Resistance of 'Conwed' Geogrid.

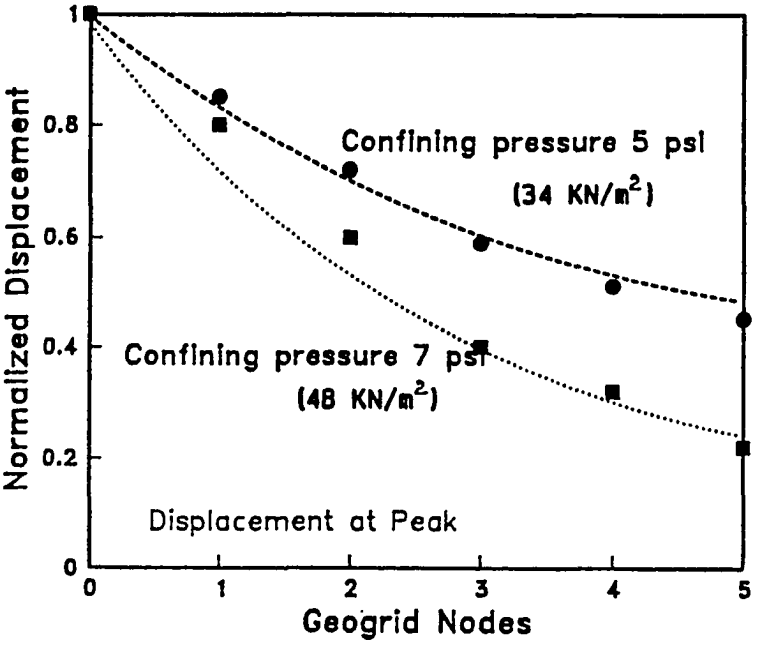

Figure 5.14 Effect of Confining Pressure on the Displacement Distribution Along the 'Tensar' Geogrid.

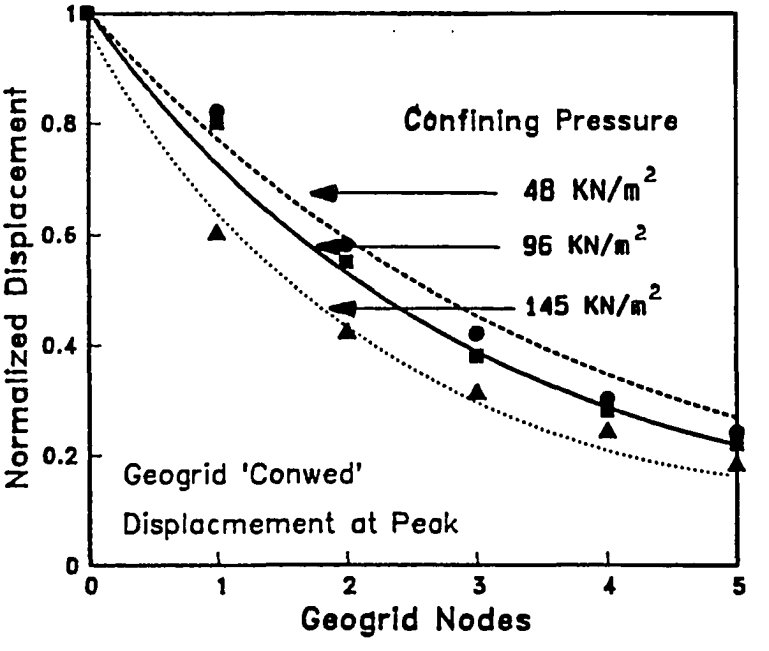

Figure 5.15 Effect of Confining Pressure on the Displacement Distribution Along the 'Conwed' Geogrid.

(v) Sleeve Length:

The interaction between the soil-inclusion system and the rigid front face of the pull-out box can affect the measured pull-out resistance. As the reinforcement is pulled-out of the box, lateral pressure develops against the rigid front face and results in an apparent increase of the geogrid pull-out resistance. This rigid boundary effect can be reduced by means of a sleeve incorporated around the slot in the front wall. These sleeves transfer the pull-out application point inside the soil mass far beyond the rigid front wall. The proposed standard ASTM testing procedure (1987) recommends the use of sleeves at the entrance with a minimum length of 500 mm (20 inch) in order to transfer the force into the soil far from the box front face.

In order to incorporate the effect of sleeve length in reducing the rigid front face effect, tests were conducted with different sleeve lengths, namely:

i) no sleeve at the front face,

ii) 8 in. sleeve length,

iii) 12 in. sleeve length.

These tests were performed with soils of average density of 104 pcf (1.67 t/m_3) and under a confining pressure of 7 psi (48.2 KN/m_2). Figure (5.16) shows the effect of the sleeve length on the 'Tensar' geogrid pull-out resistance. The results demonstrate that the increase in the sleeve length results in a reduction in the earth pressure developed at the front rigid wall and, consequently, a reduction of the pull-out resistance. The lateral pressure

developed at the facing was measured in these tests using two earth pressure cells fixed on the box rigid front wall at a 3 and 8 in. above the sleeve (see Figure 3.11). Figure (5.17) shows the development of lateral earth pressure on the front wall when no sleeves are incorporated . The initial lateral pressures recorded in both cells were approximately the same and were equal to 5 psi. The lateral earth pressure in the upper cell (cell#2) substantially increased to 15 psi, while lateral pressure of 7 psi was recorded at the lower cell. Figures (5.18) and (5.19) show the earth pressure recorded when sleeves of 8 and 12 in., respectively, were incorporated in the front face. The figures show a slight increase of earth pressure at cell#2, while the pressure readings in cell#1 remained practically constant.

The results demonstrate the significant affect of the sleeve length on the earth pressure measured at the front face. The use of the 8 in. sleeve results in a substantial reduction of the earth pressure on the front wall. The increase of the sleeve length from 8 to 12 in. has practically no effect on the lateral earth pressure. The relationship between the sleeve length and the developed lateral pressure on the front wall is shown in Figure (5.20). The figure shows that the increase in the lateral earth pressure during pull-out becomes negligible when a sleeve length of 12 in. is used. The effect of sleeve length on the displacement distribution along the geogrid is shown in Figure (5.21).

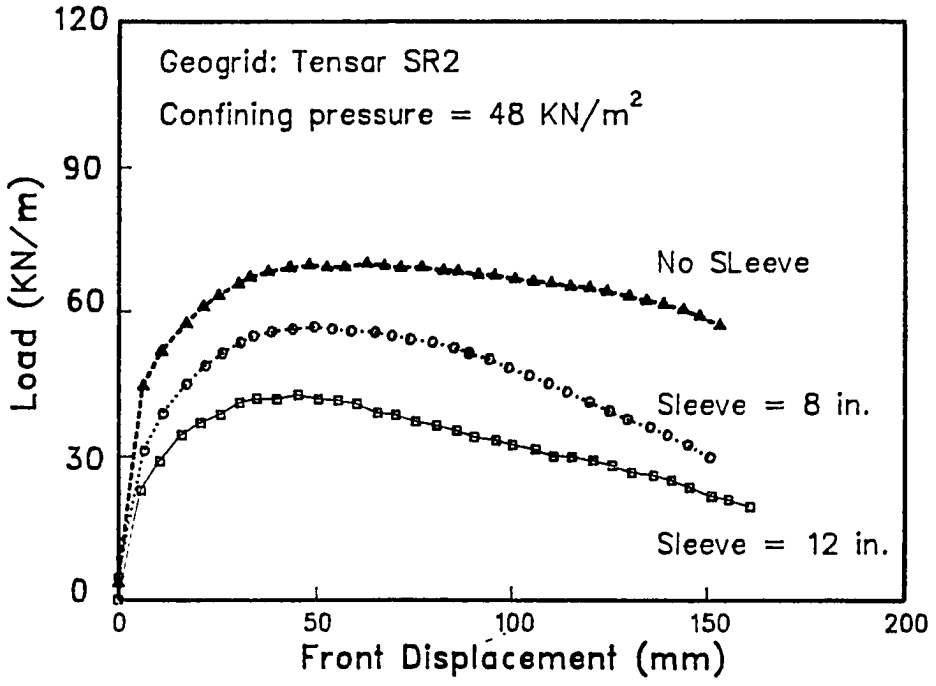

Figure 5.16 Effect of Sleeve Length on the Pull-out Response of 'Tensar' Geogrid.

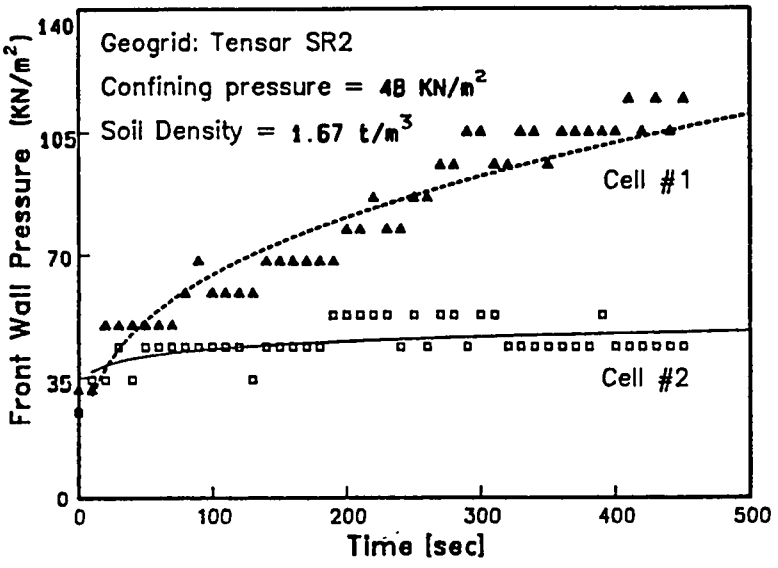

Figure 5.17 Development of Earth Pressure on the Front Wall in Case of No-Sleeve.

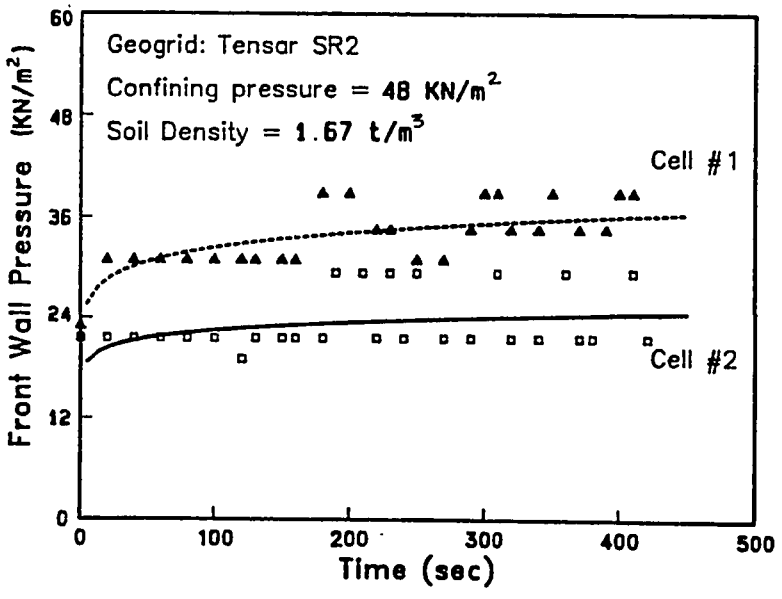

Figure 5.18 Development of Earth Pressure on the Front Wall in Case of 8 in. Sleeve.

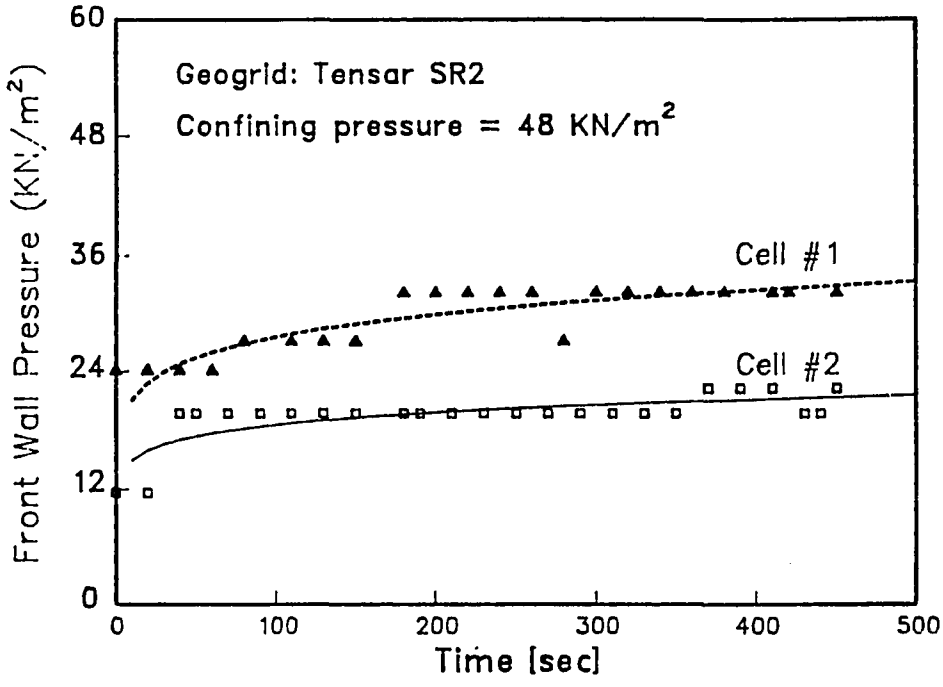

Figure 5.19 Development of Earth Pressure on the Front Wall in Case of 12 in. Sleeve.

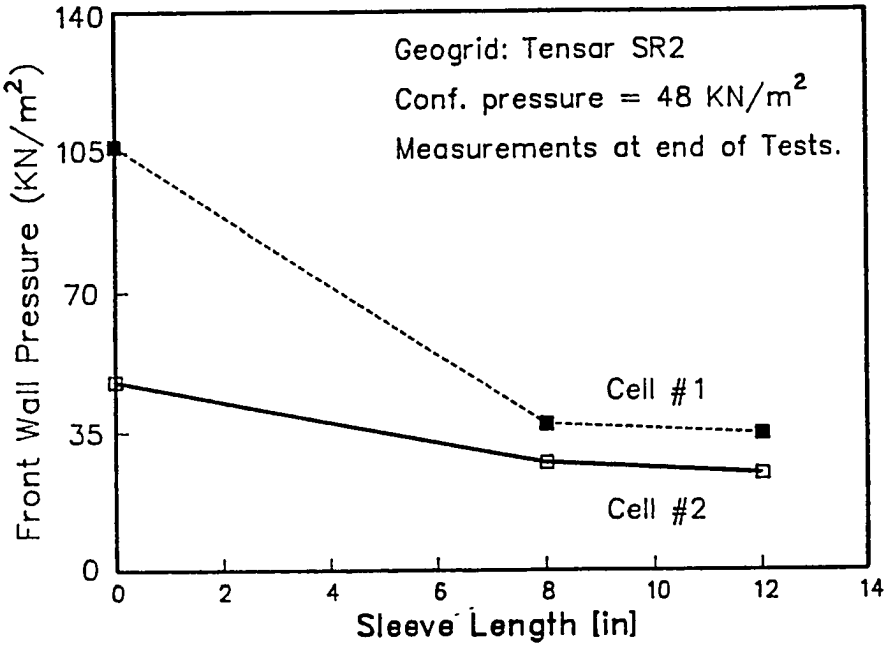

Figure 5.20 Effect of Sleeve Length on Lateral Earth Pressure.

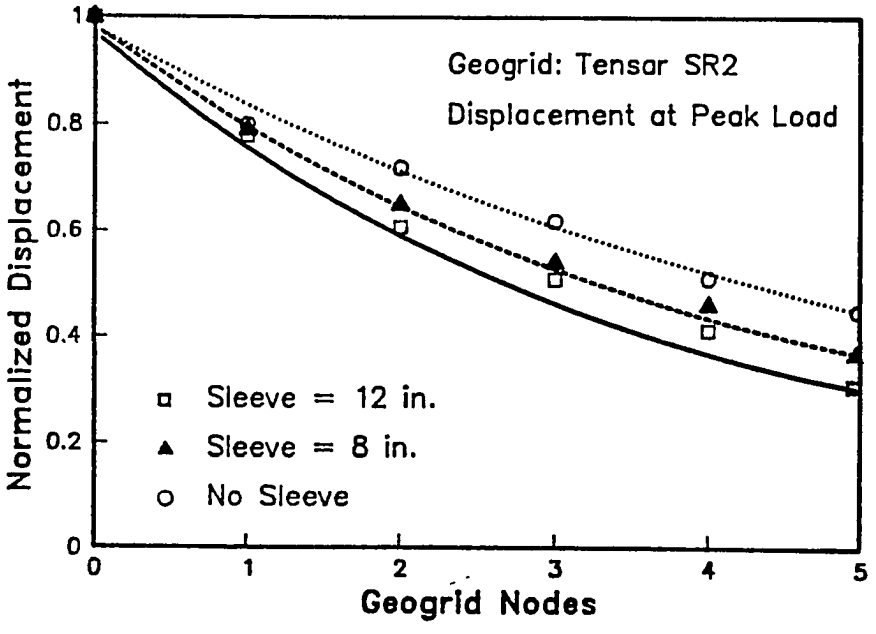

Figure 5.21 Effect of Sleeve Length on Normalized Displacement Along the Geogrid.

(vi) Thickness of the Soil :

The interaction between the soil, the geogrid and the rigid boundaries above and below the reinforcement can affect the pull-out test results. These rigid boundaries can cause an increase in the normal stresses in the vicinity of the geogrid surface if the soil thickness is small enough to restrain the soil dilatancy. Moreover, friction can develop between the top and bottom rigid boundaries and the soil which affects the soil-geogrid mobilized shear stress.

The proposed standard ASTM testing procedure (1987) recommends a minimum thickness of soil layer of 100 mm (2.5 inch) above and below the geosynthetic. In order to investigate the effect of the thickness of the soil on the pull-out response and to evaluate the proposed ASTM recommendations, pull-out tests were performed in soil samples of different thickness; namely:

i) soil thickness 10 cm above and 10 cm under the geogrid,

ii) soil thickness 10 cm above and 30 cm under the geogrid,

iii) soil thickness 30 cm above and 30 cm under the geogrid,

iv) soil thickness 40 cm above and 40 cm under the geogrid.

The above tests were performed on geogrid 'Tensar' under confining stress 7 psi (48.2 KN/m_2) and average soil density of 104 pcf(1.67 t/m_3). The effect of soil thickness on the pull-out response of the geogrid is shown in Figure (5.22) and the effect of the soil thickness on the normalized displacement along the geogrid is shown in Figure (5.23). The figures show that:

i) The decrease in soil thickness results in an apparent increase in the pull-

out strength of the geogrid.

ii) The decrease in soil thickness leads to higher shear stresses mobilized at the rear due to the developed frictional resistance.

iii) The increase in the soil thickness from 30 cm to 40 cm above and under the geogrid does not have any significant effect on the pull-out resistance of the geogrid.

These results lead to the conclusion that:

i) The proposed ASTM standard test method for measuring pull-out resistance (1987), which recommends a total pull-out box height of 20 cm, would lead to high pull-out response values due to the effect of the box boundaries above and under the reinforcement on the test results.

ii) The soil thickness of 30 cm (1 ft) above and under the reinforcement (a total of 2 ft soil thickness) is enough to eliminate the effect of the upper and the lower boundaries on the pull-out response.

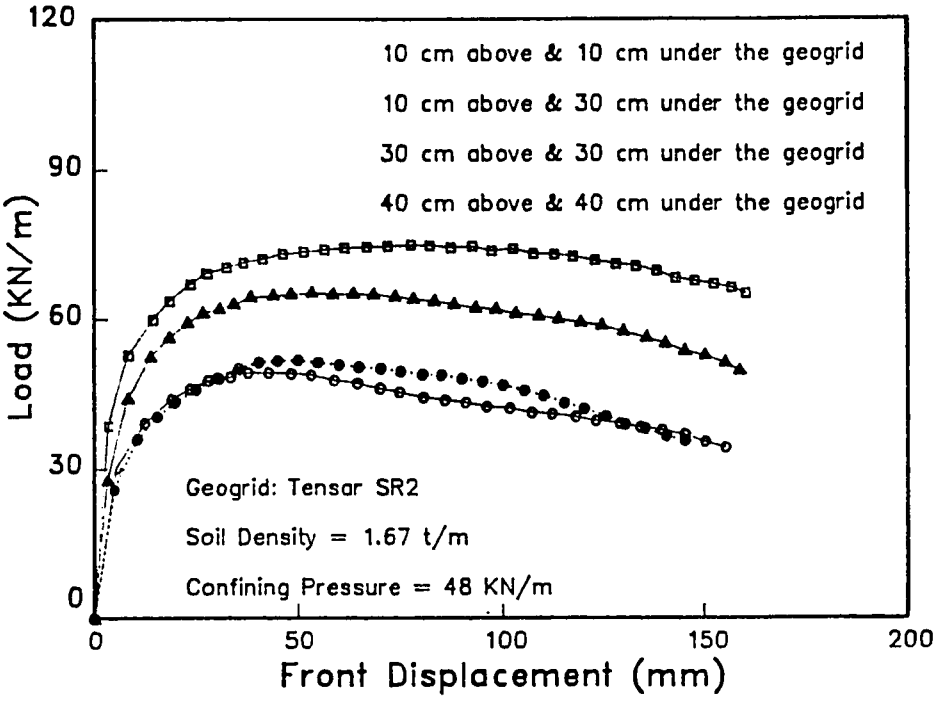

Figure 5.22 Effect of Soil Thickness on Pull-out Response.

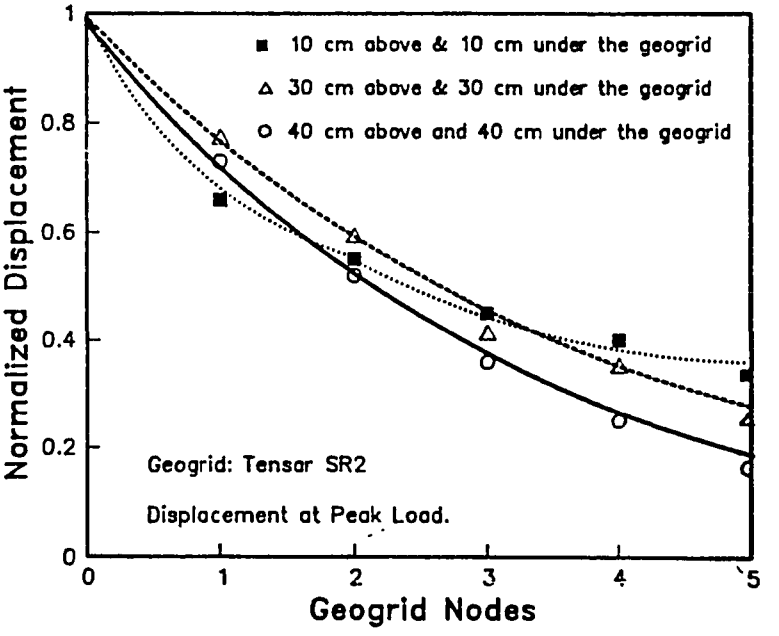

Figure 5.23 Effect of Soil Thickness on the Normalized Displacement Along the Geogrid.

CHAPTER 6

MODELING LOAD TRANSFER MECHANISM.

6.1) INTRODUCTION:

The design of soil-reinforcement systems requires an evaluation of the pull-out performance of the reinforcement with respect to three basic criteria:

i) The pull-out resistance of each reinforcement should be able to resist the working tensile force in the reinforcement with an adequate factor of safety.

ii) The front soil-reinforcement displacement, required to mobilize the pull-out resistance, should be smaller than the allowable design displacement.

iii) The long term creep load, and creep strain, should be smaller than the corresponding critical creep value.

In order to obtain the pull-out design parameters that satisfy the above criteria, a load transfer model based on the interpretation of pull-out test results has to be developed. This model should be able to evaluate the in-soil mechanical properties of the reinforcement (i.e. the in-soil stress-strain behavior of the reinforcement and its confined extension), and the soil-reinforcement properties at the interface (i.e. the interface shear stress-strain relationship and the reinforcement pull-out resistance).

The large number of factors that affect the interface properties raises difficulties in developing an interpretation procedure from pull-out test results.

These factors are usually related to:

i) testing: such as apparatus and sample dimensions, boundary conditions, strain rate, and the applied confining pressure,

ii) soil characteristics: such as its relative density, dilation properties, and fine grain portion of the soil,

iii) reinforcement: its type, geometry and extensibility.

The major concern in the interpretation of the pull-out tests results pertains to the effect of the reinforcement extensibility on the interaction pull-out parameters. Inextensible reinforcement (such as metallic strips) moves as a rigid member in the soil and the soil displacement required to mobilize the interface lateral friction is very small (Schlosser and Elias, 1978; and Schlosser et al., 1983). Such reinforcement develops a constant shear stress distribution along its length. While; for extensible reinforcement, its non-uniform extensibility results in a decreasing shear displacement distribution along its length. The interface shear stress is therefore not uniformly mobilized along the total reinforcement length. As the reinforcement extensibility depends upon its length, pull-out interface parameters become a function of the specimen length in pull-out tests. Therefore, the scale effect has to be evaluated in order to extrapolate pull-out test results to the reinforcement length in the field.

Several investigators (Jewell et al., 1984; Stewart et al., 1977) defined a soil-reinforcement resistance coefficient δ to be used in the shear strength

relationship:

$$\tau = \sigma_v \tan \delta \qquad \ldots\ldots\ldots\ldots\ldots\ldots \quad (6.1)$$

where, τ = shear stress at the interface,

σ_v = normal stress at the reinforcement level,

The pull-out resistance can then be calculated from the relationship:

$$P_r = 2 \cdot \gamma \; d \; \tan \delta \cdot L_e \qquad \ldots\ldots\ldots\ldots\ldots\ldots \quad (6.2)$$

where, P_r = pull-out resistance in force per unit width of the reinforcement,

γ = soil density,

d = thickness of soil above reinforcement,

L_e = length of reinforcement resisting pull-out force.

The disadvantage of this method is that it ignores the non-uniform shear stress distribution along the extensible reinforcement. It assumes an even distribution over the length and defines δ as the slope of the pull-out stress versus normal stress. Bonczkiewicz et al. (1988) modified the previous approach by distributing the mobilized shear stress over the actual portion of the elongated sample. They used wire extensometers to determine the sliding length of the reinforcement as the pull-out progress. The pull-out shear per unit ares can then be calculated as:

$$\text{Pull-out stress} = \frac{\text{mobilized load}}{\text{actual strained section x 2}} \qquad \ldots\ldots \quad (6.3)$$

The FHWA manual for the design of reinforced soil structures (Christopher et al., 1989) recommended a modified form of Equation (6.2), to include the

effect of extensibility, in determining the pull-out resistance:

$$P_r = F^* . \alpha . \sigma_v . L_e . c \quad \ldots\ldots\ldots\ldots (6.4)$$

where,

F^* is a pull-out resistance factor obtained from pull-out tests performed in the specific backfill,

c is the reinforced unit perimeter [c = 2 for grids and sheets],

α is a scale effect correction factor.

The scale effect correction factor represents the nonlinearity of the P_r-L_e relationship due to extensibility. For inextensible reinforcement, α is approximately 1. For extensible reinforcement, α can be determined from the equation:

$$\alpha = \frac{\tau_{avg.}}{\tau_p} \quad \ldots\ldots\ldots\ldots (6.5)$$

where τ_{avg} and τ_p are, respectively, the average and ultimate interface lateral shear stresses mobilized along the reinforcement. The disadvantage of this empirical formula is that α depends primarily upon the interface shear strain softening and not, explicitly, upon the extensibility of the reinforcement. However, the manual recommends performing pull-out tests on reinforcements with different lengths or using an analytical or numerical load transfer model to obtain the scale effect factor.

Solomone et al. (1980) proposed another methodology for obtaining the soil reinforcement resistance coefficient δ by using the slope of the relationship

between the pull-out force and the mobilized length of the reinforcement (K_r). The mobilized length of the reinforcement was found by assuming that movement at a wire gauge at a specific location along the reinforcement indicated pull-out at that point. The slope K_r can then be implemented, to determine δ, in the relationship:

$$K_r / 2b = \sigma_v \, . \, \tan \delta \qquad \ldots\ldots\ldots\ldots\ldots \quad (6.6)$$

where b is the reinforcement width. The limitation of this method is that it assumes a uniform distribution of the pull-out force along the reinforcement, in the form of the slope K_r, which is not the case in extensible reinforcement.

The review of the previous approaches shows the limitations of most of these methods regarding the assumptions of uniform shear stress-strain distributions along the reinforcement. The concept of a uniformly mobilized interface shear stress which can be used for inextensible reinforcement can not be adequately used for the interpretation of pull-out tests in extensible reinforcement. In order to develop an appropriate load transfer mechanism, an instrumentation scheme should be implemented in pull-out tests to measure the interface shear strain at different points along the reinforcement.

Different investigators evaluated the interface shear strain distribution in extensible reinforcement by obtaining measurements along the length of the pull-out specimens. Figure (6.1) shows the displacement distribution along instrumented geotextile specimen in a large box pull-out test (after Tzong and

Cheng-Kuang, 1987). Figure (6.2) shows the pull-out resistance distribution along the length of the instrumented geotextile specimen in the pull-out box (after Bonczkiewizc et al., 1988).

Leshchinsky and Field (1987) measured the load on both ends of non-woven geotextile specimens using the pull-out test apparatus shown in Figure (2.3). The relationships between the applied load versus front and rear displacements are shown in Figure (6.3). A second degree polynomial function was assumed to interpolate the displacement U(x) at any location x along the length of the fabric:

$$U(x) = K_0 + K_1 . x + K_2 . x^2 \qquad \ldots\ldots\ldots\ldots \quad (6.7)$$

A linear distribution of the elongation along the specimen could then be calculated (by integrating equation 6.7) and, consequently, the tensile force distribution along the specimen can be calculated.

Juran and Chen (1988) proposed a theoretical load transfer model derived from the (t-z) method commonly used in design of friction piles along with the appropriate constitutive equations. Figure (6.4) shows the numerical simulation of the pull-out resistance using this model along with the experimental results.

In this chapter; the displacement measurements at different points along the specimens in the pull-out tests along with the appropriate interaction laws (relating the shear strain at any point along the reinforcement to the mobilized shear stress at the interface) are used to develop a load transfer model. In this

model; the interpretation procedure for the displacement-rate controlled pull-out tests on the instrumented geogrid permits the determination of: (a) the in-soil confined material properties, (b) the soil-geogrid interface properties, and (c) the scale effect of the specimen length on the pull-out interface parameters. This procedure is evaluated through comparison of the interface properties derived from the pull-out tests with those obtained directly from the direct shear tests. The load controlled pull-out test results are also used to asses the critical creep pull-out load and to predict the long term creep displacement under a specified pull-out load.

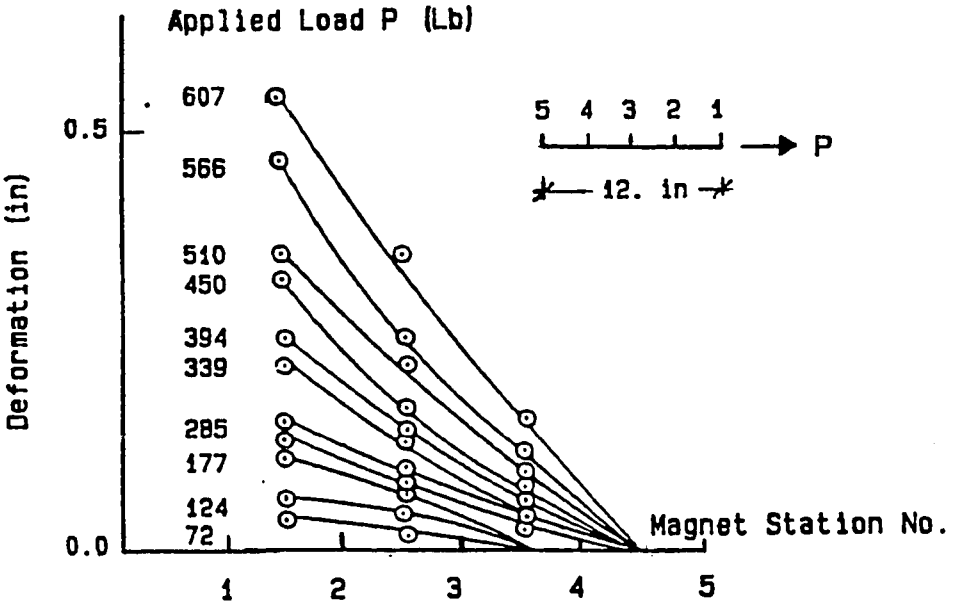

Figure 6.1 Deformation along the Geotextile.
(after Tzong and Cheng-Kuang, 1987)

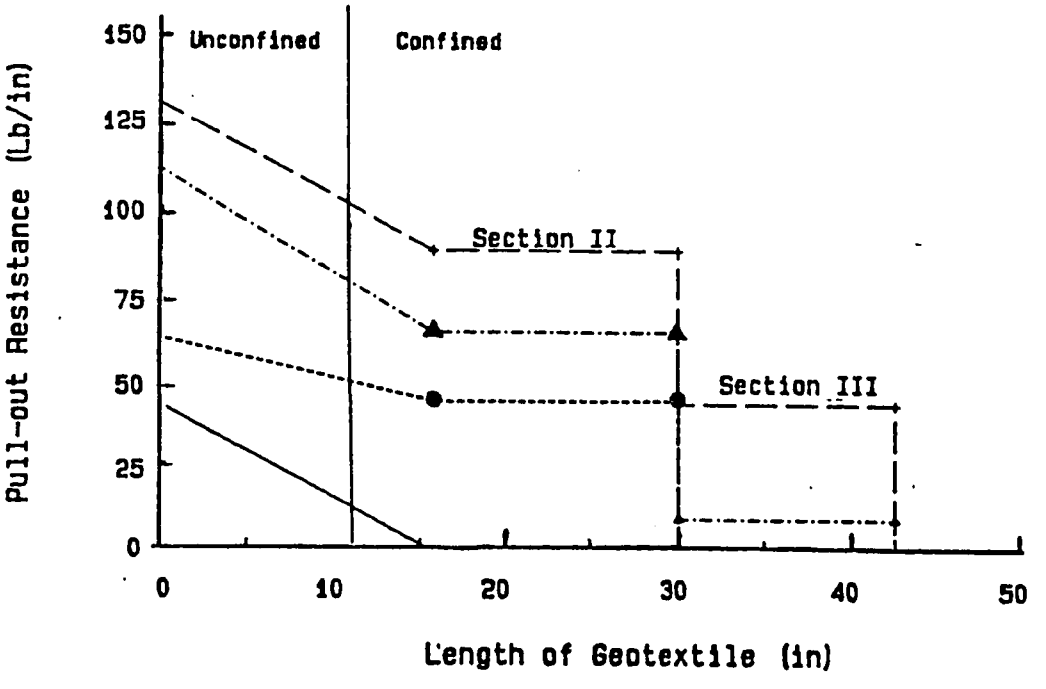

Figure 6.2 Distribution of Pull-out Resistance along Geotextile
(after Bonczkewitz et al., 1988)

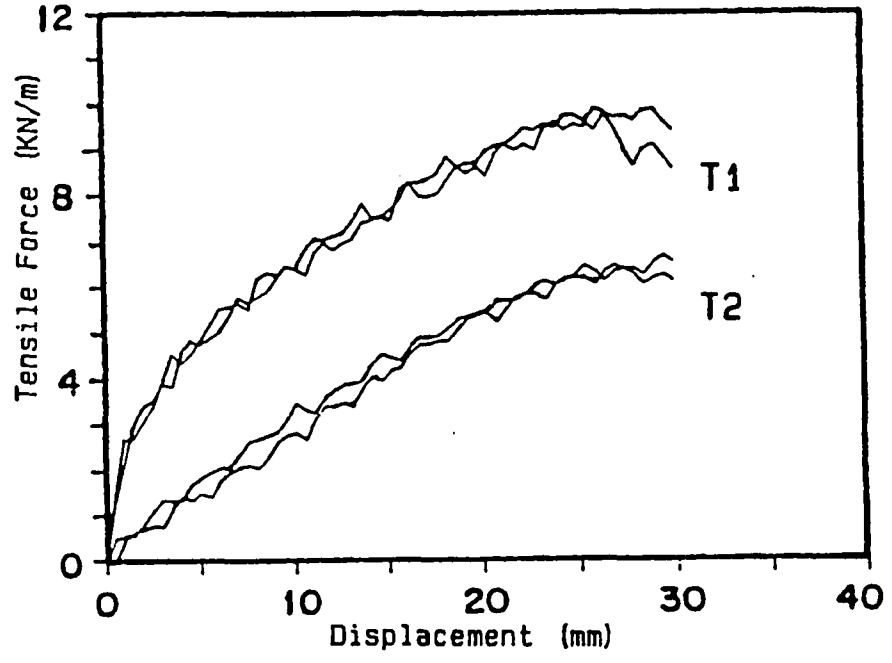

Figure 6.3 Applied Load versus Front and Rear Displacement
(after Leshchinsky and Field, 1987)

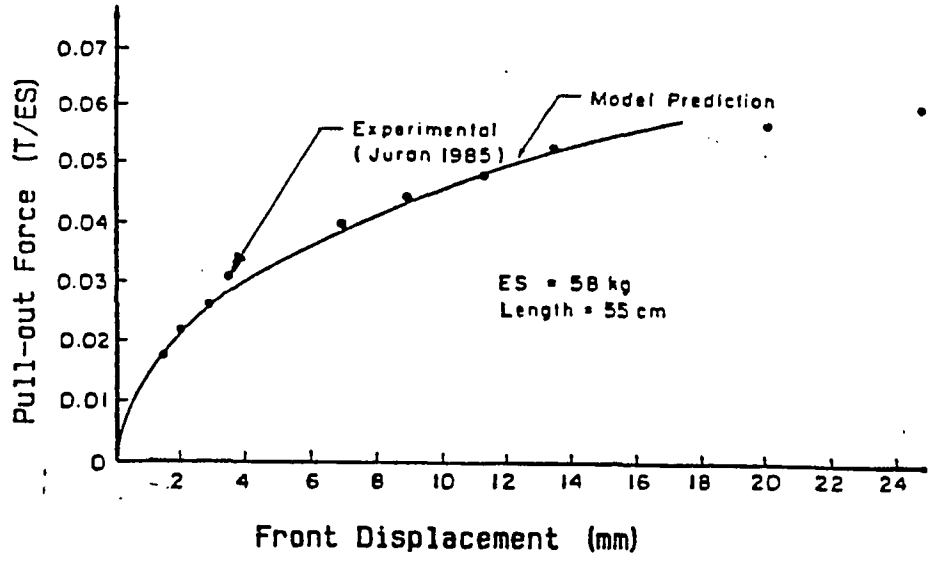

Figure 6.4 Numerical Simulation of Pull-out Test on Woven Strips
(after Juran and Chen, 1988)

6.2) MODELING LOAD TRANSFER IN DISPLACEMENT-RATE CONTROLLED PULL-OUT TESTS:

The proposed data analysis procedure is illustrated through the interpretation of the displacement-rate controlled pull-out tests results presented in the previous chapters. This procedure consists of the following steps:

(1) From the Time-Nodal displacements relationship (see Figures 4.13 and 4.14), the displacements distribution along the reinforcement can be plotted for different pull-out loads. Figures (6.5) and (6.6) show the displacement distribution along the specimen length obtained from Tests on geogrid 'Tensar' under confining pressure of 7 psi. Figure (6.7) shows the displacements distribution for geogrid 'Conwed'. From the discretized elements along the geogrid reinforcement (Figure 6.8), it can be seen that the displacement of each element i results from the elongation of the element (i.e. $\delta_{i-1} - \delta_i$) and its shear displacement δ_i.

2) The strain ϵ_i of each element i can be calculated from the relation:

$$\epsilon_i = [\, \delta_{i-1} - \delta_i \,] / \Delta x \qquad \ldots\ldots\ldots\ldots \quad (6.8)$$

where δ_{i-1} and δ_i are, respectively, the displacements at nodes i-1 and i, and Δx is the length of element i.

(3) The in-soil geogrid stress (force/unit width) versus strain can now be plotted for the front element of the geogrid. Figure (6.9) shows the confined stress-strain relationship for geogrid 'Tensar'; while Figure (6.10) shows the same relationship for geogrid 'Conwed'. For the sake of comparison, the

unconfined stress-strain relationships for the two geogrids are plotted in their respective figures. The figures show that confinement results in a substantial increase of the stiffness modulus E.t (where t is the reinforcement thickness). This comparison illustrates that the design criteria for geogrid reinforcement should be based upon the confined properties derived from pull-out tests rather than the unconfined material properties.

(4) The confined stress-strain properties (e.g. stiffness modulus E.t) obtained under a specific confining pressure are assumed to be unique for each geogrid material. The E.t values can be determined from the slope of the stress-strain curve at each loading level.

(5) The tension force T_i at each node i can be calculated from the relationship:

$$[T_{i-1} - T_i] / b = E.t. [\delta_{i-1} - \delta_i] / \Delta x \quad \ldots\ldots\ldots\ldots (6.9)$$

(6) The shear stress distribution along the specimen can be calculated from the static equilibrium equation of each element i:

$$[T_{i-1} - T_i] = \tau_i . P . \Delta x \quad \ldots\ldots\ldots\ldots (6.10)$$

where P is the geogrid perimeter [= 2b].

(7) The shear stress-strain relationship at the interface can then be plotted for all the elements of the geogrid. Figures (6.11) and (6.12) show the shear stress-displacement curves derived from the pull-out test results on the 'Tensar' geogrid; while Figure (6.13) shows the same relationship for geogrid 'Conwed'.

In order to validate the analysis procedure, the shear stress-displacement curves calculated for the 'Tensar' geogrid were compared with those obtained directly from tests performed in the large direct shear box under the same confining pressure and soil relative density. The results, shown in Figure (6.14), confirm the applicability of the proposed procedure.

The analysis of pull-out test results on the geogrid reinforcement illustrates the non-uniformity of the displacement distribution along the geogrid length (see Figures 6.5 to 6.7). The peak shear stress mobilized at the interface is a function of the sample length. Therefore, the extrapolation of the pull-out test results to reinforcements of different lengths should be considered when pull-out test results are implemented into design. The established interface properties and confined stress-strain relationships of the reinforcement could be implemented to back calculate the displacement distribution along the geogrid of any length under the same testing conditions. Thereby, laboratory pull-out test results could be extrapolated to full scale reinforcement length. The interpretation procedure to back calculate the displacement distribution and the mobilized pull-out force along reinforcement of a specified length is as follows:

(1) The reinforcement length is discretized to n number of elements, see Figure (6.8). The displacement δ_{n+1} at the end is assumed to be zero and, consequently, the mobilized force at the end T_{n+1} is also zero.

(2) The value of displacement at node (n) is assumed and the strain at element n can be calculated from equation (6.8).

(3) From the established shear stress-strain relationship (Figures 6.11 to 6.13), the shear stress at the interface of element n can be obtained.

(4) The pull-out force T_n is calculated from the equilibrium equation of element n (equation 6.10).

(5) From the confined stress-strain relationship (Figures 6.9 and 6.10), the stiffness modulus E.t (at the strain level of element n) is obtained.

(6) The pull-out force T_n can then be calculated from equation (6.9).

(7) The value of T_n from step (6) is checked with the one calculated in step (5). An iteration technique is used to obtain T_n value within a limited error.

(8) The same procedure is repeated at element n-1 and up to the facing element.

This analytical procedure was used to predict the displacements and the pull-out forces at the nodes of geogrid reinforcements of lengths 1.5 ft, 3 ft and 6 ft. The calculated displacements for the reinforcements of lengths 1.5 ft and 3 ft were compared, in Figure (6.15), with the measured ones. The figure also shows the predicted displacement distribution along geogrid reinforcement of 6 ft length. The analytical results of the pull-out forces along the geogrids are shown in Figure (6.16). The comparison between the analytical and experimental results illustrates the applicability of the proposed procedure.

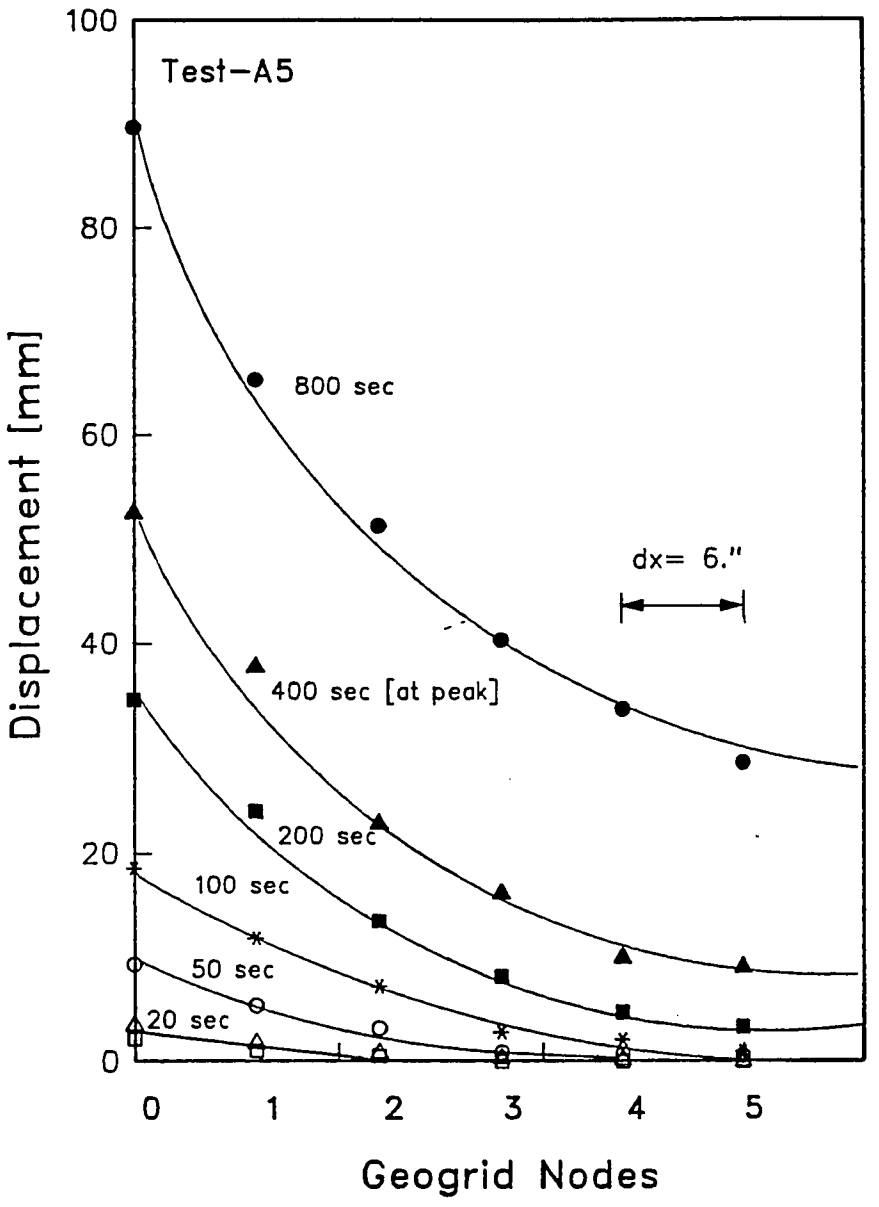

Figure 6.5 Displacement Distribution Along Geogrid 'Tensar'.

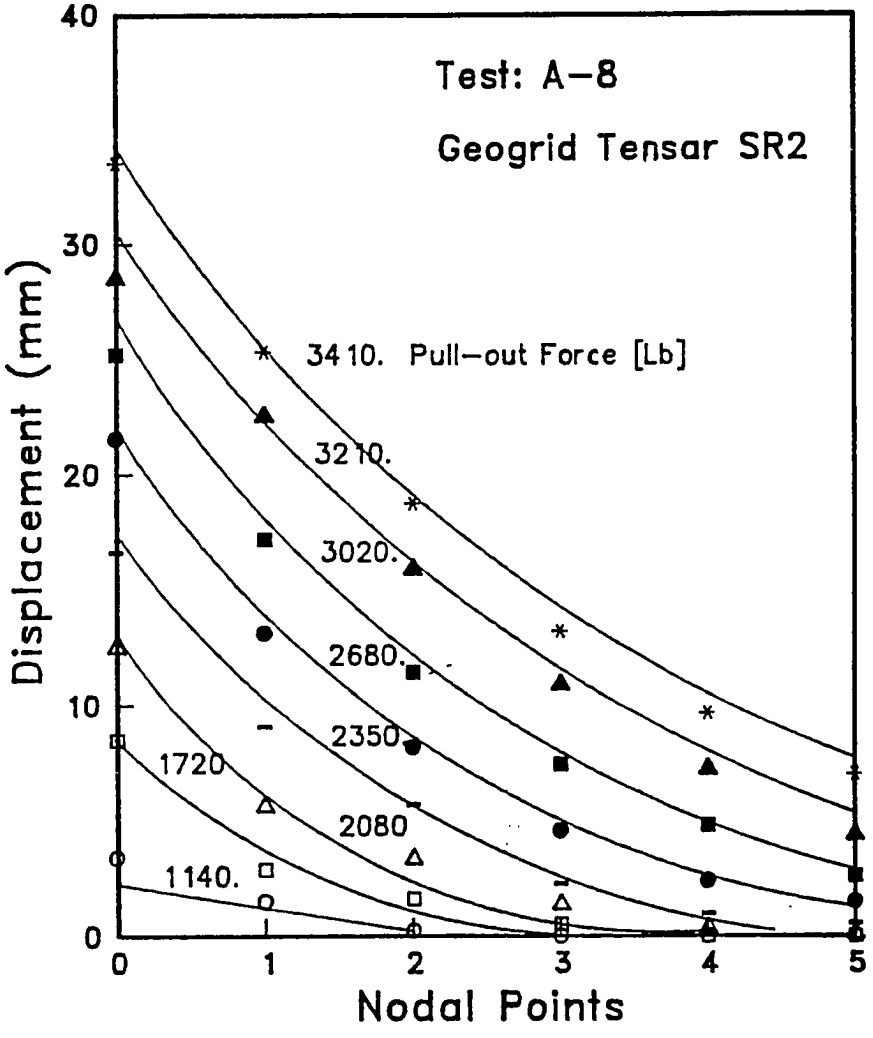

Figure 6.6 Displacement Distribution Along Geogrid 'Tensar'.

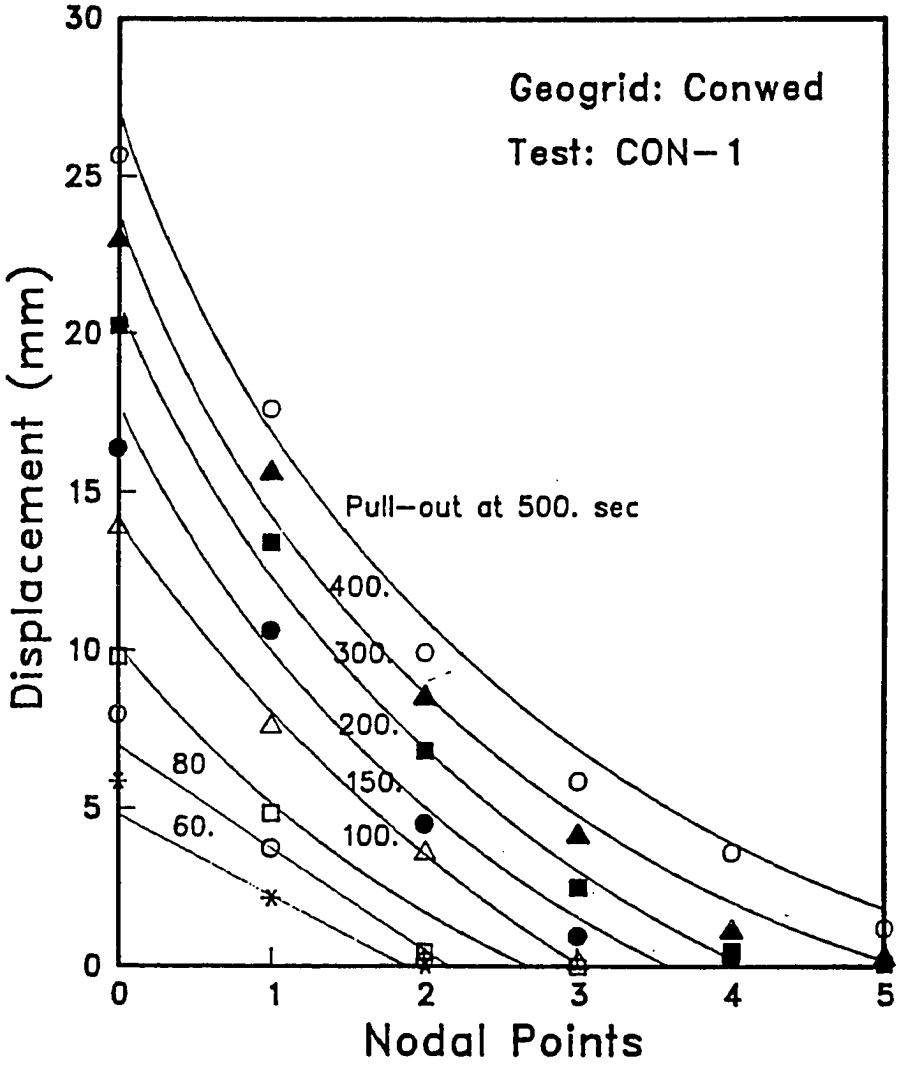

Figure 6.7 Displacement Distribution Along Geogrid 'Conwed'.

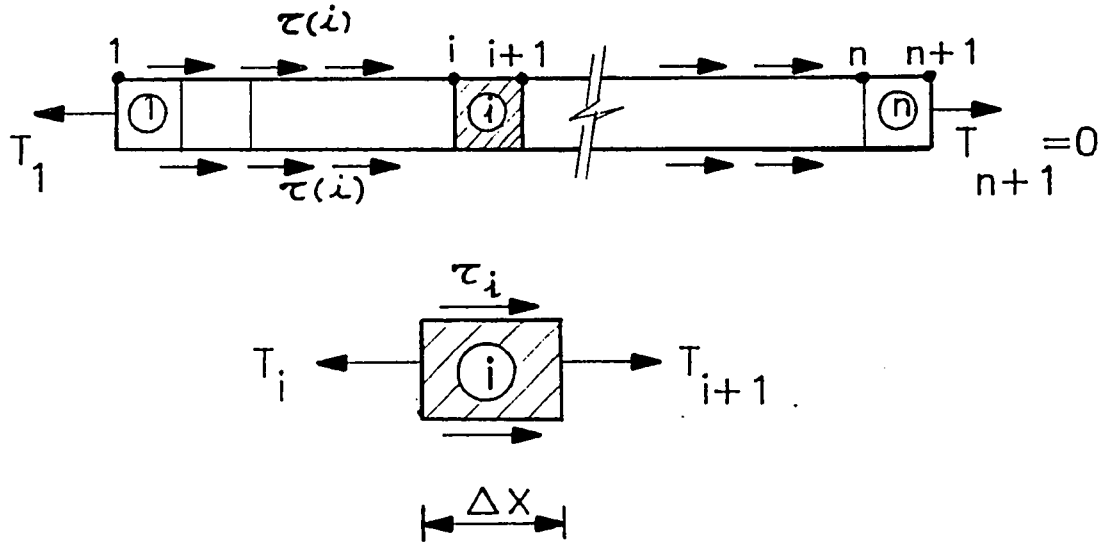

Figure 6.8 Numerical Analysis of Pull-out Tests.

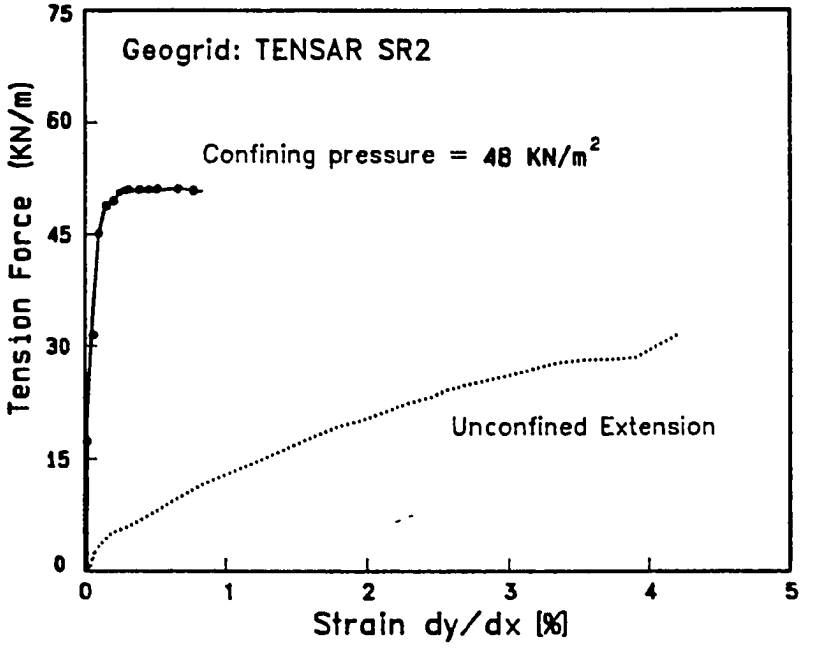

Figure 6.9 Confined and Unconfined Stress-Strain Relationship for Geogrid 'Tensar-SR2'.

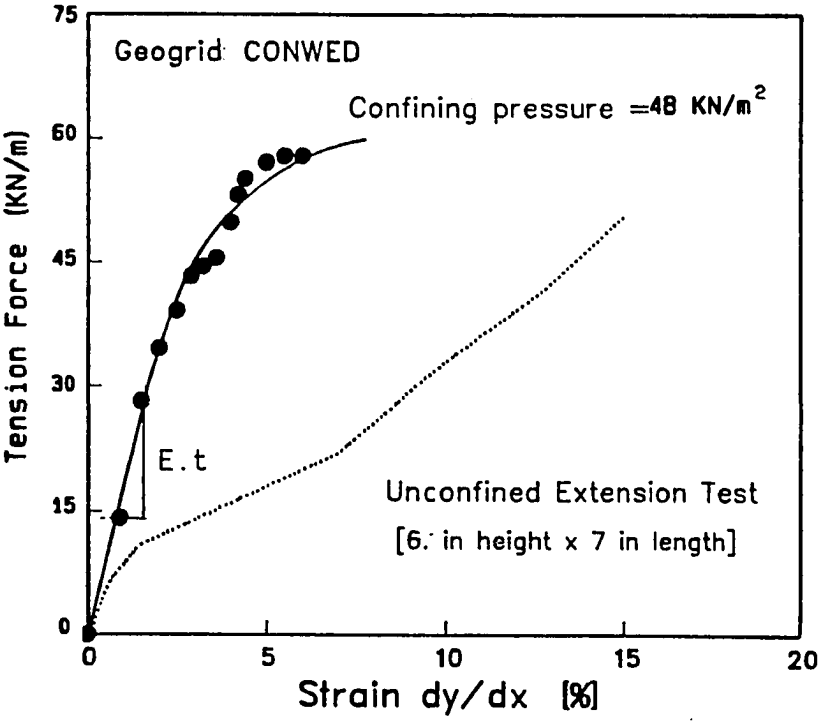

Figure 6.10 Confined and Unconfined Stress-Strain Relationship For Geogrid 'Conwed'.

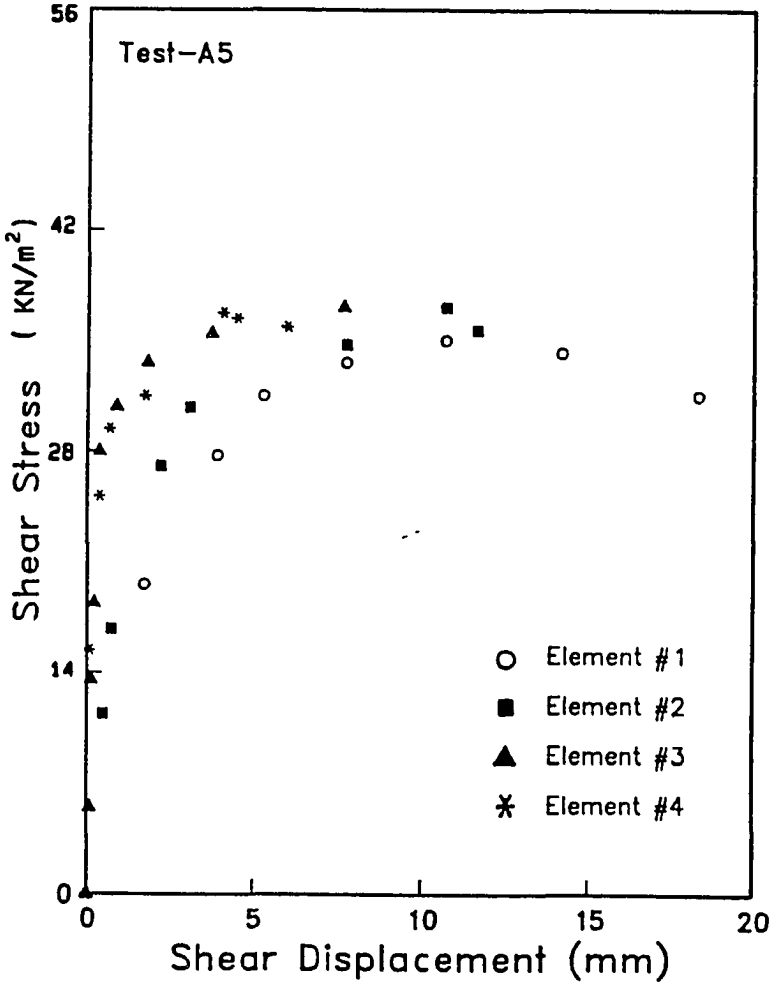

Figure 6.11 Interface Shear Stress-Displacement Relationship for Geogrid 'Tensar-SR2'.

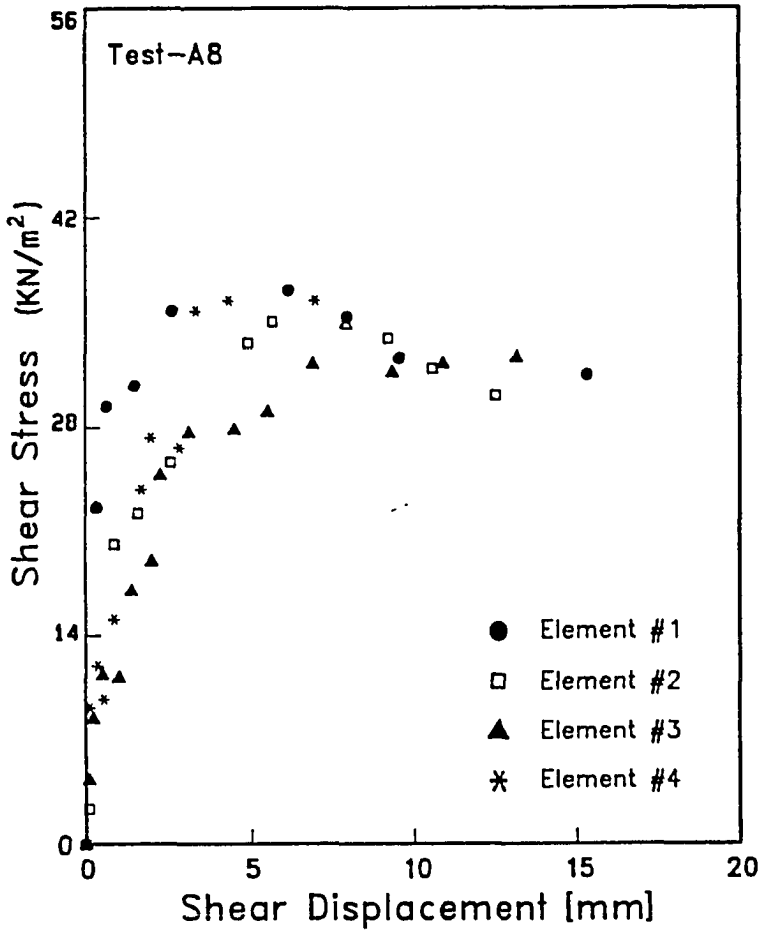

Figure 6.12 Interface Shear Stress-Displacement Relationship *for Geogrid 'Tensar-SR2'.*

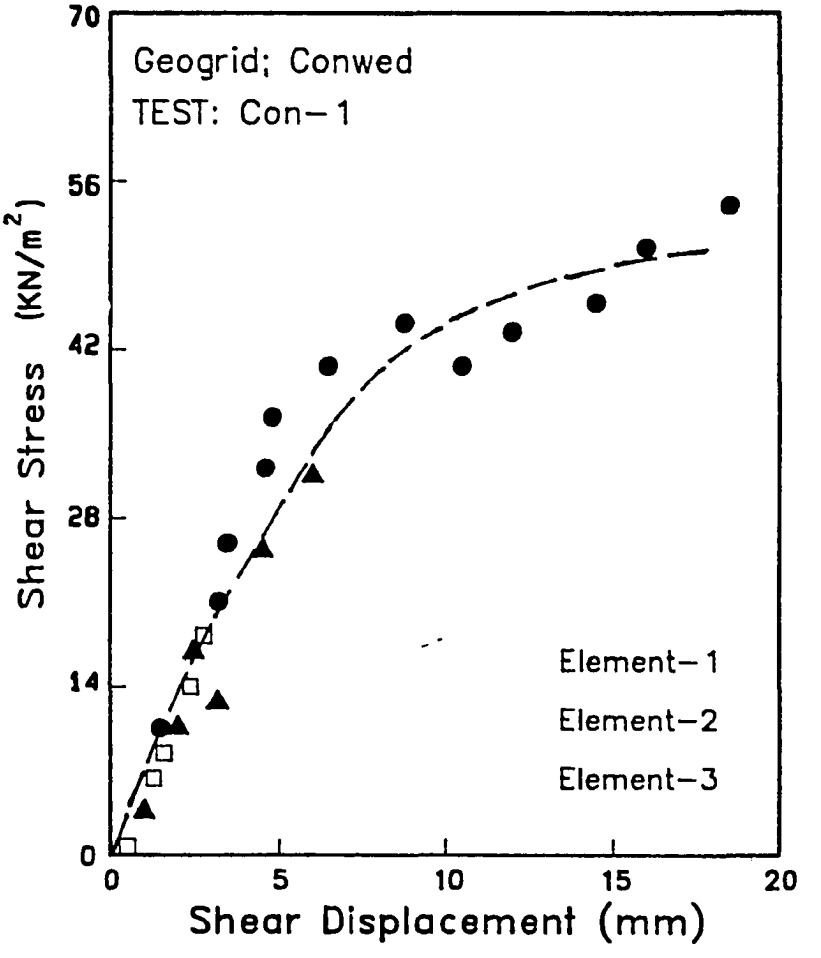

Figure 6.13 Interface Shear Stress-Displacement Relationship for Geogrid 'Conwed'.

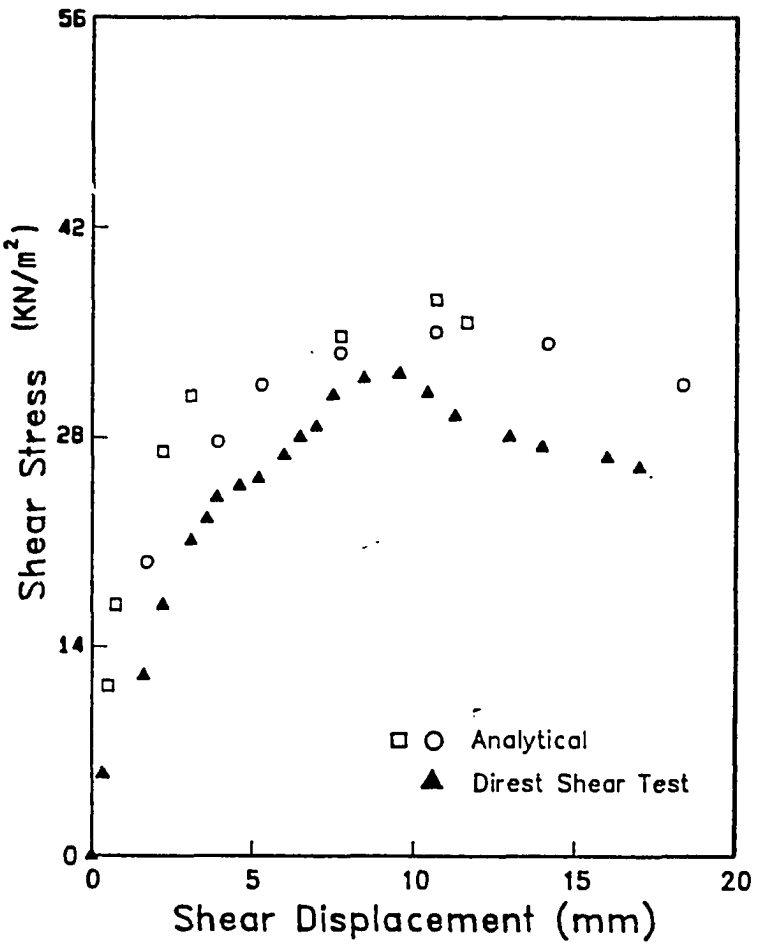

Figure 6.14 Analytical and Experimental Interface Shear Stress-Displacement Relationship for Geogrid 'Tensar-SR2'.

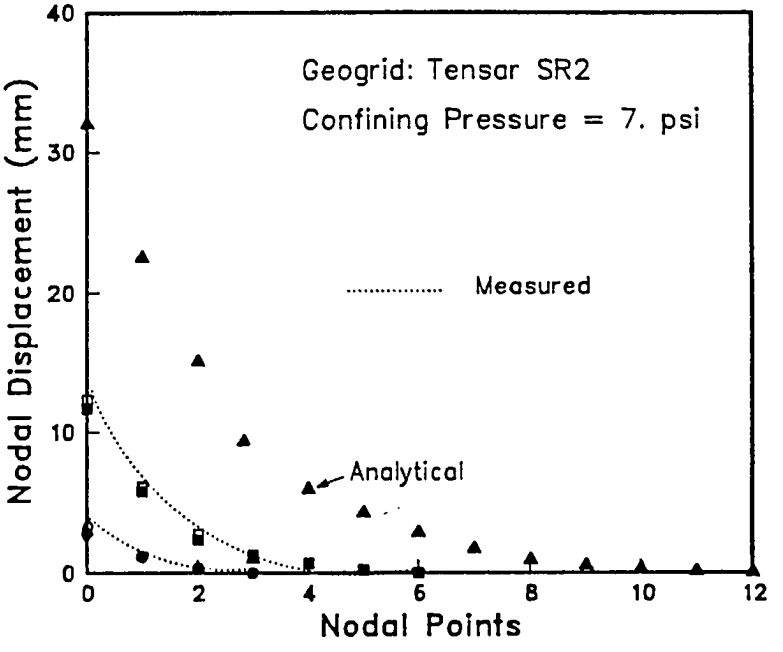

Figure 6.15 Analytical and Experimental Displacement Distribution along the Geogrid Length.

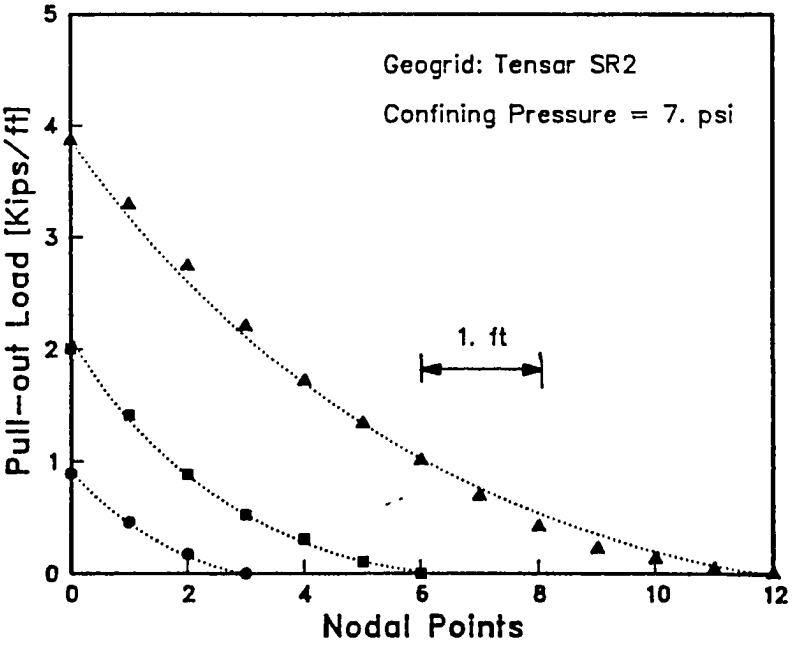

Figure 6.16 Analytical Pull-out Load Distribution along The Geogrid Length.

6.3) ANALYSIS OF LOAD-CONTROLLED PULL-OUT TESTS:

The process of time-dependent deformation of the geogrid subjected to a constant stress displays generally three stages; in addition to its instantaneous deformation. These stages are (see Figure 4.18):

i) Stage I (Primary Creep): A non-steady state creep where deformations develop at a decreasing rate.

ii) Stage II (Secondary Creep): A stage of steady state creep where the deformation rate reaches a minimum value and then stays constant.

iii) Stage III (Tertiary creep): Where the deformation develops at an increasing rate and ends at failure.

The duration and effect of any particular stage vary with the geogrid type and load. The engineering concern in the long term stability of reinforced earth structures is to determine the critical load level and displacement at which the secondary creep stabilizes and before the tertiary creep starts to develop. Since these properties depend on the time available for observations, an accurate experimental approach is a difficult and time consuming task. Deformations which may appear to be stabilizing may develop if observed for a longer period of time.

The instrumentation for displacement measurements along the geogrids permitted the calculation of creep strains when the geogrid is subjected to stepped creep loads. Pull-out tests were conducted on 'Conwed' geogrids where the specimens were subjected to creep loads of 50%, 65% and 85% of

maximum pull-out load. Figures (6.17) and (6.18) show the displacement measurement at different nodes along the geogrid at 65% Tmax and 85% Tmax, respectively. The calculated creep strains are plotted with time in Figures (6.19) and (6.20) for load levels 65% Tmax and 85% Tmax, respectively. Figure (6.20) shows accelerating creep strain at the "Conwed' geogrid when it is subjected to pull-out load of 85% Tmax. The unconfined creep strains under the same loading levels are plotted in their respective figures. The comparison between the unconfined and confined creep strains shows that confinement causes lower creep strains under the same loading levels.

The creep strain under a sustained load at time t can be analyzed by utilizing the pull-out creep test results into the relationships proposed by Singh and Mitchell (1968). These relationships are based on the following observations:

(i) A relationship between strain rate (ϵ) and time exists for many clays subjected to loadings within the range of 30% to 90% of strength. This relationship is illustrated by a form of a plot between the log-strain rate and log-time (Figure 6.21). The Figure shows that log-strain rate decreases linearly with log-time with a slope (m) independent of creep load. This relationship can be expressed as:

$$\text{Log } \epsilon = \text{Log } \epsilon(t_1,T) - m \text{ Log } (t/t_1) \quad \ldots\ldots\ldots\ldots\ldots\ldots \quad (6.11)$$

Where, ϵ = strain rate at any time t,

$\epsilon\ (t_1,T)$ = strain rate at unit time t_1 and load T.

(ii) A relationship between log-strain rate and the practical range of applied loads (T) can be expressed linearly (Figure 6.22) as:

$$\text{Log } \epsilon = \text{Log } \epsilon(t,T_0) + \alpha T \quad \ldots\ldots\ldots\ldots\ldots\ldots\ldots\ldots (6.12)$$

Where, $\epsilon(t,T_0)$ = strain rate obtained by projecting the straight line of the relationship to T = 0,

α = slope of the straight line portion of the log-strain rate versus load.

Combining equations (6.11) and (6.12) and integrating we get:

$$\epsilon = \epsilon_1 + \left(\frac{A}{1-m}\right) e^{\alpha T} (t - 1)^{1-m} \quad \text{for } m \neq 1 \quad \ldots\ldots\ldots (6.13\text{-a})$$

$$\epsilon = \epsilon_1 + A\, e^{\alpha T} \text{Log } (t) \quad \text{for } m = 1 \quad \ldots\ldots\ldots (6.13\text{-b})$$

Where $A = \epsilon(t_1,T_0)$. Equation (6.13) is a simple three parameter relationship between strain and time which is found to be applicable to different kinds of soils (Singh and Mitchell, 1968). Shrestha and Bell (1982-b) investigated its applicability to predict creep strains for different kinds of geotextiles. The relationship between log-strain rate versus log-time for geogrid 'Conwed' is shown in Figure (6.23) for different pull-out levels. The figure shows a linear relationship at load levels of 50% and 65% of Tmax. Figure (6.24) shows the relationship between the log-strain rate versus loading levels T normalized with respect to the maximum pull-out load Tmax.

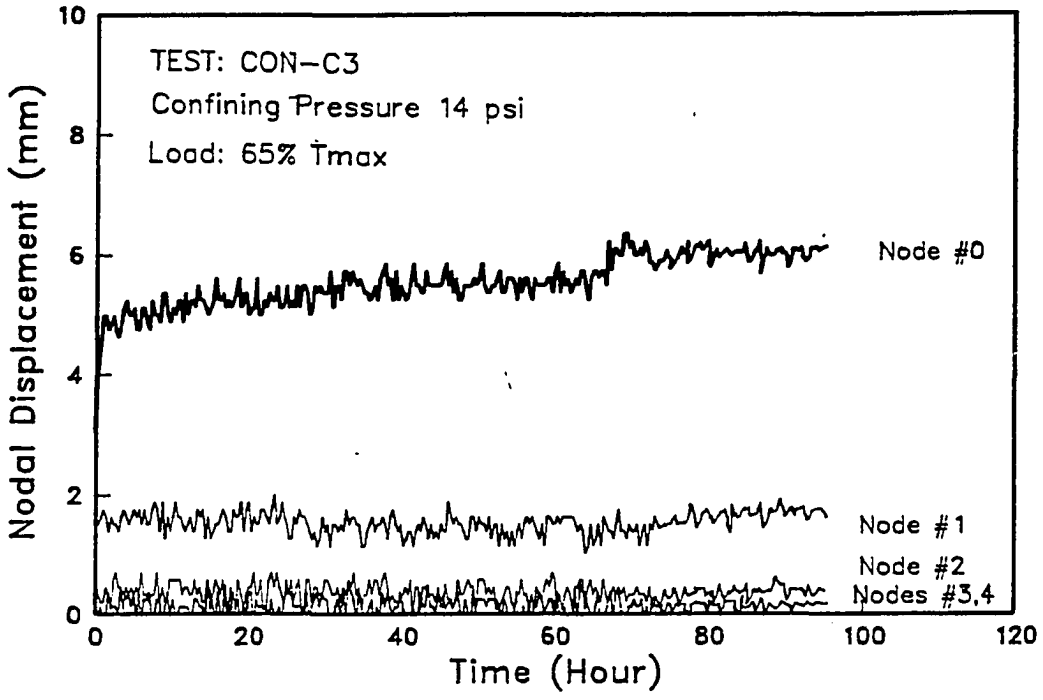

Figure 6.17 Nodal Displacements at Load-Controlled Pull-out Test on Geogrid 'Conwed'

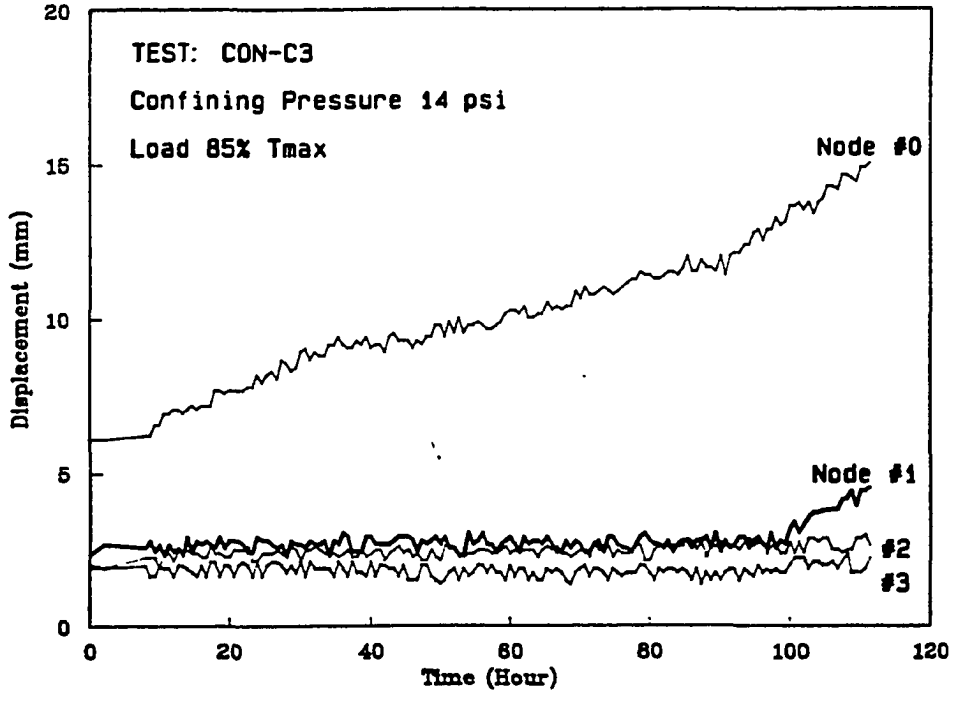

Figure 6.18 Nodal Displacements at Load-Controlled Pull-out Test on Geogrid 'Conwed'

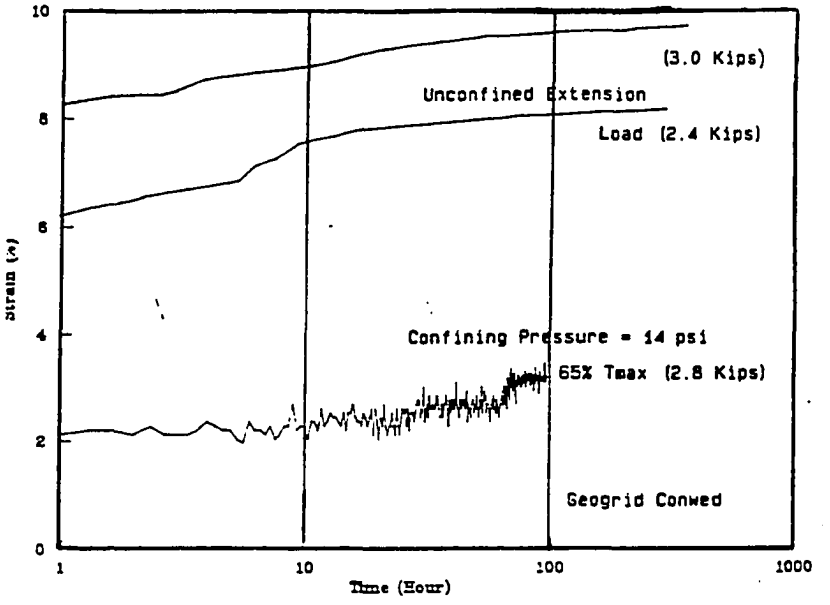

Figure 7.19 Confined & Unconfined Creep Strain for Geogrid 'Conwed'.

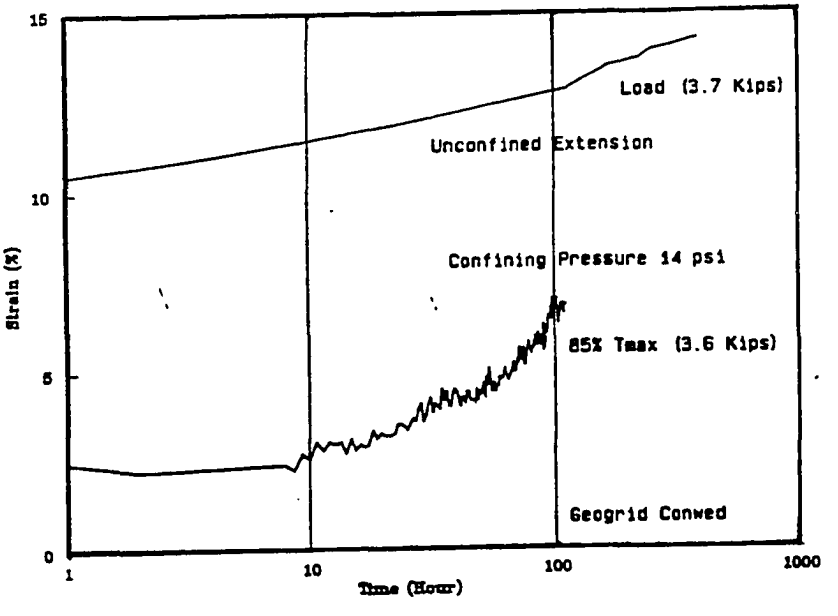

Figure 7.20 Confined & Unconfined Creep Strain for Geogrid 'Conwed'.

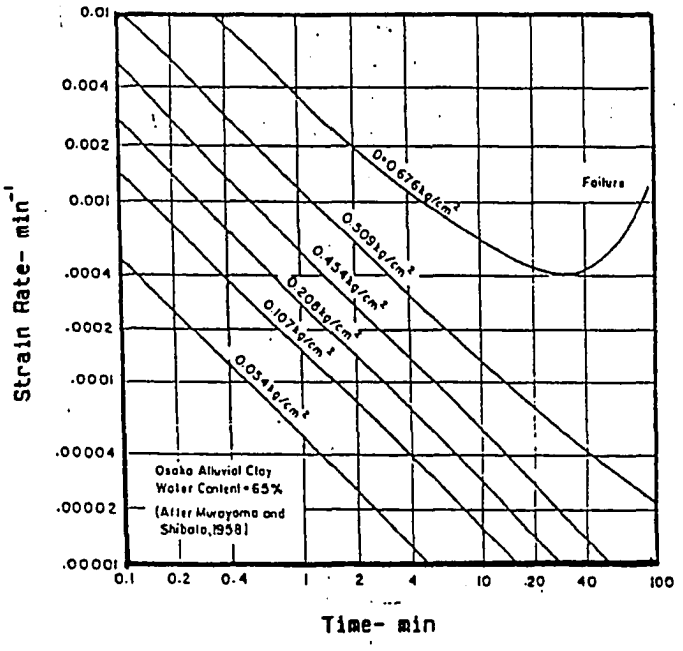

Figure 6.21 Strain-Rate versus Time Relationship.
(After Singh and Mitchell, 1968)

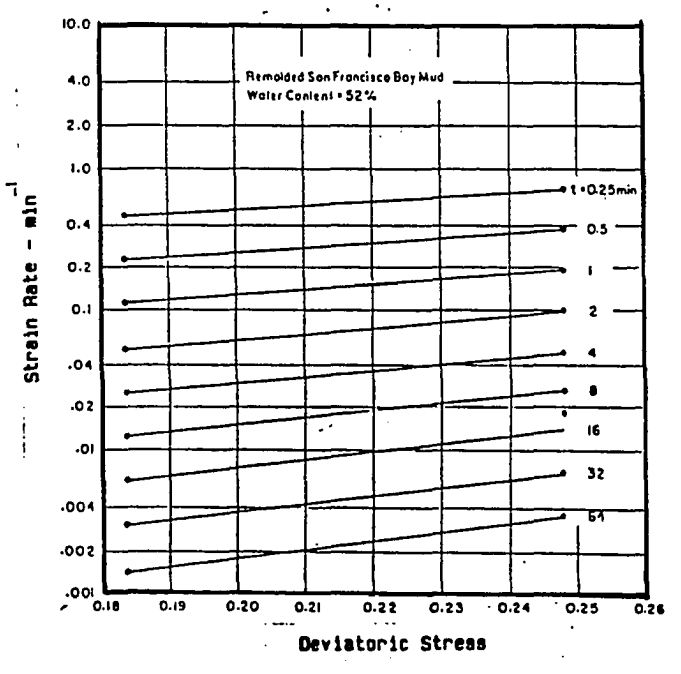

Figure 6.22 Strain-Rate versus Stress Relationship.
(After Singh and Mitchell, 1968)

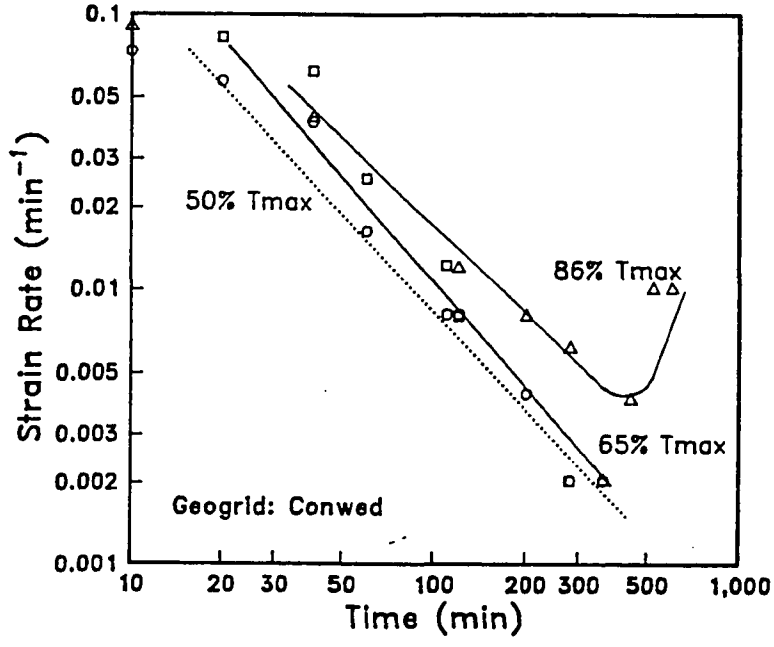

Figure 6.23 Strain-rate versus Time Relationship for Geogrid 'Conwed'.

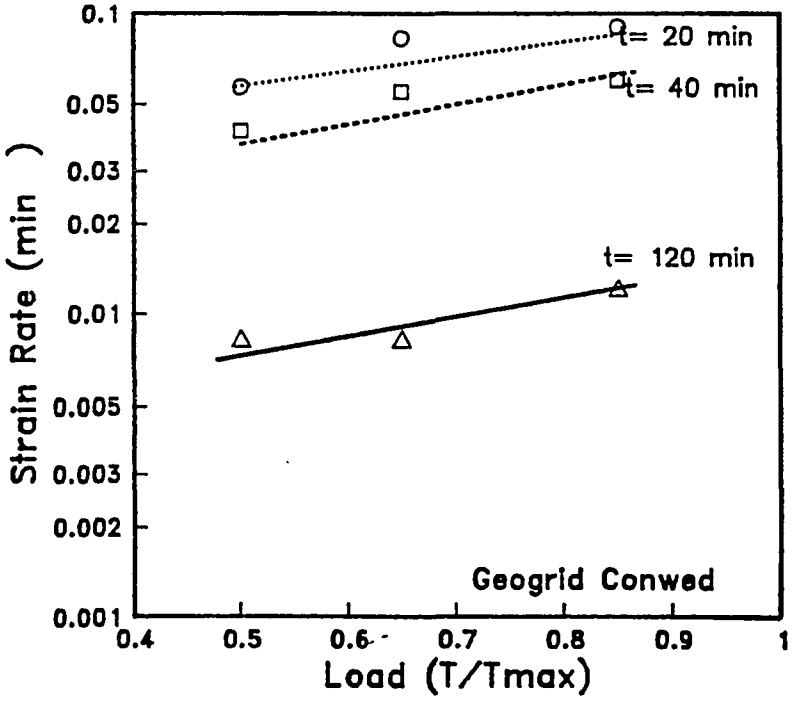

Figure 6.24 Strain-rate versus Load Relationship for Geogrid 'Conwed'.

CHAPTER 7

STABILITY ANALYSIS OF REINFORCED SOIL STRUCTURES

7.1) INTRODUCTION:

The stability analysis of reinforced soil structures involves the evaluation of the following:

(i) The external stability when the potential sliding surface develops outside the reinforced zone. In this case, the conventional slope stability procedures like modified Bishop's analysis can be used.

(ii) The internal stability of the reinforced structure when the failure surface passes through the reinforced zone. In this case, the mobilized tensile forces in the reinforcement along with the soil shear stress along the failure surface resist the driving forces induced by the weight of soil in the active zone (Figure 7.1-a).

The internal stability of the soil-reinforcement system requires the analysis of two failure criteria:

(i) Failure by pull-out of the reinforcement: the mobilized tensile forces of the reinforcement should not exceed its pull-out resistance.

(ii) Failure by breakage of the reinforcement: the mobilized tensile force in reinforcement should not exceed its ultimate tensile resistance.

Most of the internal stability analysis of the reinforced structures are

based on limit equilibrium methods which are modified to account for the reinforcement tensile resistance. These methods consider different assumptions with regard to the failure mechanism (rotational or translational), the shape of the failure surface (plane, bilinear, circular and log spiral) as well as the deformation and orientation of the reinforcement. Rowe (1984) and Hird (1986) used the limit equilibrium design method with circular sliding surface to obtain design charts for reinforced embankments on soft foundation soils. Milligan and La Rochelle (1984) developed limit equilibrium design charts with both a circular arc for rotational failure and a planner sliding surface for translational failure of embankments over soft foundations. Murray (1982) considered a bilinear slip surface to evaluate the safety factors of reinforced slopes. Jewell et al. (1984) and Schmertmann et al. (1987) presented a bilinear wedge limit analysis method to evaluate the rotational and translational failure mechanisms in steep reinforced slopes. Leshchinsky et al. (1986), Leshchinsky and Perry (1989) and Leshchinsky and Boedeker (1989) presented an analytical approach based on limit equilibrium analysis of log spiral slip surface and using variational calculus to find the rotational and translational failures in reinforced slopes.

Since the limit equilibrium analysis cannot predict the actual distribution of the tension force at the failure state, different assumptions regarding the distribution of the tensile force T were considered. In these methods the tension forces are usually assumed to follow either the K_o or the K_a Rankine's

earth pressure distribution. Leshchinsky and Perry (1989) considered T_j as a linear function of the overburden pressure; i.e:

$$T_j = T_1 \ (H - y_j)/H$$

where y_j is the is the depth of the reinforcement j. Christopher et al. (1989) considered a distribution factor (K/K_a). This ratio depends on the stiffness of the reinforced mass S_r which is primarily related to the reinforcement extensibility and its horizontal and vertical spacings in the soil mass.

Different assumptions regarding the orientation of the reinforcement at the failure surface were also considered. As the tension forces are mobilized, the reinforcement reorients itself from its horizontal position ($\beta = 0$) to an angle β (Figure 7.1-a). The orientation of the reinforcement (β) governs the magnitude of the mobilized tension forces and consequently the factor of safety. Jewell (1982) and Ingold (1982) assumed that the tension forces stay horizontal; while Brakel et al. (1982) assumed the direction of the tension forces to be tangent to the failure surface. Gourc et al. (1986) considered both limit cases assuming horizontal forces at small displacements; whereas at large deformations, the reinforcement becomes tangential to the potential failure surface. Rowe and Soderman (1985) performed finite element study to evaluate the effect of reinforcement orientation on the moment arm of the failure circle in reinforced embankments. They concluded that the moment arm for calculating the resisting moment due to geotextile force can be taken as

$$\text{moment arm} = (R+z)/2 \quad \text{for } D/B \leq 0.42$$

moment arm = z for D/B > 0.42

Where R, z, D and B are as shown in Figure (7.1-b). Leshchinsky and Perry (1989) determined that a value of β equals (Θ-ϕ) is required to mobilize the reinforcement maximum tensile force where Θ is the inclination of the failure surface with horizontal and ϕ is the friction angle of the soil.

The slope stability methods based on limit equilibrium can be used to evaluate the safety factors with respect to the failure mechanism along the assumed failure surfaces. Nevertheless, these methods can not provide an estimation of the maximum tension forces that would be generated at each reinforcement level. Consequently, they do not allow for the evaluation of the local stability of the reinforced soil mass at the level of each reinforcement with respect to the potential failure due to breakage or pull-out of the reinforcement. Moreover, these methods do not allow for an evaluation of the effect of soil dilatancy and reinforcement extensibility on the generated tension forces and structure stability. The development of a working stress analysis for the evaluation of the tensile forces of the reinforcement and the stability of the structure requires adequate constitutive equations for the soil, in-soil confined stress-strain properties of the reinforcement and an assumption pertaining the strain compatibility between the soil and the reinforcement.

This chapter presents a soil-reinforcement analytical model that associates an elasto-plastic strain hardening soil behavior, elastic-perfectly plastic response of the reinforcement and a perfect adherence at the soil-

reinforcement interface to calculate the maximum tension forces in the reinforcement. This model (Juran et al., 1988-b,c and 1990) allows for the evaluation of the effect of soil dilatancy and reinforcement extensibility on the generated tension forces.

7.2) MODELING GEOSYNTHETIC-REINFORCED SOIL WALLS:

The model used in the analysis of geosynthetic reinforced soils is based on the analogy between the response of the reinforced soil material to shearing (Figure 7.2-b) and the plane strain shear mechanism developed along the potential failure surface (Figure 7.2-a). This analogy has been assessed through numerical simulations presented by Jewell (1980) and Juran et al. (1988-b and c). The main design assumptions of this model are:

(i) The soil is assumed to be homogeneous, isotropic and follows an elasto-plastic strain hardening (and strain softening) yield function with a non-associated flow rule.

(i) An active zone develops in the soil which undergoes a rigid body movement along a plane failure surface (Figure 7.2-a).

(ii) The shear displacement of soil along the potential failure surface is assumed linear with depth and the mobilized extension of the reinforcement along the shear zone satisfies the strain compatibility with the specified soil shear strain.

(iii) The reinforcement is assumed elastic-perfectly plastic and the generated

tension force is retained by the portions of the reinforcement in the resisting zone.

The soil-geosynthetic model is based on the development of the following relationships: (i) Constitutive equations of the soil; (ii) stress-strain relationship for the reinforcement; (iii) soil-reinforcement interaction; and (iv) equilibrium conditions in the soil mass.

i) Soil Model:

The yield surface of soil is defined by a yield function that obeys Mohr-Coulomb's failure criteria. It is assumed that the soil layer along the potential sliding surface undergoes simple shearing and therefore the strain hardening is a function of the shear strain at the failure surface γ_{xy}. The yield function can then be written as :

$$F(\sigma_y, \gamma_{xy}) = \frac{\tau_{xy}}{\sigma_y} - h(\gamma_{xy}) = 0 \qquad \ldots\ldots\ldots\ldots \quad (7.1)$$

where τ_{xy} and σ_y are the mobilized shear and normal stresses along the potential sliding surface, respectively; and $h(\gamma_{xy})$ is the strain hardening function and equals tan ϕ_m where ϕ_m is the mobilized soil friction angle at the failure plane.

For dense dilating sand, it is assumed that the strain hardening function $h(\gamma_{xy})$ is parabolic (Figure 7.3) and is written as:

$$h(\gamma_{xy}) = \frac{c\ \gamma_{xy}\ (\gamma_{xy} - a)}{(\gamma_{xy} + b)^2} \qquad \ldots\ldots\ldots\ldots \quad (7.2)$$

Where the constants a, b and c are determined from the initial conditions of the strain hardening function which yield:

$$a = -4\,(\sigma_y/G)\,(\tan^2 \phi_p \,.\, L^2)\,/\,\tan \phi_{cv}$$

$$b = 2\,(\sigma_y/G)\,(\tan \phi_p \,.\, L)$$

$$c = \tan \phi_{cv}$$

and, $L = 1 + [\,1 - (\tan \phi_{cv} / \tan \phi_p)]^{1/2}$

Where G is the initial soil shear modulus and ϕ_p and ϕ_{cv} are, respectively, the soil friction angles at peak and at critical state (Figure 7.3). The determination of these constants along with the detailed mathematical formulation of the equations presented herein are shown in Appendix D.

The plastic flow of the sand is defined by its dilatancy angle υ which equals:

$$\tan \upsilon = \frac{d\epsilon_y}{d\gamma_{xy}} = \frac{1}{\mu}\left[\tan \phi_{cv} - \frac{\tau_{xy}}{\sigma_y}\right] \qquad \ldots\ldots \quad (7.3)$$

where $d\epsilon_y$ is soil extension (or compression) increment in the direction of orthogonal to the failure surface, $d\gamma_{xy}$ is the shear strain increment along the failure surface and μ is a dilatancy parameter equals μ_1 when $\phi_m \leq \phi_{cv}$ and a contracting parameter equals μ_2 for $\phi_m > \phi_{cv}$.

(ii) Reinforcement:

The reinforcement is assumed to be elastic-perfectly plastic material. The maximum tensile force of the reinforcement should not exceed either its elastic limit determined from confined tests on the reinforcement under the specified

confining pressures or its pull-out resistance.

(iii) Soil-Reinforcement Interaction:

As the tension forces are being mobilized, the reinforcement reorients itself from its original horizontal position to an angle β (Figure 7.2-a). The current inclination of the reinforcement λ_i is calculated incrementally from Figure (7.4-a) in the equation:

$$\tan \lambda_i = \frac{\tan \lambda_{i-1} + d\gamma_{xy}}{1 + d\epsilon_y} \qquad \ldots\ldots\ldots\ldots (7.4)$$

with an initial horizontal inclination $\lambda_o = \frac{\pi}{2} - \alpha$;where α is the slope of the failure surface.

The soil deformation in the direction of the reinforcement λ_i for each γ_{xy} at the level of each reinforcement can be calculated from the Mohr's circle of strain (Figure 7.4-b). The strain in soil $d\epsilon_\rho$ is given by:

$$d\epsilon_\rho = \tan \upsilon \left[1 - \frac{\cos(\lambda_i - \upsilon) \sin \lambda_i}{\sin \upsilon} \right] d\gamma_{xy} \qquad \ldots\ldots (7.5)$$

The assumption of a perfect soil-reinforcement adherence implies that the tension increment of the reinforcement $d\epsilon_R$ is equal to that of the soil in its direction (i.e. $d\epsilon_\rho$). The elastic-perfectly plastic constitutive equation of the reinforcement enables to calculate the tension stress increment $d\sigma_R$:

$$d\sigma_R = E \cdot d\epsilon_R \ , \quad \text{with } \sigma_R \leq R_T \qquad \ldots\ldots\ldots\ldots (7.6)$$

where E is the reinforcement elastic modulus and R_T is its yield stress. It should be noted that a non-linear elastic behavior of the reinforcement can be

numerically implemented in the model. The maximum tension force in the reinforcement per unit area along the failure surface is then given by:

$$\frac{T_{max}}{S_h . S_v} = \epsilon_R \frac{E.t.b}{S_h . S_v} \qquad \ldots\ldots\ldots\ldots (7.7)$$

where t and b are the thickness and width od the reinforcement, respectively; and S_h and S_v are the horizontal and vertical spacings between the reinforcements.

(iv) Equilibrium Condition:

The forces acting on the active zone are shown in Figure (7.2-a). The gravity force in the active zone is resisted by the tension forces in the reinforcement and the soil reaction along the potential sliding surface. The gravity force in the active zone is given by :

$$W = \tfrac{1}{2} \rho H_0^2 \left[\frac{1}{\tan \alpha} - \tan J \right] \qquad \ldots\ldots\ldots\ldots (7.8)$$

where ρ is the soil unit weight and J is the inclination of the wall facing with respect to vertical. The analysis of equilibrium condition in the active zone yields a nondimentional solution, relating the actual structure height H_o to the specified shear strain level γ_{xy} along the potential sliding surface :

$$H_o / \left[\frac{E.t.b}{\rho . S_h . S_v} \right] = \frac{2 \left[\Sigma^N \epsilon_R \sin(\lambda + \alpha) \cot(\alpha - \phi) - \Sigma^N \epsilon_R \cos(\lambda + \alpha) \right]}{N \left[(1/\tan \alpha) - \tan J \right]} \qquad \ldots (7.9)$$

The height of the structure H_o is minimized with respect to α in equation (7.9) in order to derive the most critical solution, i.e. $\partial H_o / \partial \alpha = 0$.

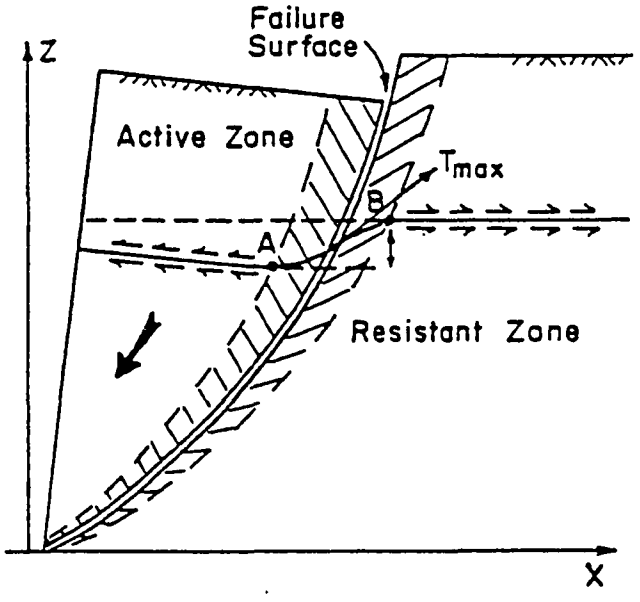

Figure 7.1-a Schematic Diagram of Failure Mechanism in Reinforced Soil Walls (After Gourc et al. 1986).

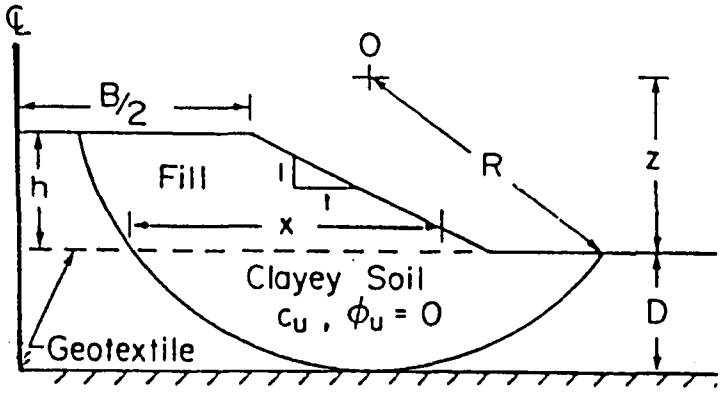

Figure 7.1-b Schematic Diagram of Failure Mechanism in Reinforced Embankments (After Rowe and Soderman, 1985).

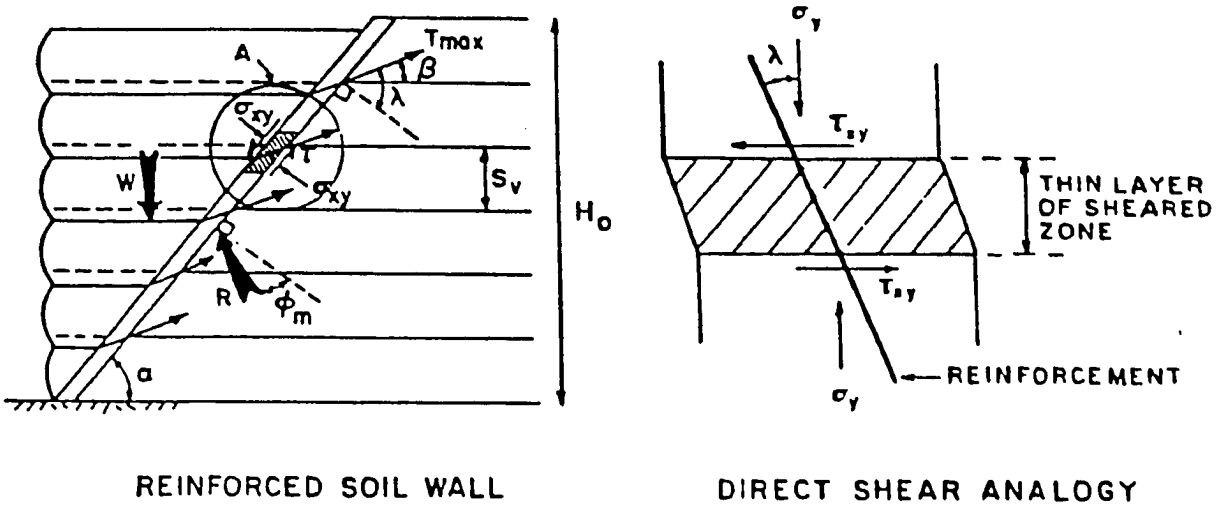

Figure 7.2 Analogy between Behavior of Reinforced Soils in Retaining Wall and in Direct Shear Test (After Juran et al. 1990)

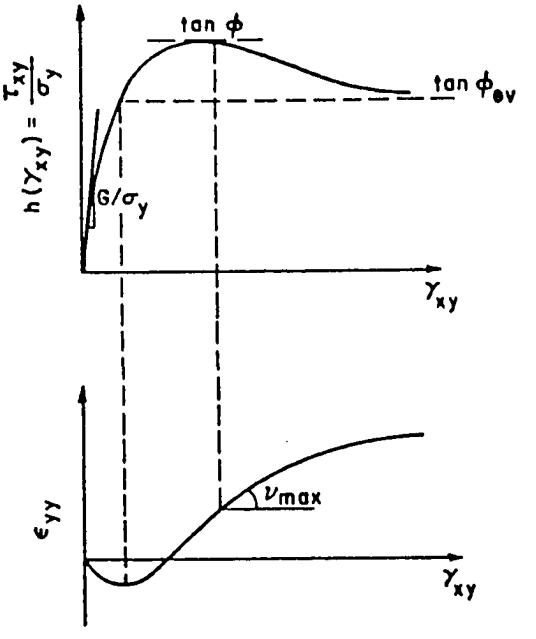

Figure 7.3 Elasto-plastic Strain Hardening of Soil.

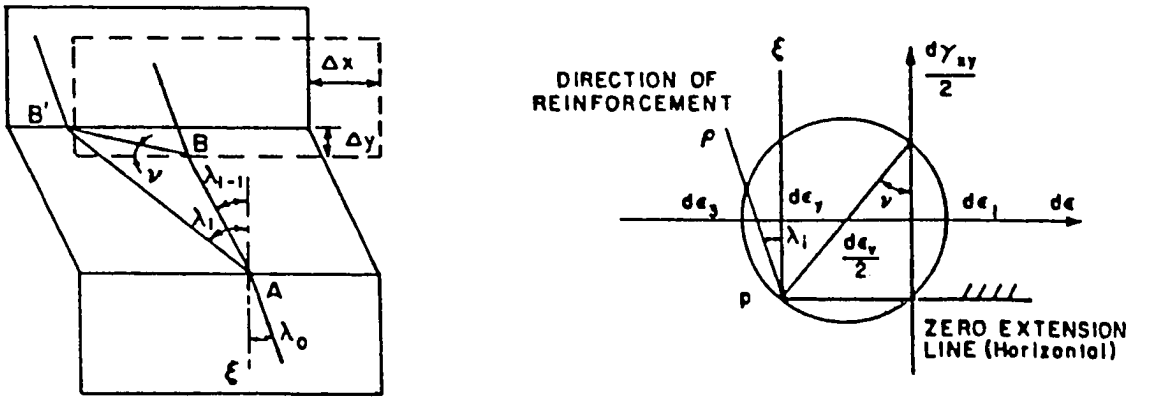

(a) Deformation of Reinforcement (b) Mohr's Circle of Strain

Figure 7.4 Modeling Behavior of Reinforced Soil.
(After Juran et al. 1990)

7.3) ANALYSIS OF BEHAVIOR OF GEOSYNTHETIC SOIL WALLS:

The formulations of the relationships of the proposed strain compatibility analysis are presented in detail in Appendix D. These relationships were implemented in a computer program to predict for each structure height the maximum tension forces mobilized in the reinforcements and the location of the potential failure plane. Figure (7.5) shows a flow chart illustrating the computational scheme. The output data can then be used to evaluate the potential failure of each reinforcement due to either breakage or sliding. The selection of the appropriate reinforcement and spacings should satisfy the required safety factors with respect to these potential failure modes, as well as design criteria pertaining the admissible strains in the reinforcements.

The maximum tensile force in the reinforcement depends on the stiffness of the reinforced soil mass which is primarily related to the extensibility and density of the reinforcement. The effect of the relative stiffness of the reinforcement on the maximum tension forces is illustrated in Figure (7.6). The relative stiffness of the reinforcement is defined as:

$$h_o = E.t.b / \rho.S_h.S_v$$

The maximum tension force is given by the non-dimensional parameter:

$$T_N = T_{max} / \rho.H.S_h.S_v$$

where H is the height of the structure. For a given soil type, a unique $T_N = f(H/h_o)$ relationship can be developed provided that the reinforcement yield strain is not exceeded (i.e. $\epsilon_R < \epsilon_y$). The relationship in Figure (7.6) was

calculated for a typical range of compacted backfill materials with the following soil parameters: ϕ_p = 40°, ϕ_{cv} = 31°, ρ = 15.5 KN/m^3 and a constant dilatancy angle = 1/3 ϕ_p = 13°, and a range of normalized shear modulus (G/σ_v). The figure illustrates several aspects of the behavior of reinforced soil wall:

1- For a given structure height, the relative stiffness, h_o, of the reinforcement significantly affects the state of stress in the soil. As h_o decreases (i.e. extensibility increases), the normalized tension forces, T_N, decreases from K_o state of stress (for quasi-inextensible reinforcement) to K_a state of stress (for highly extensible reinforcement).

2- the variation of the normalized tension forces, T_N, with the relative stiffness, h_o, depends upon the normalized shear modulus, G/σ_v, which governs the shear strain in the soil.

In order to assess the effect of soil dilatancy on the locus of maximum tension forces, two assumptions were considered: (1) constant dilatancy angle = 13°, and (2) variable, strain dependent dilatancy angle defined as in Equation (7.3) with the contractancy parameter μ_1 = 10 and the dilatancy parameter μ_2 = 0.9, for the sand used in this parametric study. It should be indicated that the assumption of variable dilatancy attempts to simulate soil volume change with an initial phase of contraction followed by a phase of dilation. Soil dilatancy is highly dependent upon the in-situ confining pressure and construction process. The two assumptions specified above yield the probable range of the actual soil behavior in a compacted backfill material. The effect of

soil dilatancy on the relationship between relative stiffness of the reinforcement, h_o, and the normalized tension forces is shown in Figure (7.7). The Figure shows that the assumption of a constant dilatancy rate (i.e., $\upsilon_m = \upsilon_{max}$) leads to more conservative results.

The effect of the reinforcement relative stiffness ,h_o, on the inclination of the failure surface is shown in Figure (7.8). The Figure illustrates the following:

1- For a given structure height, as the relative stiffness, h_o, increases ((as for quasi-inextensible reinforcement), the inclination of the failure surface increases and becomes practically vertical.

2- As the relative stiffness decreases (e.g. higher extensibility of the reinforcement), the inclination of the failure progressively approaches that of Mohr-Coulomb's failure plane (i.e. $\alpha_{cr} = \pi/4 + \phi/2$). This variation of α_{cr} is consistent with observations on both reduced scale and centrifugal model walls (Juran and Christopher 1989; and Jaber et al. 1987).

These results also conform with observations on walls reinforced with both extensible and quasi-inextensible reinforcement (Juran and Chen 1989; and Christopher et al. 1989). These observations are illustrated in Figure (7.9) for both types of reinforcement. The Figure shows practically vertical failure surfaces at the upper part of the structure when inextensible reinforcement is used. It should be noted that the vertical failure surface, when inextensible reinforcements are used, suggests a probable more critical failure height when

a log spiral failure surface is assumed.

The design charts presented in Figures (7.6) to (7.8) can be used to evaluate the local stability of each reinforcement and to predict the failure surface for the specified soil data. The analysis allows the engineer to design and analyze the structure behavior under the design working load. In order to evaluate the design assumptions considered in this analysis, the predicted tension forces are compared with those measured in model walls and embankments reinforced with different types of geosynthetics.

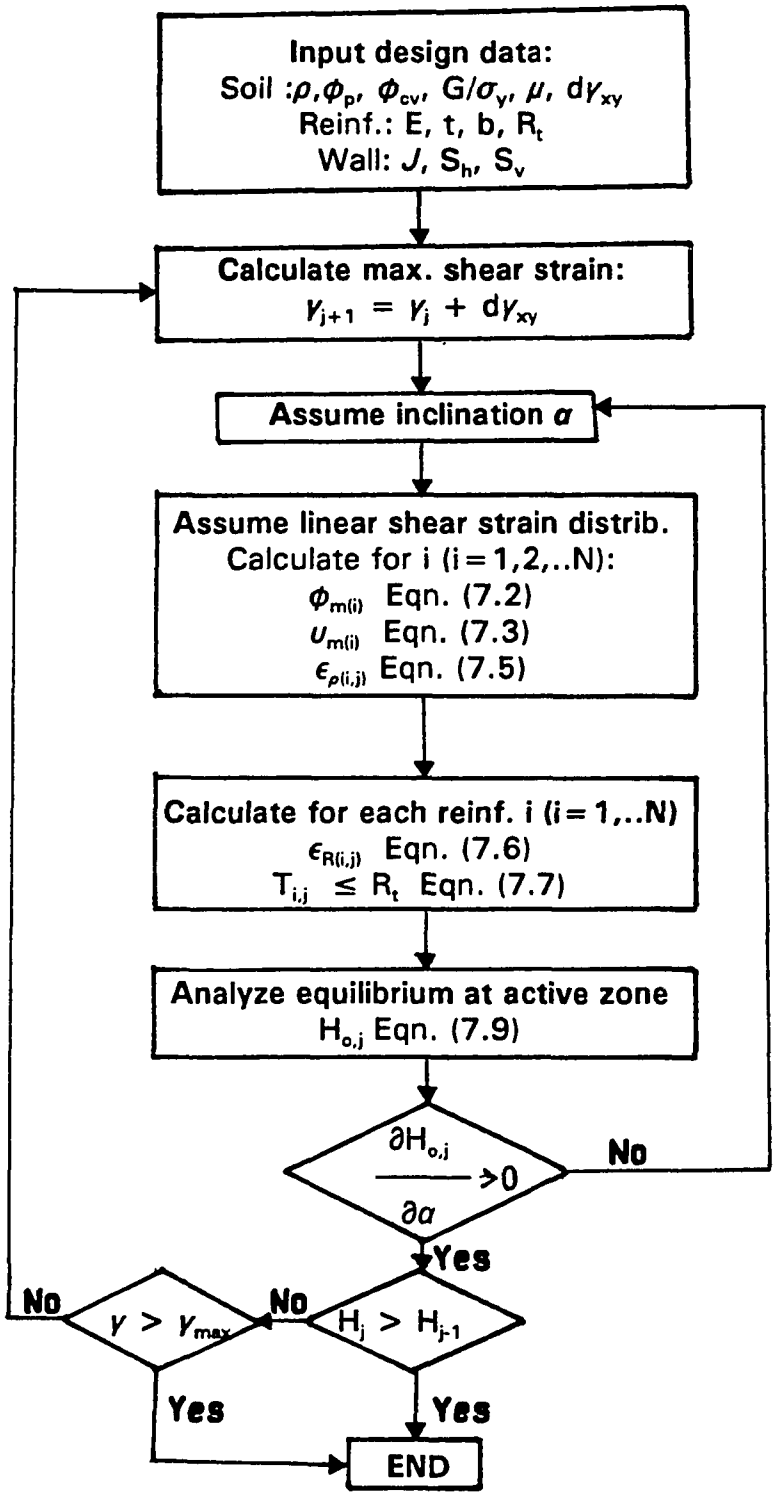

Figure 7.5 Flow Chart of Computational Scheme.

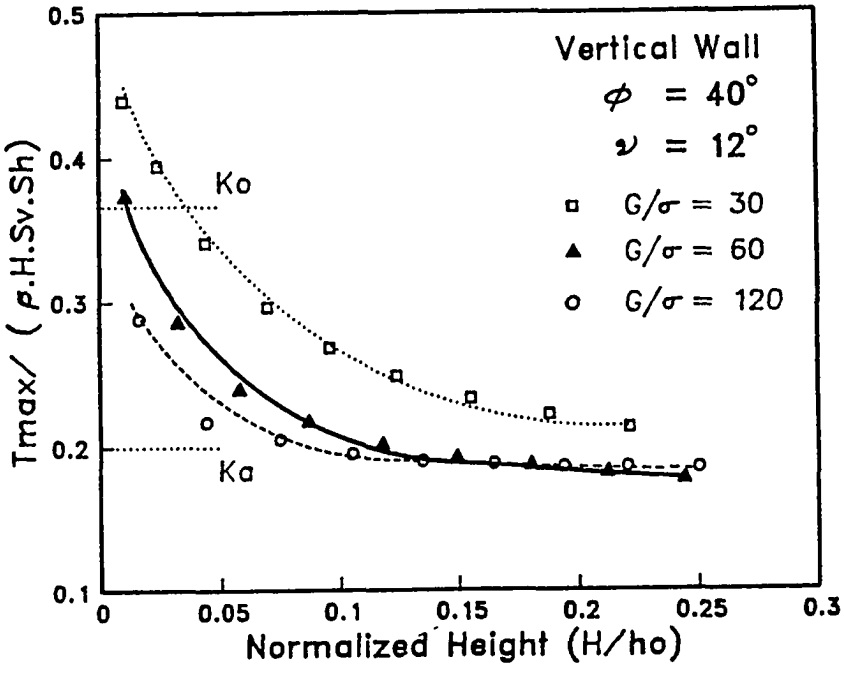

Figure 7.6 Effect of Reinforcement Stiffness, h_o, on Maximum Tension Forces.

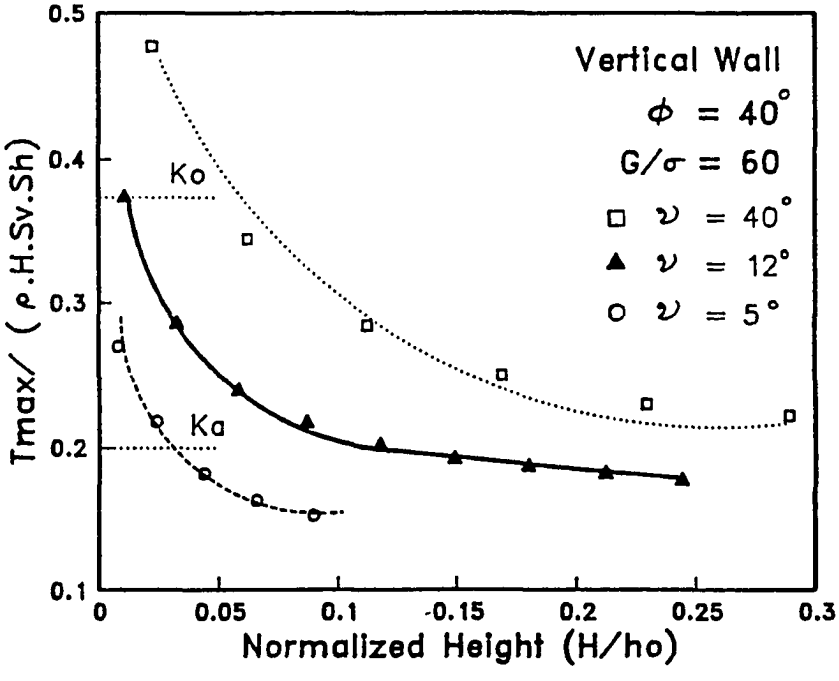

Figure 7.7 Effect of Soil Dilatancy on Maximum Tension Forces.

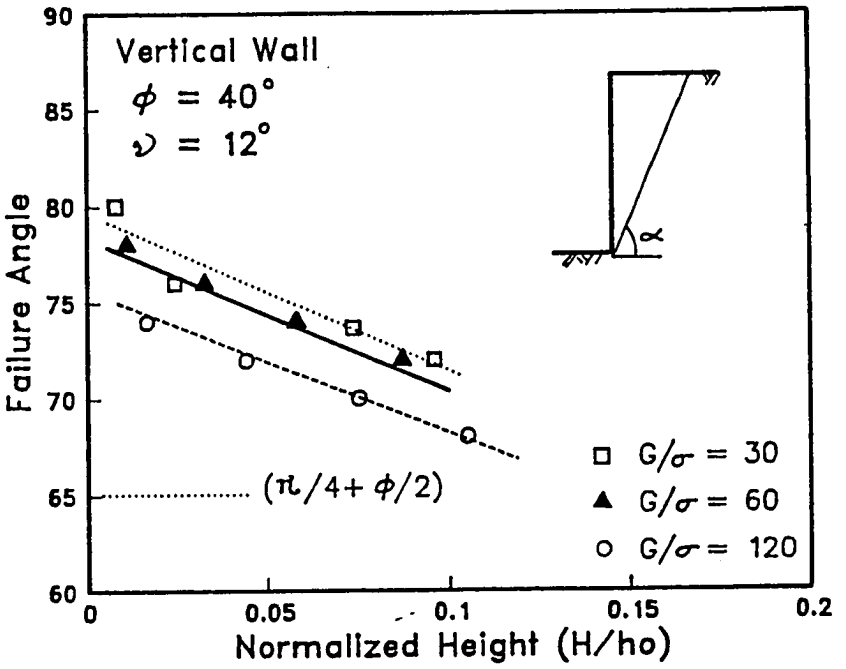

Figure 7.8 Effect of Reinforcement Stiffness, h_o, on the Inclination of Failure Surface.

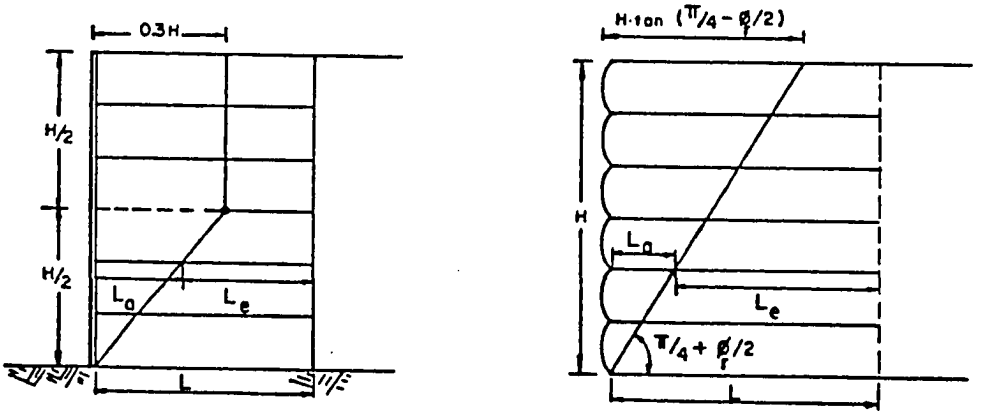

(b) inextensible reinforcements (c) extensible reinforcements

Figure 7.9 Observations on Inclination of Failure Surface for Different Reinforcements (Christopher et al. 1989).

7.4) ANALYSIS OF MODEL WALL RESULTS:

The tension forces predicted using the proposed analysis were compared with those measured in different model walls and embankments, namely:

1- Two laboratory model test walls, of 60 cm high, reinforced with non-woven geotextile strips (Juran and Christopher, 1989).

2- Three instrumented full scale reinforced soil walls of 20 ft high (Christopher et al., 1989).

3- Two instrumented embankments of 20 ft high and slope 0.5 horizontal to 1 vertical and two embankments of 25 ft high and slope 1 horizontal to 1 vertical (Christopher et al., 1989).

(i) Analysis of Laboratory Model Tests:

Figure (7.10) shows typical instrumented cross section of the model walls and the observed failure surface. The material properties of the non-woven geotextile for both walls is shown in table (7.1) and the confined-unconfined extension properties of the reinforcement are shown in Figure (7.11). For the purpose of the analysis, the reinforcement is assumed to be linearly elastic perfectly plastic material. The soil used in the study was Fontainbleau sand, compacted to an average dry density of 15.5 KN/m^3, with the following properties: $\phi_p = 40°$, $\phi_{cv} = 31.5°$, and $G/\sigma = 50$. For the sake of analysis, the two assumptions of constant and variable dilatancy angles were considered.

Figure (7.12) and (7.13) show the predicted and measured distributions of the tension forces in walls No. 1 and No. 2, respectively. The measured tension forces in the model walls are close to those predicted by K_o state of stress at the upper part of the walls and approach those predicted by K_a state of stress (i.e. Rankine's state of stress) at the lower part of the walls. The numerical analysis of the model walls, assuming a constant dilatancy rate, predicts fairly well the measured tension forces in wall No. 1 while it overestimates the tension forces in wall No. 2. The tension forces in the reinforcement are significantly affected by soil dilatancy which is difficult to assess. However, the assumption of a constant dilatancy rate appears to provide a conservative bound for the design values of tension forces in the reinforcement. For both models, the numerical simulation shows that as the lower reinforcements attain their limit tension force, the lateral thrust due to the increase in the structure height is progressively transferred to the upper reinforcement.

Wall	Reinforcement	Elastic Limit F_y/b (N/cm)	E.t (N/cm)	b (cm)	S_h (cm)	S_v (cm)	L (cm)	Failure
1	Non-woven geotextile	6	500	6	30	7	60	Breakage
2	Non-woven geotextile	6	500	5	30	5	50	Breakage

Table 7.1 Material Properties and Geometrical Parameters of Test Walls (Juran and Christopher, 1989).

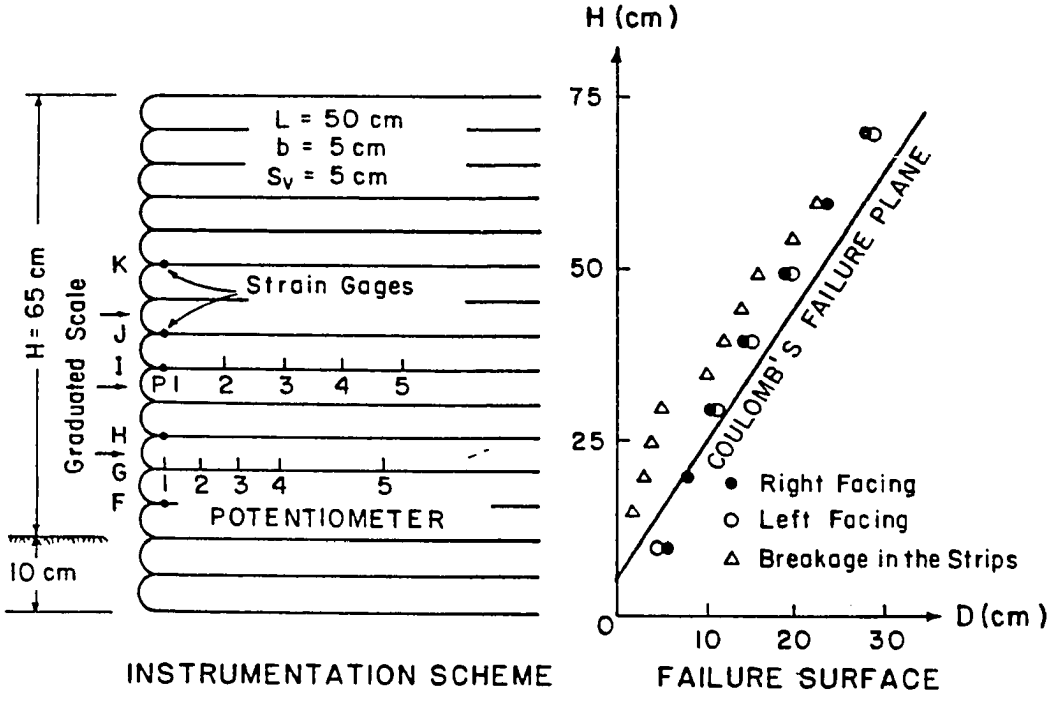

Figure 7.10 Geometry of Test Walls and Failure Surfaces.

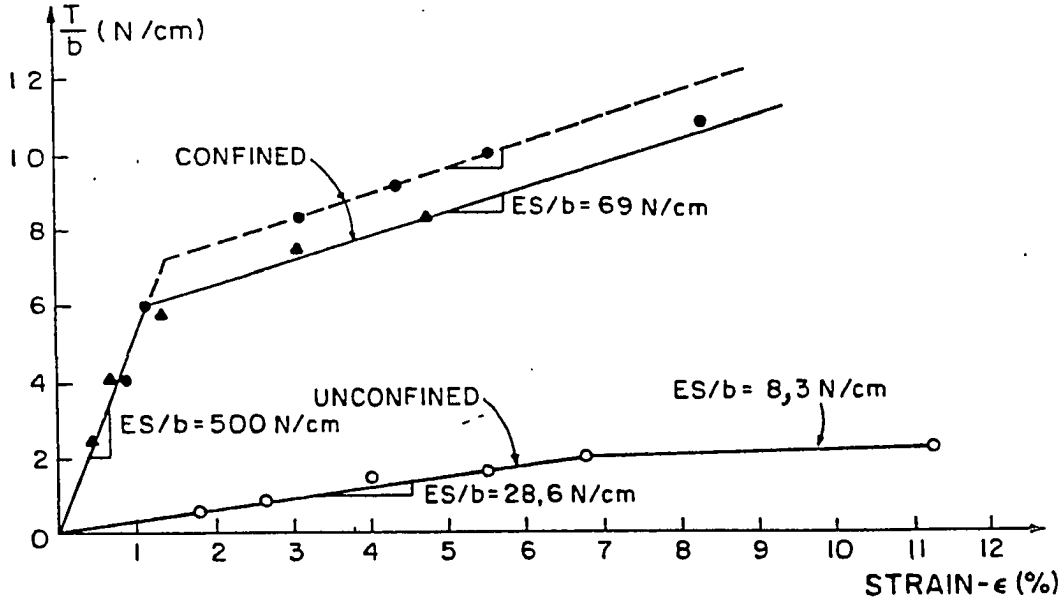

Figure 7.11 'Confined' and 'Unconfined' Extension Tests on Non-woven Geotextile (Juran and Christopher, 1989).

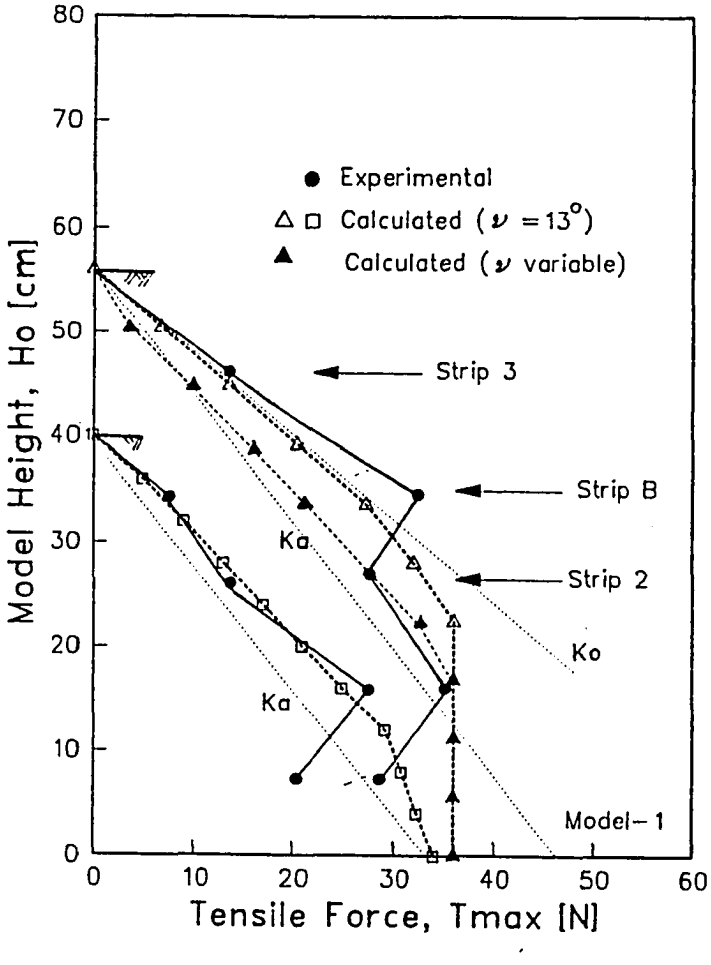

Figure 7.12 Measured and Predicted Maximum Tension Forces in Wall No. 1.

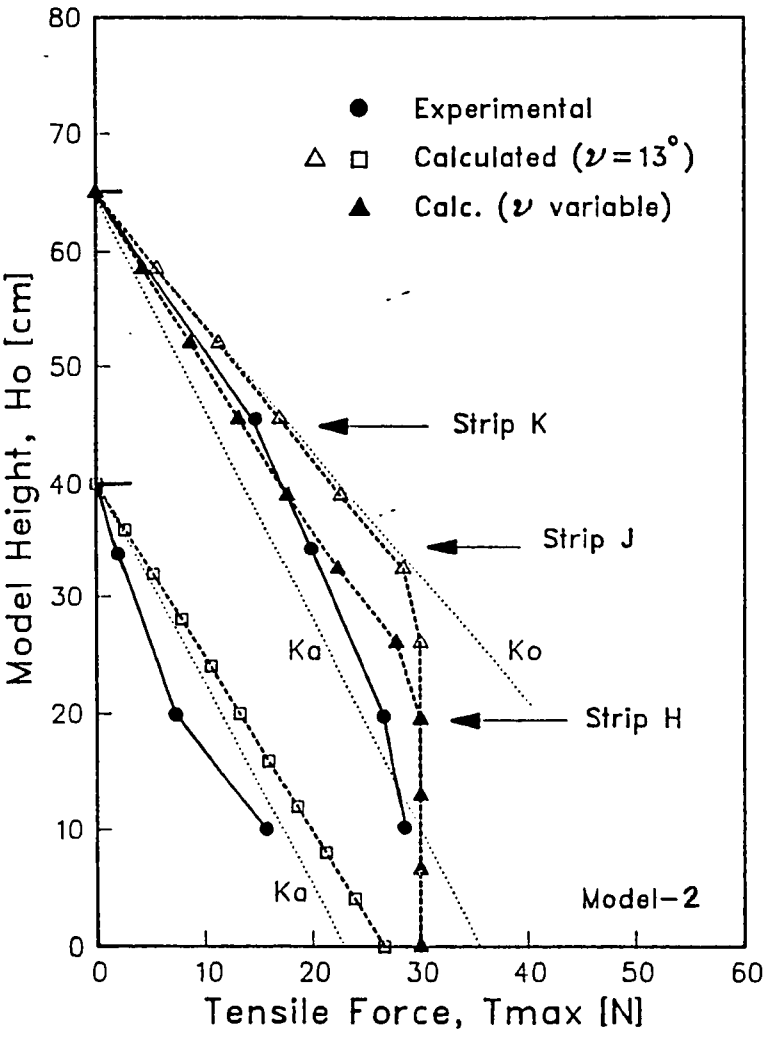

Figure 7.13 Measured and Predicted Maximum Tension Forces in Wall No. 2.

(ii) Analysis of Full-Scale Model Walls:

Three full scale model walls of 20 ft height (Christopher et al. 1989) were evaluated in this analysis. Typical geometry and soil properties of the walls are shown in Figure (7.14). Different reinforcements were used in these walls with properties shown in Table (7.2). The relative stiffness of the reinforcements in these walls are defined as $S_r = (E.t.b)/(S_h.S_v)$, and it relates to the relative stiffness parameter used in this analysis by the relationship ($h_o = S_r/\rho$) where ρ is the soil density.

Figures (7.15) to (7.17) show the comparison between the measured tension forces in the reinforcements and the predicted ones for the three walls. Two different cases of soil dilatancy were used to predict the tension forces; namely, fully mobilized soil dilatency , $\upsilon_m = \upsilon_{max}$; and variable dilatancy angle ,$\upsilon_m = f(\gamma_m)$. The figures show that the model predicts fairly well the maximum tension forces in the walls and that the assumption of fully mobilized soil dilatancy gives an upper bound of the developed tension forces.

The measured and predicted maximum tension forces in the three walls are normalized with respect to Rankine's state of stress, K_a, in Figure (7.18). The variation of K/K_a with depth illustrates the development of the state of stress in the reinforcement. The figure shows that the distribution of the maximum tension forces is close to K_o state of stress at the upper part of the wall and approaches K_a at the lower part, when the flexible reinforcements are used in walls No. 2 and No. 7.

This observation is similar to the measured and predicted behavior of non-woven geotextiles in the test walls analyzed previously. When rigid reinforcement is used, as in wall No. 3, The distribution of the maximum tension force remains close to K_o state of stresses.

Wall	Reinforcement type	S_r (K/ft^2)	S_h (ft)	S_v (ft)
2	Geogrid	56	1.0	2.5
3	Bar mats	1037	4.92	2.5
7	Gabion woven mesh	20	1.0	2.5

Table (7.2) Material Properties and Geometrical Parameters of Model Walls. (Christopher et al. 1989)

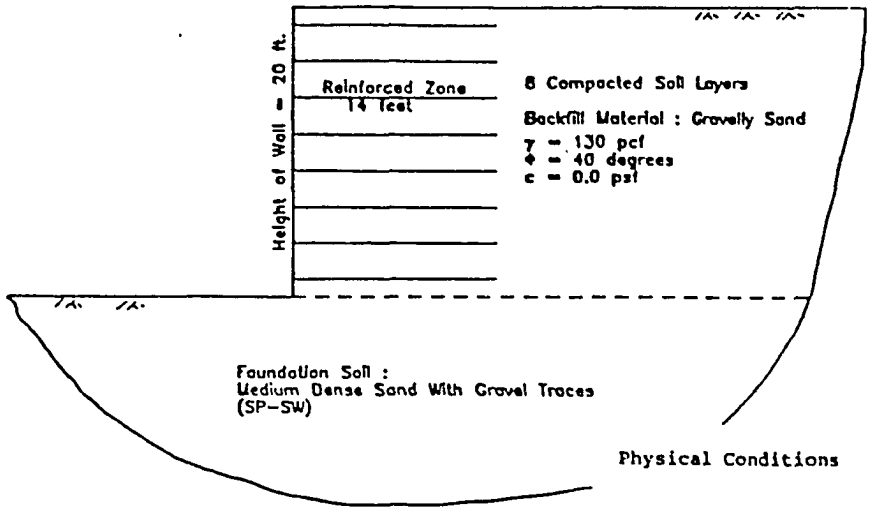

Figure 7.14 Geometry and Soil Properties of Model Walls.

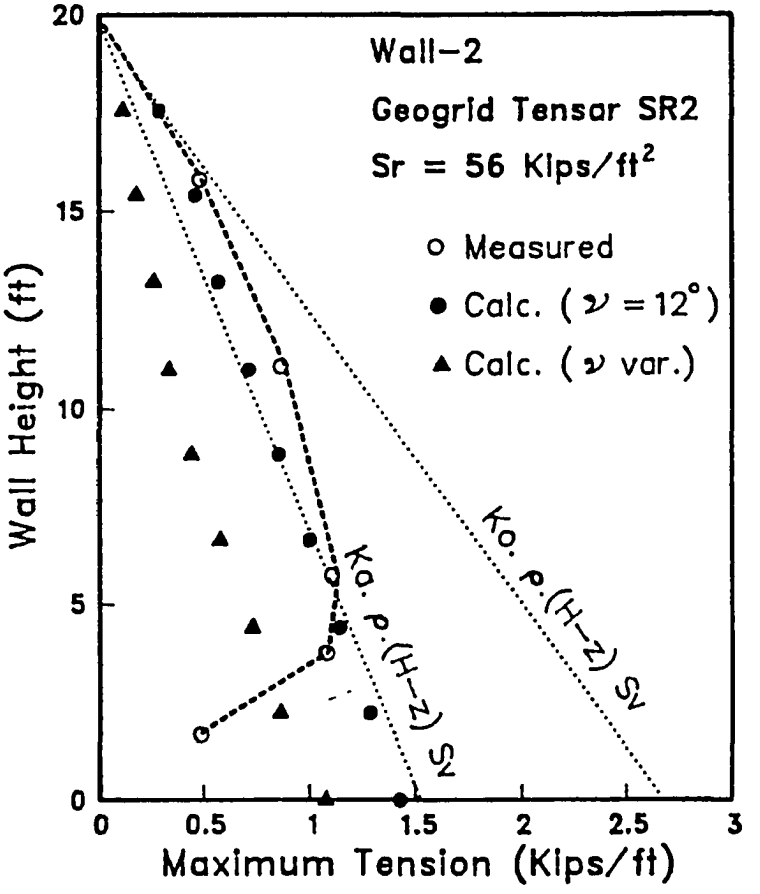

Figure 7.15 Measured and Predicted Maximum Tension Forces in Wall No. 2.

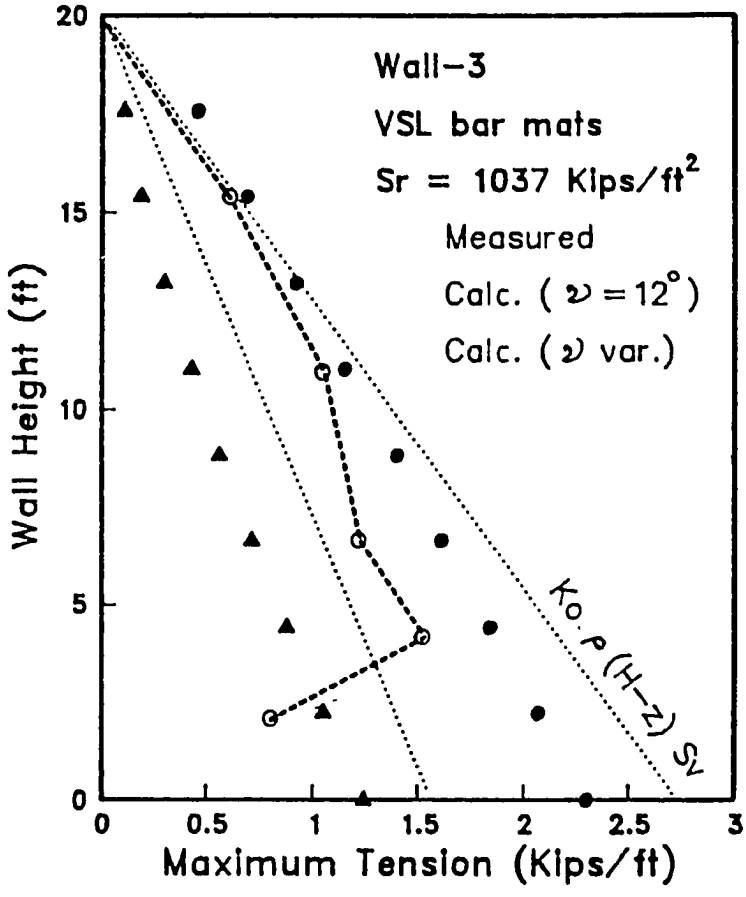

Figure 7.16 Measured and Predicted Maximum Tension Forces in Wall No. 3.

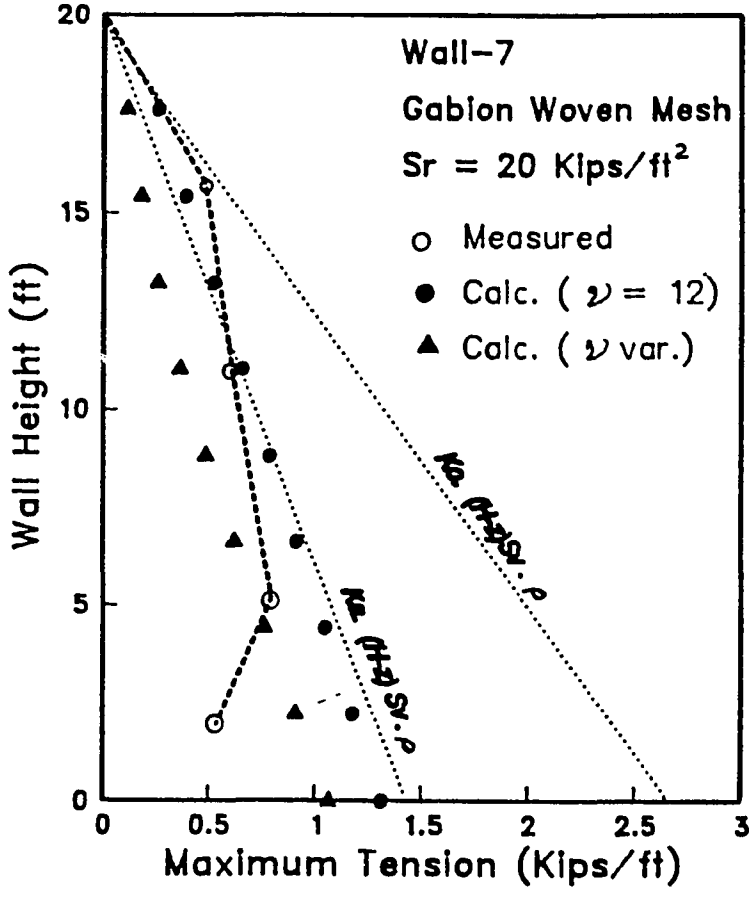

Figure 7.17 Measured and Predicted Maximum Tension Forces in Wall No. 7.

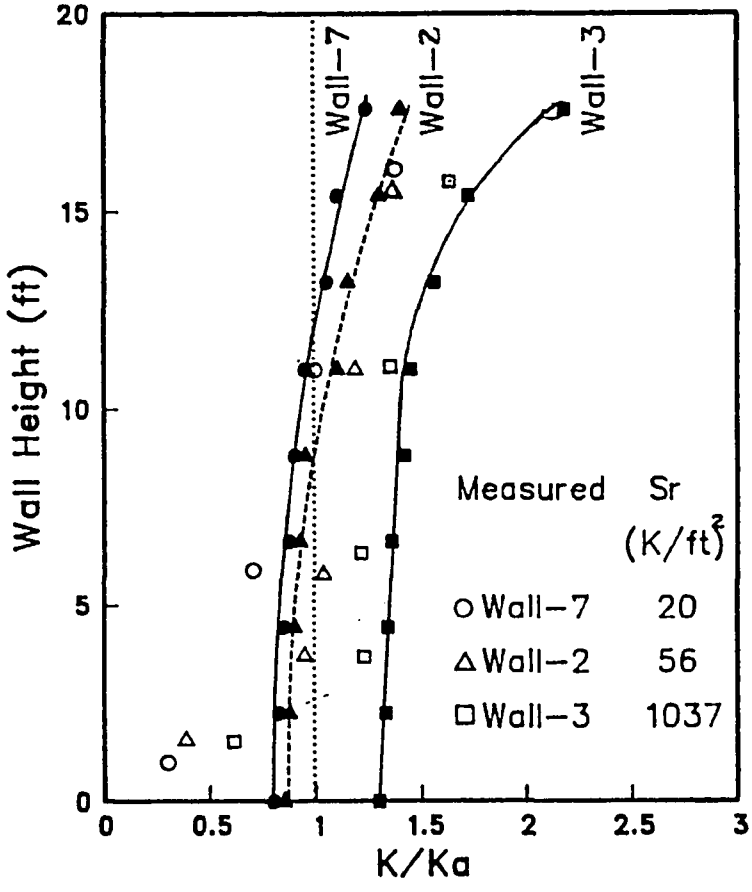

Figure 7.18 State of Stress in The Reinforcement with Depth.

(iii) Analysis of Reinforced Embankments:

The behavior of four instrumented embankments were evaluated using the proposed analysis. The geometry and properties of the embankments are shown in Table (7.3). In these embankments, eight layers of reinforcement with a uniform spacing of 2.5 ft and total length of 14 ft were used. Figures (7.19) to (7.22) show the comparison between the measured and predicted maximum tension forces in the reinforcement. Figure (7.23) shows a comparison between the predicted inclination of failure surface and the measured locus of maximum tension forces in embankment No. 1. The results show that the proposed analysis predicts fairly well the distribution of tension forces and inclination of the failure surface in the reinforced embankments.

Embankment	Slope	Reinforcement type	T_{ult} lb/in	E.A Kips/ft
1	0.5 H: 1 V	Geogrid	145.	90
2	0.5 H: 1 V	Woven geotextile	214	96
3	1 H: 1 V	Geogrid	145	90
4	1 H: 1 V	Woven Geotextile	214	24

Table 7.3 Properties of Reinforced Embankments.
(Christopher et al. 1989).

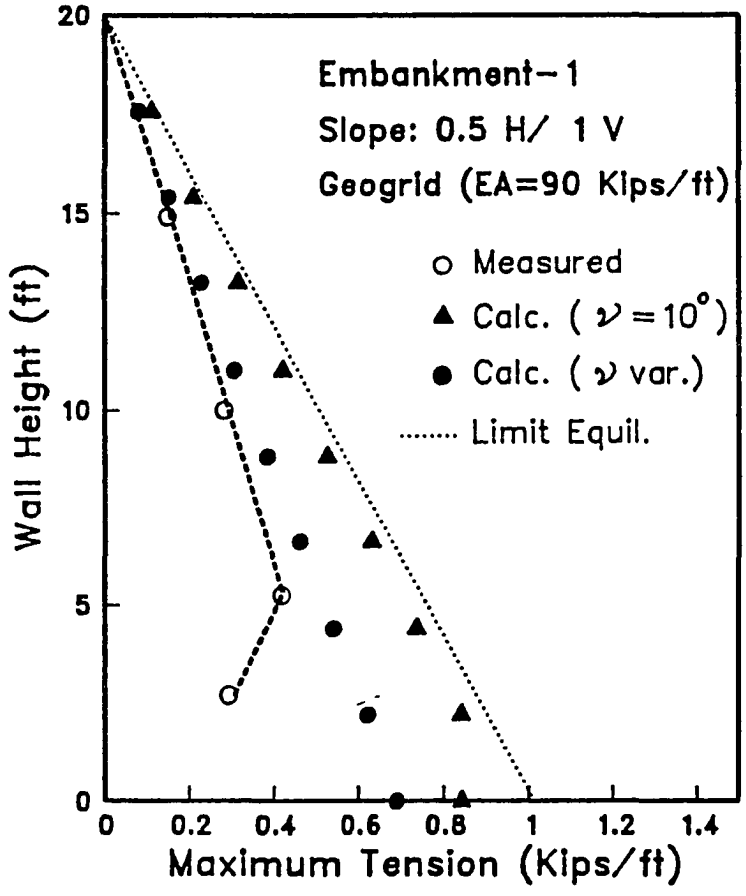

Figure 7.19 Measured & Predicted Tension Forces in Embankment 1.

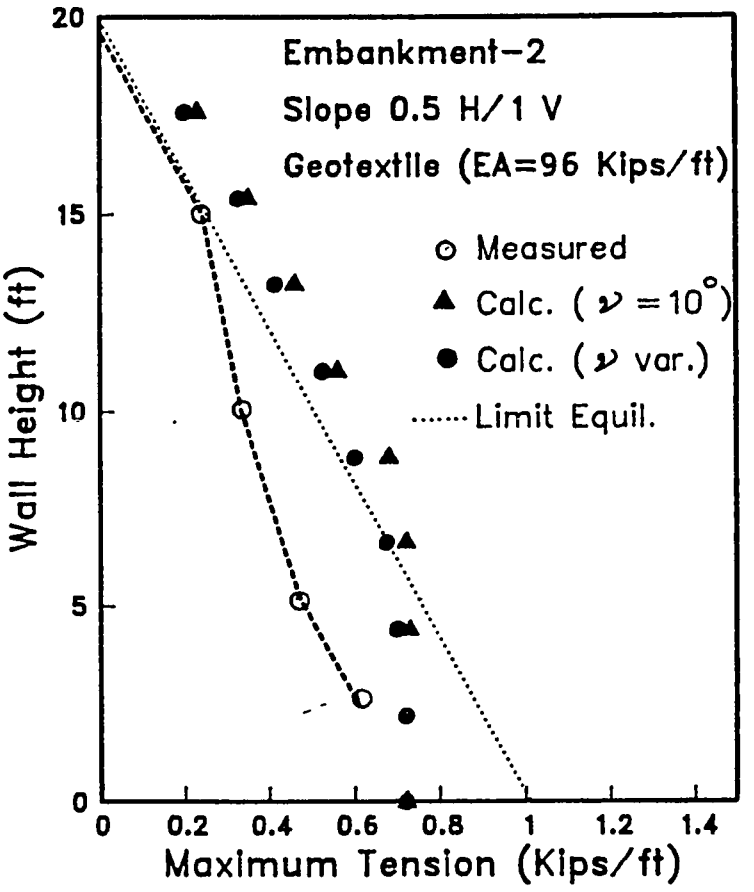

Figure 7.20 Measured & Predicted Tension Forces in Embankment 2.

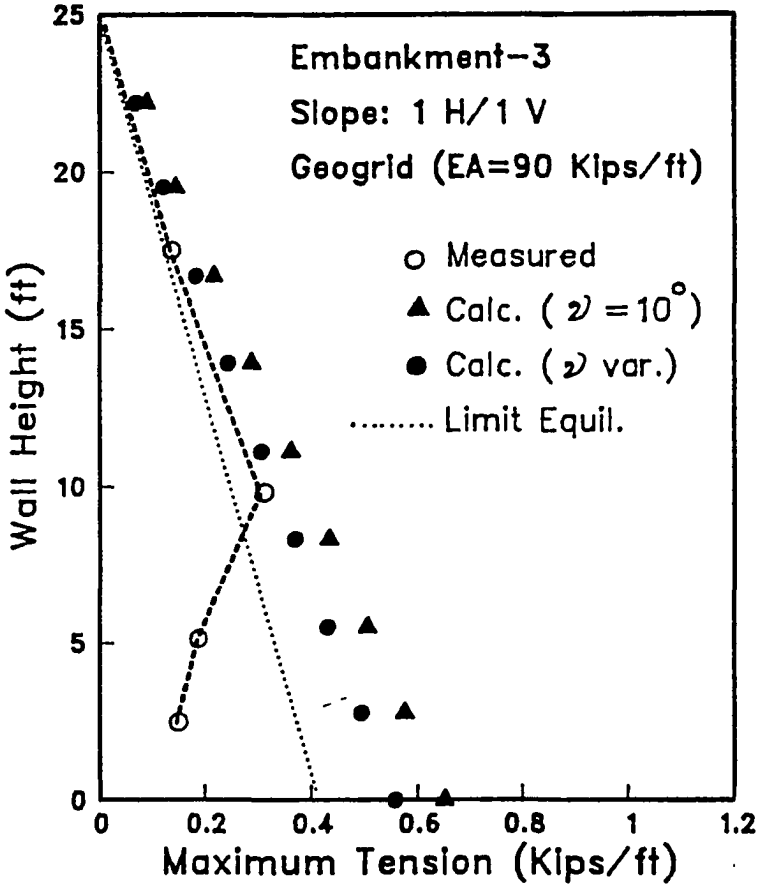

Figure 7.21 Measured & Predicted Tension Forces in Embankment 3.

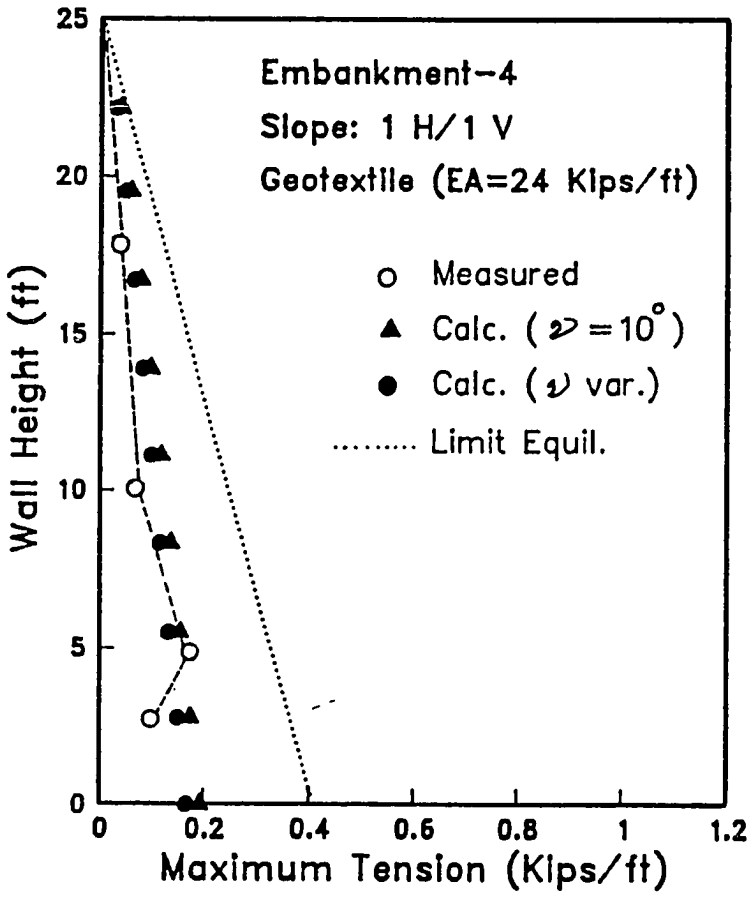

Figure 7.22 Measured & Predicted Tension Forces in Embankment 4.

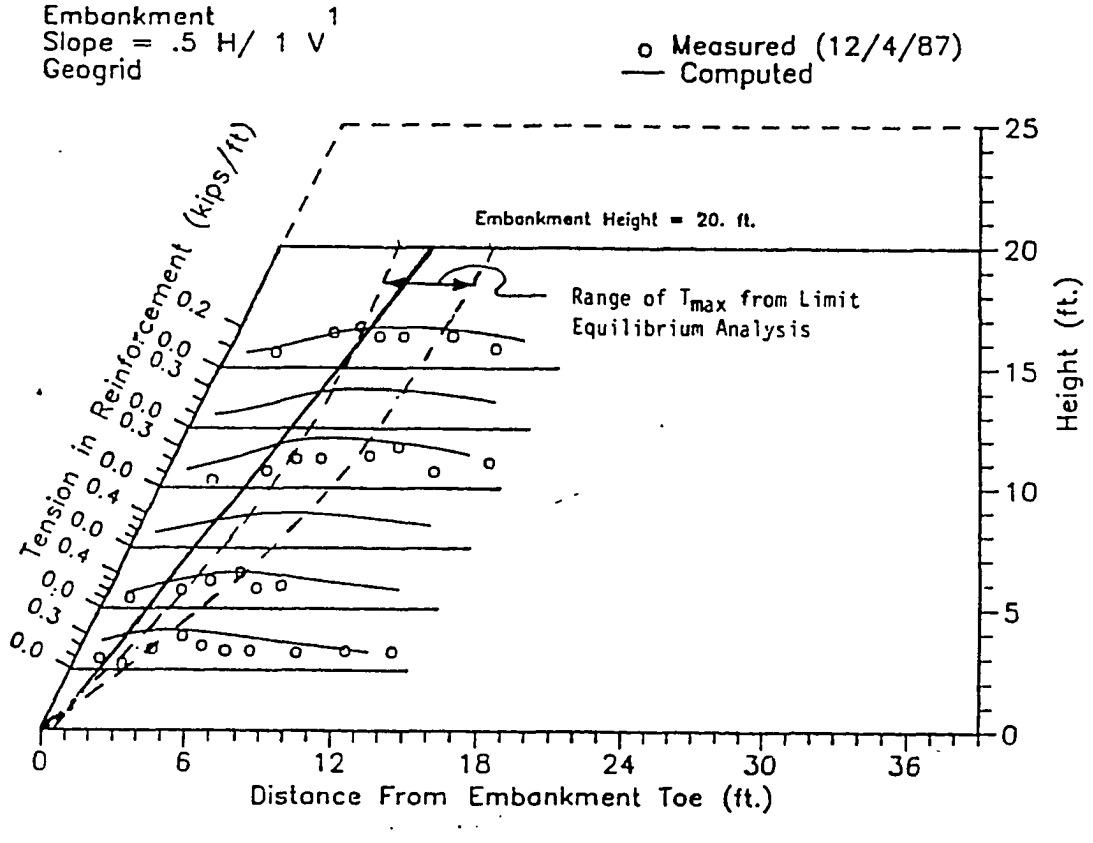

Figure 7.23 Measured & Predicted Failure Surface in Embankment 1.

CHAPTER 8

CONCLUSIONS

The pull-out box and large direct shear box were designed and constructed in order to evaluate the short term and long term interface parameters and confined stress-strain properties of the geogrids. Displacement-rate controlled tests were conducted to provide the parameters related to short-term performance of the geogrids; namely, their pull-out resistance, front displacement at peak, and interface stiffness modulus. The instrumentation of the pull-out box enabled the measurement of the nodal displacements along the confined geogrid. These measurements were utilized in a load-transfer model in order to determine the stress-strain properties of the geogrids. Load-controlled pull-out tests were conducted to evaluate the long-term parameters of the geogrids; namely, the critical creep load under specific confining pressures, and creep displacement.

The results of the pull-out tests on both 'Tensar' and 'Conwed' geogrids in granular soils illustrate the importance of soil density and the applied confining pressures on the pull-out behavior. The high soil density and confining pressure increase the geogrid frictional resistance at the interface and increase the lateral earth resistance on the transversal elements. Consequently, they restrain the displacement of the geogrid along its length and increase the geogrid pull-out resistance.

Pull-out testing program was conducted to evaluate the performance of the facility and to assess the effect of different testing parameters (i.e. testing modes, pull-out rate, soil density, confining pressure, and box boundary conditions) on the interface properties. The parametric study led to the following conclusions:

(i) The increase in the pull-out displacement-rate results in a decrease in the peak pull-out resistance and interface stiffness modulus. Pull-out tests results appears to be less sensitive to changes in displacement-rates under 6 mm/min.

(ii) Pull-out test results on the geogrid in different soil densities illustrate the influential effect of soil placement and compaction. A compaction procedure was developed and calibrated to obtain uniform soil density along the geogrid. Different soil placement techniques and compaction procedures have yet to be developed if the geogrid is to be tested in fine grained soils.

(iii) Test results on the geogrid under different confining pressures demonstrate that the peak pull-out strength is mobilized at strain levels much lower than those of the unconfined extension tests. This conclusion suggests that the design criteria of reinforced-structures should be based on the pull-out tests results rather than the unconfined extension test results.

(iv) The lateral earth pressure developed at the facing increases the soil-geogrid resistance to pull-out. The use of sleeves around the pull-out slot transfers the soil-geogrid interface resistance far behind the rigid front wall,

which imposes a practical solution to reduce the front rigid wall effect. Pull-out tests with different sleeve lengths led to the conclusion that a minimum sleeve length of 1 ft is enough to eliminate this boundary effect.

(v) Another boundary condition that influence pull-out test results is the upper and lower box boundaries. When small soil thickness is used, the rigid top and bottom plates increase soil friction at the soil-geogrid interface and restrain soil dilatancy. Pull-out tests on geogrids in different soil thicknesses demonstrate that a minimum soil thickness of 1 ft above and 1 ft under the geogrid necessary to eliminate the effect of theses boundaries on test results.

Modeling load transfer in soils reinforced with geogrids is complex and involves several interaction mechanisms. However, a simplified load-transfer model for extensible reinforcement was developed in order to rationally extrapolate laboratory pull-out test results to full-scale reinforcement lengths. Development of this model required the appropriate instrumentations to measure the displacements at different locations along the geogrid. The data analysis permitted the derivation of the soil-geogrid interaction parameters and the in-soil stress-strain relationship of the reinforcement from displacement-rate controlled pull-out tests. The confined creep characteristics were determined from the interpretation of stepped load-controlled pull-out tests.

The methods currently used for the design of geosynthetic reinforced

walls and embankments are mostly derived from conventional slope stability analysis modified to account for the reinforcement effect on the global stability of the soil mass. These methods do not provide an estimation of the tension forces mobilized at each reinforcement and, therefore, can not be used to evaluate the local stability at each reinforcement level. These limitation raised the need to development of a design approach that utilizes the interface parameters and in-soil stress-strain characteristics derived from pull-out test results . This approach considers the strain compatibility between the reinforcement and the soil under working loads and allows the evaluation of the effect of soil dilatancy and reinforcement extensibility on the generated tension forces at each reinforcement level. The predicted tension forces and failure angles are found to be consistent with the observations on reduced scale lab models, full-scale model walls, and embankments with different types of extensible reinforcements. The comparison between predicted and measured tension forces in these walls demonstrates that the two assumptions, commonly used to predict the state of stresses in the reinforcement (i.e. Ka and Ko) are too restrictive to properly simulate the observed variation of tension forces with depth for different extensible reinforcements.

REFERENCES

Al-Hussaini, M.M., (1977), "Field Experiment of Reinforced Earth Wall," Internat. Conference on the Use of Fabrics in Geotechnics, Paris, Vol. 1, pp. 119-121.

Andrawes, K.Z., McGown, A., and Murray, R.T., (1986), "The Load-Strain-Time-Temperature Behavior of Geotextiles and Geogrids," 3rd. Internat. Conference on Geotextiles, Vienna, Vol. 3, pp. 707-712.

Anderson, L.R., and Nielsen, M.R., (1984), "Pull-Out Resistance of Wire Mats Embedded in Soil," Report for the Hilfiker Company, Eureka, CA.

Bell, A.L., Green, H.M., and Laverty. K., (1982), "Factors Influencing the Selection of Woven Polypropylene Geotextiles for Earth," 2nd. Internat. Conference on Geotextiles, Las Vegas, Vol. 3, pp. 689-694.

Bonaparte, R., Holtz, R.D., and Giroud, J.P., (1987),"Soil Reinforcement Design Using Geotextiles and Geogrids," Geotextile Testing & the Design Engineer, ASTM STP 952, pp. 69-116.

Bonczkiewicz, C., Christopher, B.R., and Atmatzidis, D.K., (1988), "Evaluation of Soil-Reinforcement Interaction by Large Scale Pullout Box" Transport. Research Board, 67th Annual Meeting, Washington D.C.

Brakel, J., Coppers, M., Maagdenberg, A.C., and Risseuw, P., (1982), "Stability of Slopes Constructed with Polymer Reinforced Fabric, Test Section of Almer, Holland," 2nd. Internat. Conference on Geotextiles, Las Vegas , V. 3, pp. 727-732.

Brand, S.R., and Duffy, D.M., (1987), "Strength and Pullout Testing of Geogrids," Geosynthetics Conference, New Orleans, Vol. 1, pp.226-236.

Broms, B.B., (1977), "Triaxial Tests with Fabric-Reinforced Soil," Internat. Conference on the Use of Fabrics in Geotechnics, Paris, Vol. 3, pp. 129-133.

Christensen, R.W., and Wu, T.H., (1964), "Analysis of Clay Deformation as a Rate Process," Journal of Soil Mech. and Foundation Division, ASCE, Vol. 90, No. SM6, pp. 125-157.

Christopher, B.R., (1976),"Tensar SS2 Geogrid Evaluation", Evaluation Report to Tensar Cooperation.

Christopher, B.R., Holtz, R.D., and Bell, W.D., (1986), "New Tests for Determining the In-Soil Stress-Strain Properties of Geotextiles" 3rd. Internat. Conference on Geotextiles, Vienna, Vol. 3, pp. 683-688.

Christopher, B.R., Safder, A.G., Giroud, J.P., Juran, I., Mitchell, J.K., Schlosser, F., and Dunnicliff, J., (1989), "Reinforced Soil Structures, Design and Construction Guide," 2 Vol., FHWA Report No. RD-89043.

Colman, B.D. and Knox, A.G., (1957), "The Interpretation of Creep Failure in Textile Fibers as a Rate Process," Textile Research Journal, PP. 393-399.

Coyle, H.M., and Reese, L.C., (1966), "Load Transfer for Axially Loaded Piles in Clay," ASCE, Journ. of Soil Mech. and Found. Div., Vol. 92, No. 2, pp. 1-26.

Degoutte, G., and Mathieu, G., (1986), "Experimental Research of Friction Between Soil and Geomembranes or Geotextiles Using 30 x 30 cm_2 Shearbox," 3rd. Internat. Conference on Geotextiles, Vienna, Vol. 4, pp. 1251-1255.

El-Fermaoui, A., and Nowatzki, E., (1982), "Effect of Confining Pressure on Performance of Geotextiles in Soils," 2nd. Internat. Conference on Geotextiles, Las Vegas, Vol. 3, pp. 799-804.

Elias, V., (1979), "Friction in Reinforced Earth Utilizing Fine Grained Backfills," Internat. Conference of Soil Reinforcement, Paris, France, pp. 435-438.

Fowler, J., (1982), "Theoretical design Considerations for Fabric-Reinforced Embankments" 2nd. Internat. Conference on Geotextiles, Las Vegas, Vol. 3, pp. 665-670.

Formazin, J., and Batereau, C., (1985), "The Shear Strength Behavior of Certain Materials on the Surface of Geotextiles," Proc. of the 11th. Internat. Conference on Soil Mechanics, San Francisco, Vol. 3, pp. 1773-1775.

Forsyth, R.A., (1978), "Alternative Earth Reinforcement," Symposium on Earth Reinforcement, ASCE Convention, Pittsburgh, PA., pp. 358-362.

Gourc, J.P., Delmas, P., and Giroud, J.P., (1980), "Experiments on Soil Reinforcement with Geotextiles," ASCE Convention, Portland, Oregon.

Gourc, J.P., Ratel, A., and Delmas, P., (1986), "Design of Fabric Retaining Walls: The Displacement Method," 3rd. Internat. Conference on Geotextiles, Vienna, Vol. 3, pp. 289-294.

Greenwood, J.H., and Myles, B., (1986), "Creep and Stress Relaxation of Geotextiles," 3rd. Internat. Conference on Geotextiles, Vienna, Vol. 3, pp. 821-826.

Hausmann, M.R., and Vagneron, J.M., (1977), "Analysis of Soil-Fabric Interaction," Internat. Conference on the Use of Fabrics in Geotechnics, Paris, France, Vol. 3, pp. 139-144.

Hird, C.C., (1986), "Stability Charts for Reinforced Embankments on Soft Ground," Geotextiles and Geomembranes, 4, pp. 107-127.

Holtz, R.D., and Broms, B.B., (1977), "Walls Reinforced by Fabrics - Results of Model Tests," Internat. Conference on the Use of Fabrics in Geotechnics, Paris, France, Vol. 1, pp. 113-117.

Holtz, R.D., (1977), "Laboratory Studies of Reinforced Earth Using a Woven Polyester Fabric," Internat. Conference on the Use of Fabrics in Geotechnics, Paris, France, Vol.3, pp.149-154.

Holtz, R.D., Tobin, W., and Burke, W.W., (1982), "Creep Characteristics and Stress-Strain Behavior of a Geotextile-Reinforced Sand," 2nd. Internat. Conference on Geotextiles, Las Vegas, Vol. 3, pp 805-809.

Ingold, T. S., and Templeman, J., (1979), "The Comparative Performance of Polymer Net Reinforcement," Internat. Conference on Soil Reinforcement, Paris, Vol .1

Ingold, T.S., (1982), "An Analytical Study of Geotextile Reinforced Embankments," 2nd. Internat. Conference on Geotextiles, Las Vegas, Vol. 3, pp 683-688.

Ingold, T.S., (1983), "Laboratory Pull-out Testing of Grid Reinforcement in Sand," Geotech. Testing Journal, 6(3), pp. 101-111.

Jaber, M., Mitchell, J.K., Shen, C.K., and Hua, Z.K., (1987), "Behavior of Reinforced Soil, Centrifuge Model Tests," FHWA Report No. DTFH61-84-00073.

Jacobsen, H. M., (1985), "Stability of Earth Structures Reinforced by Geotextiles," Proc. of the 11th. Internat. Conference on Soil Mechanics and Foundation Engineering, San Francisco, Vol. 3, pp. 1781-1785.

Jewell, R.A., (1980), "Some Effects of Reinforcement on the Mechanical Behavior of Soils," Ph.D. Thesis, Cambridge University, Cambridge, England.

Jewell, R.A., (1982), "A Limit Equilibrium Design Method for Reinforced Embankments on Soft Foundations," 2nd. Internat. Conference on Geotextiles, Las Vegas, Vol. 3, pp. 671-676.

Jewell, R.A., Milligan, G., Sarsby, R.W., and Dubois, D., (1984), "Interaction between Soil and Geogrids ", Proceedings, Polymer Grid Reinforcement, London, pp. 18-30.

Johnston, R.S., (1985), "Pull-out Testing of Tensar Geogrids," Thesis presented to University of California at Davis for M.Sc. Degree.

Juran, I., Knochenmus, G., Acar, Y.B., and Arman, A.,(1988), "Pull-out Response of Geotextiles and Geogrids (Synthesis of Available Experimental Data)," Proc. of Symp. on Geotextiles for Soil Improvement, ASCE, Geotech. Special Publication 18, pp. 92-111.

Juran, I., Guermazi, A., Chen, C.L., and Ider, M.H., (1988-b), "Modeling and Simulation of Load Transfer in Reinforced Soil: Part 1," Internat. Journal of Numer. and Analytical Methods in Geomechanics, Vol. 12, pp. 141-155.

Juran, I., Ider, H., Chen, C.L., and Guermazi, A., (1988-c), "Numerical Analysis of the Response of Reinforced Soils to Direct Shearing: Part 2," Internat. Journal of Numer. and Analytical Methods in Geomechanics, Vol. 12, pp. 157-171.

Juran, I., and Chen, C.L., (1988), "Soil-Geotextile Pull-out Interaction Properties, Testing and Interpretation," Transp. Research Board, 67th Annual Meeting, Washington D.C.

Juran, I., and Chen, C.L., (1989), "Strain Compatibility Design Method for Reinforced Earth Walls," Journal of Geotech. Engineering, ASCE, Vol. 115, No.4, pp. 435-456.

Juran, I., and Christopher, B., (1989), "Laboratory Model Study of Geosynthetic Reinforced Soil Retaining Walls," Journal of Geotech. Engineering., ASCE, Vol. 115, No. 7, pp. 905-926.

Juran, I., Ider, H., and Farrag, K., (1990), "Strain Compatibility Analysis for Geosynthetic Reinforced Soil Walls," Journal of Geotech. Engineering, ASCE, Vol. 116, No. 2, pp. 312-329.

Knochenmus, G., (1987), "Review of the Available Pull-out Testing Facility," Report submitted to Louisiana Transport. Research Center, Research Project 87-1G7.

Knochenmus, G., (1989), "Stress-Strain Behavior of Non-woven Geotextiles under Confined Conditions," Thesis presented to Louisiana State University for M.Sc. Degree, 194 p.

Koerner, B., (1986), "Direct Shear/Pull-out Tests on Geogrids," Report No. 1, Dept. of Civil Eng., Drexel Univ., Philadelphia, PA.

Leshchinsky, D., and Reinschmidt, A.J., (1985), "Stability of Membrane Reinforced Slopes," Journal of Geotech. Engineering, ASCE, Vol. 111, No. 11, pp. 1285-1300.

Leshchinsky, D., Volk, J.C., and Reinschmidt, A.J., (1986), "Stability of Geotextile-Reinforced Earth Railroad Embankments," Geotextiles and Geomembranes, 3, pp. 105-128.

Leshchinsky, D., and Perry, E.B., (1987), "A Design Procedure for Geotextile-Reinforced Walls," Geosynthetics Conference, New Orleans, pp. 95-107.

Leshchinsky, D., and Field, D.A., (1987), "In-Soil Load Elongation, Tensile Strength and Interface Friction of Non-Woven Geotextiles," Geosynthetics Conference, New Orleans, Vol. 1, pp. 238-249.

Leshchinsky, D., and Perry, E.B., (1989), " On the Design of Geosynthetic Reinforced Walls," Geotextile and Geomembranes, 8, pp. 311-323.

Leshchinsky, D., and Poedeker, R., (1989), "Geosynthetic Reinforced Soil Structures," Journal of Geotech. Engineering, ASCE, Vol. 115, No. 10, pp. 1459-1478.

Martin, J.P., Koerner, R.M., and Whitty, J.E., (1984), "Experimental Friction Evaluation of Slippage Between Geomembranes, Geotextiles and Soils," Proc. Int. Conf. on Geomembranes, Denver, pp. 191-196.

McGown, A., Andrawes, K.Z., and Kabir, M.H., (1982), "Load-Extension Testing of Geotextiles Confined In-Soil," 2nd. Internat. Conference on Geotextiles, Las Vegas, Vol. 3, pp. 793-798.

Milligan, V., and La Rochelle, P., (1984), "Design Methods for Embankments over weak soils," Polymer Grid Reinforcement, London, pp. 95-102.

Mitchell, J.K., Campanella, R.G., and Singh, A., (1968), "Soil Creep as a Rate Process," Journal of the Soil Mech. and Foundation Division, ASCE, pp. 231-253.

Mitchell J.K., (1969), "Shearing Resistance of Soils as a Rate Process," Journal of the Soil Mechanics and Foundation Division, ASCE, pp. 29-61.

Mitchell, J.K., and Villet, W.C., (1987), "Reinforcement of Earth Slopes and Embankments," Transport. Research Board, NCHRP Report No. 290.

Miyamori, T., Iwai, S., Makiuchi, K., (1986), "Frictional Characteristics of Non-Woven Fabrics," 3rd. Internat. Conference on Geotextiles, Vienna, Vol. 3, pp. 701-705.

Murayama, S. and Shibata, T., (1961) "Rheological Properties of Clays," Proc. 5th. Int. Con. on Soil Mech. and Foundations, Paris, pp. 269-273.

Murray, R.T., (1982), "Fabric Reinforcement of Embankments and Cuttings," 2nd. Internat. Conference on Geotextiles, Las Vegas, V. 3, pp. 707-713.

Myles, B., (1982), "Assessment of Soil Fabric Friction by Means of Shear," 2nd. Internat. Conference on Geotextiles, Las Vegas, Vol. 3, pp. 787-791.

Myles, B., (1987), "A Review of Existing Tension Testing Methods," Geotextiles Testing and the Design Engineer, ASTM STP 952, pp. 57-68.

Palmeira, E., and Milligan, G., (1989), "Large Scale Direct Shear Tests on Reinforced Soil," Soils and Foundations, Japanese Society of Soil Mech. and Found. Eng., Vol. 29, No. 1, pp. 18-30.

Richards, E.A., and Scott, J.D., (1985), "Soil Geotextile Friction Properties," 2nd. Canadian Symp. on Geotextile & Geomembrane, pp. 13-24.

Richards, E.A., and Scott, J.D., (1986), "Stress-Strain Properties of Geotextiles," 3rd. Internat. Conference on Geotextiles, Vienna, Vol. 3, pp. 873-878.

Rowe, R.K., (1984), "Reinforced Embankment, Analysis and Design," Journal of Geotech. Engineering, ASCE, Vol. 110, No. 2, pp. 231-246.

Rowe, R.K., Ho, S.K., and Fisher, D., (1985), "Determination of Soil-Geotextile Interface Strength Properties," 2nd. Canadian Symposium on Geotextiles, pp. 25-34.

Rowe, R.K., and Soderman, K.L., (1985), "An Approximate Method for Estimating the Stability of Geotextile-Reinforced Embankments'" Can. Geotech. Journal, Vol. 22, pp. 392-398.

Rowe, R.K., and Ho, S.K., (1986), "Determination of Geotextile Stress-Strain Characteristics using a Wide Strip Tests", 3rd. Internat. Conf. on Geotextiles, Vienna, pp. 885-890

Saxena, S.K., and Budiman, J.S., (1985), "Interface Response of Geotextiles," Proc. of the 11th. Internat. Conference on Soil Mechanics and Foundation Engineering, San Francisco, Vol. 3, pp. 1801-1804.

Shen, C.K., Romsted, K. and Hermann, L.R. (1976),"Integrated Study of Reinforced Earth, II-Behavior and Design," Journal of the Geotech. Div., ASCE, 102-GT6, pp. 577-590.

Siel, B.D., Tzong, W.H., and Chou, N.N., (1987), "In-Soil Stress-Strain Behavior of Geotextile," Geosynthetics Conference, New Orleans, Vol.1, pp. 260-265.

Singh, A. and Mitchell, J.K., (1968), "General Stress-strain-Time Functions for Soils", Journ. Soil. Mech. and Found. Division, ASCE, SM1, Jan., pp. 21-46.

Singh, A. and Mitchell, J.K., (1969), "Creep Potential and Creep Rupture of Soils," Proc. 7th. ICSMFE, Mexico, vol. 1.

Shrestha, S.C., and Bell, J.R., (1982-a), "A Wide Strip Tensile Test of Geotextiles," 2nd. Internat. Conference on Geotextiles, Las Vegas, Vol. 3, pp. 739-744.

Shrestha, S.C., and Bell, J.R., (1982-b), "Creep Behavior of Geotextile Under Sustained Loads," 2nd. Internat. Conference on Geotextiles, Las Vegas, Vol. 3, pp. 769-774.

Schlosser, F., and Elias, V., (1978), "Friction in Reinf. Earth," ASCE National Convention, Pittsburgh, PA., pp. 735-764.

Schlosser, F., and Guilloux, A., (1979) "Friction Between Soil and Strips in Reinforced Earth Structures," Intern. Conference of the Reinforcement of Soils, Paris,France, Vol. 1.

Schlosser, F., Jacobsen, H.M., and Juran, I., (1983),"Soil Reinforcement," 8th. European Conference on Soil Mechanics and Foundation Engineering, Helsinki.

Schmertmann, G.R., Chouery, C., Johnson, R., and Bonaparte, R.,(1987) "Design Charts for Geogrid Reinforced Soil Slopes," Geosyunthetic Conference, New Orleans, pp. 108-120.

Solomone, W.G., Boutrup, E., Holtz, R.D., Kovacs, W.D., and Sulton, C.D., (1980), "Fabric Reinforcement Designed Against Pull-out," The Use of Geotextiles for Soil Improvement, ASCE, Portland, Oregon, pp. 80-177.

Stewart, J.R., Williamson, and Mohnen, (1977), "Guidelines for use of Fabrics in Construction and Maintenance of Low-Volume Roads", USDA Forest Service, Portland, Oregon.

Tzong, W.H., and Cheng-Kuang, S., (1987), "Soil-Geotextile Interaction Mechanism in Pullout Test," Geosynthetics Conference, New Orleans, Vol. 1, pp. 250-259.

Vyalov, S.S., (1986), "Rheological Fundamentals of Soil Mechanics," Developments in Geotechnical Engineering 36, Elsevier.

Williams, N.D., and Houlihan, M.F., (1987), "Evaluation of Interface Friction Properties Between Geosynthetics and Soils," Geosynthetics Conference, New Orleans, Vol. 2, pp. 616-627.

APPENDIX A

EQUIPMENT DETAILS & SPECIFICATIONS.

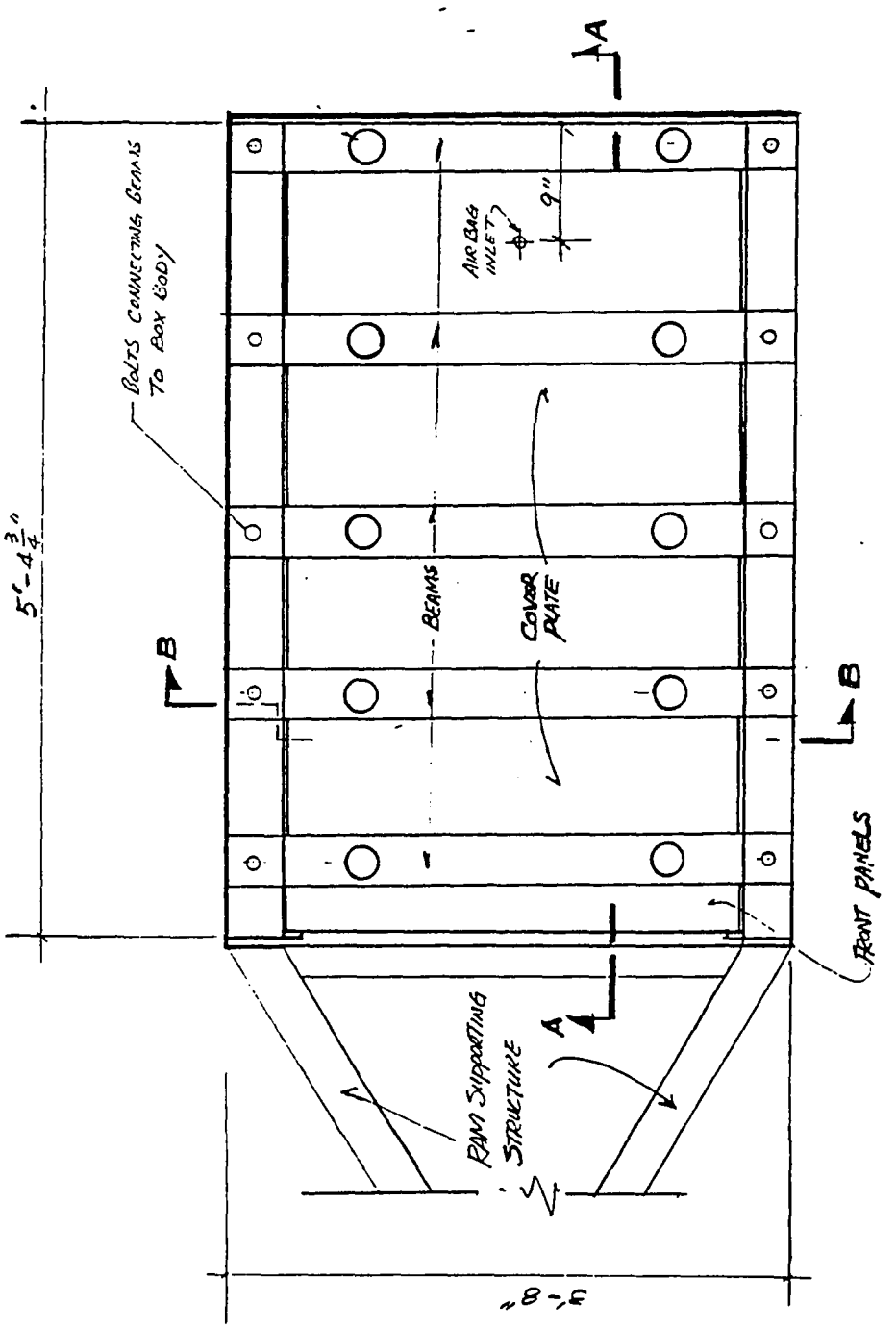

Figure A-1. Top View of the Pull-out Box

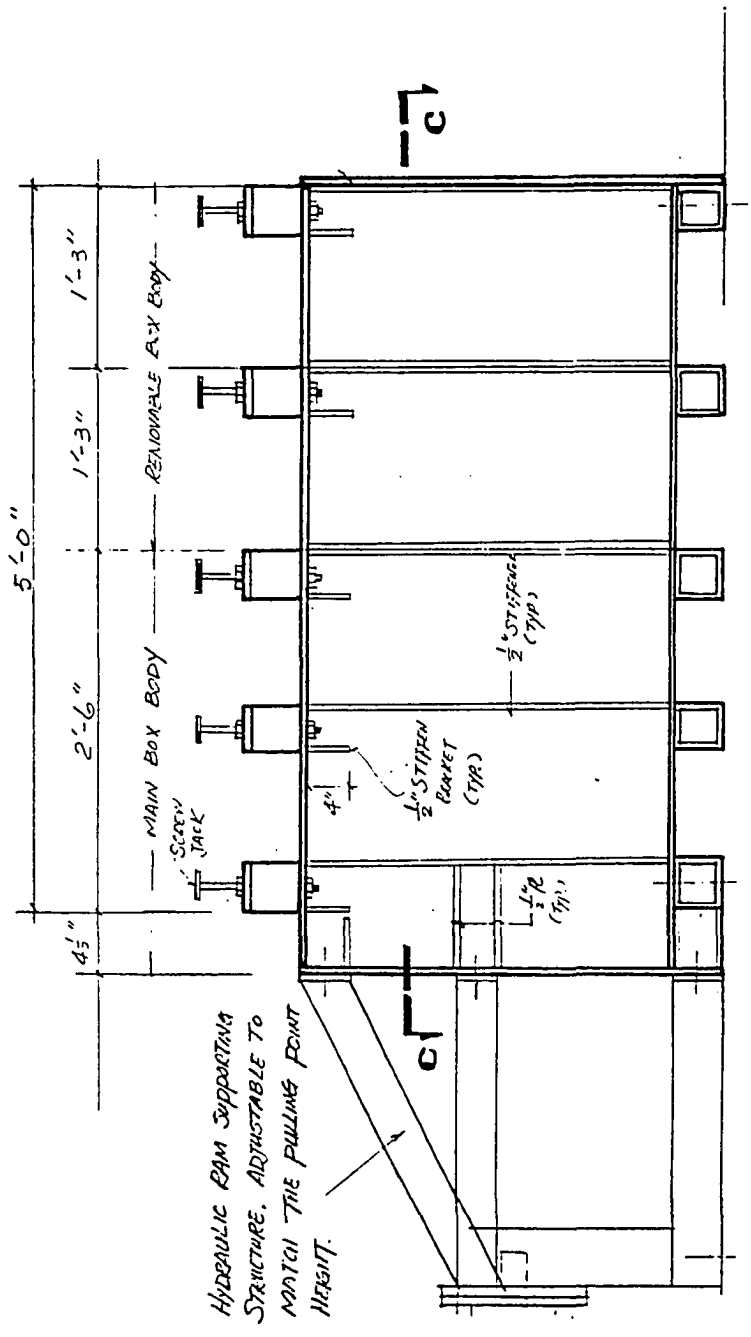

Figure A-2. View of the Pull-out Box.

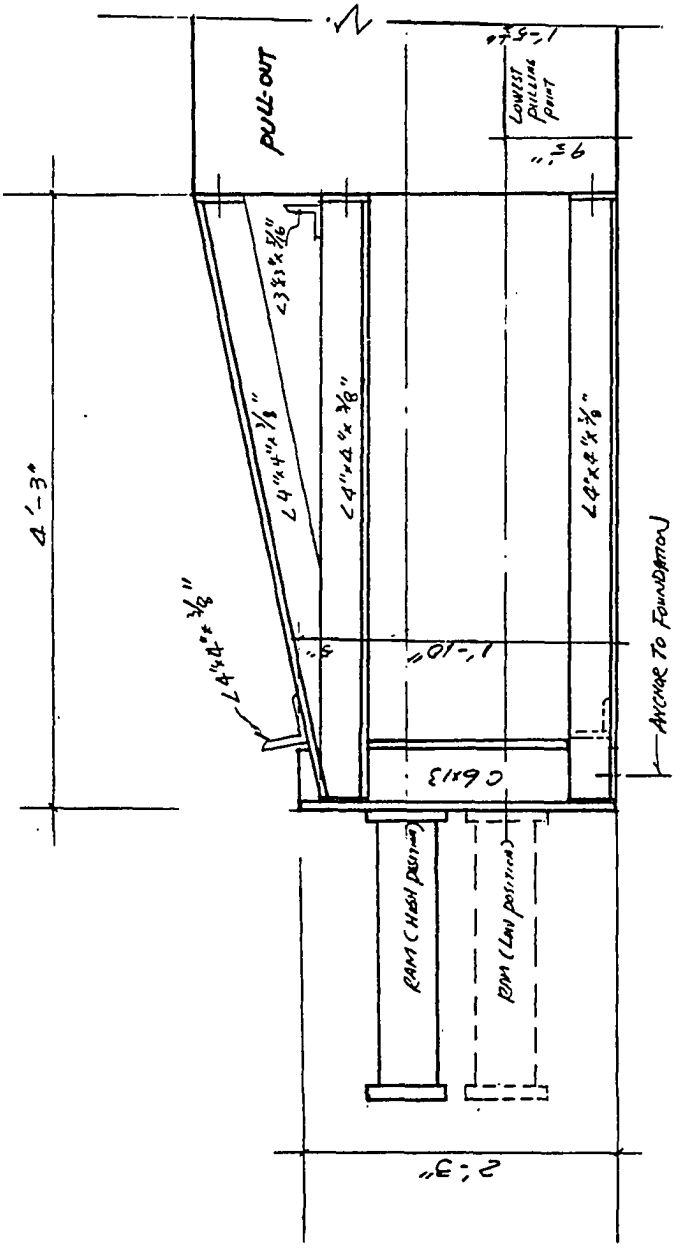

Figure A-3. Detail of the Loading Frame.

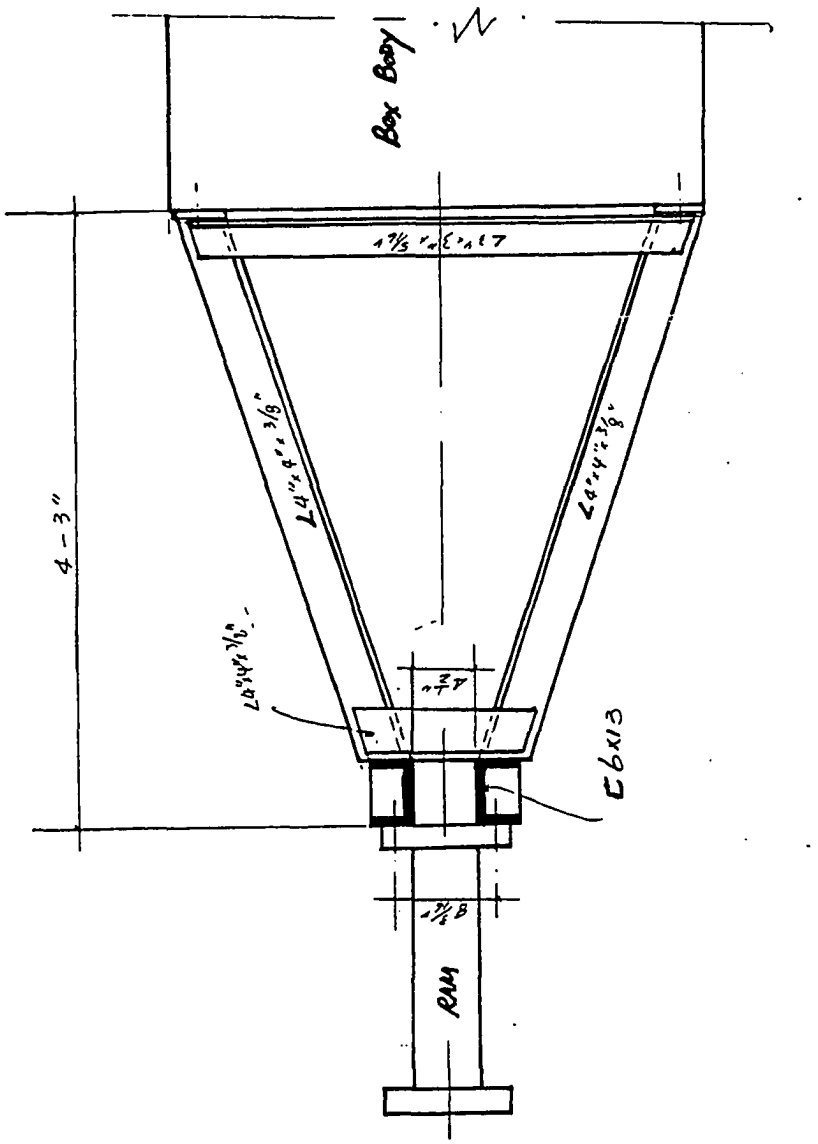

Figure A-4. Detail of the Loading Frame.

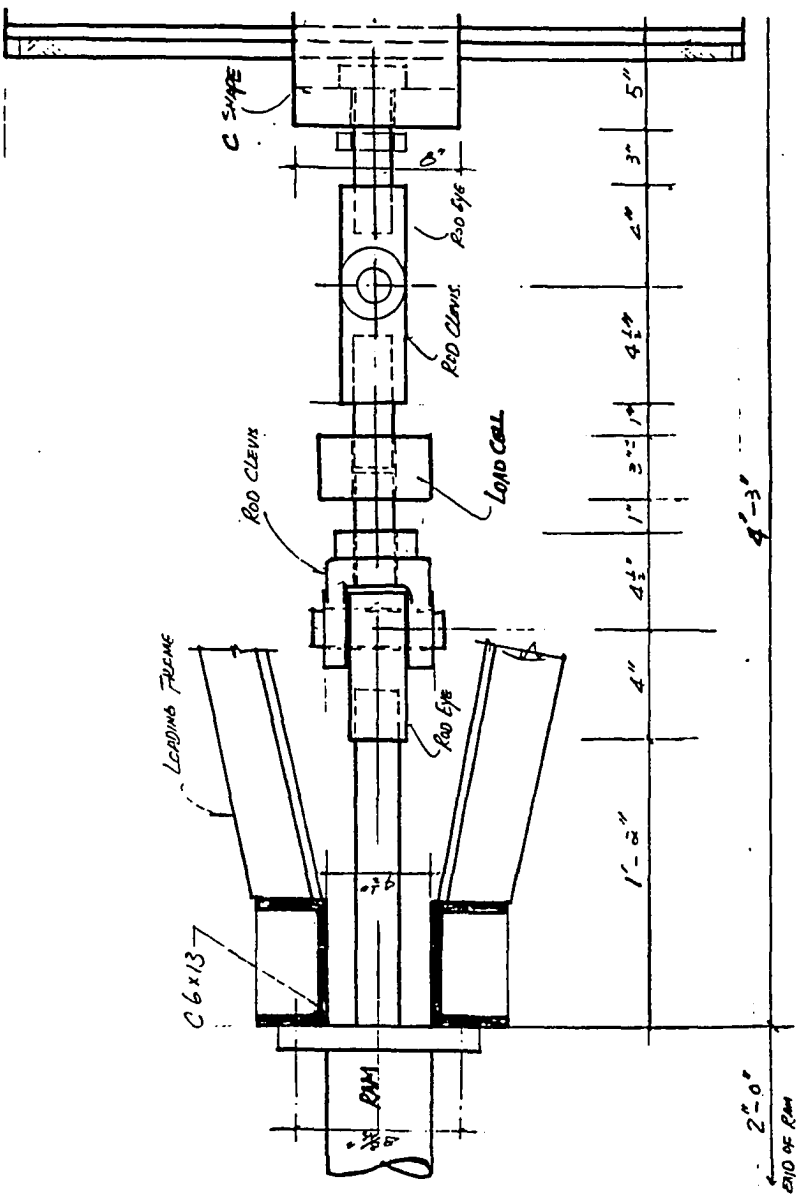

Figure A-5. Detail of Load Cell Connections.

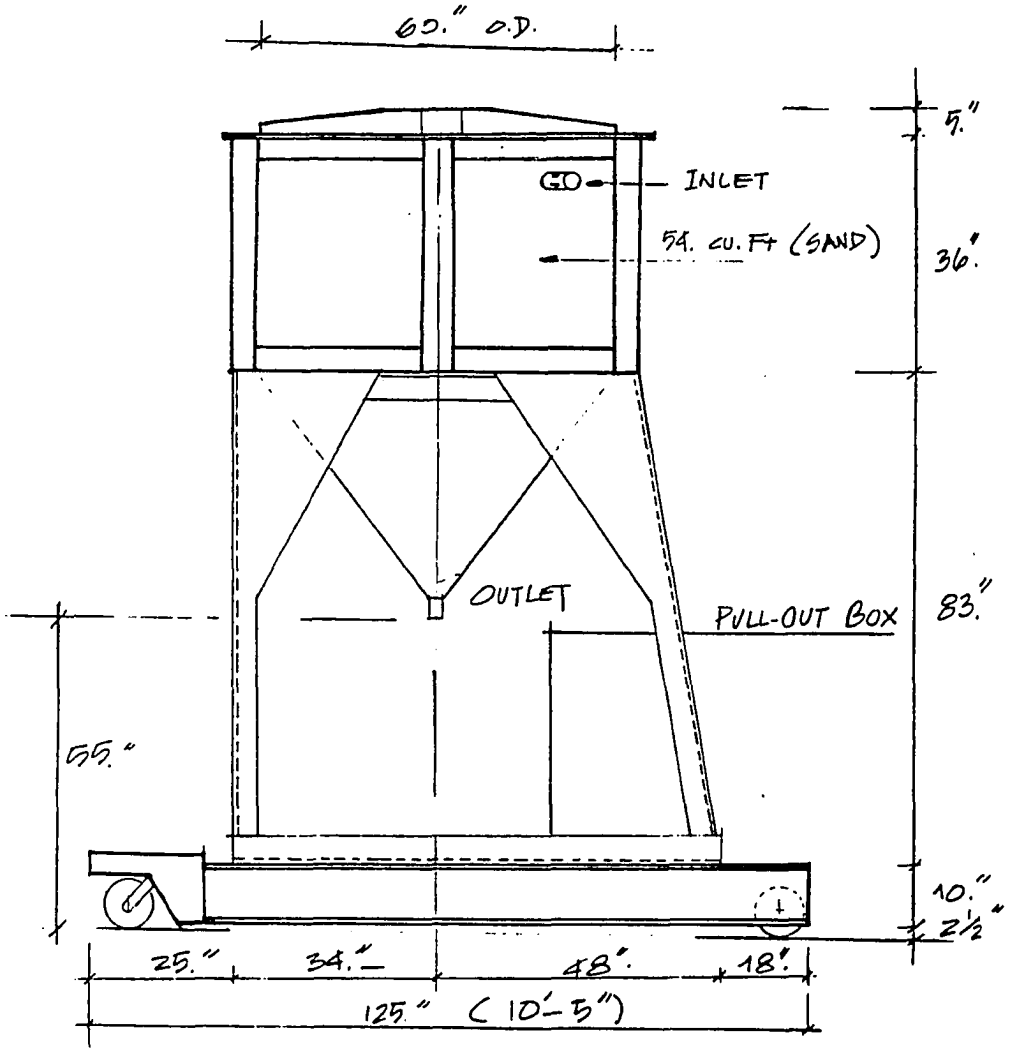

Figure A-6. Detail of Hopper.

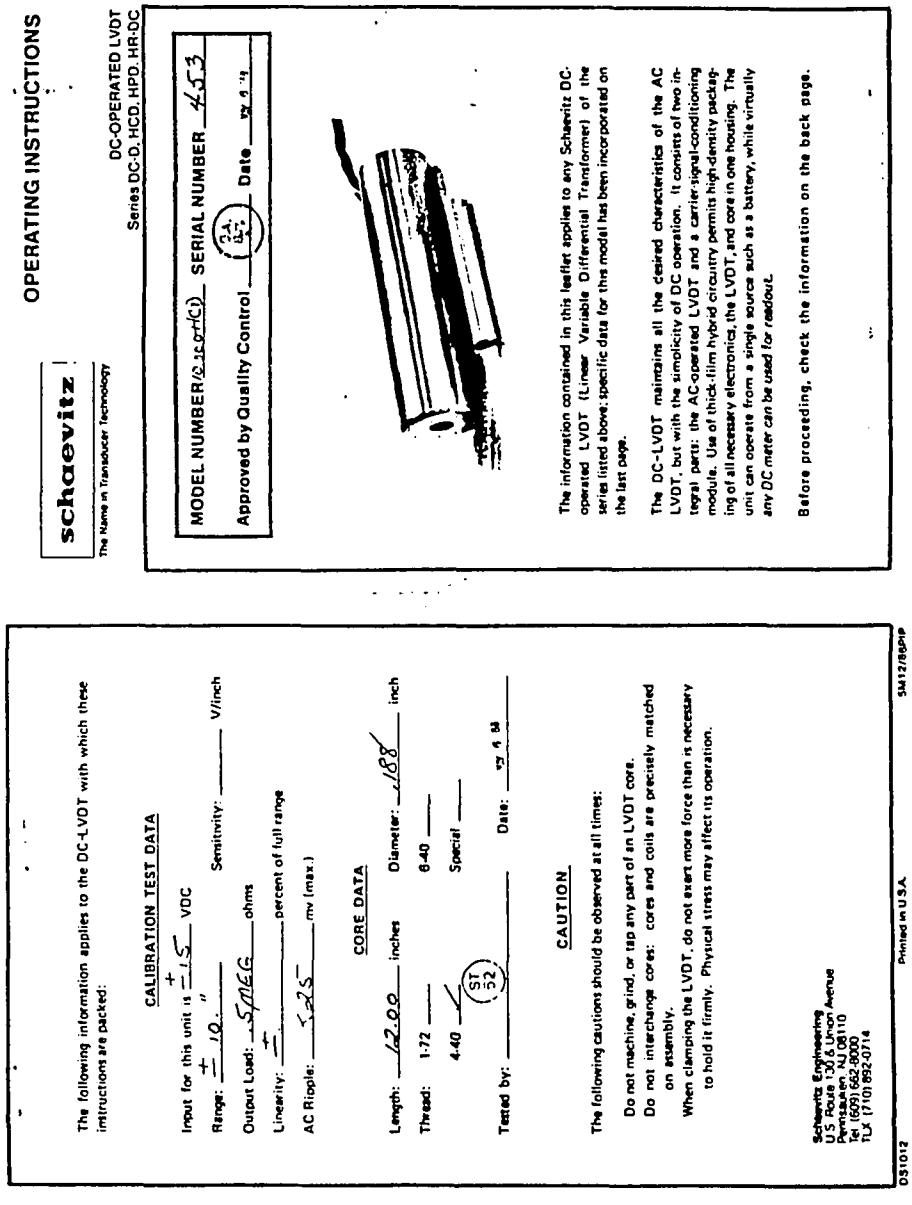

Figure A-7. Specifications of the LVDT's.

STRAIN GAGE LOAD CELL

MODEL 3187 - 20K S/N 751 CALIBRATION DATE 3/19/90

SPECIFICATIONS:

RATED CAPACITY-TENSION & COMPRESSION... 20,000 Lbs.
MAX. LOAD (without zero shift).....50% overload (150% of rated capacity
SIGNAL SENSOR.....4 arm bonded strain gage bridge
BRIDGE RESISTANCE.....350 ohms nominal
MAX. BRIDGE EXCITATION.....20 volts DC or AC RMS
COMPENSATED TEMP. RANGE.....70° F. to 170° F.
USEABLE TEMP. RANGE.....-65° F. to +200° F.
*EFFECT OF TEMP. ON ZERO.....±0.002% of rated capacity/°F.
*EFFECT OF TEMP. ON OUTPUT.....±0.002% of reading/°F.
NONLINEARITY.....±0. % of rated capacity
OUTPUT.....COMP. - 2.998 mV/V at rated cap.
TENS. +3.003 mV/V at rated cap.

*Within compensated temperature range

ELECTRICAL CONNECTIONS:

RECEPTACLE: PT02E-10-6P or MS-3102 A-14S-5P PIG
MATING CONNECTOR: PT06W-10-6S or MS-3106 E-14S-5S TAILS

PINS	FUNCTION	RESISTANCE
RED A (+) and (-) D BLK	Excitation	358.3 ohms
GRN B (+) and (-) C WHT	Signal	350.7 ohms

CALIBRATION:

A precision wire wound resistor, when shunted across one leg of the strain gage bridge, produces an electrical signal equivalent to an applied load. This shunt calibration is valid only when used with high input impedance indicators. The equivalent values below were determined by factory calibration.

LOAD VALUE	ACROSS PINS	RESISTOR VALUE
14,539 Lbs. compression	GRN B and D BLK	40 K ohms
14,526 Lbs. tension	GRN B and A RED	40 K ohms

Figure A-8. Specifications of the Load Cell.

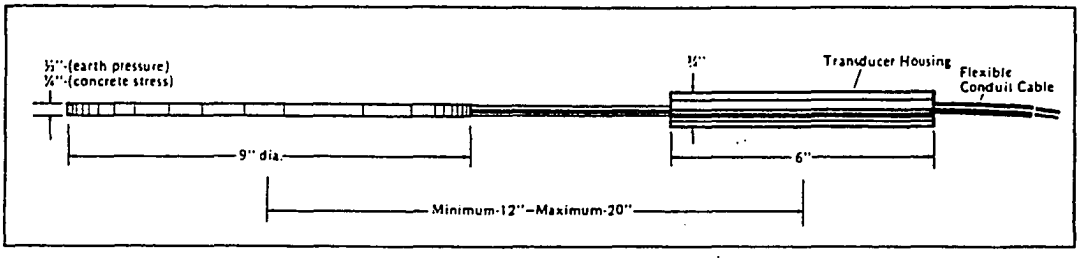

Geokon offers the following four basic types of transducers:

Pneumatic (Models 2510 and 2520). This transducer is a Petur Model P-100 and is connected to the readout location via twin pneumatic tubes (Model T-102). It is read out using the Petur Model C-102 Readout Box.

Semiconductor Strain Gage – Conventional style pressure transducer compatible with many existing dataloggers where 5 volt DC or AC excitation is provided. The signal output is large enough to be scanned directly without further amplification. They may also be read remotely using the Geokon Model RB-101 Readout Box.

Resistance Strain Gage – These transducers are compatible with other resistance strain gage systems such as load cells, borehole deformation gages etc. They may be read out using conventional strain indicator or readout boxes (Vishay P350A, Vishay P3500 etc.).

Vibrating Wire (Model 4500H). This transducer is compatible with the rest of the Geokon line of vibrating wire instruments and is recommended for use with the Model GK-4 Datalogger or GK-401 Readout Box. It incorporates all of the advantages of the vibrating wire system of measurements.

SPECIFICATIONS

Model Number		EP Cell 2510 CS Cell 2520	3500 3600	3650 3660	4800E 4800C
Transducer type	–	Pneumatic	Semiconductor strain gage	Resistance strain gage	Vibrating wire
Typical ranges available	psi	15 to 3000*	25,100,500 1000,3000,5000	25,100,500 1000,3000,5000	50,100,500 1000,3000,5000
Over-range capacity	% F.S.	3000 psi max.	200	200	150
Accuracy	% F.S.	0.4*	1	0.5	0.25
Resolution	% F.S.	0.4*	infinite	infinite	0.1
Thermal effect on zero	% F.S./°F	zero	<0.05	<0.02	<0.05
Excitation voltage	V	–	max.6v (DC or AC)	max.10v (DC or AC)	5v sq.wave
Signal output	mv/v	–	20	3	1200-2000Hz frequency
Bridge resistance	ohms	–	150in 115out	350	coil 150
Transducer housing dia.	in.	1.5	1.625	2.25	1
Transducer housing length	in.	6	6	6	6
Weight (less cable	lbs.	5 7	5 7	5 7	5 7
Connecting leads	–	Polyethylene twin tubes	4-cond. shielded	4-cond. shielded	2-cond. shielded
Readout box	–	Petur C-102	Geokon RB-101	Vishay P350A	Geokon GK-401

*Depends on pressure gage in readout box.

Figure A-9. Specifications of the Pressure Gauges.

APPENDIX B

COMPACTION CONTROL AND DENSITY CALIBRATION.

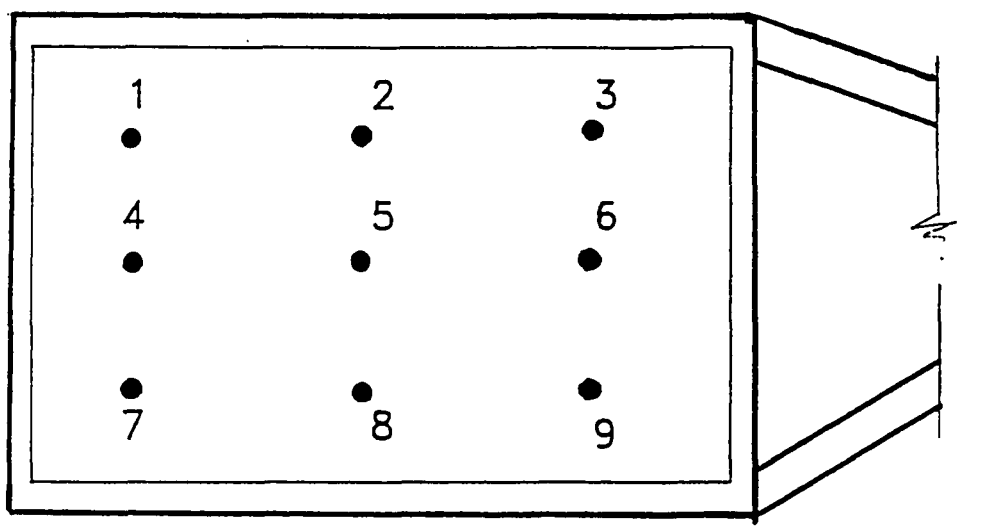

Figure B-1. Points od Density Measurements.

pt	blows	layer 2	layer 3 up	layer 3 down	layer 4
1	0	99.1 (0)	101.9 (+0.8)	102.6 (+1.0)	103.8 (+0.1)
	40	102.3 (+0.6)	101.9 (−0.7)	104.4 (+0.8)	104.7 (−0.5)
	110	103.8 (+0.3)	105.3 (+1.0)	106.2 (+1.1)	106.7 (−0.2)
	200	104.1 (−0.1)	108.0 (+2.9)	108.2 (+1.2)	108.4 (−0.1)
2	0	99.3 (+0.2)	102.2 (+1.1)	102.7 (+1.1)	103.5 (−0.2)
	40	102.4 (+0.7)	102.6 (0)	104.3 (+0.7)	105.9 (+0.7)
	110	103.2 (−0.3)	103.4 (−0.9)	104.0 (−0.9)	107.5 (+0.6)
	200	104.7 (+0.5)	104.3 (−0.8)	105.7 (−1.3)	108.9 (+0.4)
3	0	98.4 (−0.7)	101.4 (+0.3)	101.6 (+0.5)	103.2 (−0.5)
	40	100.8 (−0.9)	101.7 (−0.9)	102.2 (−0.4)	105.2 (0)
	110	103.4 (−0.1)	104.3 (0)	104.6 (+0.3)	107.0 (+0.1)
	200	104.3 (+0.1)	103.1 (−2.0)	105.8 (+0.7)	108.0 (−0.5)
4	0	98.7 (−0.4)	99.9 (−1.2)	100.6 (−1.0)	102.9 (−0.8)
	40	100.7 (−1.0)	102.5 (−0.1)	102.8 (−0.8)	104.7 (−0.5)
	110	103.1 (−0.4)	103.9 (−0.4)	105.7 (+0.6)	106.1 (−0.8)
	200	103.4 (−0.8)	104.0 (−1.1)	106.3 (−0.7)	107.4 (−1.1)
5	0	100.6 (+1.5)	101.3 (+0.2)	102.2 (+0.6)	103.2 (−0.5)
	40	102.6 (+0.9)	104.9 (+2.3)	104.4 (+0.8)	105.0 (−0.2)
	110	103.8 (+0.3)	105.2 (+0.9)	105.5 (+0.4)	107.5 (+0.6)
	200	103.6 (−0.6)	106.5 (+1.4)	107.9 (+0.9)	109.1 (+0.6)
6	0	98.5 (−0.6)	99.8 (−1.3)	99.6 (−2.0)	103.0 (−0.7)
	40	101.8 (+0.1)	102.2 (−0.4)	103.5 (−0.1)	103.9 (−1.3)
	110	103.8 (+0.3)	103.5 (−0.8)	104.5 (−0.6)	104.6 (−2.3)
	200	104.8 (+0.6)	104.7 (−0.4)	107.8 (+0.8)	109.9 (+1.4)

Table B-1. Density Measurements at Each Layer.
(Variable Falling Height).

Table B-1 (Continued)..

pt	blows	layer 2	layer 3 up	layer 3 down	layer 4
7	0	/	98.9 (−2.2)	104.6 (+3.0)	104.6 (+0.9)
	40	/	104.6 (+2.0)	105.8 (+2.2)	106.1 (+0.9)
	110	/	106.3 (+2.0)	107.2 (+2.1)	107.8 (+0.9)
	200	/	106.4 (+1.3)	107.4 (+0.4)	108.1 (−0.4)
8	0	/	102.8 (+1.7)	104.1 (+2.5)	104.7 (+1.0)
	40	/	105.1 (+2.5)	105.5 (+1.9)	105.2 (0)
	110	/	106.9 (+2.6)	107.4 (+2.3)	107.4 (+0.5)
	200	/	107.8 (+2.7)	108.1 (+1.1)	108.5 (0)
9	0	/	102.5 (+1.4)	104.2 (+2.6)	104.3 (+0.6)
	40	/	103.9 (+1.3)	105.6 (+2.0)	105.7 (+0.5)
	110	/	104.5 (+0.2)	107.5 (+2.4)	107.5 (+0.6)
	200	/	106.4 (+1.3)	107.9 (+0.9)	108.3 (−0.2)

pt	blows	layer 2	layer 3 up	layer 3 down	layer 4
1	0	101.1 (-0.8)	101.9 (-0.9)	104.1 (+0.8)	104.6 (+0.5)
	40	103.8 (0)	104.3 (+0.2)	105.7 (+0.7)	105.9 (+0.1)
	110	105.8 (+0.5)	106.1 (+0.1)	106.6 (-0.3)	107.0 (-0.4)
	200	106.0 (-0.3)	105.2 (-1.6)	108.0 (0)	108.1 (-0.9)
2	0	101.7 (-0.2)	103.1 (+0.3)	102.9 (-0.4)	103.8 (-0.3)
	40	104.7 (+0.9)	104.6 (+0.5)	105.3 (+0.3)	105.5 (-0.3)
	110	105.5 (+0.2)	106.3 (+0.3)	107.3 (+0.4)	107.3 (-0.1)
	200	105.2 (-0.9)	107.4 (+0.6)	107.6 (-0.4)	108.7 (-0.3)
3	0	102.5 (+0.6)	103.8 (+1.0)	103.5 (+0.2)	103.9 (-0.2)
	40	104.1 (+0.3)	103.9 (-0.2)	104.5 (-0.5)	105.6 (-0.2)
	110	104.9 (-0.4)	105.3 (-0.7)	106.4 (-0.5)	106.9 (-0.5)
	200	106.0 (-0.3)	105.8 (-1.0)	108.4 (+0.4)	107.2 (-1.8)
4	0	102.4 (+0.5)	102.9 (+0.1)	103.7 (+0.4)	104.7 (+0.6)
	40	103.1 (-0.7)	105.0 (+0.9)	104.9 (-0.1)	106.4 (+0.6)
	110	105.3 (0)	105.5 (-0.5)	106.8 (-0.1)	107.1 (-0.3)
	200	108.2 (+1.9)	106.7 (-0.1)	109.1 (+1.1)	109.6 (+0.6)
5	0	102.1 (+0.2)	102.2 (-0.6)	102.6 (-0.7)	104.2 (+0.1)
	40	103.5 (-0.3)	103.5 (-0.6)	104.6 (-0.4)	106.1 (+0.3)
	110	106.0 (+0.7)	106.8 (+0.8)	107.5 (+0.6)	107.1 (-0.3)
	200	107.2 (+0.9)	108.0 (+1.2)	107.7 (-0.3)	110.0 (+1.0)
6	0	101.5 (-0.4)	102.7 (-0.1)	103.2 (-0.1)	103.5 (-0.6)
	40	103.4 (-0.4)	103.2 (-0.9)	105.2 (+0.2)	105.2 (-0.6)
	110	104.1 (-1.2)	106.7 (+0.7)	106.8 (-0.1)	107.5 (+0.1)
	200	105.2 (-1.1)	107.5 (+0.7)	107.1 (-0.9)	108.3 (-0.7)

Table B-2. Density Measurements at Each Layer.
(Constant Falling Height).

Table B-2 (Continued).

pt	blows	layer 2	layer 3 up	layer 3 down	layer 4
7	0	/	103.9 (+1.1)	103.8 (+0.5)	103.9 (-0.2)
	40	/	103.9 (-0.2)	105.7 (+0.5)	105.5 (-0.3)
	110	/	105.3 (-0.7)	107.5 (+0.6)	108.3 (+0.9)
	200	/	108.3 (+1.5)	109.1 (+1.1)	110.0 (+1.0)
8	0	/	104.1 (+1.3)	103.9 (+0.6)	104.7 (+0.6)
	40	/	104.3 (+0.2)	106.4 (+1.4)	106.7 (+0.9)
	110	/	107.5 (+1.5)	108.3 (+1.4)	107.5 (+0.1)
	200	/	107.6 (+0.8)	107.8 (-0.2)	110.4 (+1.4)
9	0	/	103.7 (+0.9)	104.5 (+1.2)	103.6 (+0.5)
	40	/	104.4 (+0.3)	106.0 (+1.0)	105.1 (-0.7)
	110	/	108.4 (+2.4)	108.2 (+1.3)	107.6 (+0.2)
	200	/	106.8 (0)	107.3 (-0.7)	109.1 (+0.1)

APPENDIX C

PULL-OUT TEST RESULTS.

(a)

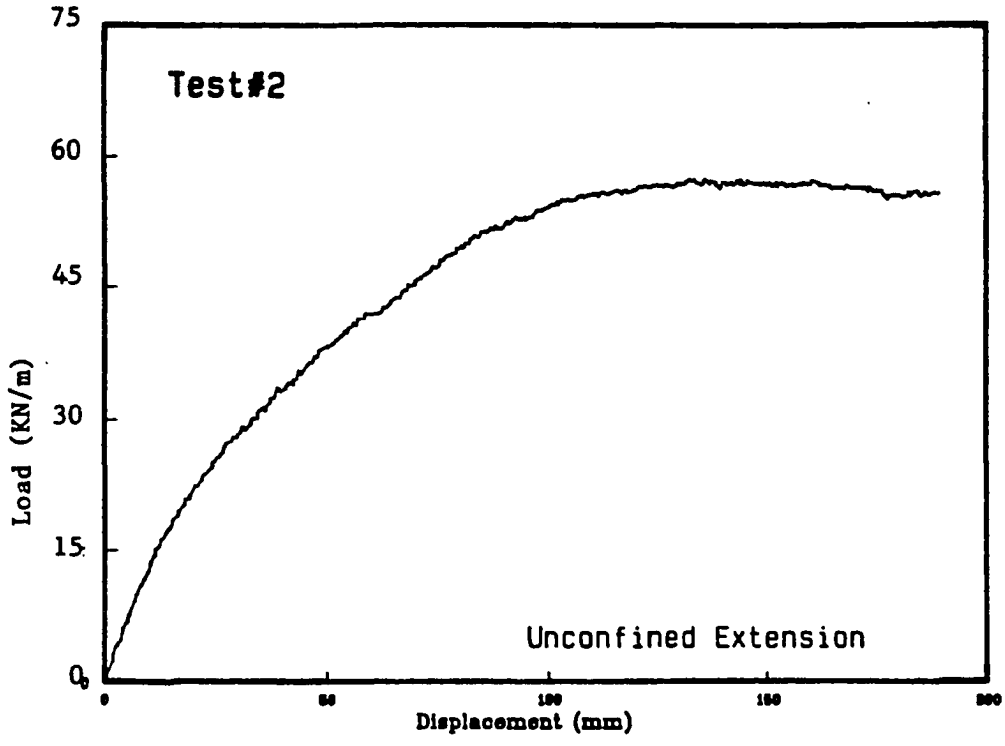

(a)

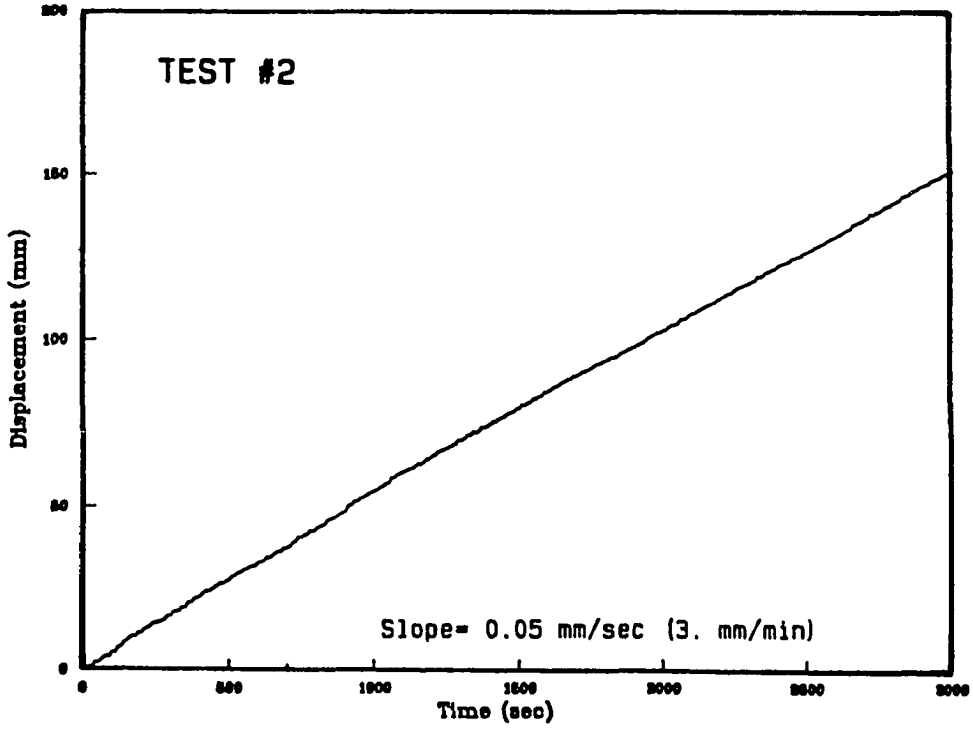

(b)

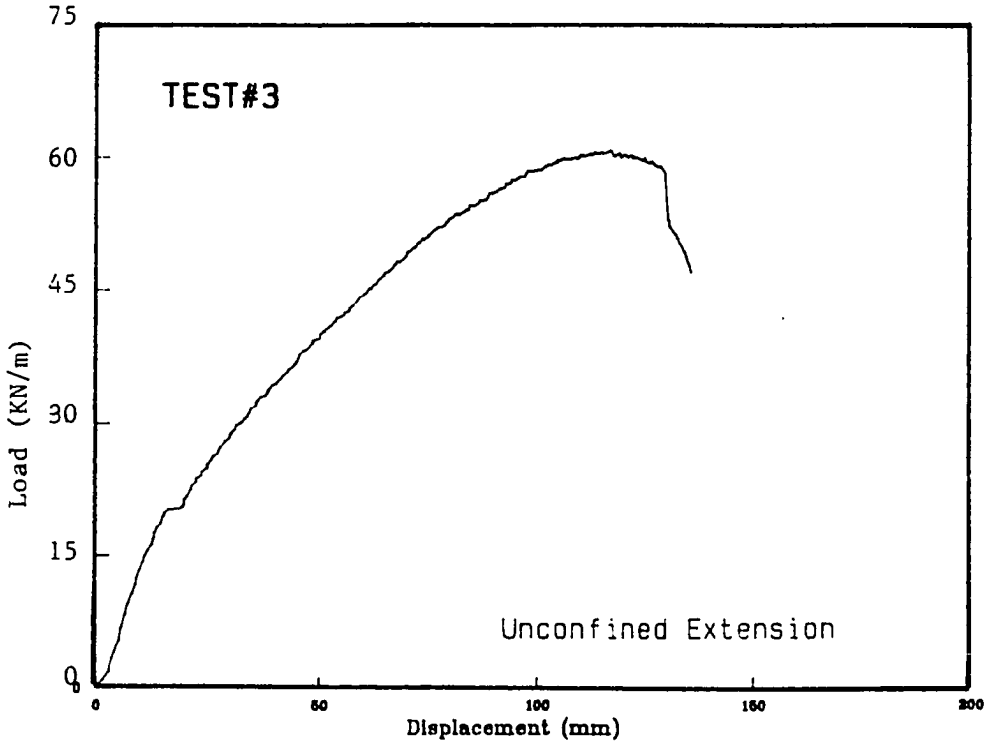

(a)

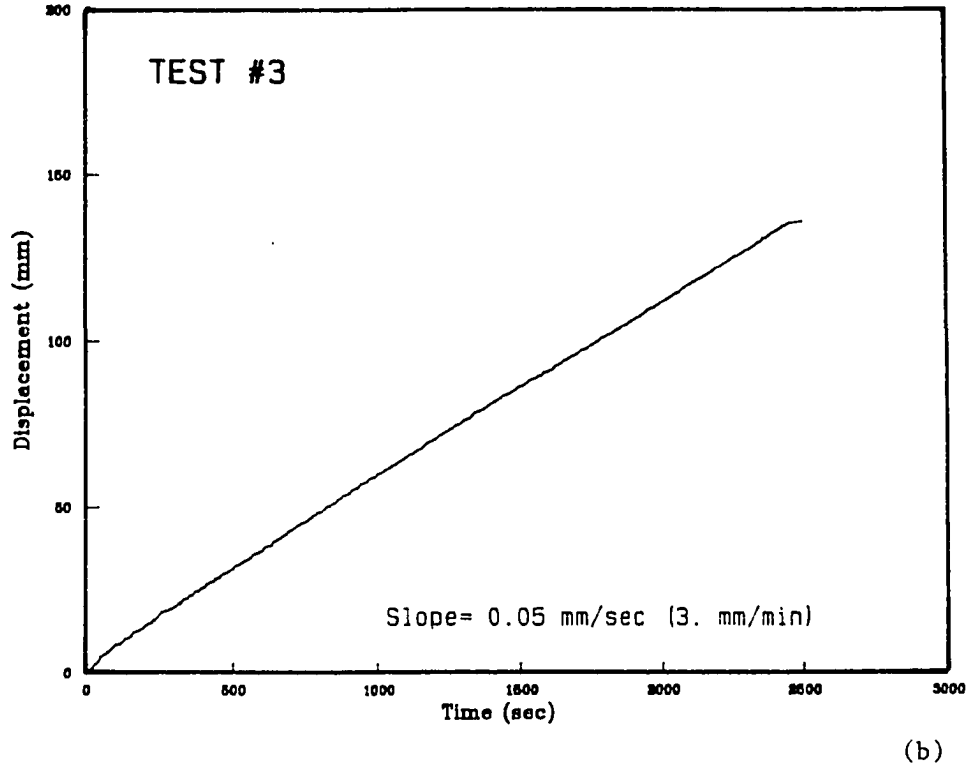

(b)

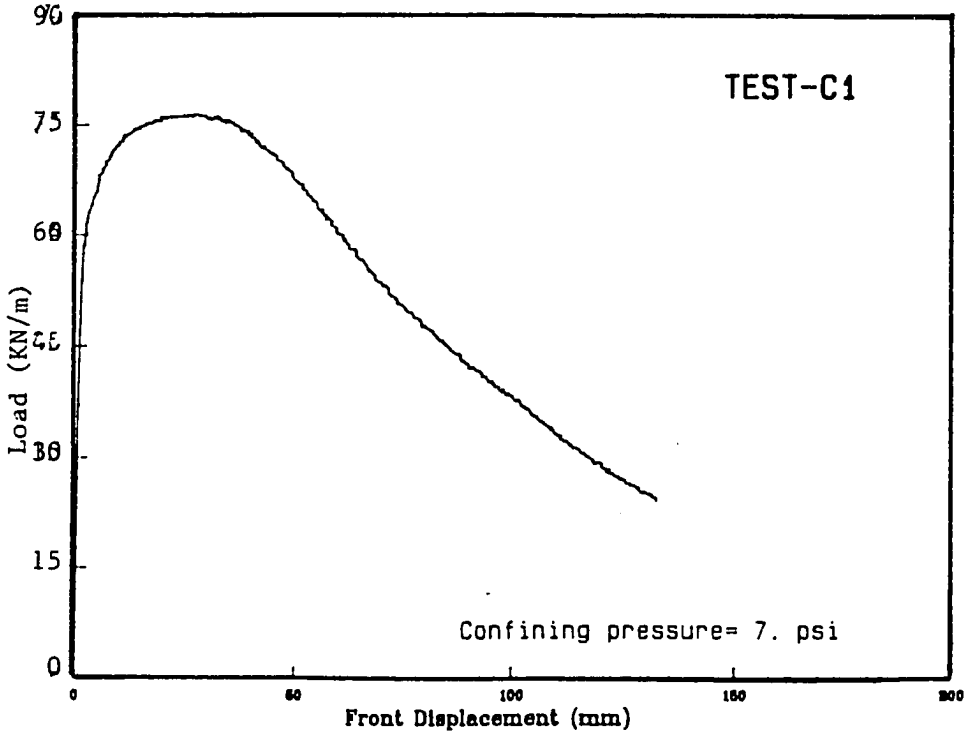

(a)

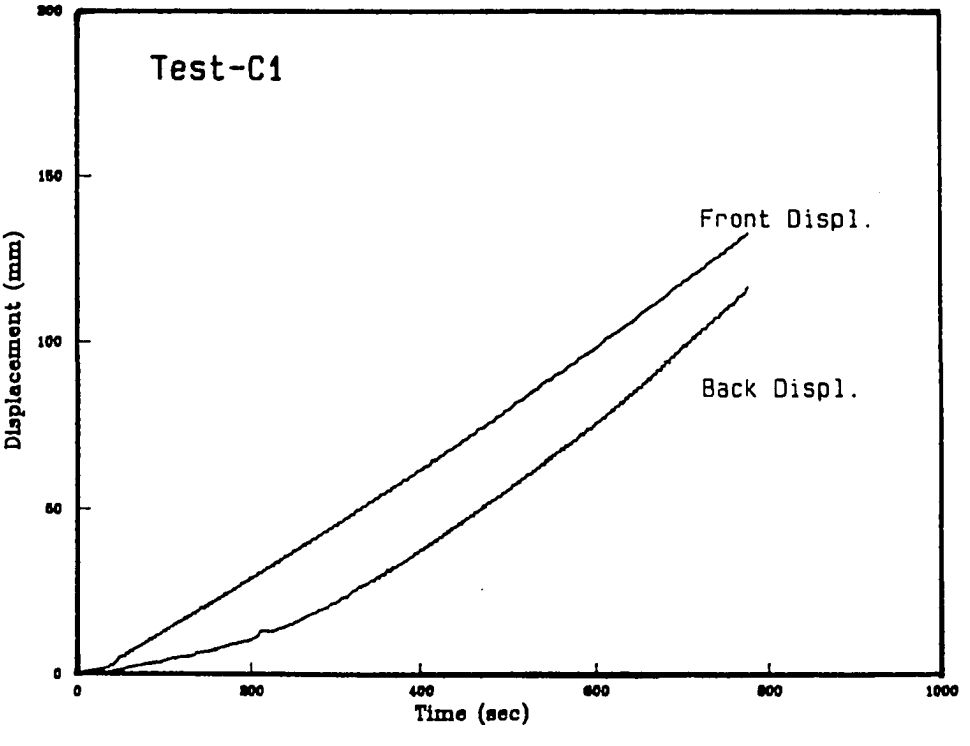

(b)

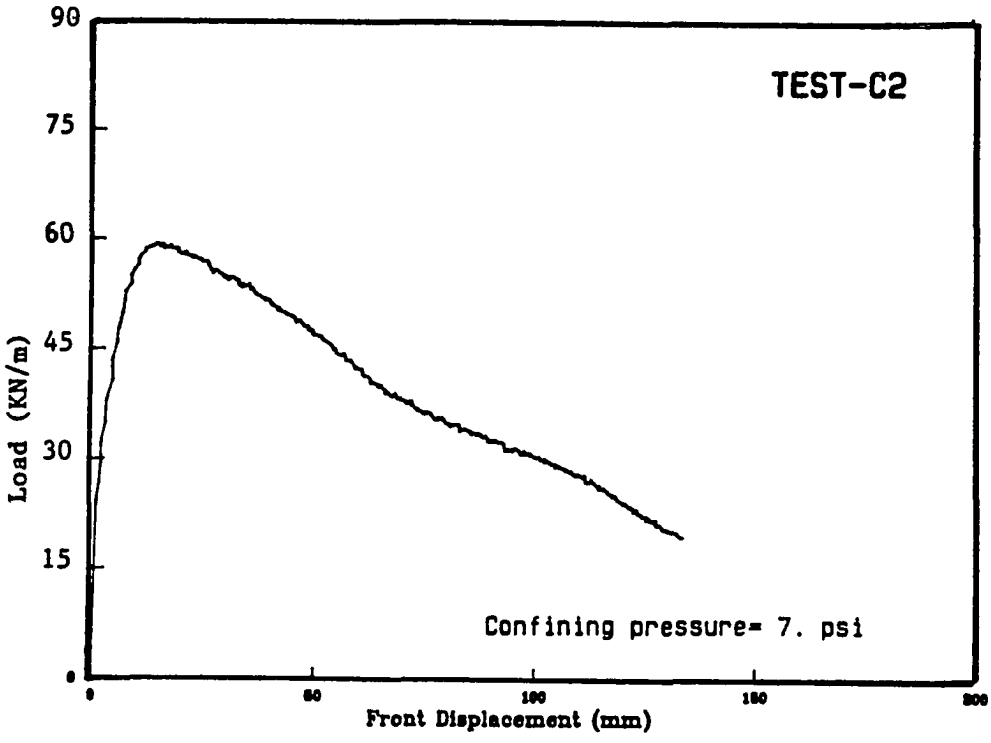

(a)

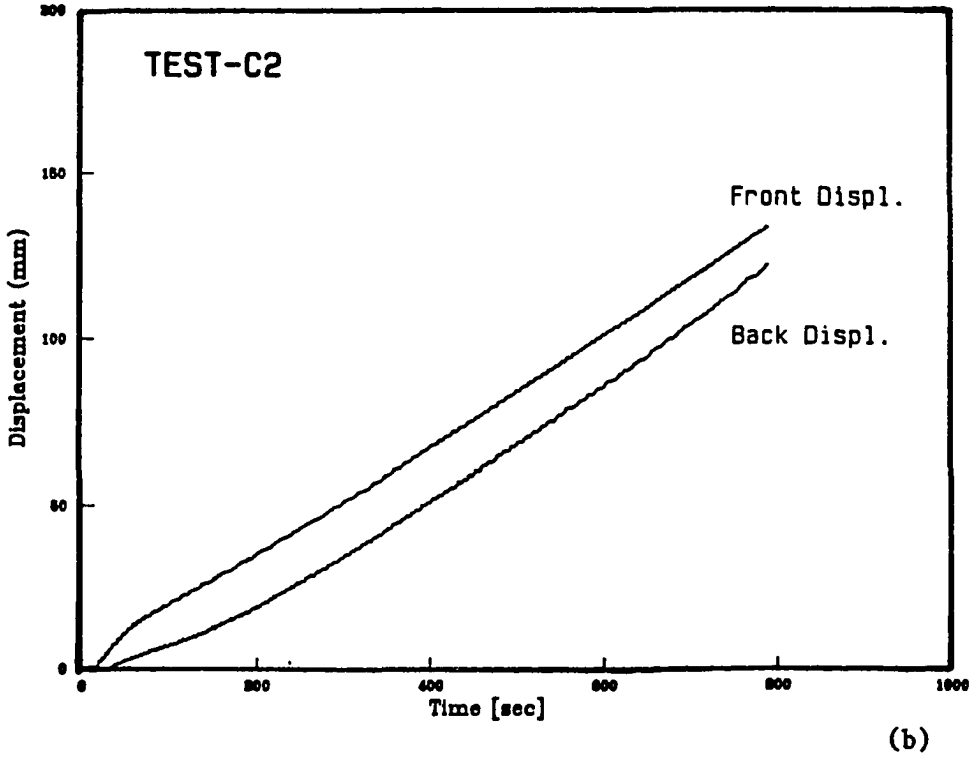

(b)

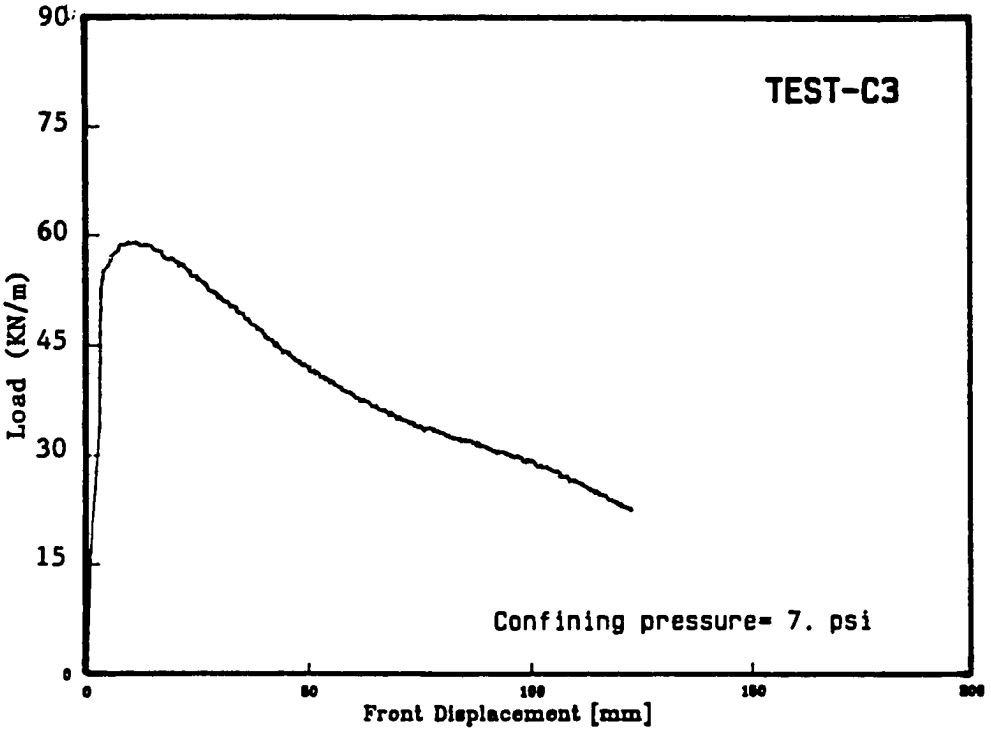

(a)

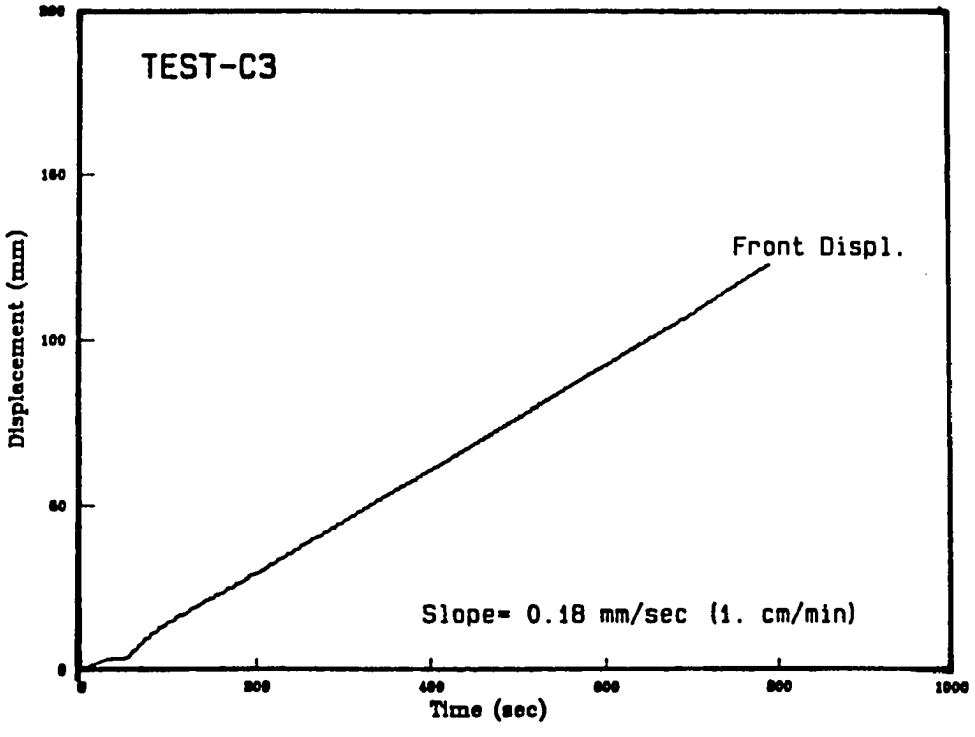

(b)

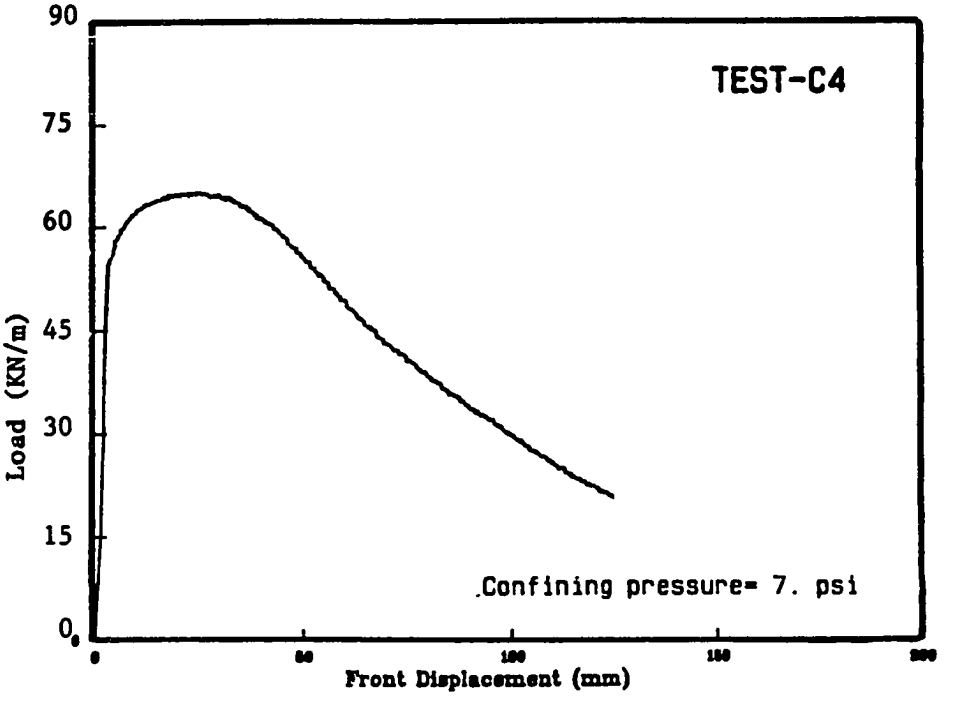

(a)

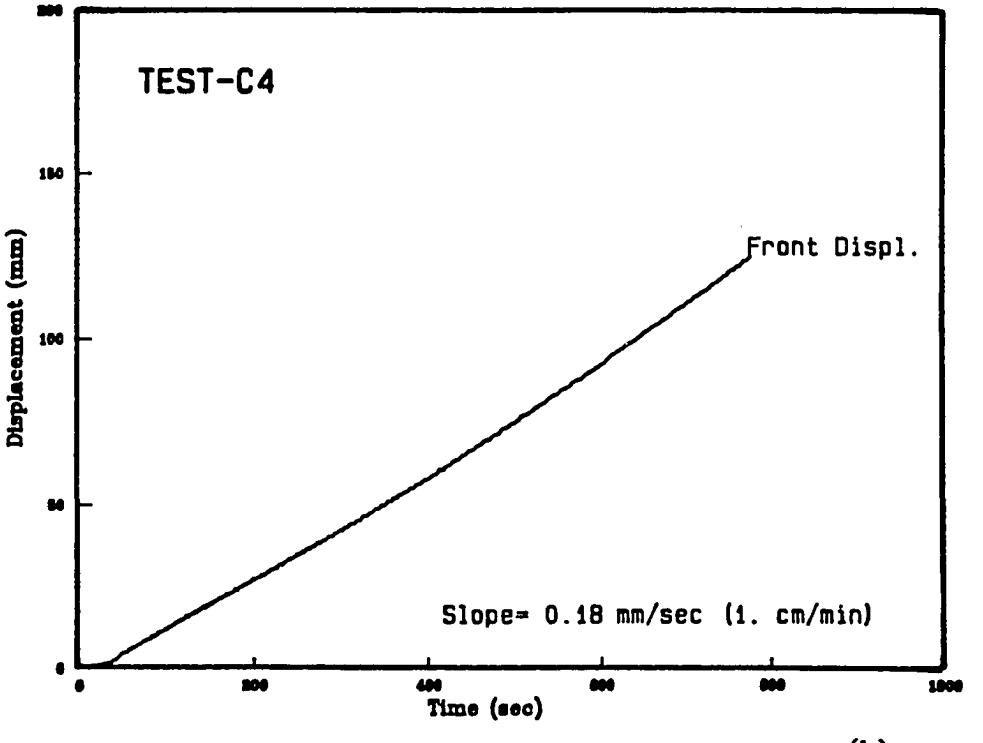

(b)

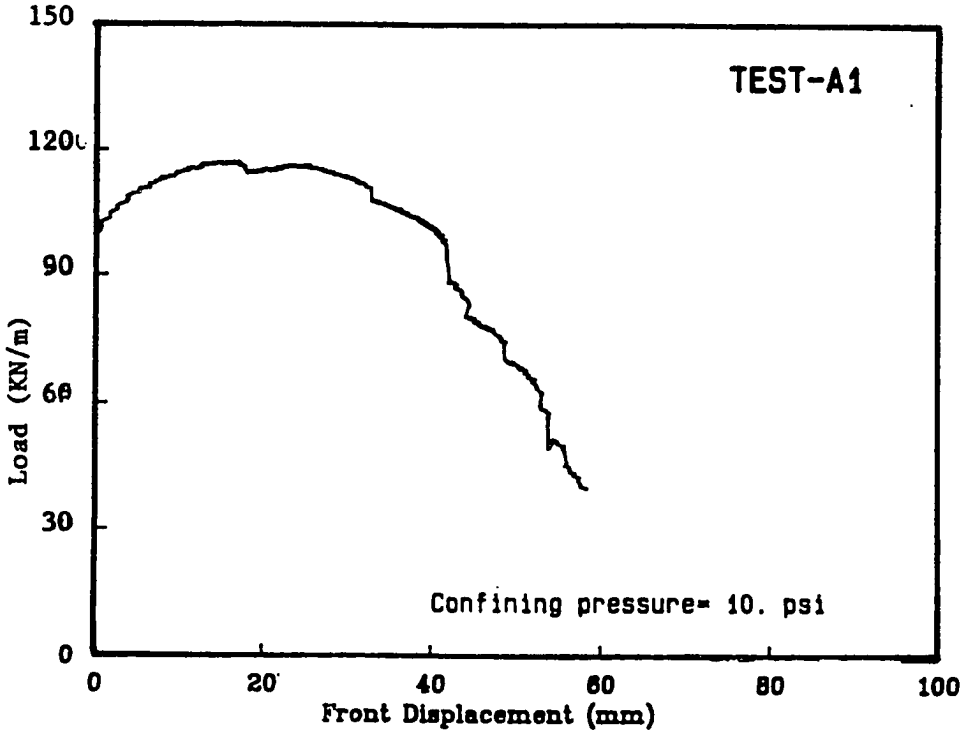

(a)

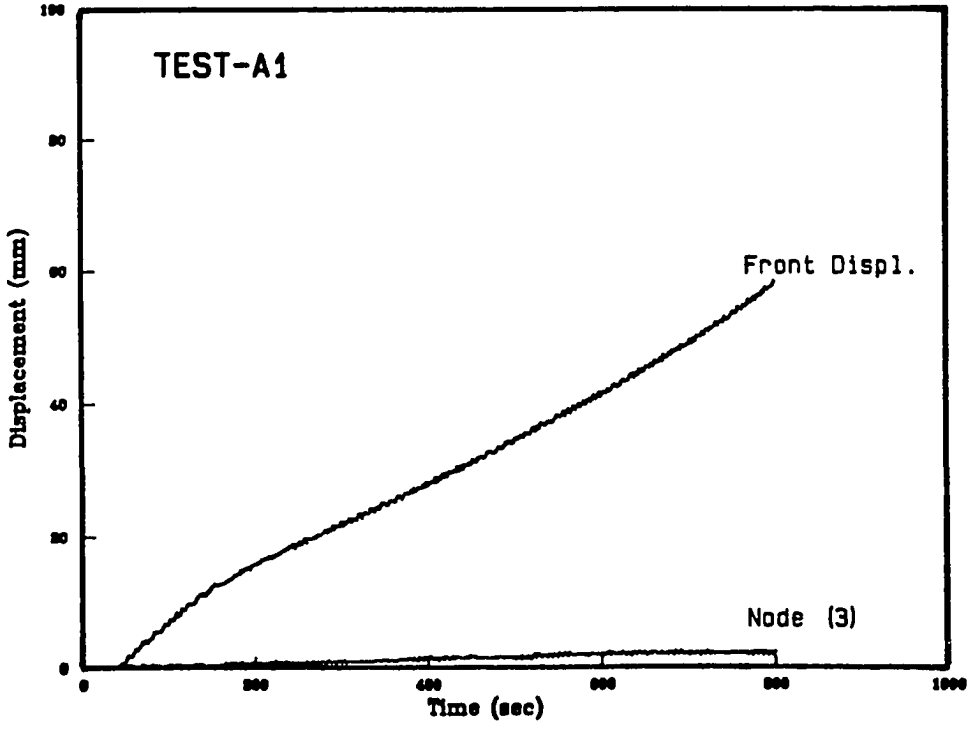

(b)

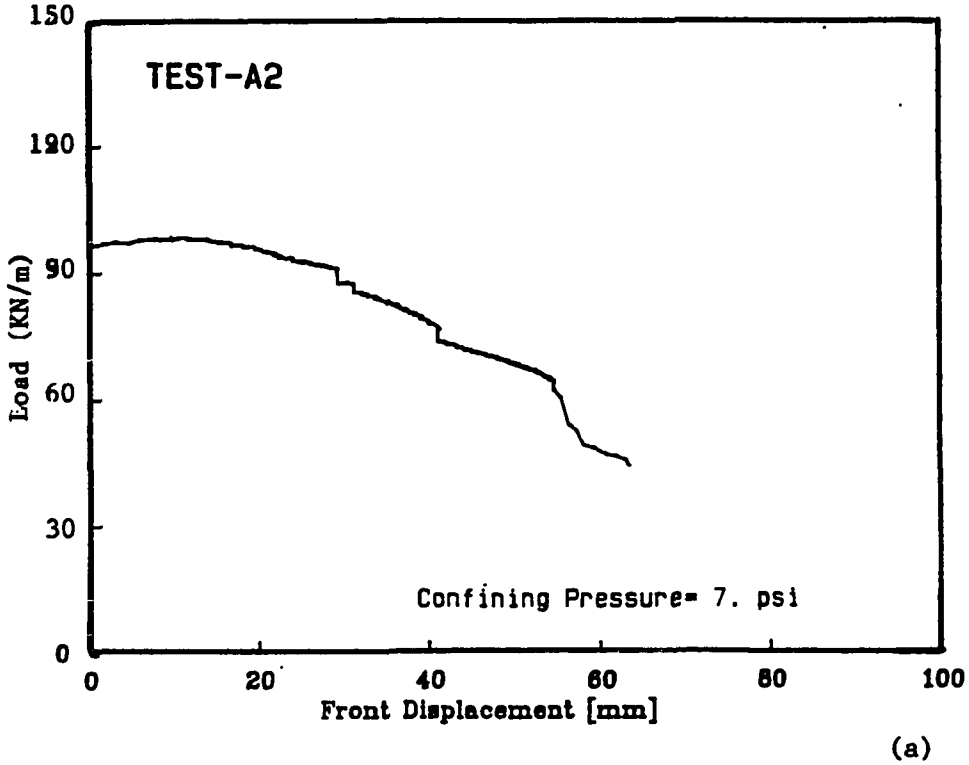

(a)

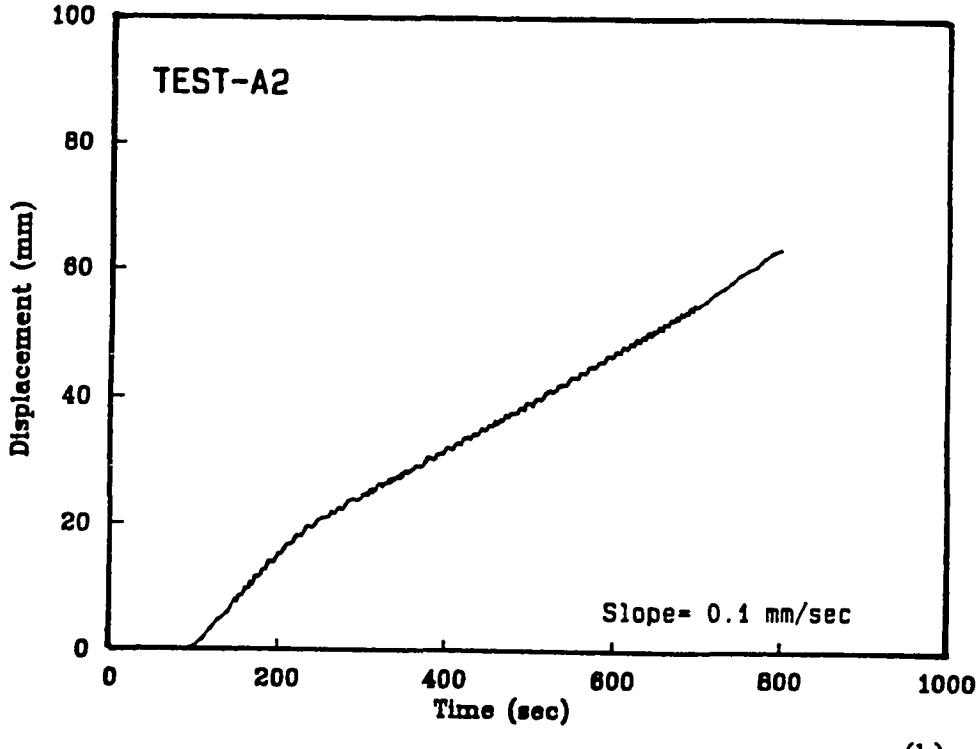

(b)

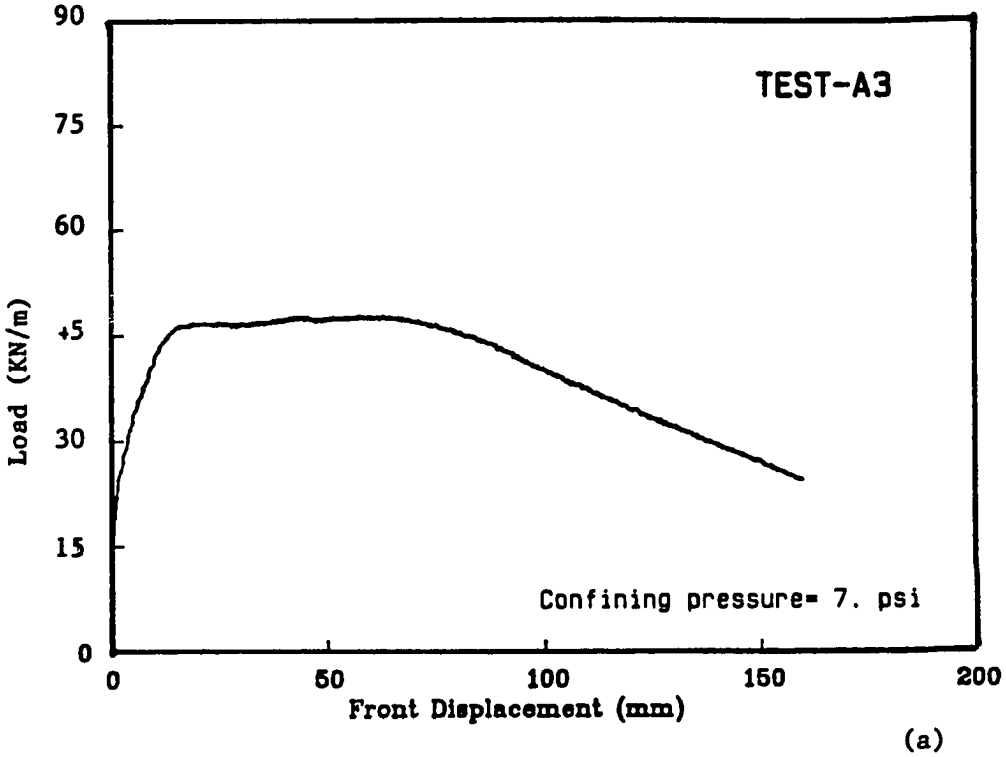

(a)

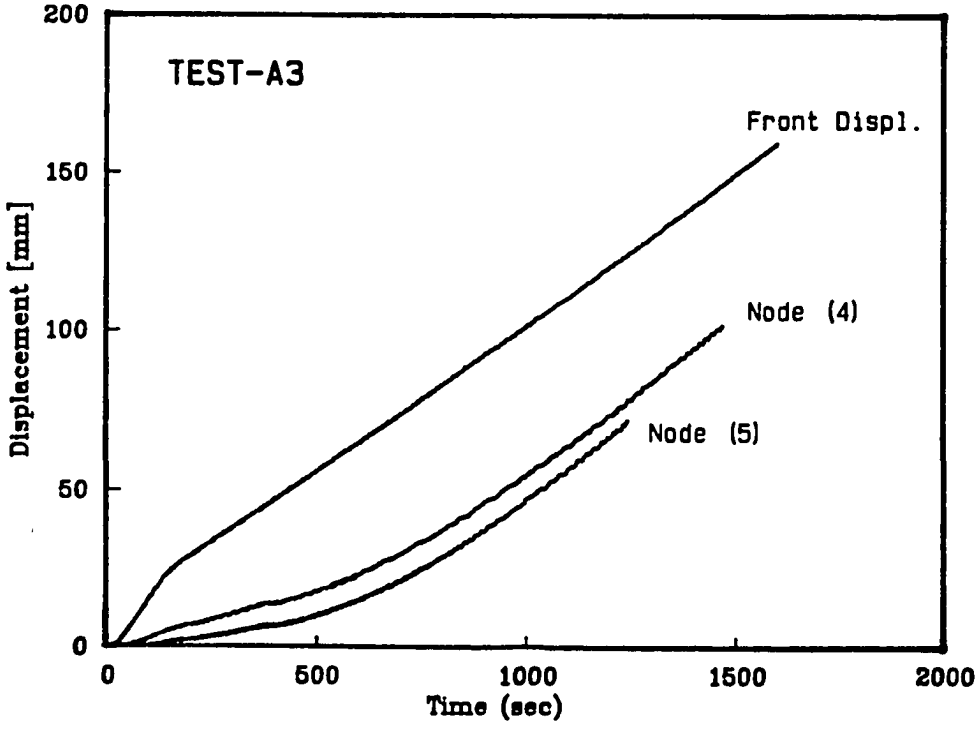

(b)

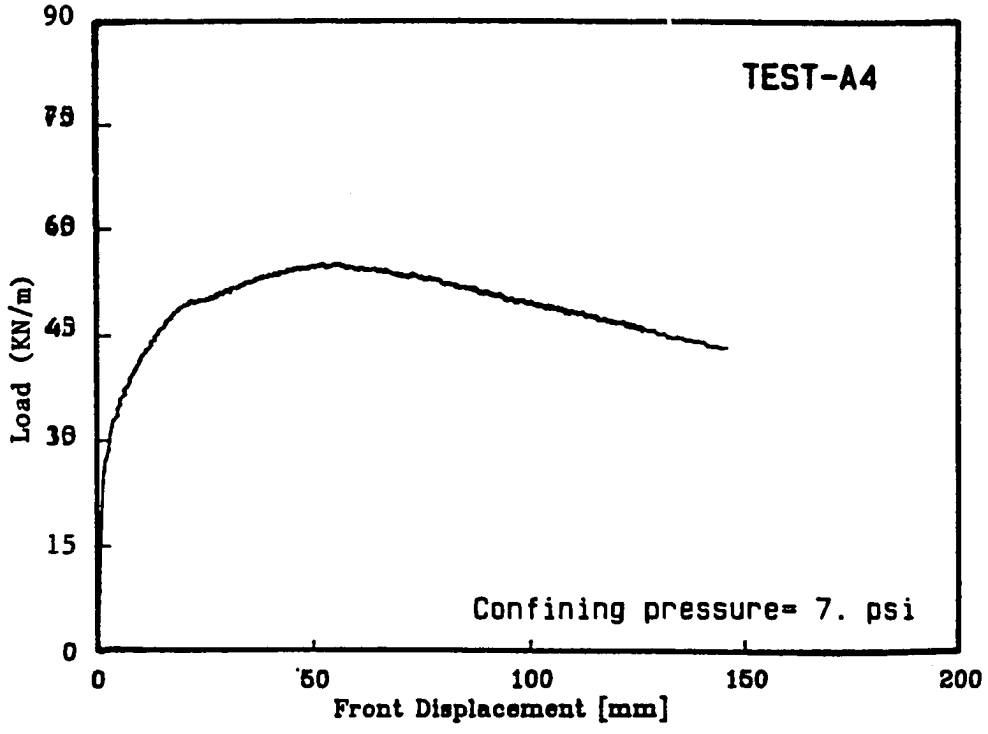

(a)

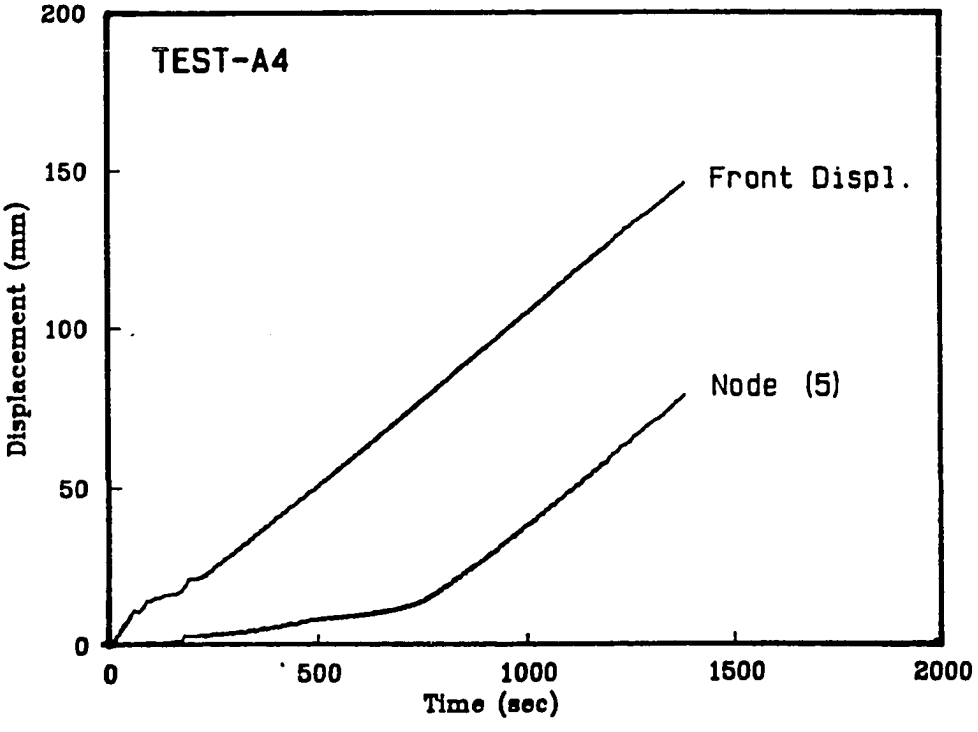

(b)

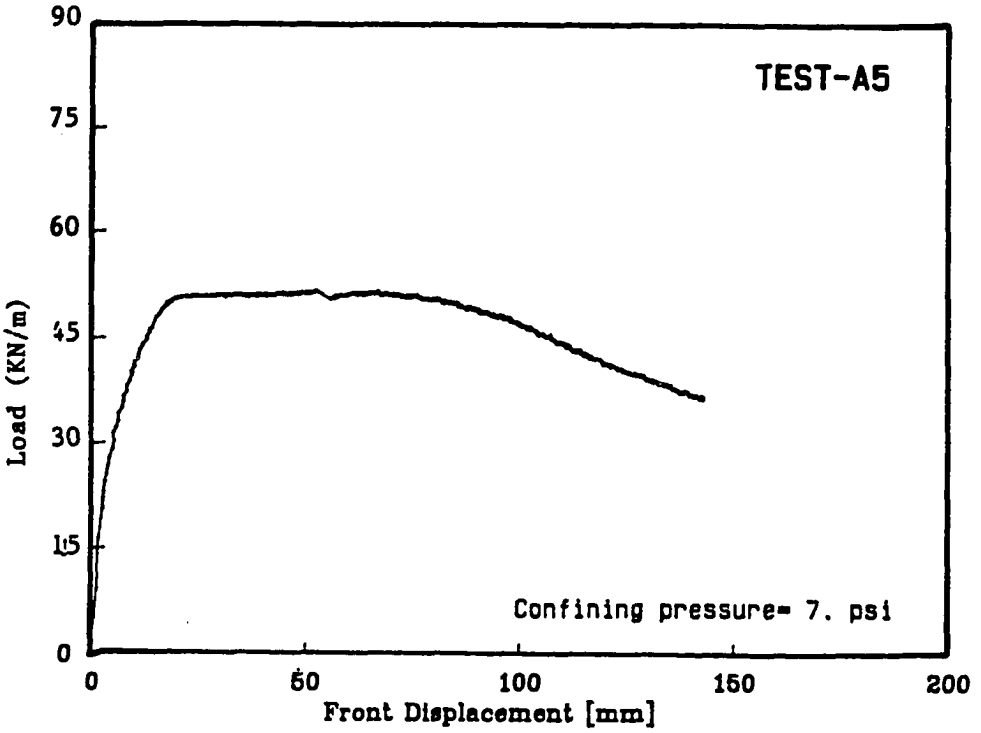

(a)

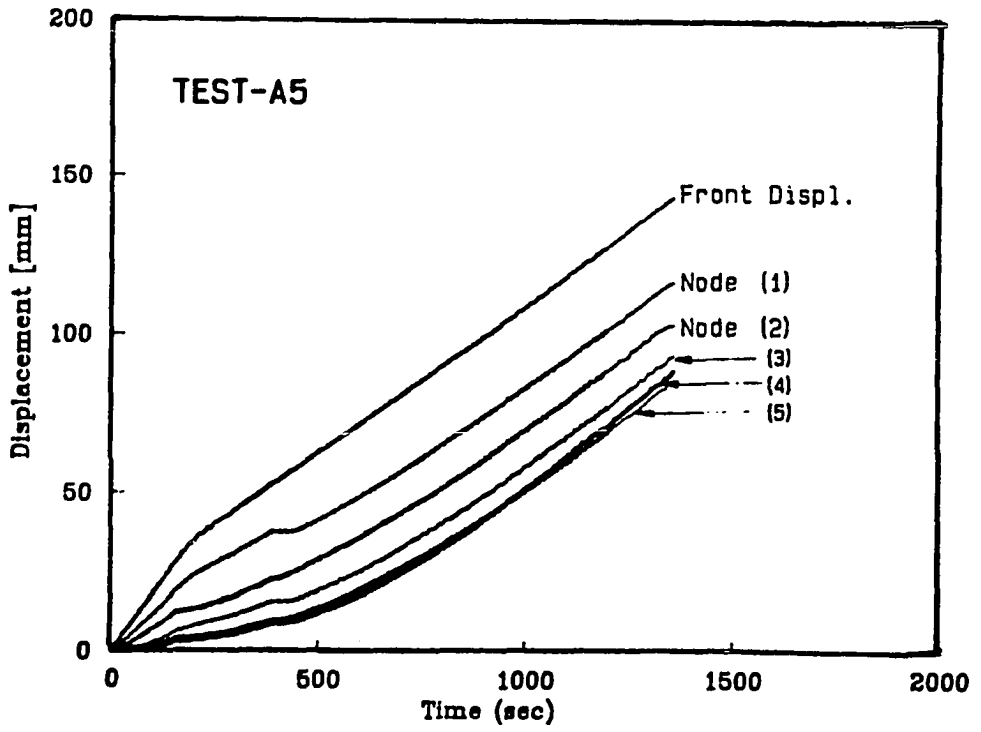

(b)

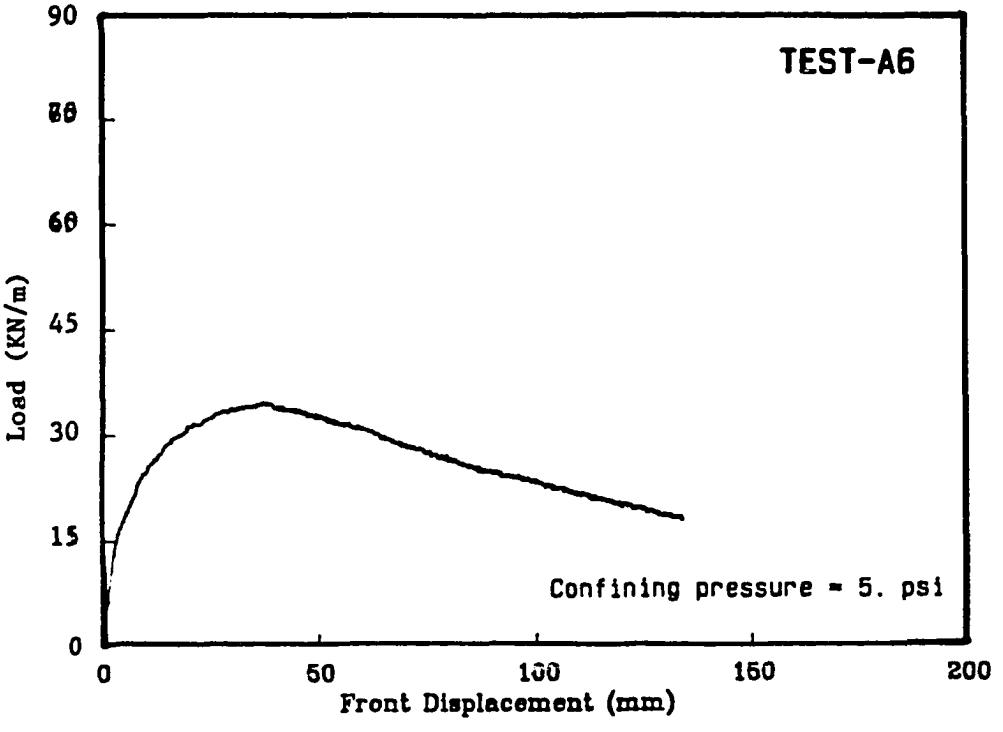

(a)

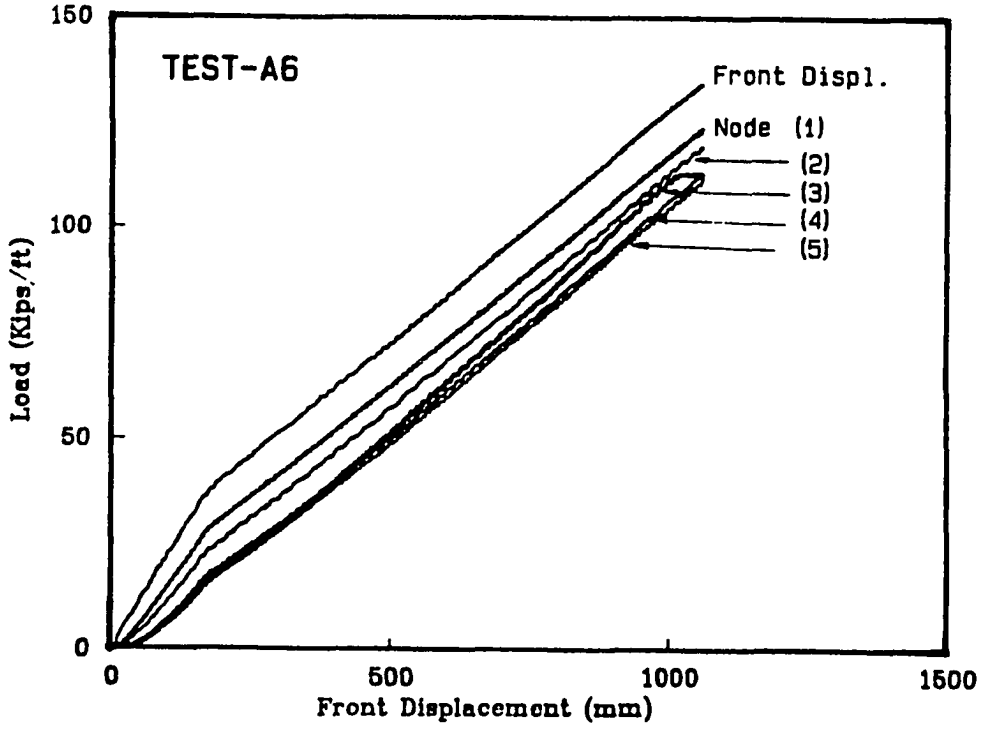

(b)

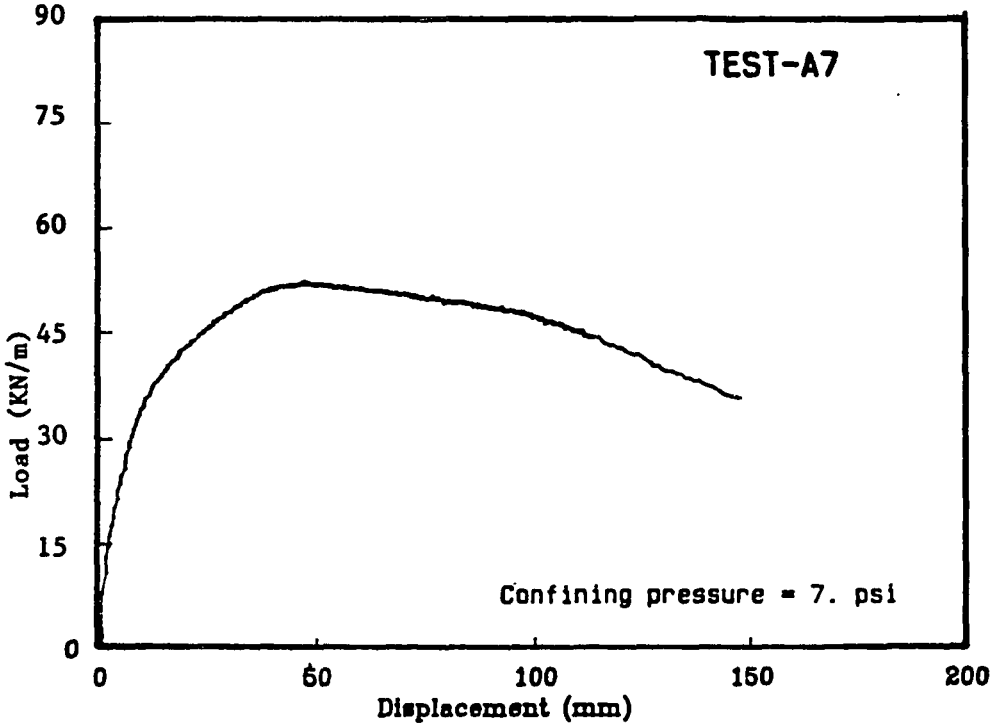

(a)

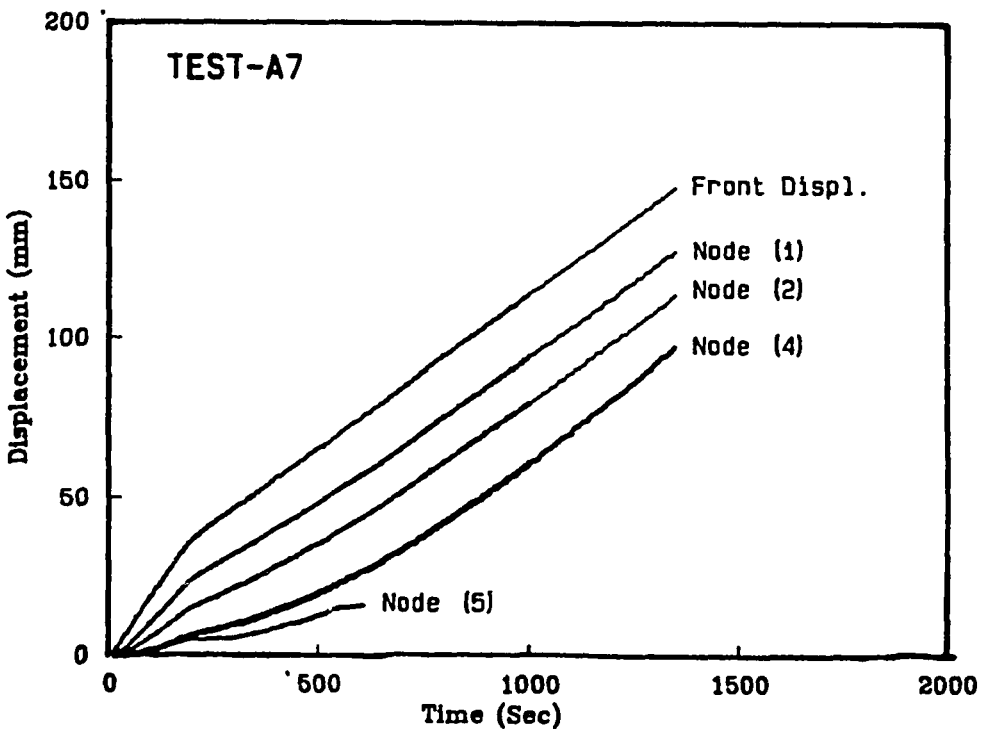

(b)

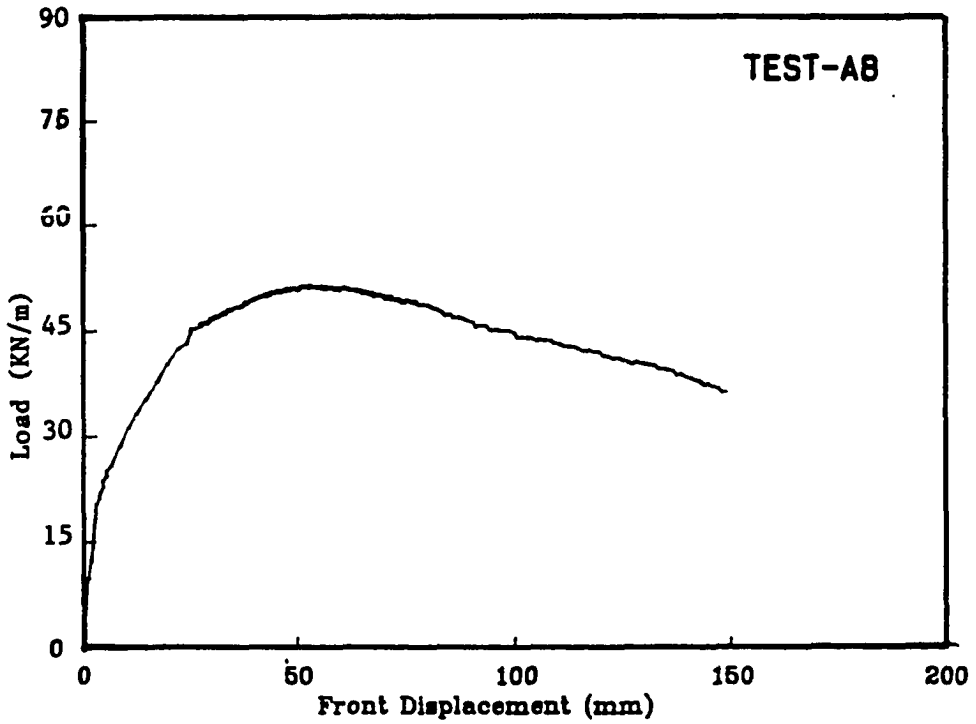

(a)

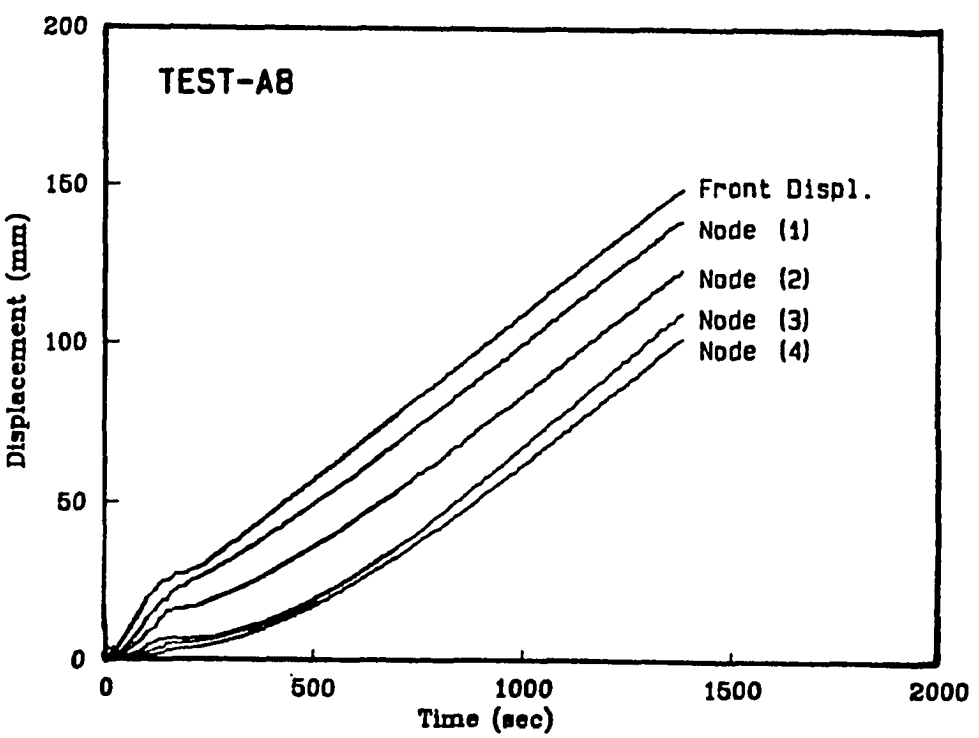

(b)

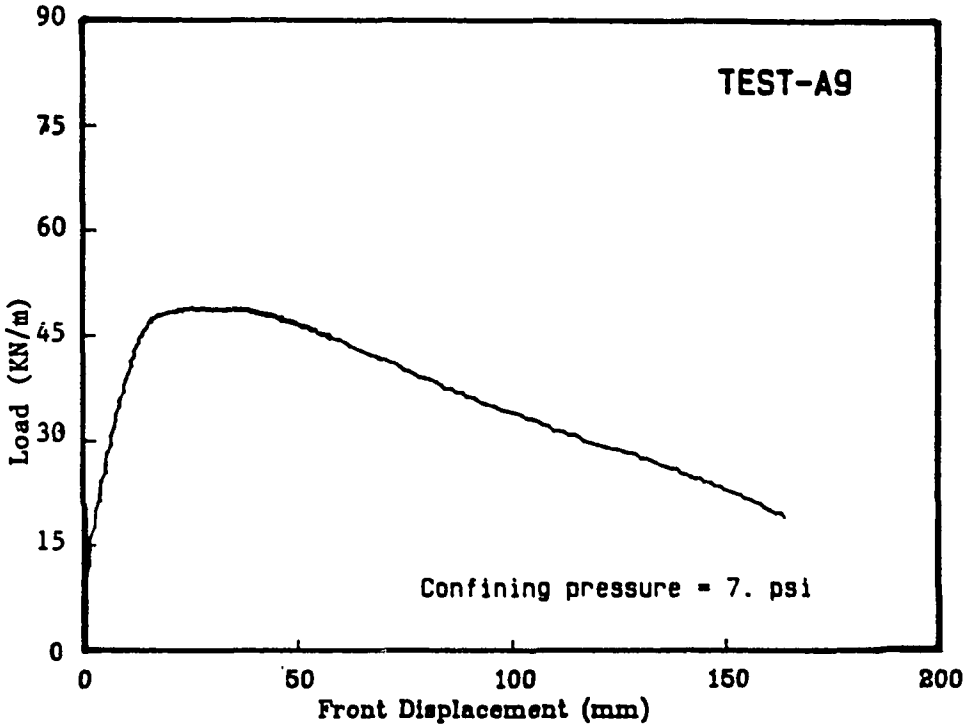

(a)

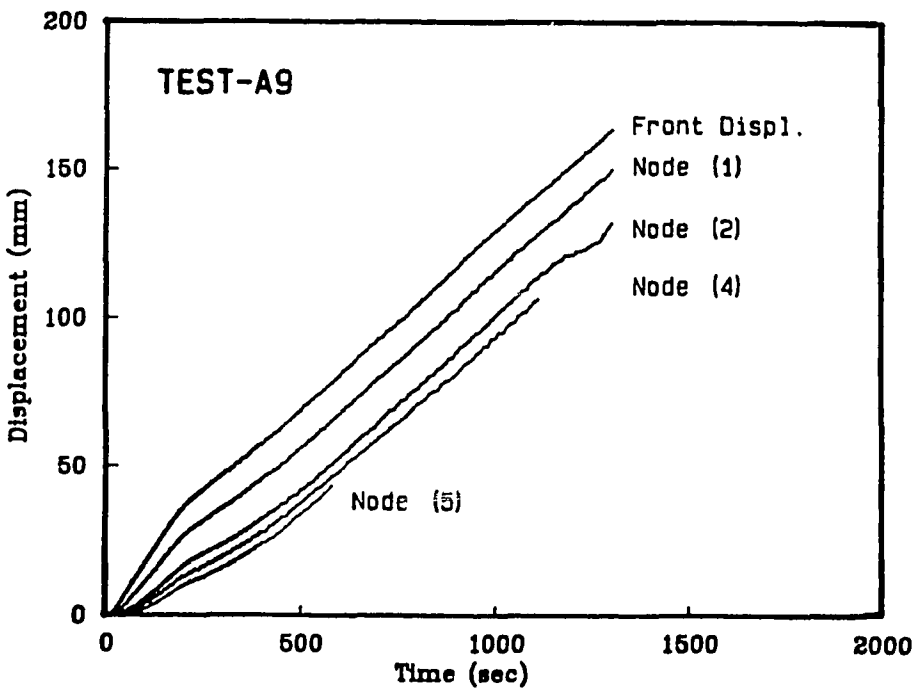

(b)

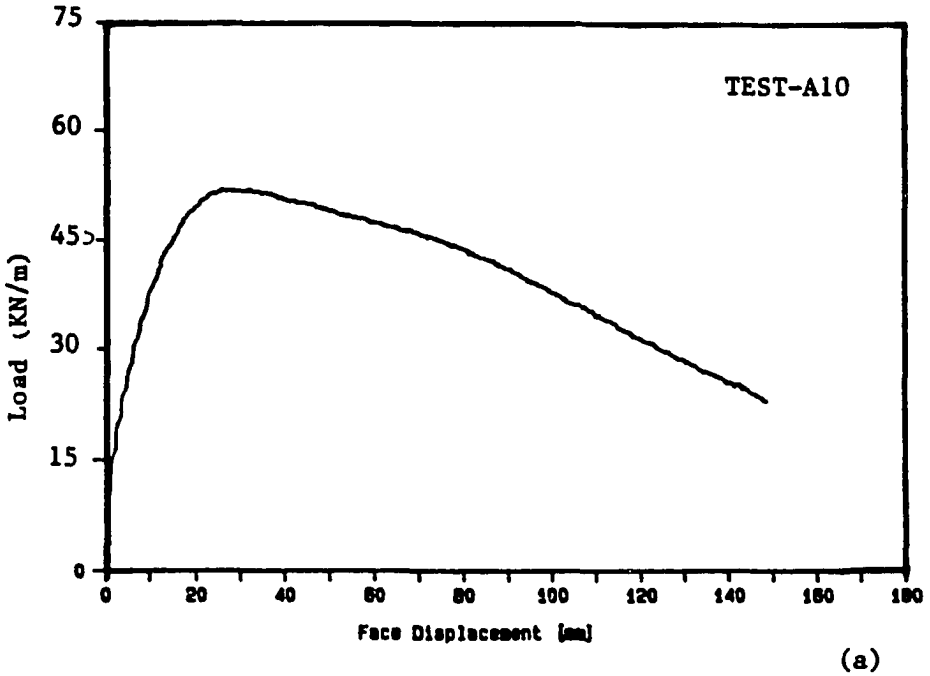

(a)

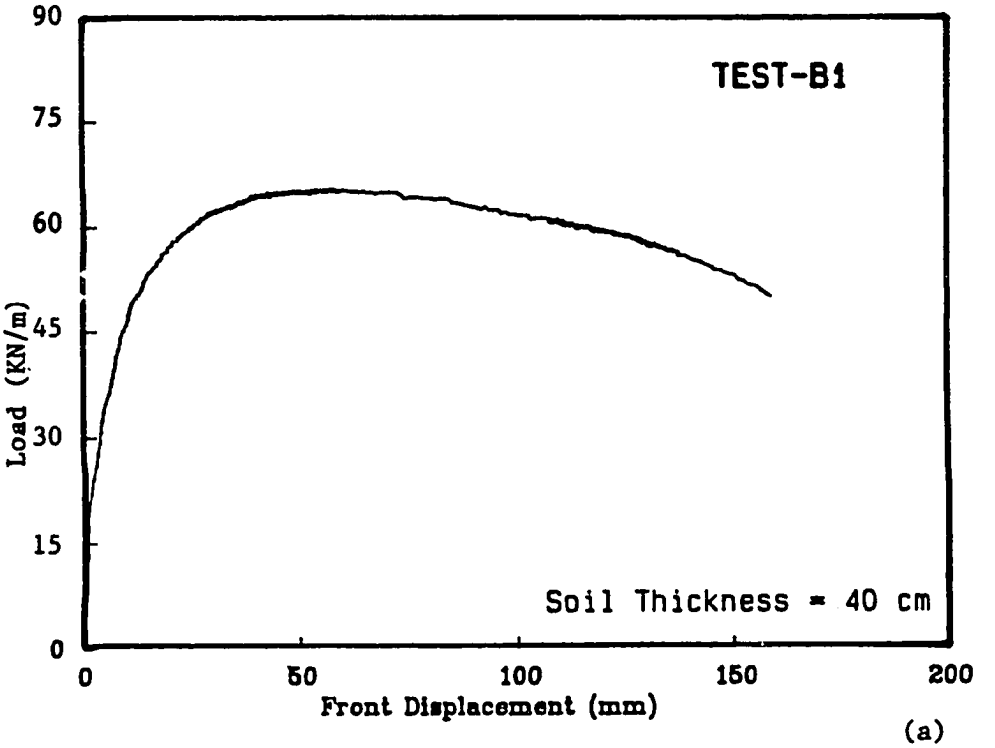

(a)

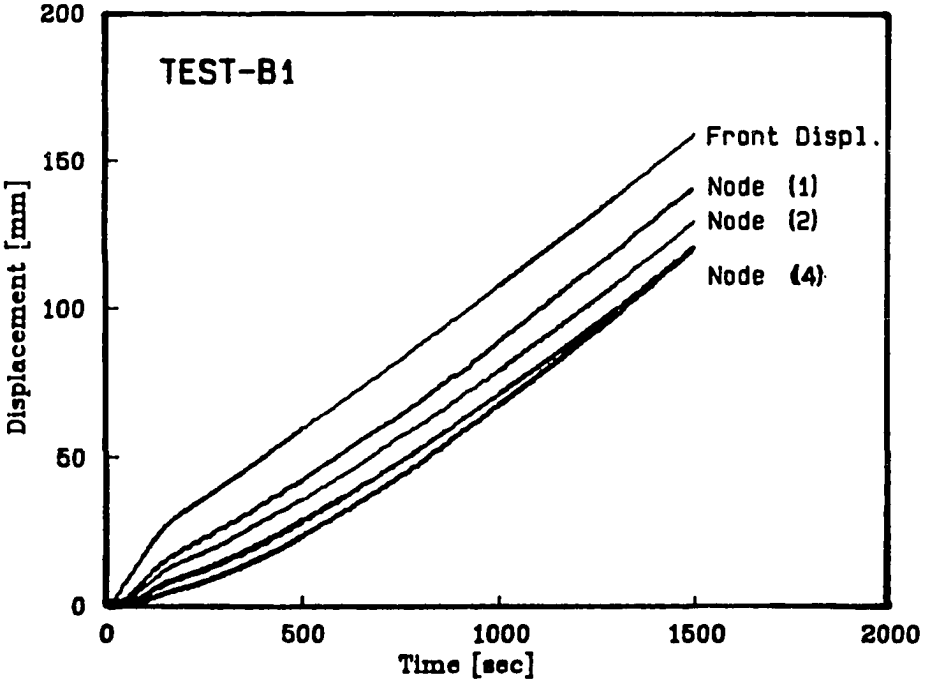

(b)

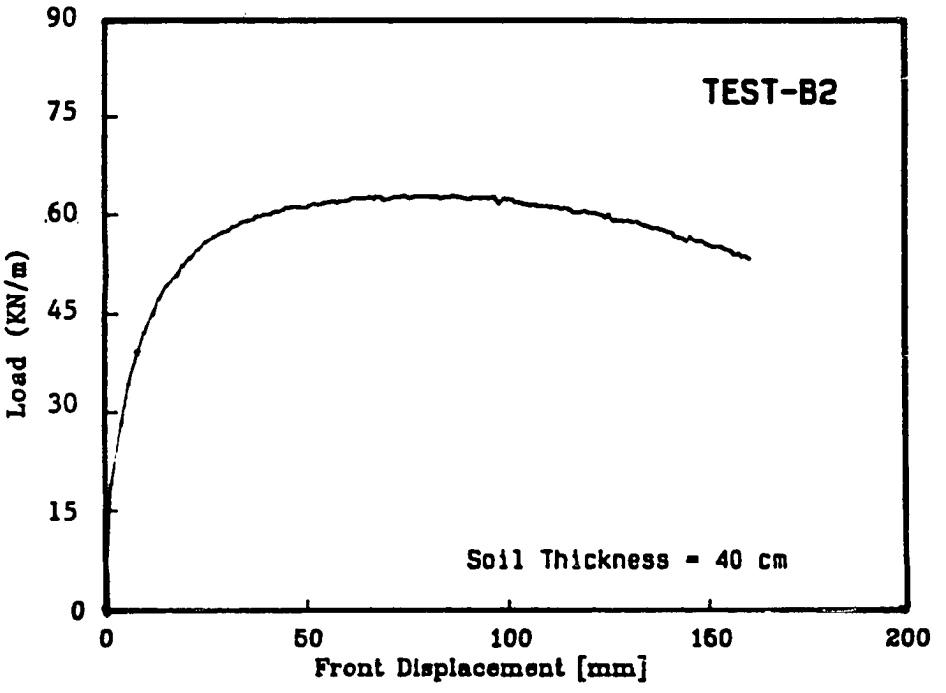

(a)

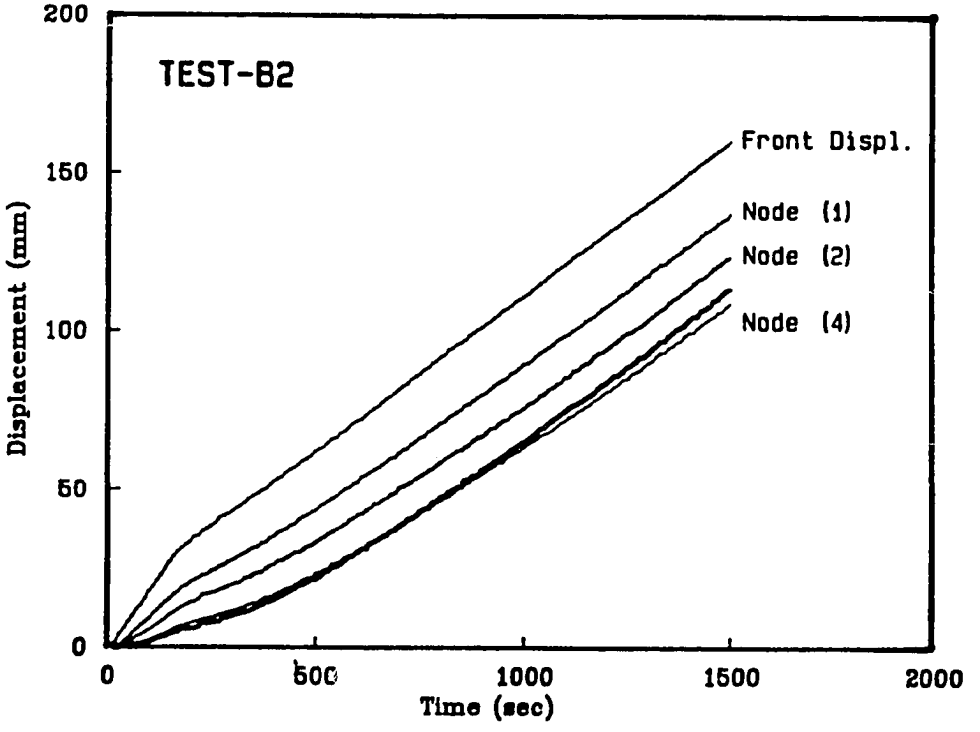

(b)

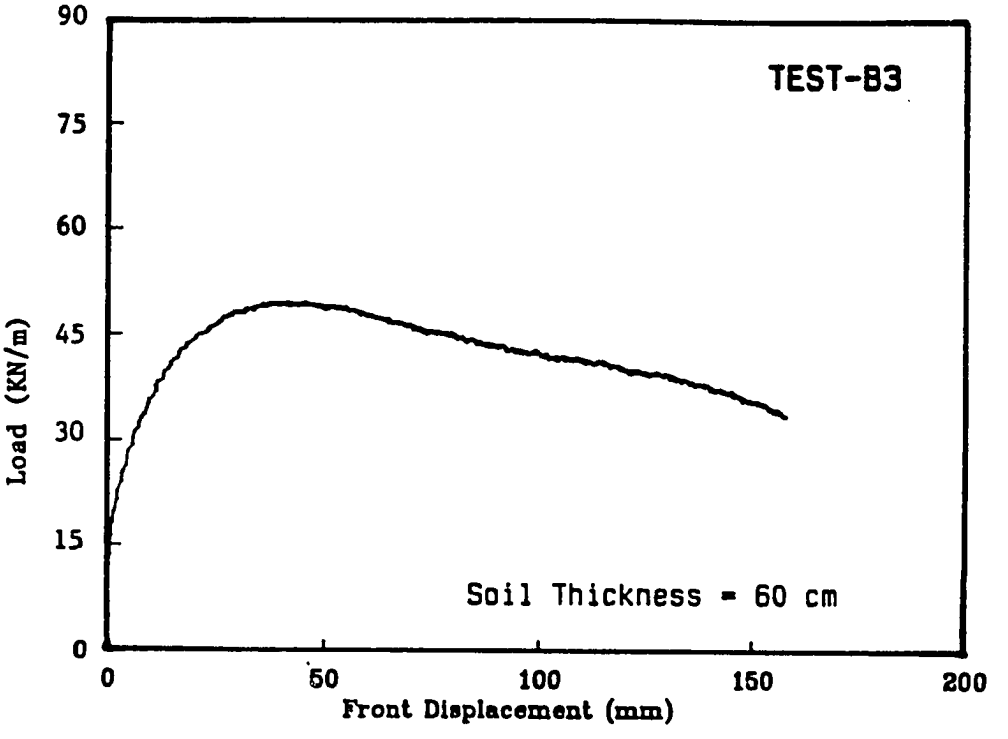

(a)

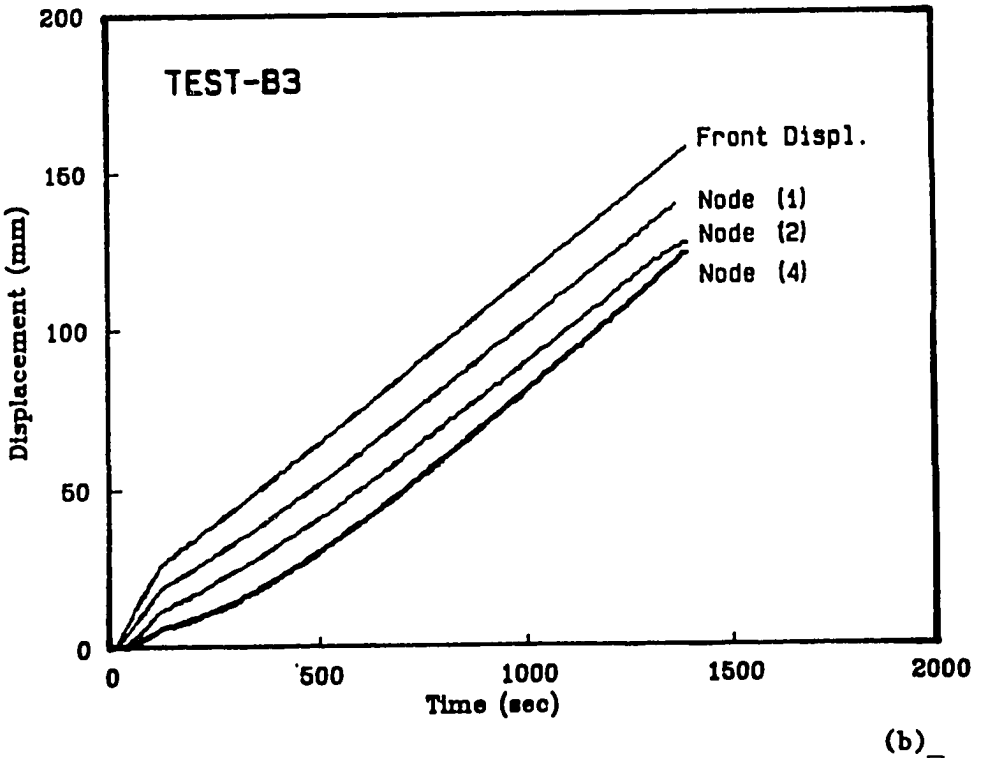

(b)

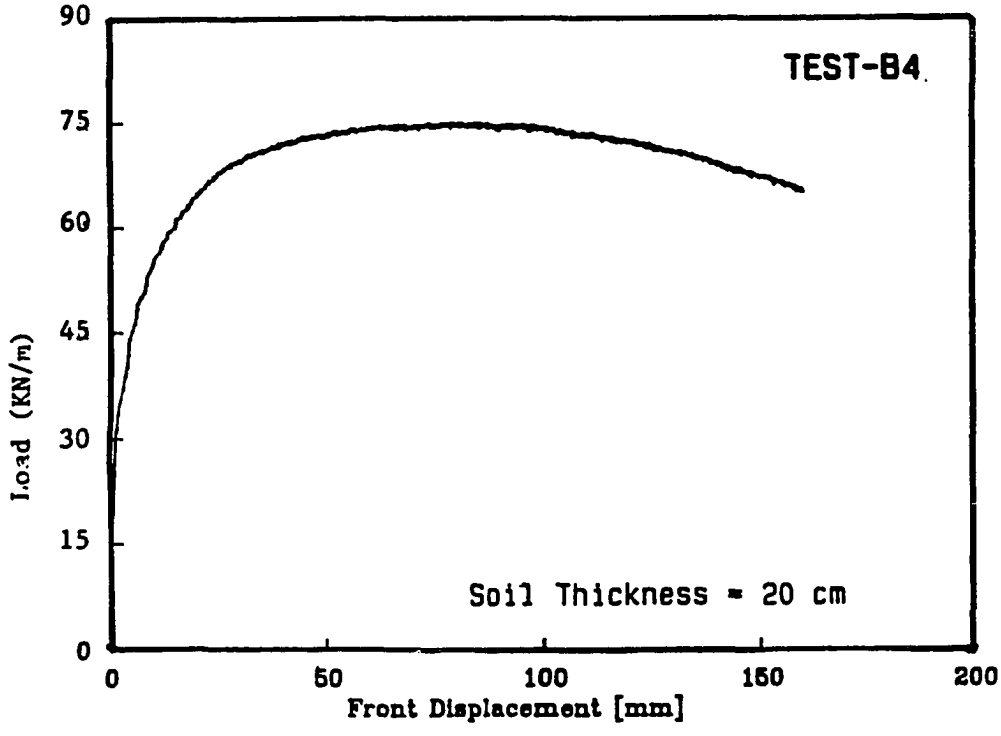

(a)

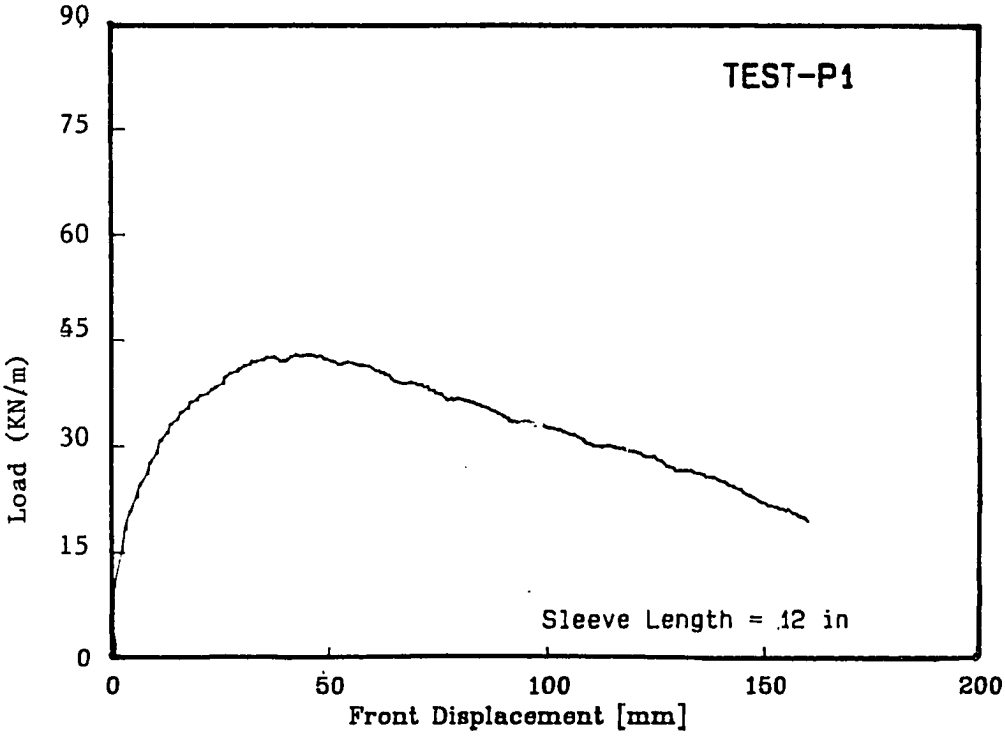

(a)

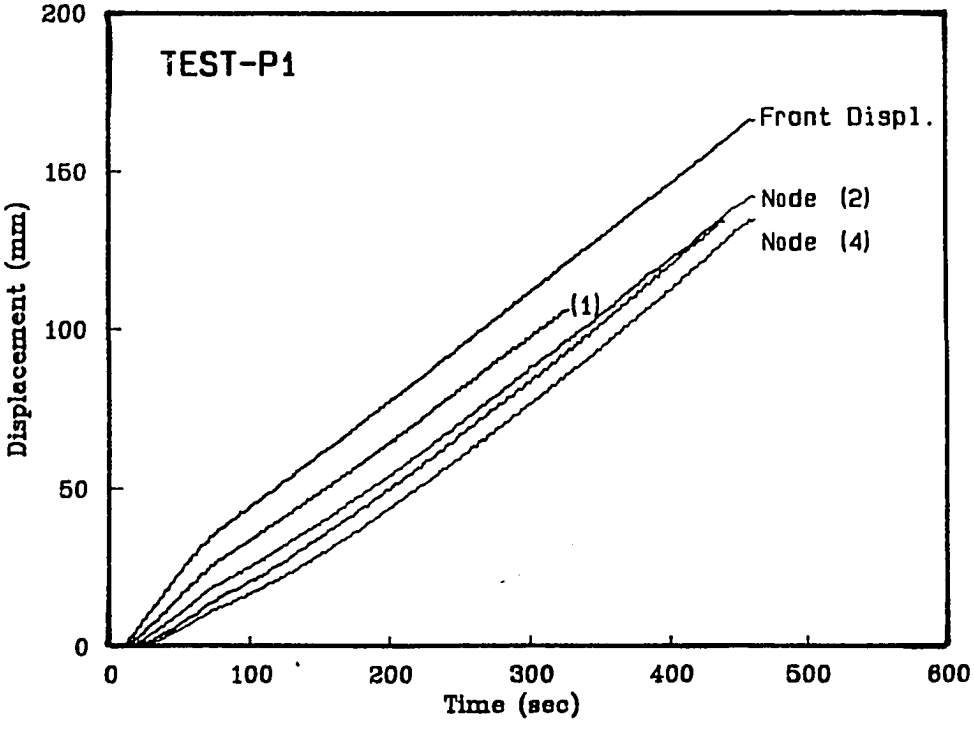

(b)

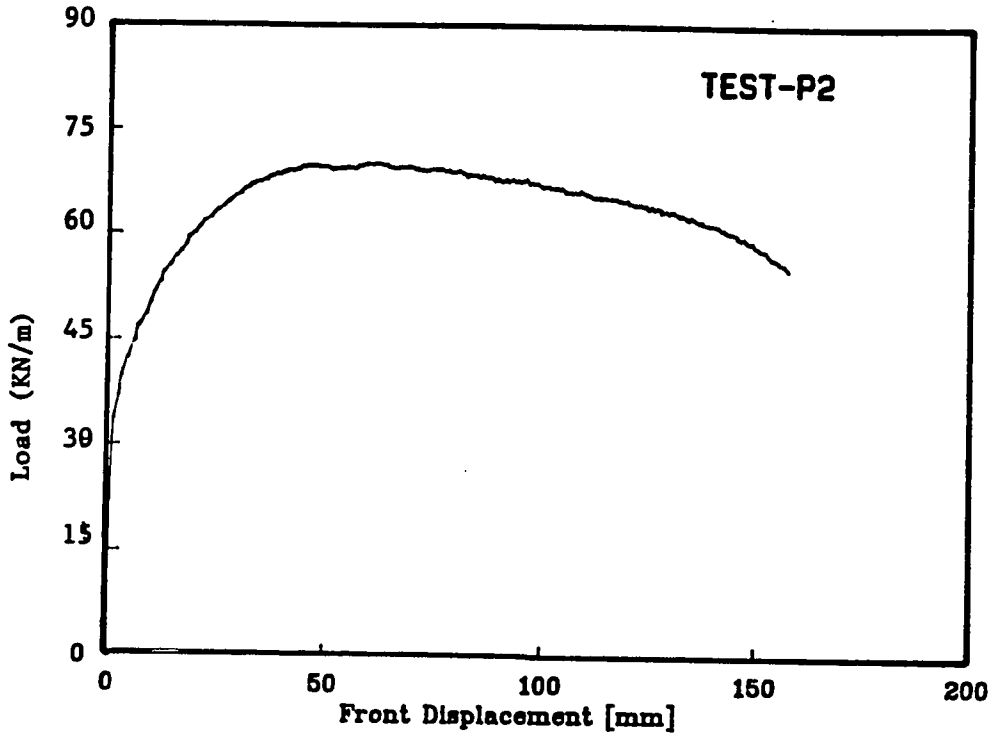

(a)

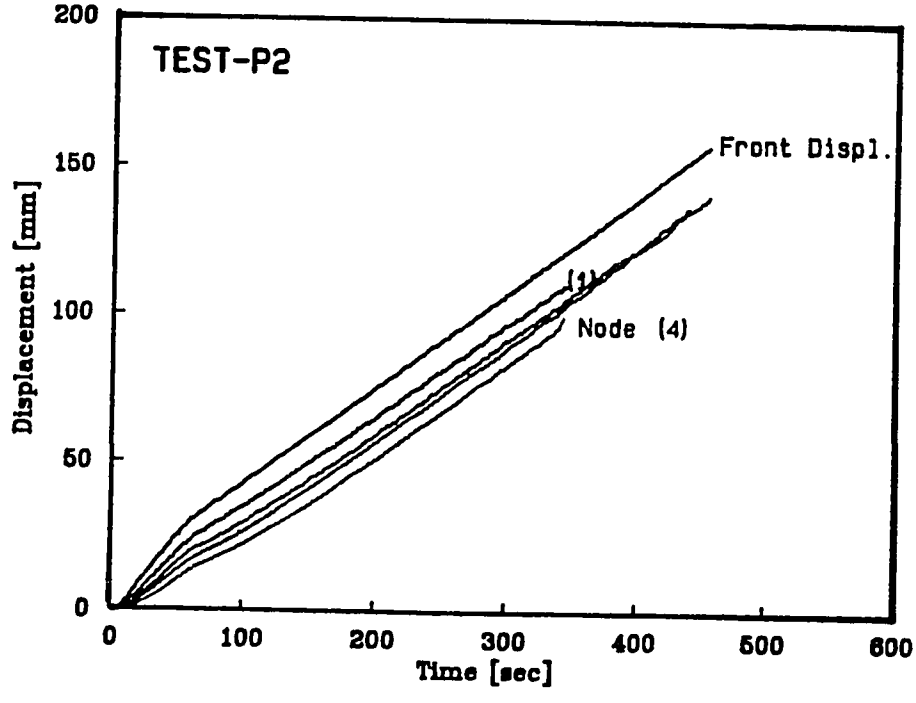

(b)

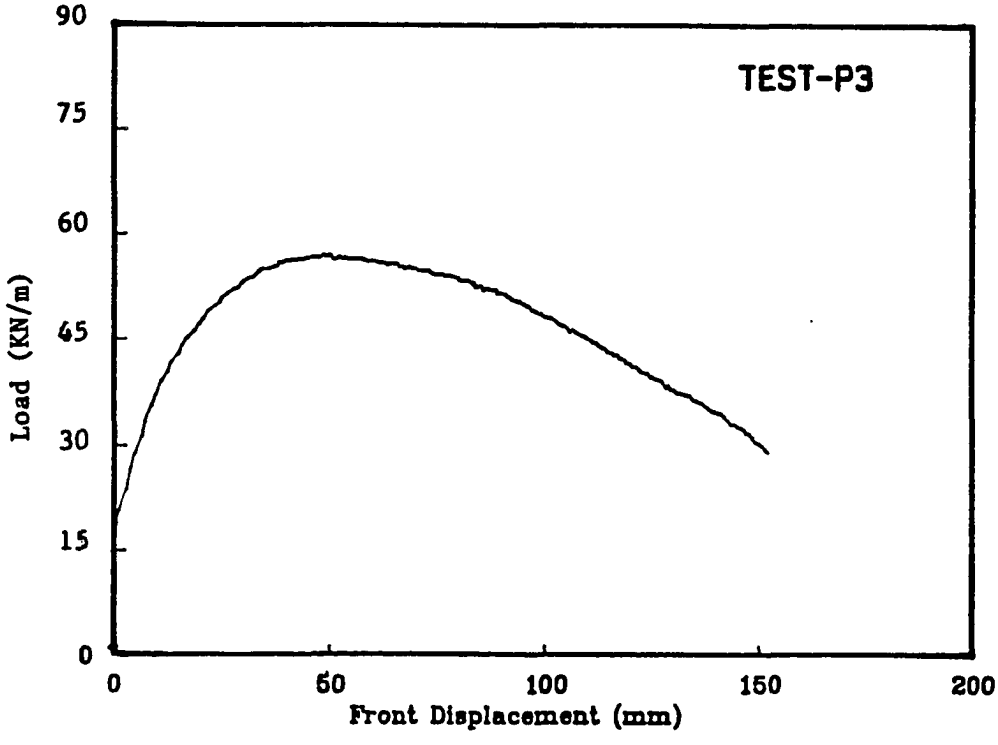

(a)

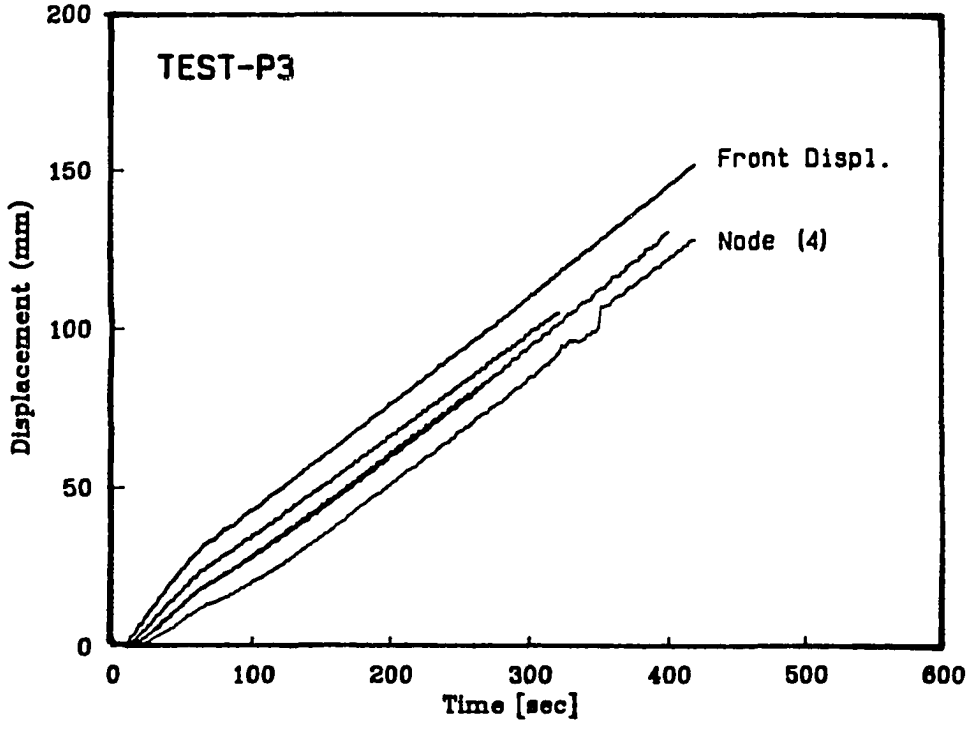

(b)

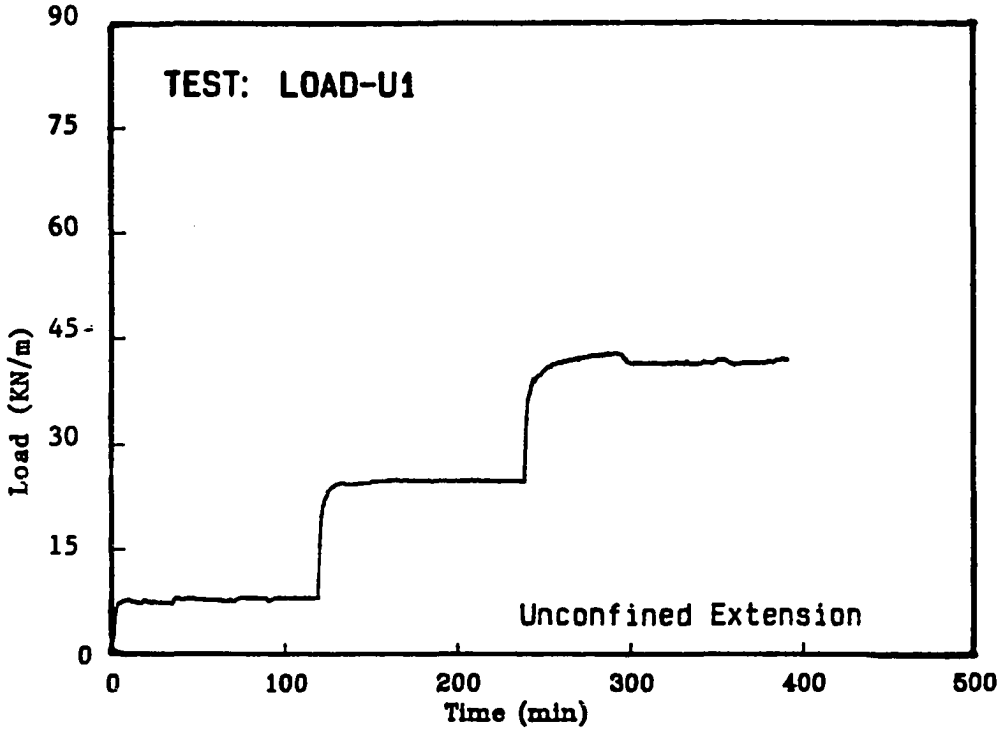

(a)

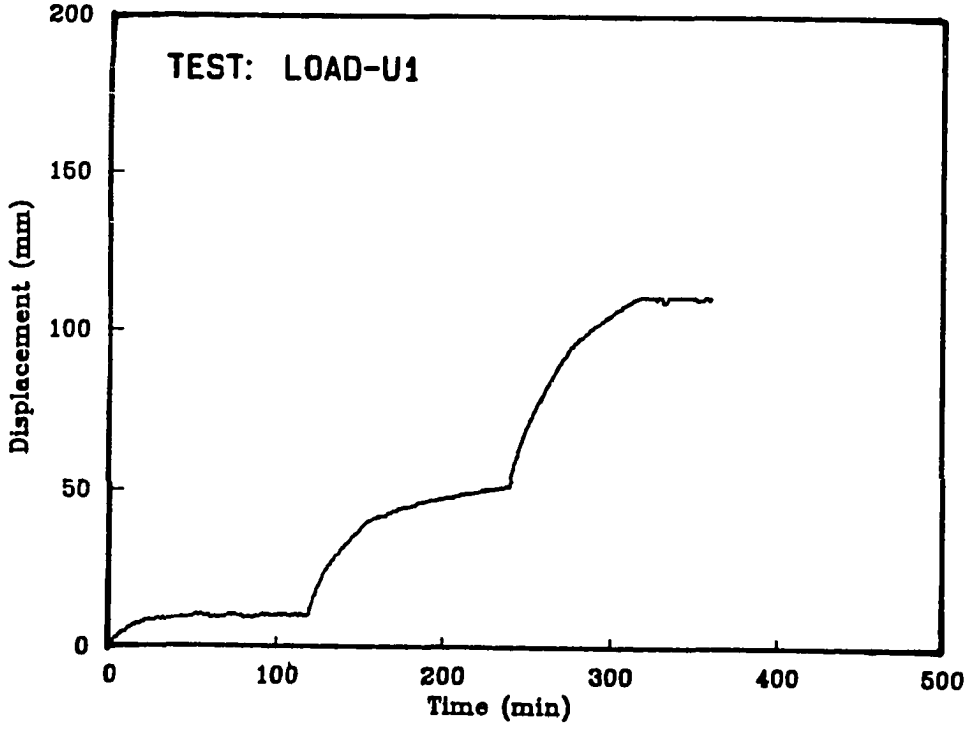

(b)

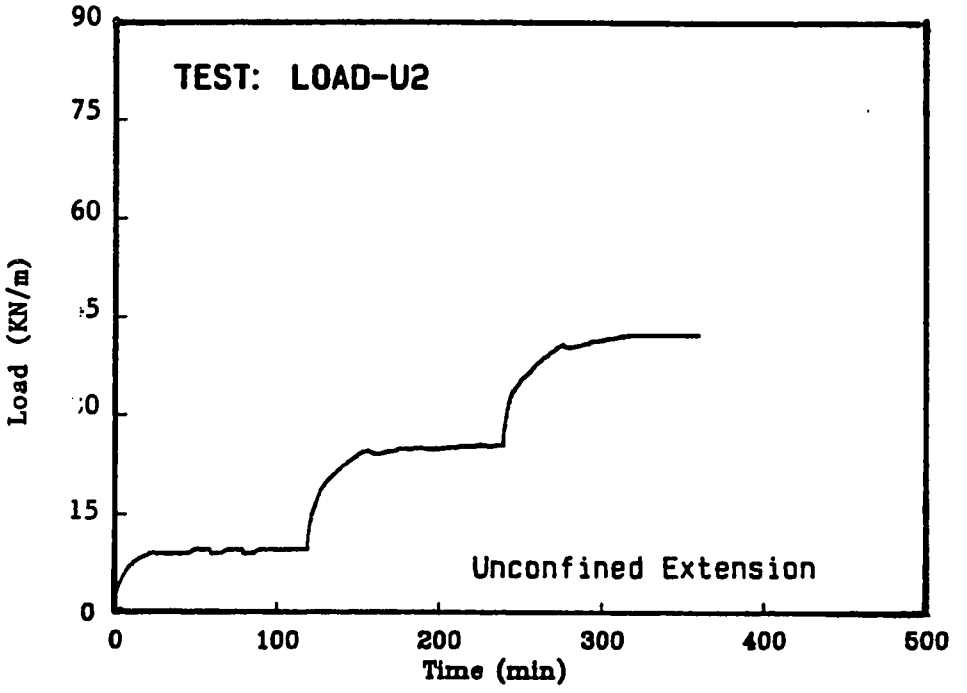

(a)

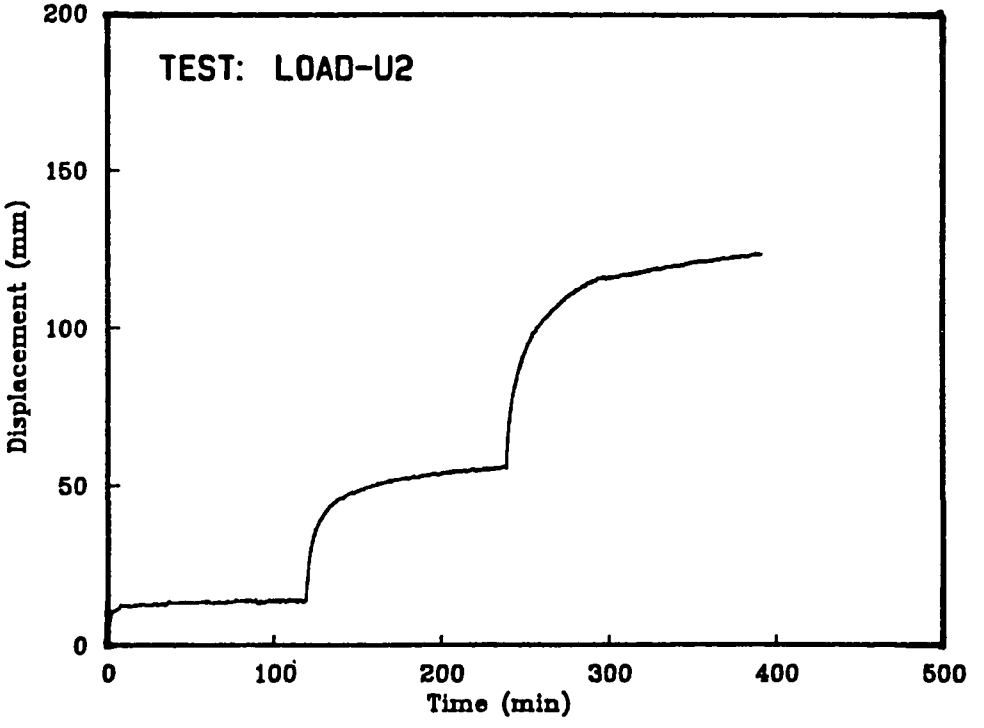

(b)

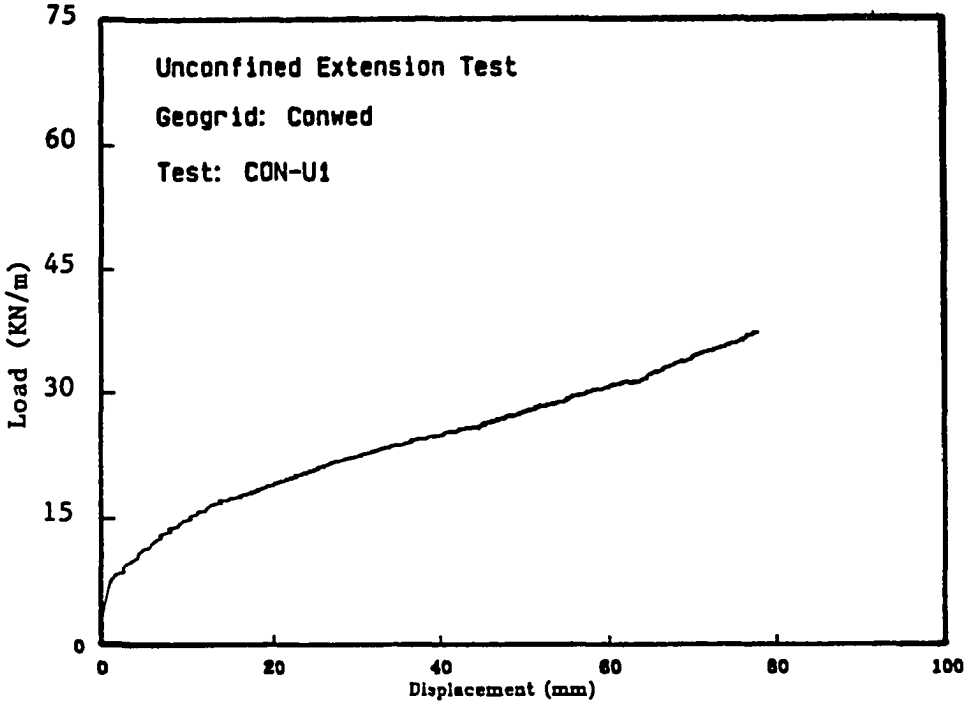

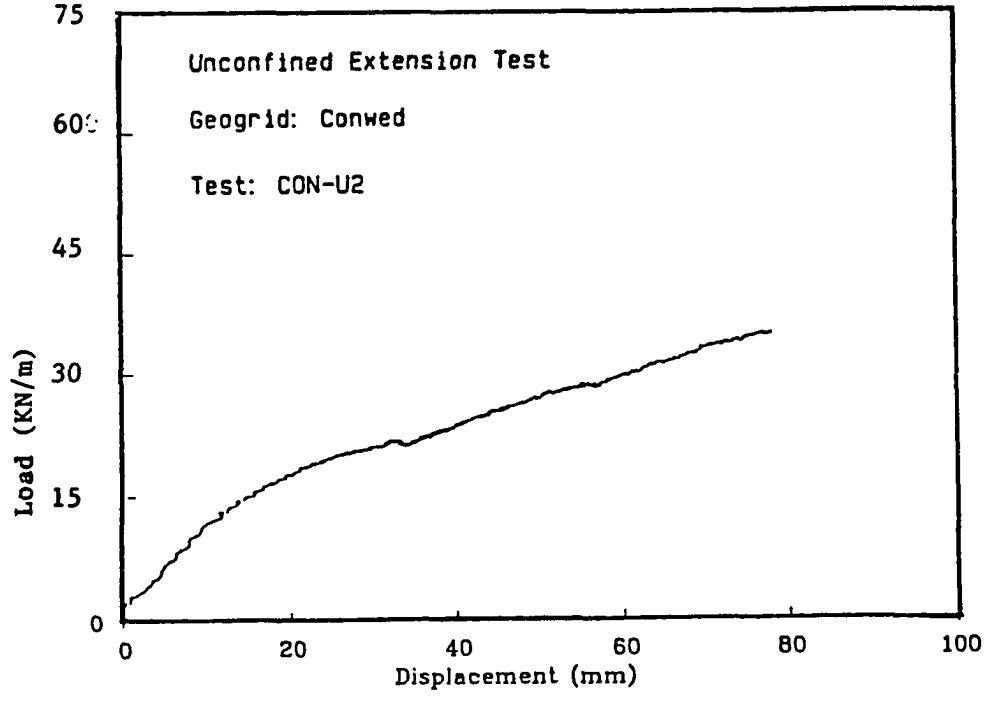

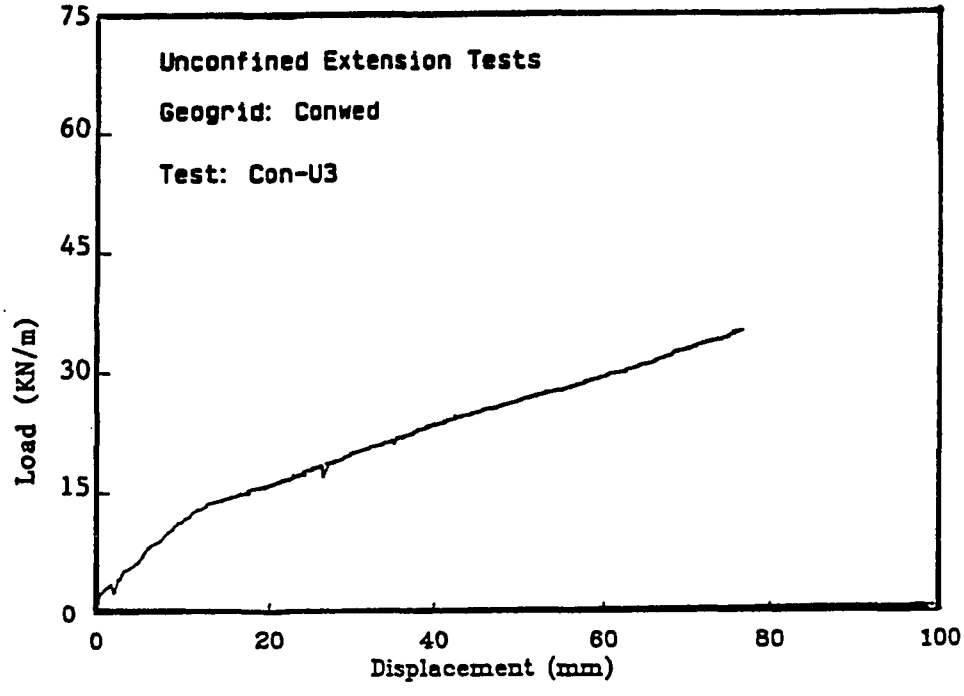

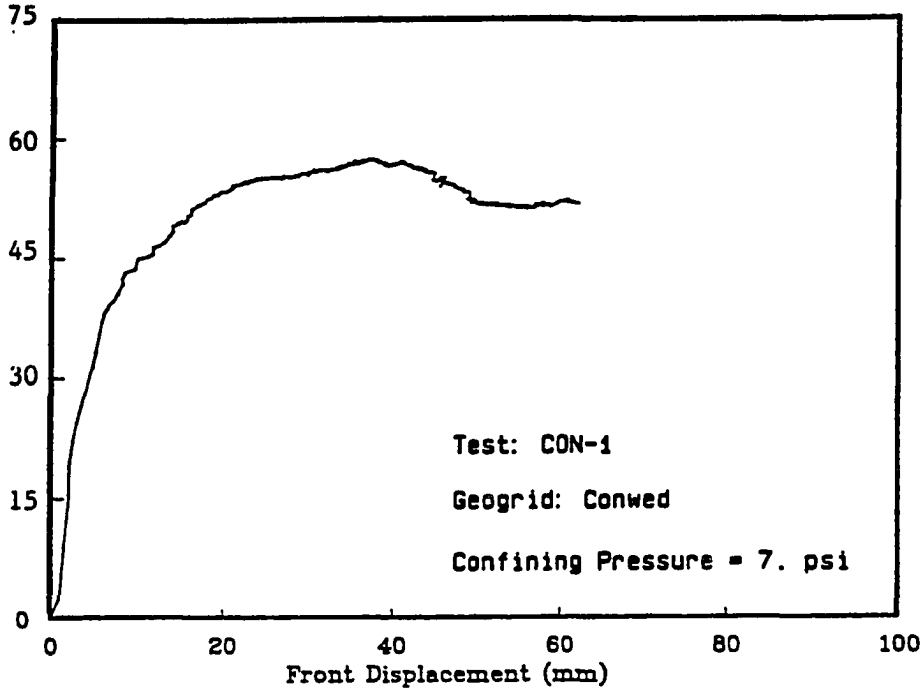

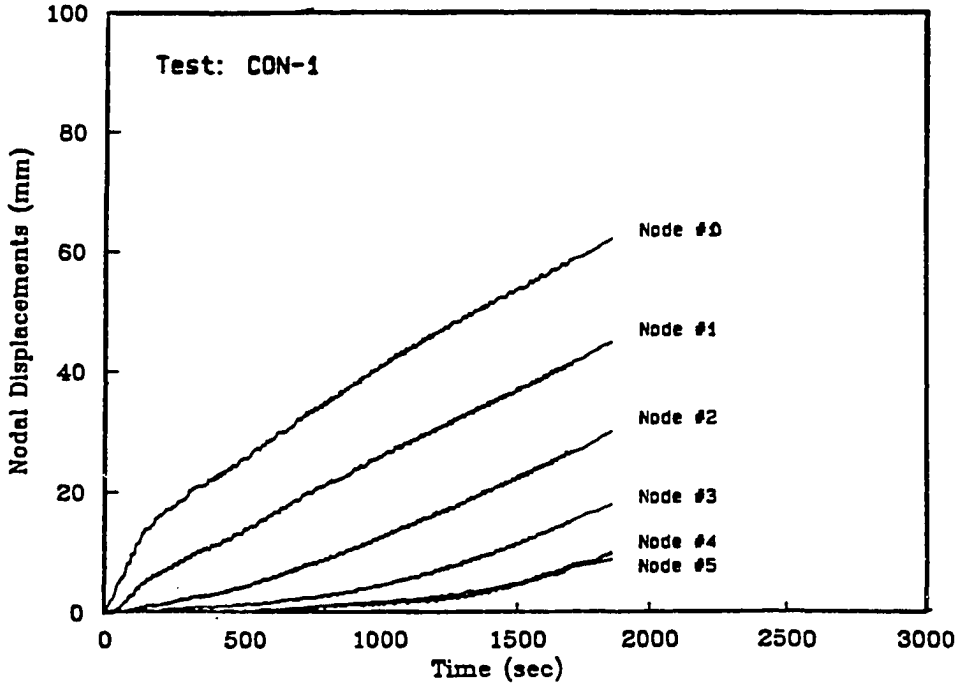

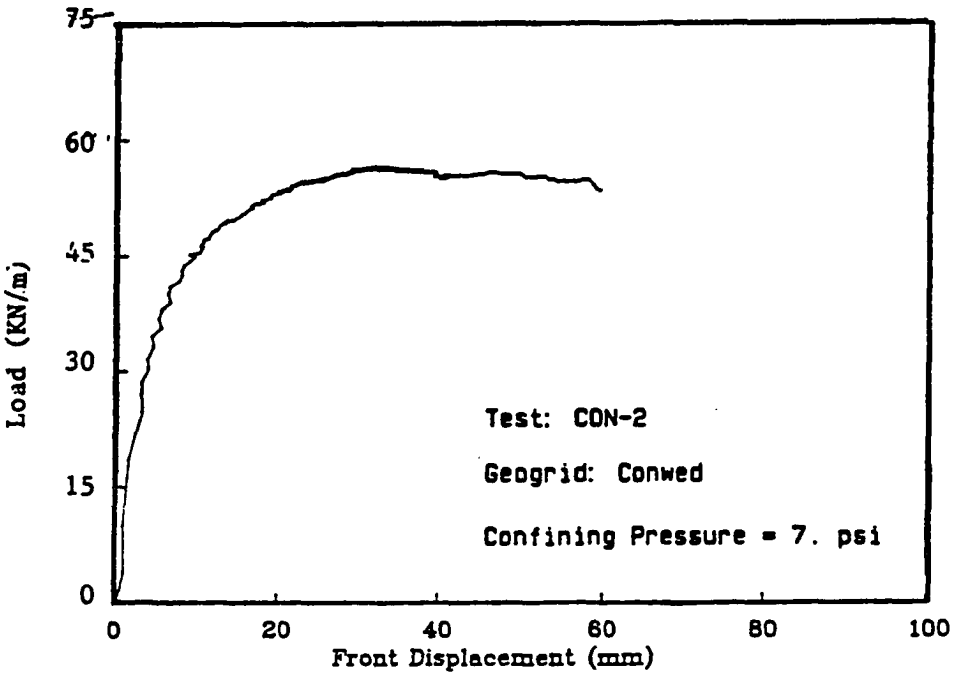

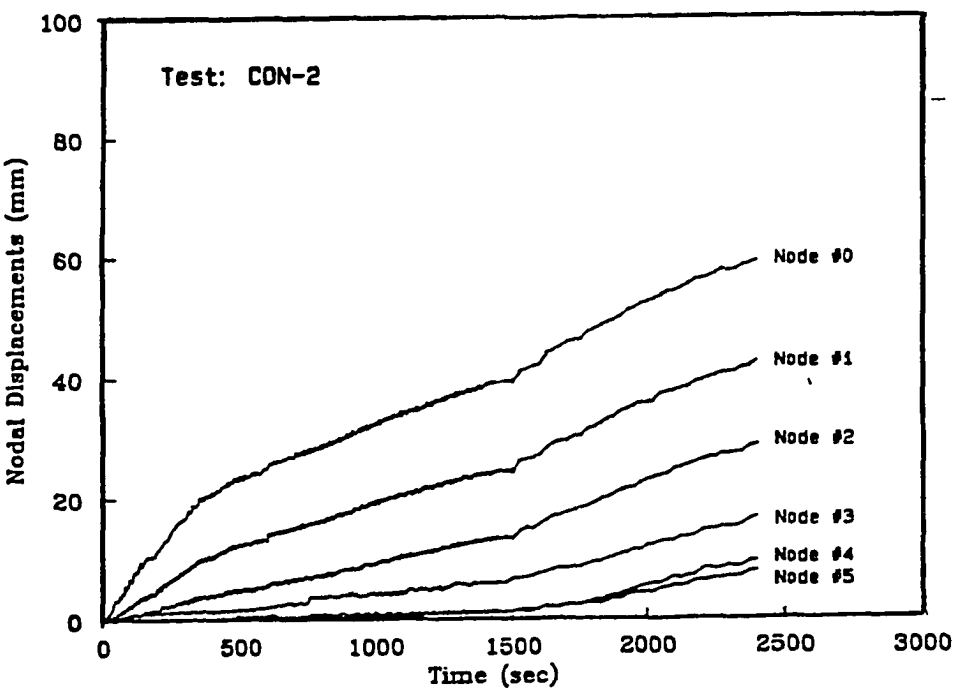

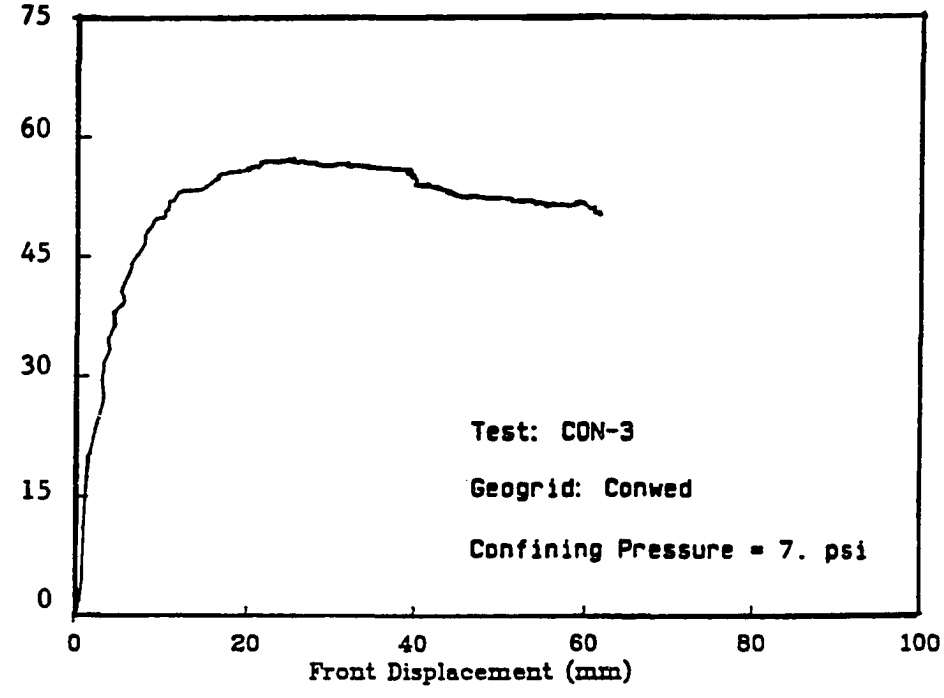

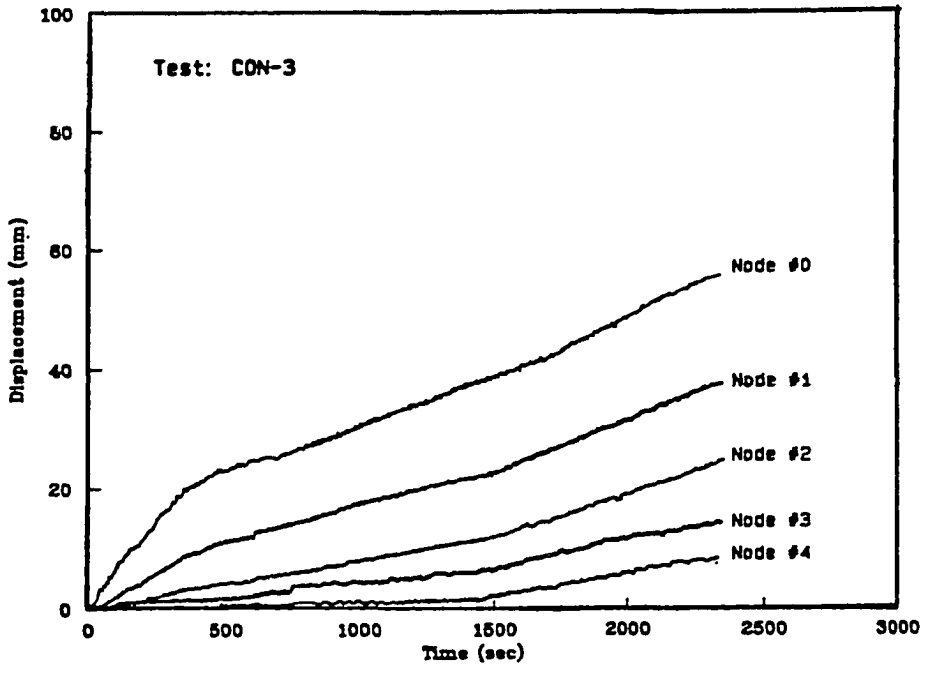

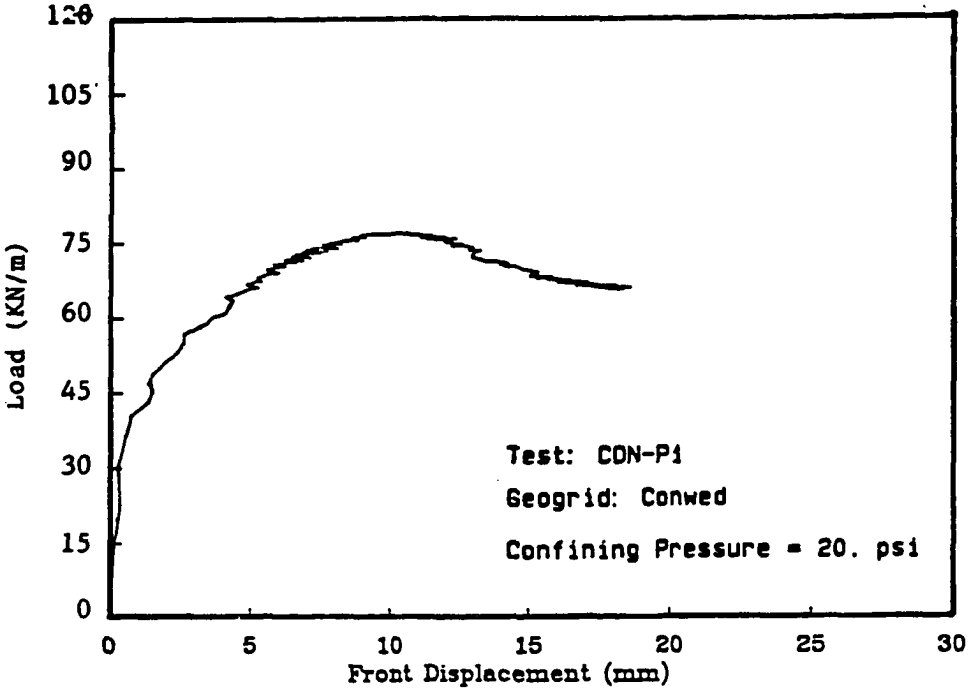

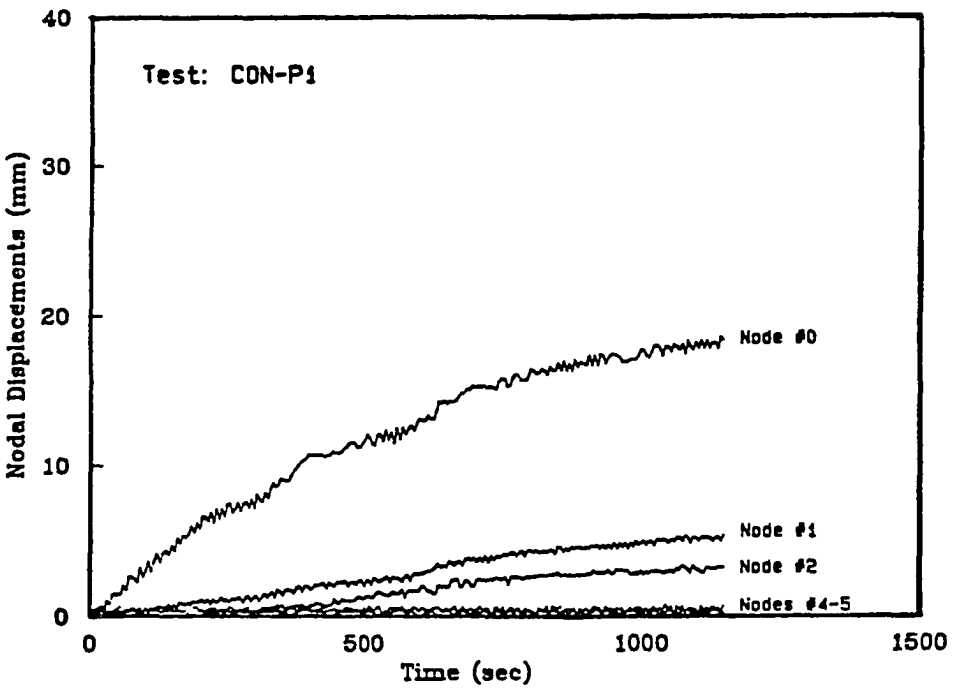

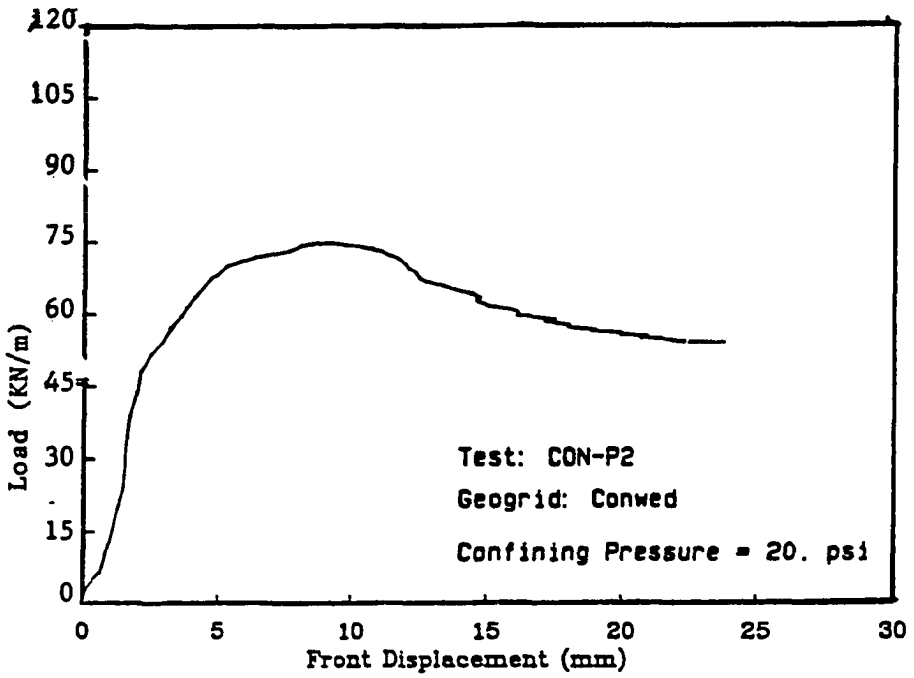

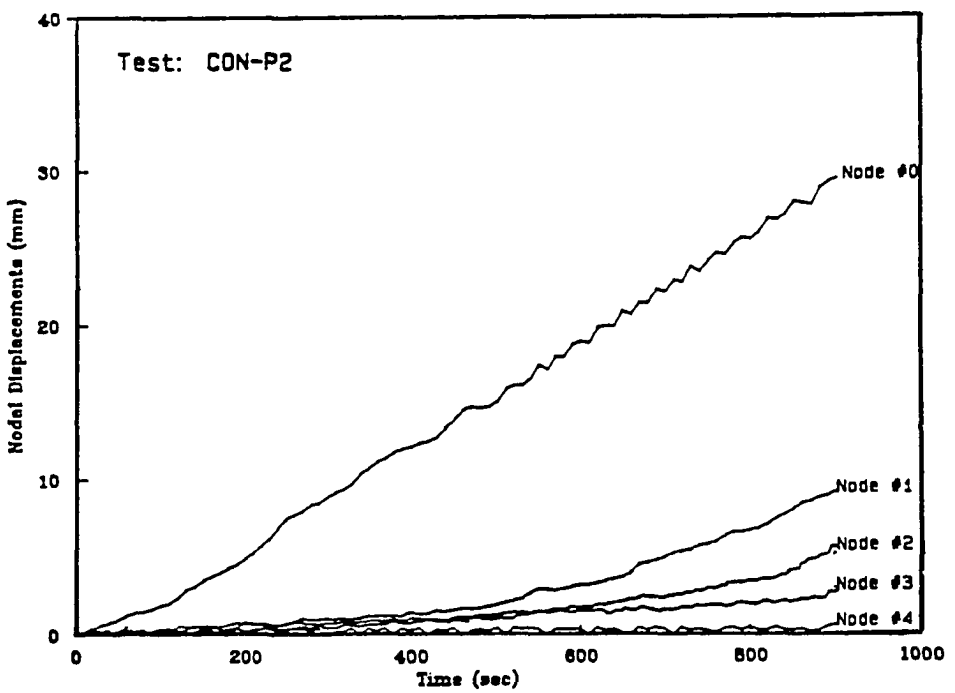

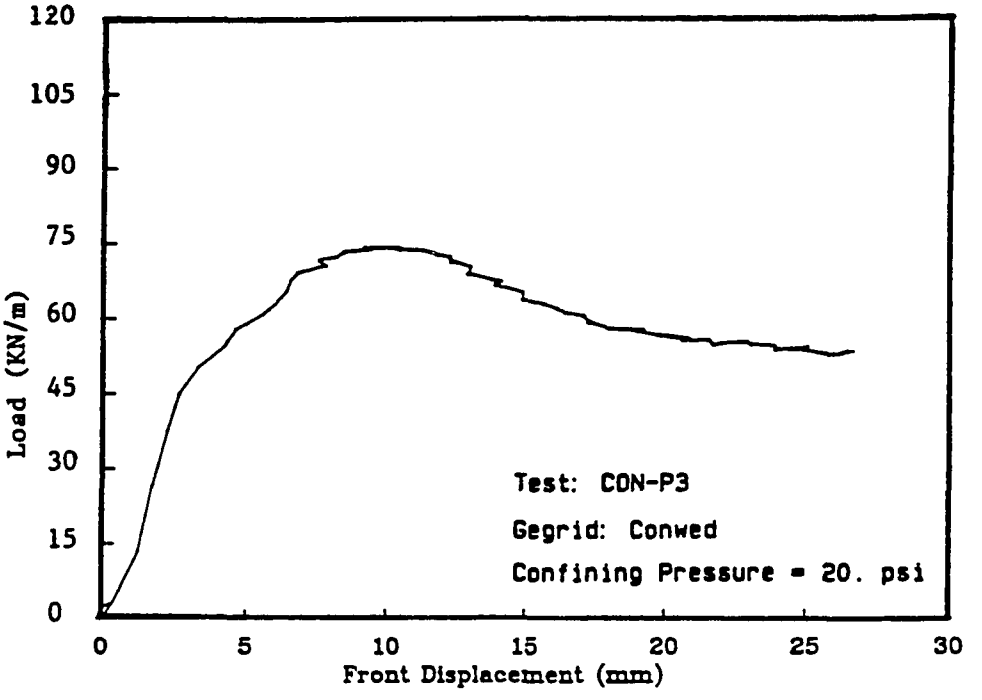

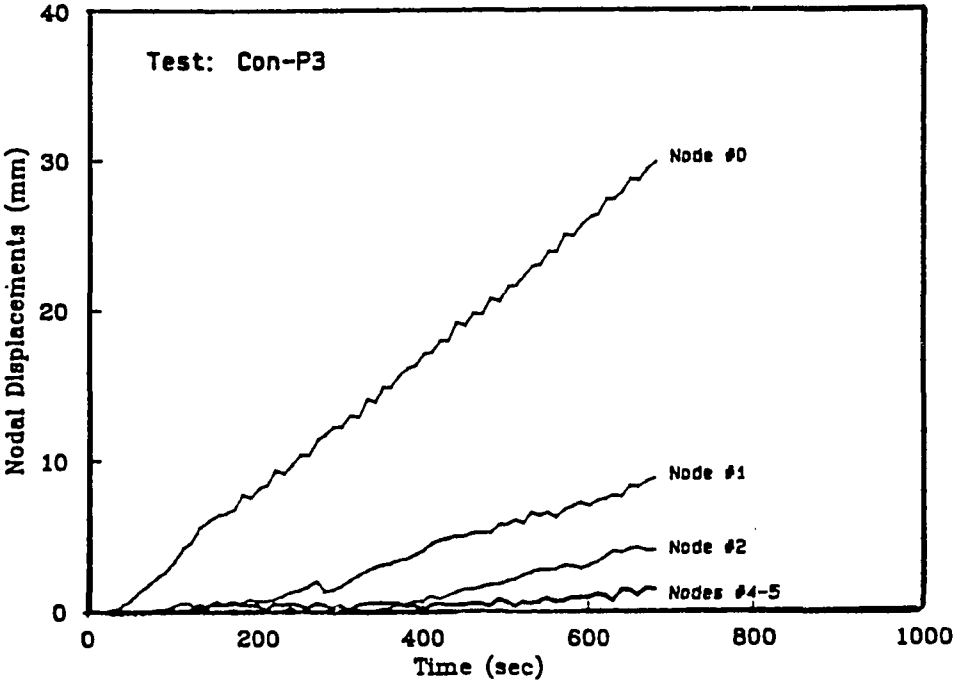

APPENDIX D

FORMULATION OF SOIL-REINFORCEMENT MODEL RELATIONSHIPS.

(I) soil Yield Function:

The soil is assumed to follow Mohr-Coulomb yield criteria:

$$\tau_{xy} = h(\gamma_{xy}) \cdot \sigma_y$$

where τ_{xy} and σ_y are the soil mobilized shear and normal stresses along the failure surface, $h(\gamma_{xy})$ is a strain hardening (and softening) function relating the current yield surface to the actual state of strain. As soil cohesion c = 0, the function $h(\gamma_{xy}) = \tan \phi_m$, where ϕ_m is the mobilized soil friction along the failure surface, then:

$$\frac{\tau_{xy}}{\sigma_y} = h(\gamma_{xy})$$

and the yield function (Figure D.1) is:

$$F(\sigma,\gamma_{xy}) = \frac{\tau_{xy}}{\sigma_y} - h(\gamma_{xy}) = 0 \qquad \ldots\ldots\ldots\ldots\ldots\ldots \text{(D.1)}$$

For dense dilating sand, the strain hardening (strain softening) function $h(\gamma_{xy})$ is assumed parabolic; i.e.:

$$h(\gamma_{xy}) = \tan \phi_m = \frac{c \cdot \gamma_{xy} (\gamma_{x,y} - a)}{(\gamma_{xy} + b)^2} \qquad \ldots\ldots\ldots \text{(D.2)}$$

The constants a, b and c are determined from the initial conditions as follows:

(i) the initial tangent of $h(\gamma_{xy}) = G/\sigma_y$; i.e.:

$$\frac{d[h(\gamma_{xy})]}{d\gamma_{xy}} = \frac{G}{\sigma_y} \qquad (\text{at } \gamma_{xy} = 0)$$

$$\frac{(\gamma_{xy} + b)^2 (2c.\gamma_{xy} - c.a) - 2\, c.\gamma_{xy} (\gamma_{xy} - a) (\gamma_{xy} + b)}{(\gamma_{xy} + b)^4} = \frac{G}{\sigma_y}$$

$$\therefore \quad \frac{-c.a}{b^2} = \frac{G}{\sigma_y} \qquad \ldots\ldots\ldots \text{(D.3-a)}$$

(ii) at peak shear strain, $h(\gamma_{xy}) = \tan \phi_p$

and $\dfrac{d[h(\gamma_{xy})]}{d\gamma_{xy}} = 0 \qquad$ (for $\gamma_{xy} = \gamma_p$)

i.e., $(\gamma_p + b)\,(2.c.\gamma_p) = 2.c.\gamma_p\,(\gamma_p - a)$

$$\therefore \quad \gamma_p = \frac{a.b}{2b+a}$$

substituting, $h(\gamma_p) = \dfrac{-a^2.\, b}{4b\,(a + b)} = \tan \phi_p \qquad \ldots\ldots\ldots \text{(D.3-b)}$

(iii) at critical state, $\lim_{\gamma \to \infty} h(\gamma_{xy}) = \tan \phi_{cv}$

i.e., $\lim_{\gamma \to \infty} h(\gamma_{xy}) = \lim_{\gamma \to \infty} \left[\dfrac{c.\gamma^2_{xy} - a.c.\gamma_{xy}}{\gamma^2_{xy} + 2.b.\gamma_{xy} + b^2} \right] = c$

$$\therefore \quad c = \tan \phi_{cv} \qquad \ldots\ldots\ldots \text{(D.3-c)}$$

solving equations (D.3-a), (D.3-b) and (D.3-c) we get:

$$b = 2\,(\sigma_y/G).\, \tan \phi_p\, .\, [1. + 1.-(\tan \phi_{cv}/ \tan \phi_p)\,]$$

$$a = -4\,(\sigma_y/G).\, \tan^2 \phi_p\, .\, [1. + 1.-(\tan \phi_{cv}/ \tan \phi_p)\,]^2 / \tan \phi_{cv}$$

(II) Soil-Reinforcement Interaction:

From the deformation in reinforcement during shearing, Figure (D.2), we get:

$$\tan \lambda_i = \frac{a+\Delta x}{h+\Delta y} = \frac{a/h + \Delta x/h}{1 + \Delta y/h}$$

Then,

$$\tan \lambda_i = \frac{\tan \lambda_{i-1} + d\gamma_{xy}}{1 + d\epsilon_y} \qquad \ldots\ldots\ldots (D.4)$$

From Mohr's circle of strain (Figure D.3), we get

$$d\epsilon_R = d\epsilon_y + x = d\epsilon_R + L \sin \lambda$$

Where $d\epsilon_R$ is the incremental strain in the reinforcement. From Figure (D.3) we get : $L/\sin \gamma = d\epsilon_y/\sin \upsilon$

and $\sin \gamma = \cos (\lambda + \upsilon)$, substituting:

$$L = \cos (\lambda + \upsilon).\ d\epsilon_y / \sin (\upsilon)$$

then,

$$d\epsilon_R = d\epsilon_y + \left(\frac{\cos (\lambda + \upsilon).\ \sin \lambda}{\sin \upsilon} \right) d\epsilon_y$$

since $d\epsilon_y = \tan \upsilon .\ d\gamma_{xy}$, we get:

$$d\epsilon_R = \tan \upsilon \left(1. + \frac{\cos (\lambda + \upsilon).\ \sin \lambda}{\sin \upsilon} \right) d\gamma_{xy} \qquad \ldots\ldots\ldots (D.5)$$

(III) Equilibrium Equations:

For a potential failure surface α, Figure (D.4) shows the forces acting on the active zone.

The horizontal equilibrium for any slice J (j=1,2...N), neglecting the forces between slices, is:

$$T_j \cdot \cos \beta_j = R_j \cdot \sin (\alpha - \phi_j)$$

where T_j is the tension force of the reinforcement at level (j) = E.t.b ϵ_{Rj}, β is the reinforcement inclination with the horizontal, and $\cos \beta = \sin (\lambda_j + \alpha)$, and R_j is the soil reaction along the failure surface.

$$\epsilon_{Rj} \cdot \text{E.t.b.} \sin (\lambda_j + \alpha) = R_j \cdot \sin (\alpha - \phi_j)$$

then,

$$\Sigma^N R_j = \text{E.t.b.} \; \Sigma^N \epsilon_{Rj} \cdot \frac{\sin(\lambda_j + \alpha)}{\sin(\alpha - \phi_j)} \qquad \ldots\ldots\ldots\ldots \text{(D.6)}$$

The weight of the soil mass in the active zone (Figure D.4) is:

$$W = \tfrac{1}{2} \rho \cdot H^2 [\, (1/\tan \alpha) - \tan J \,] \cdot S_h \qquad \ldots\ldots\ldots \text{(D.7)}$$

where H is the wall height, J is the inclination of the wall facing with vertical, and S_h is the horizontal spacing of the reinforcement. The vertical equilibrium in the active zone is:

$$\Sigma^N R_j \cos (\alpha - \phi_j) - \Sigma^N T_j \sin \beta = W \qquad \ldots\ldots\ldots \text{(D.8)}$$

Substituting equation (D.6) into equation (D.8), we get:

$$\text{E.t.b.} \left\{ \Sigma^N \epsilon_{Rj} \cdot \frac{\sin(\lambda_j + \alpha)}{\tan(\alpha - \phi_j)} - \Sigma^N \epsilon_{Rj} \cdot \cos(\lambda_j + \alpha) \right\} = W$$

Substituting equation (D.7) and rearranging the equation, we get the non-dimensional relationship:

$$H/\left[\frac{E.t.b}{\rho.S_h.S_v}\right]_{.} = \frac{2\left[\Sigma^N \epsilon_{Rj} \sin(\lambda_j+\alpha) \cot(\alpha-\phi_j) - \Sigma^N \epsilon_{Rj} \cos(\lambda_j+\alpha)\right]}{N[(1/\tan\alpha) - \tan J]} \quad \ldots (D.9)$$

The most critical solution in terms of the critical height H under a specific shear strain γ_{xy} can then be obtained by minimizing H in equation (D.9) with respect to the failure angle α . These formulations are implemented in a computer program to obtain the critical height and the tension force distribution at each reinforcement level for incremental shear strains.

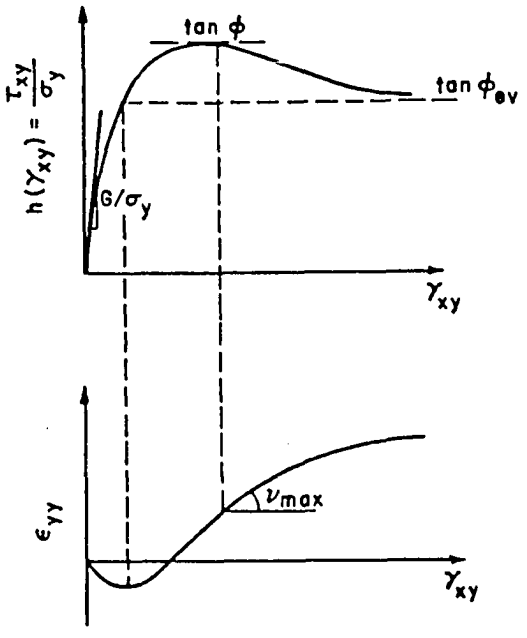

Figure D.1 Elasto-plastic Strain Hardening function of the Soil.

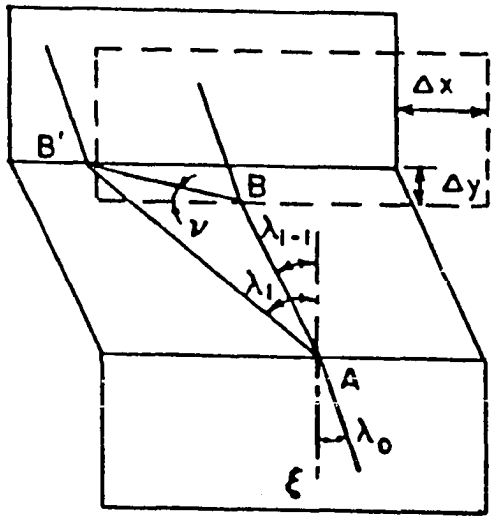

Figure D.2 Deformation of the Reinforcement during Shearing.

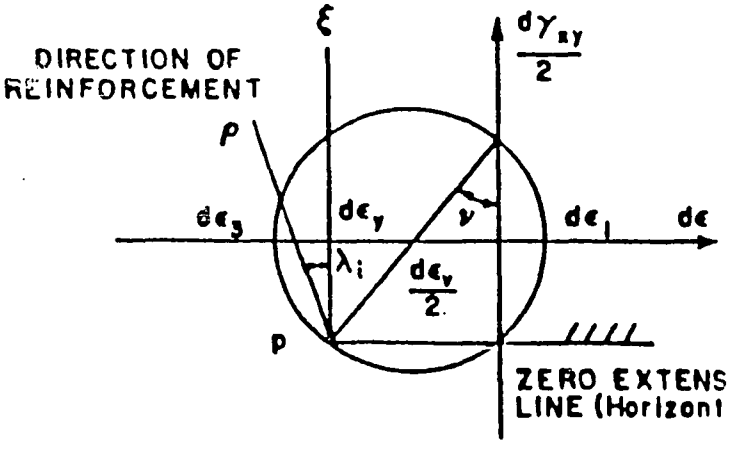

Figure D.3 Mohr's Circle of Strain Increments in Soil.

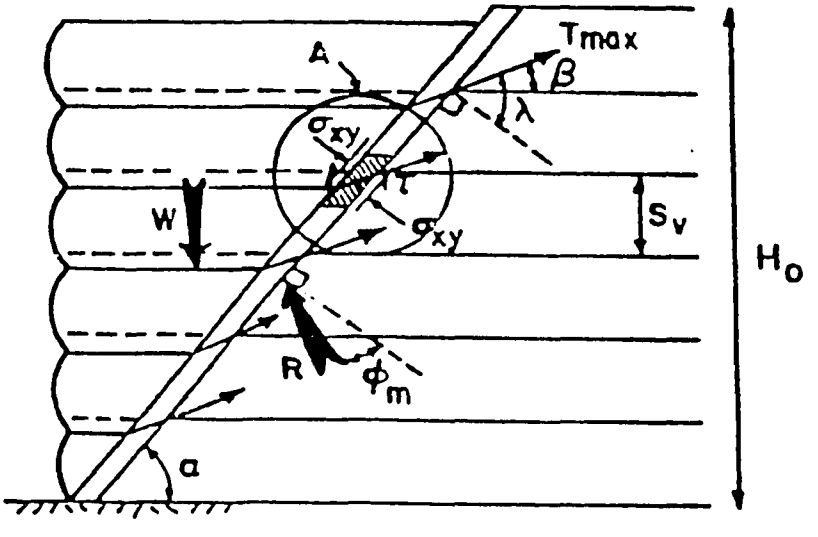

Figure D.4 Failure Mechanism in Reinforced Soil Walls.

VITA

Mr. Khalid A. Farrag was born in Alexandria, Egypt on Aug. 15, 1955. He got his B.S. degree in Civil Engineering from Cairo University on 1977. He worked as a Civil Engineer in Egypt and Saudi Arabia from 1978 till 1984. He Got his M.S. degree in Civil Engineering from Louisiana State University on Dec. 1986, and his Ph.D. degree in Civil Engineering on Dec. 1990.

DOCTORAL EXAMINATION AND DISSERTATION REPORT

Candidate: Khalid A. Farrag

Major Field: Civil Engineering

Title of Dissertation: Interaction Properties of Geogrids in Reinforced Soil Walls, Testing and Analysis.

Approved:

Major Professor and Chairman

Dean of the Graduate School

EXAMINING COMMITTEE:

Date of Examination:

Nov. 19, 1990